

# Improving Dispersion Energy Calculations

by

Monika Kodrycka

A dissertation submitted to the Graduate Faculty of  
Auburn University  
in partial fulfillment of the  
requirements for the Degree of  
Doctor of Philosophy

Auburn, Alabama  
December 14, 2019

Keywords: quantum chemistry, intermolecular interactions, dispersion,  
symmetry-adapted perturbation theory

Copyright 2019 by Monika Kodrycka

Approved by

Konrad Patkowski, Chair, Associate Professor of Chemistry and Biochemistry  
Vincent Ortiz, Ruth W. Molette Professor of Chemistry and Biochemistry  
Michael McKee, Professor Emeritus of Chemistry and Biochemistry  
Evangelos Miliordos, Assistant Professor of Chemistry and Biochemistry  
Luke Oeding, Associate Professor of Mathematics and Statistics

## Abstract

Various approaches were investigated and developed to improve dispersion energy calculations. The highest levels of *ab initio* electronic structure theory available were applied to study nine characteristic points on the CO–CO, N<sub>2</sub>–N<sub>2</sub>, and CO–N<sub>2</sub> potential energy surfaces. To obtain the desired spectroscopic accuracy, corrections beyond the state-of-the-art CCSD(T)/CBS level of theory were calculated, including higher-orders of coupled-cluster theory (up to full single, double, triple, and quadruple excitations, CCSDTQ), relativistic effects, and core-core and core-valence correlation. The significance of post-CCSD(T) effects was emphasized. These effects are particularly important for the CO–CO complex: their magnitude can exceed 3% of the CCSD(T) interaction energy. In order to enhance the dispersion calculations for the D3 atom-pairwise dispersion correction by Grimme, new forms of damping were designed: a linear combination of error functions and a piecewise-linear function. Furthermore, the possibility of creating a damped dispersion function without higher than  $C_6$  dispersion coefficients was explored. Last but not least, second-order dispersion and exchange-dispersion corrections in SAPT were improved by applying the F12 methods, resulting in  $E_{\text{disp}}^{(20)}$ -F12 and  $E_{\text{exch-disp}}^{(20)}$ -F12. In order to improve scaling of these methods, we proposed three approximate Ansätze: EBC, optimized diagonal, and fixed-amplitude. Moreover, the density-fitting algorithm was introduced to speed up the calculations and to overcome the memory bottleneck.

## Acknowledgments

I would like to thank all the people who contributed to this incredible journey. First and foremost, I would like to thank Dr. Konrad Patkowski for being a phenomenal advisor. He has provided me with opportunities and challenges that have made me a better scientist, and helped to broaden my horizons. His knowledge, talent, and passion have always been very inspiring and motivating.

I want to extend a special thanks to Dr. Filip Pawłowski for all the invaluable discussions. Thanks to him my adventure with the quantum world began many years ago and thanks to him I am at this place today.

I would like to thank Dr. Dmytro Bykov and Dr. Dmitry Liakh for being superb advisors during my internship at Oak Ridge National Lab. They have taught me massively parallel techniques and how to think about algorithms from a totally different perspective.

I also was very lucky to have had the support from the Molecular Sciences Software Institute (MolSSI). A special thanks goes to Dr. Levi Naden who was an incredible mentor. He taught me not only good programming practices, but also how to stand out from the crowd and succeed as a young scientist.

I would like to acknowledge the efforts and guidance of my thesis committee: Dr. Vincent Ortiz, Dr. Michael McKee and Dr. Evangelos Miliordos. Each has provided their own distinct insight of the field of chemistry.

To my mom, Małgorzata Kodrycka, my sincere thanks for bringing me up to always be smart and pursue my dreams. She always emphasized the importance of education and supported my academic career in the USA. I would like to thank my grandmother, Ewa Szreder, for unconditional love, good vibes and constant prayers.

Last but not least, I would like to thank Britni Arrington who has been my constant companion for her unbelievable support, kindness, and an open heart. She always reminds me that there is life beyond science and puts a big smile on my face whenever I need it. I have felt so alive with our amazing adventures.

## Table of Contents

Abstract . . . . .	ii
Acknowledgments . . . . .	iii
List of Abbreviations . . . . .	xiv
1 Introduction . . . . .	1
2 Electronic Structure Theory . . . . .	6
2.1 The Electronic Schrödinger Equation . . . . .	6
2.2 Hartree-Fock Method . . . . .	8
2.3 Correlated Methods . . . . .	12
2.3.1 Configuration Interaction Method . . . . .	12
2.3.2 Coupled-Cluster Method . . . . .	14
2.3.3 Many-Body Perturbation Theory . . . . .	15
2.3.4 Symmetry-Adapted Perturbation Theory . . . . .	18
2.3.5 Slow Convergence of Electron Correlation . . . . .	21
2.3.6 Explicitly Correlated F12 methods . . . . .	23

2.3.7	Density Functional Theory . . . . .	28
2.4	Calculations of Noncovalent Interactions . . . . .	32
2.5	Counterpoise Correction (CP) . . . . .	34
2.6	Orbital and Auxiliary Basis Sets . . . . .	34
3	Triple bonds and coupled-cluster convergence: CCSDTQ interaction energies for complexes involving CO and N <sub>2</sub> . . . . .	37
3.1	Previous studies on CO–CO, N <sub>2</sub> –N <sub>2</sub> , and CO–N <sub>2</sub> . . . . .	39
3.2	Results and Discussion . . . . .	40
3.2.1	CCSD(T) interaction energies . . . . .	42
3.2.2	Higher-order Coupled-Cluster Corrections . . . . .	46
3.2.3	Core-core and Core-valence Correlation, Relativistic, and DBOC Effects . . . . .	51
3.2.4	Total Interaction Energies . . . . .	52
3.3	Summary . . . . .	58
4	Deducing the Optimal Damping Function for the D3 Dispersion Correction to Density Functional Theory . . . . .	60
4.1	Introduction . . . . .	60
4.2	Overview of Damping Functions Used in the DFT+D Approaches . . . . .	61
4.3	Damping Function Development . . . . .	64
4.4	New Forms of Damping Functions . . . . .	65
4.4.1	Damping Function Expressed by an Error Function . . . . .	67

4.4.2	Piecewise-linear Function . . . . .	68
4.5	Results and Discussion . . . . .	69
4.5.1	Performance of Erf-based Damping Functions . . . . .	71
4.5.2	Performance of Piecewise Linear Damping Functions . . . . .	72
4.5.3	Dispersion expressions with $C_6$ only . . . . .	75
4.6	Summary . . . . .	76
5	Explicitly Correlated Dispersion and Exchange Dispersion Energies in Symmetry-Adapted Perturbation Theory . . . . .	85
5.1	F12 Dispersion Energy . . . . .	87
5.2	F12 Exchange Dispersion Energy . . . . .	93
5.3	SAPT-F12(MP2) . . . . .	95
5.4	Test Systems . . . . .	96
5.5	Tests on the A24 Database . . . . .	99
5.6	Density-Fitting Approximation in SAPT-F12 . . . . .	102
5.7	Summary . . . . .	110
6	Conclusions . . . . .	112
6.1	Future and Outlook . . . . .	113
	Bibliography . . . . .	114
	Appendices . . . . .	124

A	Triple bonds and coupled-cluster convergence: CCSDTQ interaction energies for complexes involving CO and N <sub>2</sub> . . . . .	125
B	A Platinum, gold, and silver standards of intermolecular interaction energy calculations . . . . .	127
C	Explicitly correlated dispersion and exchange dispersion energies in symmetry-adapted perturbation theory . . . . .	129



## List of Figures

2.1	Helium ground state wave functions with both electrons confined at the circle of radius $0.5 a_0$ calculated with the CI approach using increasing basis size with maximum principal quantum number $n_{max}$ . The figure comes from Ref. [1] . . . . .	22
3.1	The stationary points on the CO–CO, N <sub>2</sub> –N <sub>2</sub> , and CO–N <sub>2</sub> potential energy surfaces considered in this work. . . . .	42
4.1	The number of occurrences of intermolecular $\frac{r_{AB}}{R_0^{AB}}$ values in the training and validation sets. The functions that damp the $C_6$ dispersion term in three DFT-D3 variants are also plotted. . . . .	67
4.2	Error function curves with different values of $\alpha_i$ and $r_i$ . . . . .	68
4.3	Damping functions based on one erf function for a) $C_6$ and b) $C_8$ terms in Eq. 4.10 with optimized parameters. . . . .	70
4.4	Damping functions based on a linear combination of two erf functions a) the $C_6$ term and one erf function for b) $C_8$ term with optimized parameters. . . . .	71
4.5	The piecewise linear damping functions with 6 constrained parameters for different functionals. . . . .	71
4.6	The MCURE values for functionals utilizing the new erf-based damping function compared to DFT-D3 with original and modified damping parameters. . . . .	72
4.7	The CRMSE values of density functionals with the piecewise linear damping function utilizing 6 and 13 constrained and unconstrained damping parameters with the $C_6$ and $C_8$ coefficients, compared to DFT-D3 with original [2, 3] and modified damping parameters [4]. . . . .	75

4.8	The CRMSE values of density functionals with the piecewise linear damping function utilizing 6 and 13 unconstrained damping parameters with the $C_6$ and $C_8$ coefficients, compared to DFT-D3 with original [2, 3] and modified damping parameters [4]. The additional parameter $\gamma$ was introduced to reformulate the “effective distance” (Eq. 4.15). . . . .	75
4.9	The CRMSE values of density functionals with the $C_6$ -based damping function utilizing 10 and 21 unconstrained parameters with and without $\gamma$ compared to DFT-D3 with original [2, 3] and modified [4] damping parameters. . . . .	76
4.10	The piecewise linear damping functions with 6 constrained, and 6 and 13 unconstrained parameters for different functionals. . . . .	78
4.11	The piecewise linear damping functions with 10 and 21 unconstrained parameters including only the $C_6$ coefficient for different functionals. . . . .	79
5.1	Schematic representation of double excitations in the local MP2 method. The figure comes from Ref. [5]. . . . .	96
5.2	Convergence of $E_{\text{disp}}^{(20)}$ -F12 and $E_{\text{exch-disp}}^{(20)}$ -F12 as a function of basis set for the $\text{CH}_4\text{-CH}_4$ complex. This Figure was adapted from [6]. . . . .	98
5.3	Relative errors on the A24 database [7] for $E_{\text{disp}}^{(20)}$ -F12 computed with the aDZ/aTZ-RI basis sets. This Figure was adapted from Ref. [6]. . . . .	100
5.4	Relative errors on the A24 database [7] for $E_{\text{disp}}^{(20)}$ -F12 computed with the aTZ/aTZ-RI basis sets. Figure was adopted from Ref. [6]. . . . .	101
5.5	Relative errors on the A24 database [7] for $E_{\text{exch-disp}}^{(20)}$ -F12 computed with the aDZ/aTZ-RI basis sets. . . . .	101
5.6	Relative errors on the A24 database [7] for $E_{\text{exch-disp}}^{(20)}$ -F12 computed with the aTZ/aTZ-RI basis sets. . . . .	101
5.7	Relative errors on the A24 database [7] for the sum $E_{\text{disp}}^{(20)}$ -F12+ $E_{\text{exch-disp}}^{(20)}$ -F12 computed with the aTZ/aTZ-RI basis sets. . . . .	102

## List of Tables

2.1	List of basis sets utilized in the dissertation. . . . .	36
3.1	CCSD(T) and CCSD(T)-F12 interaction energies (in $\text{cm}^{-1}$ ) for the global minimum ( $C_{2h}$ ) geometry of the CO dimer, Fig. 3.1. The extrapolated value (rows “ext.”) in the $X$ column is computed using interaction energies in bases $a(X-1)Z$ and $aXZ$ . The letter M in the basis set stands for the hydrogenic set of midbond functions from the same $aXZ$ basis. . . . .	43
3.2	CCSD(T) and CCSD(T)-F12 interaction energies (in $\text{cm}^{-1}$ ) for the global minimum ( $C_{2h}$ ) geometry of the $\text{N}_2$ dimer, Fig. 3.1. The extrapolated value (rows “ext.”) in the $X$ column is computed using interaction energies in bases $a(X-1)Z$ and $aXZ$ . The letter M in the basis set stands for the hydrogenic set of midbond functions from the same $aXZ$ basis. . . . .	44
3.3	CCSD(T) and CCSD(T)-F12 interaction energies (in $\text{cm}^{-1}$ ) for the global minimum geometry of the CO– $\text{N}_2$ complex, Fig. 3.1. The extrapolated value (rows “ext.”) in the $X$ column is computed using interaction energies in bases $a(X-1)Z$ and $aXZ$ . The letter M in the basis set stands for the hydrogenic set of midbond functions from the same $aXZ$ basis. . . . .	45
3.4	Post-CCSD(T) interaction energy contributions for the CO–CO dimer (in $\text{cm}^{-1}$ ). The core and relativistic corrections used the aug-cc-pCVXZ and aug-cc-pCVXZ-DK bases, respectively. . . . .	48
3.5	Post-CCSD(T) interaction energy contributions for the $\text{N}_2$ – $\text{N}_2$ dimer (in $\text{cm}^{-1}$ ). The core and relativistic corrections used the aug-cc-pCVXZ and aug-cc-pCVXZ-DK bases, respectively. . . . .	49
3.6	Post-CCSD(T) interaction energy contributions for the CO– $\text{N}_2$ dimer (in $\text{cm}^{-1}$ ). The core and relativistic corrections used the aug-cc-pCVXZ and aug-cc-pCVXZ-DK bases, respectively. . . . .	50

3.7	Geometrical parameters and interaction energies for the CO–CO complex, computed by us as explained in the text (upper part) and taken from literature (lower part). All distances, angles, and interaction energies are given in bohr, degrees, and $\text{cm}^{-1}$ , respectively. $E_{\text{int}}$ represents our best interaction energy estimate computed according to Eq. (3.2). . . . .	54
3.8	Geometrical parameters and interaction energies for the $\text{N}_2$ – $\text{N}_2$ complex, computed by us as explained in the text (upper part) and taken from literature (lower part). All distances, angles, and interaction energies are given in bohr, degrees, and $\text{cm}^{-1}$ , respectively. $E_{\text{int}}$ represents our best interaction energy estimate computed according to Eq. (3.2). . . . .	55
3.9	Geometrical parameters and interaction energies for the CO– $\text{N}_2$ complex, computed by us as explained in the text (upper part) and taken from literature (lower part). The dihedral angle $\phi=0^0$ and all distances, angles, and interaction energies are given in bohr, degrees, and $\text{cm}^{-1}$ , respectively. $E_{\text{int}}$ represents our best interaction energy estimate computed according to Eq. (3.2). . . . .	56
3.10	Differences between the global ( $C_{2h}$ ) and local minima ( $C_{2h}$ and $C_s$ ) well depths for the CO–CO complex calculated at different levels of theory. The MP2, CCSD, and CCSD(T) values were obtained from the MP2-F12/(a5Z,a6Z), CCSD-F12b/(a5Z,a6Z), and CCSD(T**)-F12b/(a5Z,a6Z) extrapolations, respectively, and the higher-level corrections were computed in the basis sets specified in Sec. 3.2.1. . . . .	57
4.1	Damping parameters for one erf each for $C_6$ and $C_9$ with and without an $s_8$ factor. . . . .	80
4.2	Damping parameters for a combination of error functions with and without the $s_8$ factor. The parameter $c_2$ is calculated as a difference $1 - c_1$ . . . . .	81
4.3	Parameters for the piecewise linear damping function with 6 constrained coefficients. . . . .	82
4.4	Parameters for the piecewise linear damping function with 6 unconstrained coefficients. . . . .	82

4.5	Parameters for the piecewise linear damping function with 13 constrained coefficients. . . . .	83
4.6	Parameters for the piecewise linear damping function with 13 unconstrained coefficients. . . . .	83
4.7	Parameters for the $C_6$ only piecewise linear damping function with 10 unconstrained coefficients and the $\gamma$ parameter. . . . .	84
5.1	Orbital spaces used in this work. . . . .	88
5.2	The calculation times (in s) for the DF and non-DF $E_{\text{disp}}^{(20)}$ -F12(ODA)+ $E_{\text{exch-disp}}^{(20)}$ -F12(ODA) corrections performed on the Hopper Supercomputer at Auburn University using 1 core. The results do not include the time for SCF calculations. . . . .	111

## List of Abbreviations

AE	All-Electron
BSSE	Basis Set Superposition Error
CBS	Complete Basis Set
CC	Coupled-Cluster Theory
CI	Configuration Interaction
CP	Counterpoise Correction
CPHF	Coupled Perturbed Hartree-Fock
DF	Density-Fitting
DFT	Density Functional Theory
DKH	Douglas-Kroll-Hess
EBC	Extended Brillouin Condition
FC	Frozen-Core

GBC	Generalized Brillouin Condition
GGA	Generalized Gradient Approximation
GTO	Gaussian-Type Orbital
HF	Hartree-Fock Theory
LDA	Local Density Approximation
ML	Machine Learning
MO	Molecular Orbital
MP	Møller-Plesset Theory
QMC	Quantum Monte Carlo
RI	Resolution of the Identity
RS	Rayleigh-Schrödinger
SAPT	Symmetry-Adapted Perturbation Theory

## **Chapter 1**

### **Introduction**

Computational chemistry is a field that models chemical phenomena in order to predict, understand, and validate experimental measurements. The models used vary significantly in terms of their theoretical and computational complexity, from approximate empirical and semi-empirical ones through DFT methods to very accurate frameworks based on, among others: wavefunction theory, perturbation theory versions, or Quantum Monte Carlo (QMC) [8]. A particular challenge for computational chemistry, and for our research group, surrounds the examination of noncovalent interactions. Although these interactions are known as “weak” with a typical strength of the order of 1 kcal/mol, it has been shown that they can reach 100 kcal/mol and even more for large supramolecular complexes [9]. The omnipresent character of noncovalent interactions makes them a significant subject of study, hence their accurate investigation and understanding is crucial for explaining a vast variety of phenomena in chemistry, physics, biology, as well as materials science. All noncovalent interactions are composed of the same four basic components: electrostatics,



exchange-repulsion, induction, and dispersion. Although each of them is of high importance, this research is narrowed down to the most ubiquitous forces in nature and at the same time the most demanding ones to compute, dispersion forces.

The London dispersion forces are a special type of van der Waals interaction, which arise from the interaction between the instantaneous multipole moments of fluctuating charge distributions. They were described for the first time by Eisenschitz and London in 1930 [10], and this work turned out to be a breakout in the study of intermolecular interactions. The dispersion force explained the mysterious origin of the attraction between noble gas atoms. London's mathematical description of the dispersion interaction between two atoms ( $A$  and  $B$ ) is based on a straightforward application of second-order perturbation theory, where the Coulomb interaction is treated with a multipole expansion [11]:

$$E_{disp} = \left( -\frac{3}{2} \frac{I_A I_B}{I_A + I_B} \alpha_A \alpha_B \right) \frac{1}{R^6} = -\frac{C_6}{R^6}, \quad (1.1)$$

where  $I_A$  and  $I_B$  are the first ionization potentials of atoms  $A$  and  $B$ , respectively,  $\alpha_A$ ,  $\alpha_B$  are the dipole polarizabilities, and  $C_6$  is a van der Waals coefficient. It has been believed for a long time that dispersion is only a long range effect, which according to Eq. 1.1 decays like  $R^{-6}$ , however, recent studies proved that dispersion needs to be taken with special care also at short and intermediate distances [12], including the repulsive part of the potential.

It is fascinating what an important role dispersion interactions play in our world. The fundamental example is a gecko which, thanks to purely dispersion-driven noncovalent interactions, has an ability to climb up smooth vertical surfaces, even flat glass [13]. In ultracold physics and chemistry, long-range dispersion interactions are essential

for low-energy and low-temperature collisions between atoms and molecules [14]. In biochemistry, they are responsible for the formation of the helical structure of some proteins and stabilization of the DNA double helix [15]. In chemistry, dispersion explains, among others, the different boiling points of alkanes, the greater stability of branched over linear alkanes [16], and the stability of singly bonded diamondoid dimers [17]. It also constitutes a significant control component for reactivity and catalysis, especially in the case of larger molecules [18]. Such a broad spectrum of applications justifies the need for accurate dispersion models. However, from a computational point of view, this is a formidable task. The difficulty lies in the fact that dispersion interactions are purely quantum mechanical phenomena, originating from the correlated motion of electrons. Therefore, they are particularly demanding for electronic structure theory, and very often we need to reach for sophisticated wavefunction-based quantum chemistry methods, such as coupled-cluster singles and doubles with perturbative inclusion of triples (CCSD(T)) [19] or symmetry adapted perturbation theory (SAPT) [20, 21]. While these methodologies are reliable at capturing dispersion, their unfavorable scaling with respect to the system size prevents their application for large molecular systems. It seems that there are a few ways to avoid this obstacle. A very popular approach of reducing the complexity of current algorithms is simply introducing approximations. Another way of cutting the computational expense is achieved by applying parallel computing techniques, which allow for utilization of modern computational resources, such as computers with distributed memory equipped with many CPUs and GPUs. Thanks to these advances, the calculations of interaction energies with a spectroscopic accuracy, that is, accuracy of  $1 \text{ cm}^{-1}$ , has become feasible for systems with a few atoms. In order to attain such an accuracy, one needs to go beyond the “gold standard”

of noncovalent interactions (CCSD(T) converged to the complete basis set (CBS) limit), and include higher-order coupled-cluster excitations, core correlation, relativistic effects, and the effects beyond the Born-Oppenheimer approximation. Such an approach is in fact very expensive, but turns out to be essential for studies of dispersion bound systems in terms of theoretical as well as experimental aspects, and more details will be discussed in Chapter 2.

In recent years, we have observed a considerable growth in demand for the accurate benchmark interaction energies of noncovalent complexes including the construction and applications of sets (databases). They are of great importance for creating and testing more approximate methods, such as density functional theory (DFT) [22], semiempirical methods [23], or machine learning (ML) [24]. The requirement for a well constructed database of noncovalent interactions is to be unbiased, and it can be achieved by taking into the account following factors: radial diversity, angular diversity, and interaction type diversity [25]. The classification of types of interactions usually goes beyond the chemical intuition, so that SAPT comes in handy and allows one to decompose energy into fundamental forces. Moreover, ternary diagrams are a valuable help for representing the degree of diversity in a benchmark database [4].

Having these tools in mind, let us turn our attention towards density functional theory (DFT). This method is broadly used across different computational fields due to its attractive low scaling. Thus, it is utilized for calculations when conventional wavefunction methods prove too expensive. Nevertheless, the local or semilocal character of conventional DFT leads to a neglect of the long-range correlation, which captures attractive van der Waals forces. The quest to incorporate dispersion interactions into DFT has become

one of the hottest topics in computational chemistry and several approaches have been proposed to date, with the most successful being “DFT plus atom-atom dispersion” (DFT-D3 and its successor DFT-D4) [2, 22]. While DFT-D3/DFT-D4 works effectively at medium and large intermolecular distances, there is still some room for improvement at short distances. This aspect will be presented in detail in Chapter 3.

This work is structured as follows: In Chapter 2 we review the standard *ab initio* methods and describe the strategy for calculating noncovalent interactions. Chapter 3 elucidates the importance of the highest levels of *ab initio* electronic structure theory for some dispersion dominated complexes, such as: CO–CO, N<sub>2</sub>–N<sub>2</sub>, and CO–N<sub>2</sub>. In Chapter 4, we present new forms of damping functions for the D3 atom-pairwise dispersion correction by Grimme [2]: a linear combination of error functions and a piecewise-linear function. Moreover, we show the possibility of designing a damped dispersion function without higher than  $C_6$  dispersion coefficients. Last but not least, in Chapter 5 a novel development in SAPT is presented - explicitly correlated dispersion  $E_{\text{disp}}^{(20)}$ -F12 and exchange dispersion energies  $E_{\text{exch-disp}}^{(20)}$ -F12. We implement and investigate three Ansätze: fixed, optimized diagonal and fully optimized, for the dispersion amplitudes. Their comparison leads to the deduction of the most accurate and the most computationally efficient approach. We also present the comparison of  $E_{\text{disp}}^{(20)}$ -F12 and  $E_{\text{exch-disp}}^{(20)}$ -F12 with the SAPT-F12(MP2) method [26]. In order to speed up the calculations, the density fitting approximation [27, 28, 29] was introduced, which gave rise to DF- $E_{\text{disp}}^{(20)}$ -F12 and DF- $E_{\text{exch-disp}}^{(20)}$ -F12.

## Chapter 2

### Electronic Structure Theory

#### 2.1 The Electronic Schrödinger Equation

The heart of electronic structure methods is solving the famous non-relativistic time-independent Schrödinger Equation, which takes the form [30, 31]:

$$\widehat{H}\Psi = E\Psi, \quad (2.1)$$

where  $\widehat{H}$  is the Hamiltonian operator for a molecular system consisting of  $M$  nuclei and  $N$  electrons and  $\Psi$  is the wavefunction. The wavefunction is a function which depends on  $3N$  spatial coordinates  $r_i$  and  $N$  spin coordinates of the electrons  $\sigma_i$ , being collectively termed  $x_i$ , and the  $3M$  spatial coordinates of the nuclei  $R_I$ :

$$\Psi \equiv \Psi(x_1, x_2, \dots, x_N, R_1, R_2, \dots, R_M), \quad (2.2)$$

$\widehat{H}$  is a differential operator which represents the total energy (expressed using atomic units):

$$\widehat{H} = -\frac{1}{2} \sum_{i=1}^N \nabla_i^2 - \frac{1}{2} \sum_{A=1}^M \frac{1}{M_A} \nabla_A^2 - \sum_{i=1}^N \sum_{A=1}^M \frac{Z_A}{r_{iA}} + \sum_{i=1}^N \sum_{j>i}^N \frac{1}{r_{ij}} + \sum_{A=1}^M \sum_{B>A}^M \frac{Z_A Z_B}{R_{AB}} \quad (2.3)$$

Here,  $M_A$  is the ratio of the mass of nucleus  $A$  to the mass of the electron, and  $Z_A$  is the atomic number of nucleus  $A$ . The first two terms describe the kinetic energy of the electrons and nuclei, respectively, where the Laplacian operator  $\nabla_p^2$  is defined as a sum of differential operators (in Cartesian coordinates):

$$\nabla_p^2 = \frac{\partial^2}{\partial x_p^2} + \frac{\partial^2}{\partial y_p^2} + \frac{\partial^2}{\partial z_p^2}. \quad (2.4)$$

The remaining terms correspond to the attractive electrostatic interaction between the nuclei and the electrons and the repulsive potential due to the electron-electron and nucleus-nucleus interactions, respectively.  $r_{ij}$ ,  $r_{iA}$ , and  $r_{AB}$  are the distances between electron  $i$  and electron  $j$ , electron  $i$  and nucleus  $A$ , and nucleus  $A$  and nucleus  $B$ , respectively.

The importance of the Schrödinger equation lies in the fact that it describes the motion and interaction of all electrons and nuclei in a molecule. However, solving it analytically for systems containing more than one electron becomes mathematically unfeasible. In order to make the problem easier, the Born-Oppenheimer approximation [32] is applied, where only the motion of electrons is taken into account since nuclei are much heavier than electrons, and consequently move at a much slower rate. This approximation leads to a separation of the wavefunction and Hamiltonian in terms of the electronic and nuclear

parts. The electronic part explicitly depends on the electronic coordinates  $r$  and parametrically depends on the nuclear coordinates  $R$ . Therefore, the complexity of solving the Schrödinger equation is reduced, yielding a simplified Hamiltonian, known as the electronic Hamiltonian, given by:

$$\widehat{H}_{elec} = -\frac{1}{2} \sum_{i=1}^N \nabla_i^2 - \sum_{i=1}^N \sum_{A=1}^M \frac{Z_A}{r_{iA}} + \sum_{i=1}^N \sum_{j>i}^N \frac{1}{r_{ij}} \quad (2.5)$$

for which the kinetic energy of the nuclei is omitted, and the nuclear-nuclear repulsion contribution is constant. Nevertheless, even within this framework, solving the time-independent Schrödinger equation is still intractable, so that many schemes, called quantum-chemical methods or *ab initio* methods, have been developed to find approximate numerical solutions, and the most popular of them will be presented in the following sections.

## 2.2 Hartree-Fock Method

The first, simplest *ab initio* method that the quantum chemist would think about to solve the time-independent Schrödinger equation is the Hartree-Fock (HF) method. It is the cornerstone for more advanced electronic structure methods which describe a many-electron system more accurately. The Hartree-Fock method simplifies the many-body problem of the Schrödinger equation by transforming it into a one-body problem where each electron only interacts with a mean field created by the other electrons. The total wave function for an  $N$ -electron system is made up of the spin orbitals (functions of the coordinates of a single electron) as a Slater determinant [33]:

$$\Psi_0(x_1, x_2, \dots, x_N) = \frac{1}{\sqrt{N!}} \begin{vmatrix} \chi_1(x_1) & \chi_2(x_1) & \dots & \chi_N(x_1) \\ \chi_1(x_2) & \chi_2(x_2) & \dots & \chi_N(x_2) \\ \vdots & \vdots & & \vdots \\ \chi_1(x_N) & \chi_2(x_N) & \dots & \chi_N(x_N) \end{vmatrix}. \quad (2.6)$$

The desired feature of the above expression for the wavefunction is that it satisfies the Pauli exclusion principle for fermions, as well as it enforces the antisymmetry when any two fermions are exchanged, that is  $\Psi_0(x_1, x_2) = -\Psi_0(x_2, x_1)$ . The combination of a Slater determinant with the electronic Hamiltonian leads to the energy expression for the system which can be written in terms of sums over occupied spinorbitals  $i$  and  $j$  as:

$$E_{HF} = \langle \Psi_0 | \widehat{H} | \Psi_0 \rangle = \sum_i \langle i | h | i \rangle + \frac{1}{2} \sum_{ij} \langle ij | | ij \rangle. \quad (2.7)$$

The first term on the r.h.s of Eq. 2.7 is the core part integral and the second term is a compact notation for the Coulomb and exchange integrals, defined respectively:

$$\langle i | h | j \rangle = \int \chi_i^*(x_1) h(r_1) \chi_j(x_1) dx_1 \quad (2.8)$$

$$\begin{aligned} \langle ij | | ij \rangle &= \langle ij | ij \rangle - \langle ij | ji \rangle \\ &= \int \chi_i^*(x_1) \chi_j^*(x_2) r_{12}^{-1} \chi_i(x_1) \chi_j(x_2) dx_1 dx_2 \\ &\quad - \int \chi_i^*(x_1) \chi_j^*(x_2) r_{12}^{-1} \chi_j(x_1) \chi_i(x_2) dx_1 dx_2. \end{aligned} \quad (2.9)$$



Now, it can be shown that minimizing Eq. 2.7 with respect to the HF wave function  $\Psi_0$ , under the constraint that the spin orbitals are orthonormal, we obtain the set of spin orbitals which are the solution of the following integral-differential equations, the Hartree-Fock equations:

$$F\chi_i = \varepsilon_i\chi_i. \quad (2.10)$$

Here,  $F$  is the Fock operator,  $\chi_i$  is the  $i$ -th canonical spin orbital and  $\varepsilon_i$  is the corresponding orbital energy. The Fock operator is defined as:

$$F(1) = h(1) + J(1) - K(1). \quad (2.11)$$

The  $h(1)$  is the core-Hamiltonian being a sum of the one-electron kinetic energy operator and the electron-nuclear attraction operator:

$$h(1) = -\frac{1}{2}\nabla_1^2 - \sum_A \frac{Z_A}{r_{1A}}. \quad (2.12)$$

The Coulomb  $J(1)$  and exchange operators  $K(1)$ , when acting on spin orbital  $i$  containing electron 1 are given by:

$$J(1)\chi_i(1) = \sum_j \int \chi_j^*(2)\chi_j(2)r_{12}^{-1}\chi_i(1)dx_2 \quad (2.13)$$

$$K(1)\chi_i(1) = \sum_j \int \chi_j^*(2)\chi_i(2)r_{12}^{-1}\chi_j(1)dx_2. \quad (2.14)$$

The Coulomb operator can be viewed as the classical Coulomb repulsion that the electron number 2 occupying orbital  $\chi_j$  is impacting on the electron number 1 in the orbital  $\chi_i$  while

the exchange operator does not have a classical interpretation and is the consequence of the antisymmetry of the  $N$ -electron wave function (Slater determinant). In order to make the Hartree-Fock equations applicable to calculations for molecules, and at the same time tractable for computational implementation, they need to be converted to a problem of linear algebra. To do that, a basis set is introduced. Specifically, orbitals are expanded as linear combinations of a set of  $K$  known functions  $\Phi_\mu$ , the basis functions, with some coefficients  $C_{\mu i}$ :

$$\chi_i(\vec{r}) = \sum_{\mu=1}^K C_{\mu i} \Phi_\mu(\vec{r}), \quad (2.15)$$

and subsequently introduced into Eq. 2.10. This leads to a generalized eigenvalue problem, so called the Hartree-Fock-Roothaan equation [34], which can be expressed in the matrix form as:

$$\mathbf{FC} = \mathbf{SC}\epsilon, \quad (2.16)$$

where  $\mathbf{F}$  is denoted as the Fock matrix,  $\mathbf{S} = \langle i|j \rangle$  is the overlap matrix,  $\mathbf{C}$  is the  $M \times M$  matrix of molecular orbital (MO) coefficients, and  $\epsilon$  are the energy eigenvalues.

The number of basis functions employed in calculations is usually significantly greater than the number of occupied orbitals, hence the Hartree-Fock-Roothaan equations also produce a set of unoccupied (or virtual) orbitals. These are useful for correlated wave-function methods, discussed in the following section.

## 2.3 Correlated Methods

The Hartree Fock method is called a mean-field theory, which implies that the electron-electron interactions are not considered between all individual electron pairs, but rather the  $i^{\text{th}}$  electron is interacting with an averaged electrostatic potential created by the rest of the electrons. The missing *electron correlation energy* is defined as the difference between the exact (nonrelativistic) energy and the complete basis set Hartree-Fock energy [35]:

$$E_{corr} = E_{exact} - E_{HF}^{\infty} \quad (2.17)$$

Even though the correlation energy accounts for only around 1% of the total electronic energy, its inclusion is crucial for predicting many chemical properties.

### 2.3.1 Configuration Interaction Method

Configuration interaction (CI) [35] is conceptually the most straightforward and most intuitive method to improve upon Hartree-Fock theory by adding a description of the correlated motions of electrons. The idea behind this approach is to express the exact wave function as a linear combination of all possible Slater determinants constructed from molecular spin orbitals as follows:

$$|\Psi_{\text{FCI}}\rangle = c_0|\Phi_0\rangle + \sum_{ia} c_i^a|\Phi_i^a\rangle + \sum_{\substack{i<j \\ a<b}} c_{ij}^{ab}|\Phi_{ij}^{ab}\rangle + \sum_{\substack{i<j<k \\ a<b<c}} c_{ijk}^{abc}|\Phi_{ijk}^{abc}\rangle + \dots, \quad (2.18)$$

where  $|\Phi_0\rangle$  is the reference wave function (usually the Hartree-Fock Slater determinant);  $|\Phi_i^a\rangle$  refers to a singly excited determinant where one electron from occupied spin orbital

$i$  from the reference wavefunction is excited to a virtual spin orbital  $a$ , etc. up to  $N$ -tuply excited determinants;  $c_0, c_i^a, \dots$  are expansion coefficients that are optimized with the variational method (i.e. the minimization of the expectation value of the Hamiltonian with the CI wavefunction). The accuracy of CI calculations depends on two factors: the level of excitation and basis sets utilized for construction of excited determinants. In the case when all possible excitations are taken into account and the complete basis set is applied, the resulting FCI wave function is the exact solution of the Schrödinger equation within the Born-Oppenheimer approximation. However, this situation is not achievable. Even the application of FCI in a finite basis is restricted to rather small systems due to the number of determinants needed for calculations, which grows like the following binomial function:

$$N_{det} = \binom{K}{n_\alpha} \binom{K}{n_\beta}, \quad (2.19)$$

where  $K$  is the number of orbitals,  $n_\alpha$ , and  $n_\beta$  are the number of alpha and beta electrons, respectively. Therefore, truncated CI wave functions with finite basis sets are commonly utilized in practice, leading to a hierarchy of CI methods such as: CI with single excitations (CIS), CI with single and double excitations (CISD), CI with single, double, and triple excitations (CISDT) and so forth. Nevertheless, it needs to be stressed that the main limitations of truncated CI are the lack of size-consistency and size-extensivity. The former means that the energy of a system composed of two non-interacting fragments is not equal to the sum of the energies of two fragments from a truncated CI wave function approach:

$$E_A + E_B \neq E_{AB}(r_{AB} = \infty) \quad (2.20)$$

while the latter says that the correlation energy does not asymptotically grow linearly as the number of particles grows.

### 2.3.2 Coupled-Cluster Method

Coupled-cluster (CC) [36, 37] is a broadly used algorithm for high level calculations which was devised to be size-consistent and size-extensive even in a truncated form. Due to its accuracy, very often, it becomes the method of choice for the investigation of molecular electronic structure as well as for generating accurate benchmark interaction energies. Thus, it plays a very important role not only in the realm of noncovalent interactions, where the electron correlation needs to be treated with special care, but also in the development of modern quantum chemistry methods. Before we embark on more details about CC calculations which will be discussed in the next chapter, let us first turn our attention to a theoretical aspect of the method. This framework attempts to reproduce the exact wavefunction by an exponential expansion of a reference wavefunction (usually the HF wavefunction):

$$|\Psi_{\text{CC}}\rangle = e^{\hat{T}}|\Phi_0\rangle, \quad (2.21)$$

where  $\hat{T}$  is the cluster operator which controls the types of excitations that are taken into account [38]:

$$\hat{T} = \hat{T}_1 + \hat{T}_2 + \hat{T}_3 + \dots \quad (2.22)$$

The practical calculations employ a truncated  $\hat{T}$  since the complexity of CC scales like  $\mathcal{O}(N^{2n+2})$ , where  $N$  is the number of basis functions and  $n$  is the largest excitation level. It leads to the class of CC methods such as CC with singles and doubles (CCSD), CC with

singles, doubles, and triples (CCSDT) and so on. In this fashion, CCSD means that the cluster operator is limited to single and double excitations:

$$\hat{T}_{CCSD} = \hat{T}_1 + \hat{T}_2 = \sum_{i,a} t_i^a |\Phi_i^a\rangle + \sum_{\substack{i>j \\ a>b}} t_{ij}^{ab} |\Phi_{ij}^{ab}\rangle. \quad (2.23)$$

Here,  $t_i^a$  and  $t_{ij}^{ab}$  stand for the singles and doubles amplitudes, respectively, which are the coefficients of the CCSD wavefunction. Unfortunately, the CCSD method is still not precise enough for many applications, so that the inclusion of triple excitations is used for achieving better accuracy. It motivates us to move to CCSDT, for which we pay a high price since it scales like  $\mathcal{O}(N^8)$ . Alternatively, triple excitations can be approximated perturbatively as in the CCSD(T) method [19], leading to a more attractive accuracy-to-cost ratio with overall computational scaling of  $\mathcal{O}(N^7)$ . The CCSD(T) method is called the “gold standard” of electronic structure methods, and, when combined with the complete basis set (CBS), it provides highly accurate bond energies as well as molecular properties. In the context of interaction energies, CCSD(T) usually performs as well as CCSDT due to favorable error cancellation [39]. Nevertheless, we will see in Chapter 3 that going beyond CCSD(T)/CBS and including higher order coupled-cluster excitations up to CCSDTQ is necessary to precisely compute interaction energies between triply bound systems.

### 2.3.3 Many-Body Perturbation Theory

Perturbation theory is one of the mathematical tools which has been applied since early quantum chemistry to find solutions to the time-independent Schrödinger equation which

include a description of electron correlation. This approach provides a set of comprehensive expressions for generating a series of approximations to the exact energy  $E$  and exact wave function  $\Psi$ . The commonly used technique of obtaining these formulas is the Rayleigh-Schrödinger (RS) perturbation theory.

In the RS perturbation theory, the Hamiltonian is partitioned into two parts:

$$H(\lambda) = H_0 + \lambda V, \quad (2.24)$$

where the eigenfunctions and eigenvalues for the zeroth-order Hamiltonian  $H_0$  are known, and  $\lambda$  is a perturbation strength parameter from the range:  $0 < \lambda \leq 1$ . Moreover, the exact wave function  $\Psi$  and energy  $E$  can each be expanded as the following infinite series:

$$\Psi = \Psi^{(0)} + \lambda \Psi^{(1)} + \lambda^{(2)} \Psi^{(2)} + \dots \quad (2.25)$$

$$E = E^0 + \lambda E^{(1)} + \lambda^{(2)} E^{(2)} + \dots \quad (2.26)$$

Once Eq. 2.25 and Eq. 2.26 are substituted into the Schrödinger equation, we can collect terms that have the same power of  $\lambda$  which provides the  $n$ -th order Schrödinger equation:

$$H_0 \Psi^{(n)} + V \Psi^{(n-1)} = \sum_{k=0}^n E^{(k)} \Psi^{(n-k)}. \quad (2.27)$$

Finally, projecting the left side of the above formula onto  $\Psi^{(0)}$ , we get the desired expressions for energies of different orders:

$$E^{(0)} = \langle \Psi^{(0)} | H^0 | \Psi^{(0)} \rangle \quad (2.28)$$

$$E^{(1)} = \langle \Psi^{(0)} | V | \Psi^{(0)} \rangle \quad (2.29)$$

$$E^{(2)} = \langle \Psi^{(0)} | V | \Psi^{(1)} \rangle \quad (2.30)$$

...

$$E^{(n)} = \langle \Psi^{(0)} | V | \Psi^{(n-1)} \rangle. \quad (2.31)$$

The perturbed first-order wave function is usually obtained by taking a linear combination of the zeroth-order excited states that forms a complete set as:

$$\Psi^{(1)} = \sum_n c_n^{(1)} \Psi_n^{(0)}, \quad (2.32)$$

where  $c_n^{(1)}$  are to be determined coefficients.

The Møller-Plesset (MP) perturbation theory is a particular case of the RS perturbation theory, where the zeroth-order Hamiltonian is the sum of the Fock operators:

$$H_0 = \sum_i F(i) \quad (2.33)$$

and the perturbation is defined as follows:

$$V = \sum_{i < j}^N r_{12}^{-1} - \sum_i^N (J(i) - K(i)). \quad (2.34)$$

As a result, the zeroth-order wave function is the Hartree-Fock wave function, and the sum of the zeroth- and first-order energy is the Hartree-Fock energy, while higher order corrections accounts for the electron correlation energy. In the case of the second-order



Møller-Plesset perturbation theory, the first-order wave function is given by:

$$\Psi^{(1)} = \frac{1}{4} \sum_{ijab} t_{ab}^{ij} |\Psi_{ij}^{ab}\rangle \quad (2.35)$$

and the second-order energy reads:

$$E^{(2)} = \frac{1}{4} \sum_{ijab} \frac{|\langle ij || ab \rangle|^2}{\epsilon_i + \epsilon_j - \epsilon_a - \epsilon_b}, \quad (2.36)$$

where  $i$  and  $j$  are the occupied spin orbitals,  $a$  and  $b$  are the virtual (unoccupied) spin orbitals. The quantities  $\epsilon_i$ ,  $\epsilon_j$ ,  $\epsilon_a$ , and  $\epsilon_b$  denote the corresponding HF orbital energies.

### 2.3.4 Symmetry-Adapted Perturbation Theory

Symmetry-adapted perturbation theory (SAPT) [20, 21] is a very powerful framework for calculations of noncovalent interactions between molecules. The primary advantage of utilizing SAPT is that it provides the interaction energy decomposed in terms of meaningful quantities, such as: electrostatics, exchange-repulsion, induction, and London dispersion. This proves to be an invaluable tool for investigating the physical origins for interactions throughout chemistry.

In SAPT, we begin with unperturbed complexes (isolated monomers) and treat the interaction energy as a small quantity resulting from the mutual perturbation of monomers by the Coulombic intermonomer interactions. Therefore, the first step requires finding exact solutions of the Schrödinger equation for isolated monomers A and B, respectively:

$$H_X \Psi_X = E_X \Psi_X, \quad X = A, B, \quad (2.37)$$

where  $H_X$ ,  $\Psi_X$  and  $E_X$  stand for the Hamiltonian, wave function, and energy from monomer X, respectively. Subsequently, we define the intermolecular perturbation  $V$ , that is a sum of all Coulomb repulsions between the electrons of monomer A and B, the repulsions between the nuclei of A and B, all attractive interactions between the electrons of monomer A and the nuclei of monomer B, and *vice versa*. Therefore, the Hamiltonian of the dimer is split into contributions from each fragment and the interaction:

$$H(\lambda) = H_A + H_B + \lambda V = H_0 + \lambda V. \quad (2.38)$$

The unperturbed Hamiltonian  $H_0$  has a solution in the form of the product of the individual monomer wave functions:  $\Psi^{(0)} = \Psi_A \Psi_B$ , and the eigenenergy is  $E^{(0)} = E_A + E_B$ . Once the machinery of ordinary RS perturbation theory described in the previous subsection and the partitioning of Hamiltonian from Eq. 2.38 are utilized (which is known as polarization approximation) [40], we obtain the interaction energy expressed as follows:

$$E_{int} = E(\lambda = 1) - E^{(0)} = E_{pol}^{(1)} + E_{pol}^{(2)} + \dots, \quad (2.39)$$

The first- and second-order corrections are of high importance since they include best physically recognizable terms (electrostatics, induction as well as dispersion) and are given by:

$$E_{pol}^{(1)} = \langle \Psi_A \Psi_B | V | \Psi_A \Psi_B \rangle \quad (2.40)$$

$$E_{pol}^{(2)} = \sum_{m \neq 0} \frac{|\langle \Psi_A \Psi_B | V | \Psi_{A,m} \Psi_B \rangle|^2}{E_A - E_{A,m}} + \sum_{n \neq 0} \frac{|\langle \Psi_A \Psi_B | V | \Psi_A \Psi_{B,n} \rangle|^2}{E_B - E_{B,n}}$$

$$+ \sum_{m \neq 0} \sum_{n \neq 0} \frac{|\langle \Psi_A \Psi_B | V | \Psi_{A,m} \Psi_{B,n} \rangle|^2}{E_A + E_B - E_{A,m} - E_{B,n}}, \quad (2.41)$$

where the three consecutive sums represent  $E_{\text{ind},B \rightarrow A}^{(2)}$ ,  $E_{\text{ind},A \rightarrow B}^{(2)}$ , and  $E_{\text{disp}}^{(2)}$ , respectively.

Unfortunately, the conceptually simple polarization approximation is not fully practical and reliable because: 1) we rarely know the exact solutions of Eq. 2.37 for monomer A and B, 2) the unperturbed wave function  $\Psi^{(0)}$  does not satisfy the Pauli exclusion principle when we swap two electrons between monomers. A natural way of circumventing the first problem is by setting the zeroth-order Hamiltonian as:

$$H_0 = F_A + F_B, \quad (2.42)$$

where  $F_X$  is the Fock operator of monomer X. The second limitation is fixed by the antisymmetrizer operator  $\mathcal{A}$  which, acting on the zeroth-order wave function  $\Psi^{(0)}$  forces it to be antisymmetric. Such a procedure gives rise to the so-called exchange corrections in the perturbation series, which is required for a proper description of electron exchange between the monomers. Currently, many-electron SAPT is a well-established theory providing some levels of approximations, starting from the simplest SAPT0 going up to the highest, most accurate approach, SAPT2+3 [41]. In SAPT0, the interaction energy is expressed as:

$$E_{\text{int}}^{\text{SAPT0}} = E_{\text{elst}}^{(10)} + E_{\text{exch}}^{(10)} + E_{\text{ind,resp}}^{(20)} + E_{\text{exch-ind,resp}}^{(20)} + E_{\text{disp}}^{(20)} + E_{\text{exch-disp}}^{(20)} + \Delta E_{\text{HF}}^{(2)}. \quad (2.43)$$

The first two corrections on the right-hand side of the above formula represent the electrostatic interaction energy of molecular charge distributions and the correction for the

exchange energy. The  $E_{\text{ind,resp}}^{(20)}$  and  $E_{\text{exch-ind,resp}}^{(20)}$  terms are the induction energy, and its exchange counterpart, which describe the mutual polarization of the monomers in the field of their corresponding partners. These contributions are calculated including the relaxation of monomer HF orbitals in response to the electrostatic potential of the other monomer. It needs to be pointed out, that the response, denoted by subscript “resp”, is performed by solving the coupled perturbed Hartree-Fock (CPHF) equations [42] for each monomer.  $E_{\text{disp}}^{(20)}$  and  $E_{\text{exch-disp}}^{(20)}$  are the dispersion and exchange-dispersion energies, respectively, which describe the correlated motion of electrons between the fragments. Finally, the  $\Delta E_{\text{HF}}^{(2)}$  term approximately accounts for the third- and higher-order induction and exchange induction effects via a supermolecular HF calculation:

$$\Delta E_{\text{HF}}^{(2)} = E_{\text{int}}^{\text{HF}} - E_{\text{elst}}^{(10)} - E_{\text{exch}}^{(10)} - E_{\text{ind,resp}}^{(20)} - E_{\text{exch-ind,resp}}^{(20)}. \quad (2.44)$$

Higher-order levels of SAPT are out of the scope of this dissertation, but the reader is referred to [43].

### 2.3.5 Slow Convergence of Electron Correlation

Electronic structure methods described in the previous subsections suffer from the same serious drawback, namely they show a slow convergence to the complete basis set limit (CBS). The source of this issue originates from the inability of the wave function, which is expressed by an expansion in orbital products, to describe the region where two electrons approach each other ( $r_{12} \rightarrow 0$ ). Although some strategies to enhance the basis set convergence have been proposed, such as the CBS extrapolation [44, 45] and/or midbond

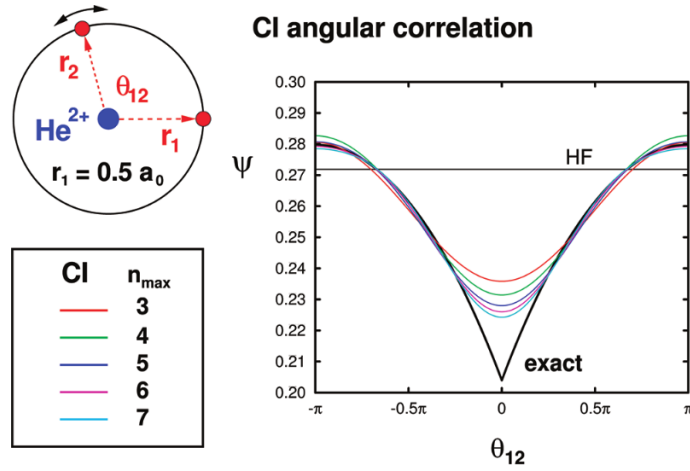


Figure 2.1: Helium ground state wave functions with both electrons confined at the circle of radius  $0.5 a_0$  calculated with the CI approach using increasing basis size with maximum principal quantum number  $n_{max}$ . The figure comes from Ref. [1]

functions [46, 47, 48], the capture of the interelectronic cusp still remains a severe limitation. In order to illustrate the problem, Fig. 2.1 shows the behavior of the CI wave function calculated with different sizes of basis sets for helium with both electrons orbiting on a circle of the same radius. Once the basis set size is increased with the maximum principal quantum number  $n_{max}$ , we approach the basis set limit, but this approach is incredibly slow and does not reproduce the cusp created by the exact wavefunction. However, the non-smoothness of the many-body wave function can be locally resolved by the cusp condition proposed by Kato [49]:

$$\left. \frac{\partial \Psi}{\partial r_{12}} \right|_{r_{12}=0} = \frac{1}{2} \Psi(r_{12} = 0). \quad (2.45)$$

The above formula implies that the exact wave function must be linear in the electronic distance for small values of  $r_{12}$ :

$$\Psi_{\text{exact}}(r_1, r_2) = \Psi(r_1, r_2) \left(1 + \frac{1}{2}r_{12} + \dots\right) \quad (2.46)$$

As we can see, the interelectronic distance  $r_{12}$  contribution needs to be included explicitly in the wavefunction to speed up the basis set convergence of correlation energies. This has been achieved in the explicitly correlated R12/F12 methods [50, 1, 51] which are the subject of the next section.

### 2.3.6 Explicitly Correlated F12 methods

In recent years, the F12 explicitly correlated methods became mainstream of electronic structure tools to calculate accurate ground-state energies [50], and they still flourish when extended to multireference methods for systems with significant static correlation [52, 53]. In order to overcome the slow basis set convergence, explicitly correlated methods incorporate the  $r_{12}$  factor into the wavefunction, depending on the distances between electrons  $i$  and  $j$ . This idea was originally proposed by Hylleraas [54] for helium and goes back to 1927. Initially, such a concept leads to numerous complicated three- and four-electron integrals, which became a major impediment in developing explicitly correlated methods for many-electron systems. A conceptual breakthrough was achieved by Kutzelnigg who devised a practical way of including  $r_{12}$ -dependent terms into conventional quantum chemistry methods [55]. The success of his methodology hung on the resolution of identity (RI), a technique which allows one to approximate many-electron integrals in terms of sums of products of simpler two-electron integrals. This achievement gave rise to the R12 [56, 57]

and later F12 [50, 1, 51] methods, being effectively adapted to the framework of second-order perturbation theory [58, 59] as well as coupled-cluster theory [60, 61, 62, 63, 64].

### Explicitly Correlated Second-Order Møller-Plesset Methods

The second order Møller-Plesset perturbation theory stands out among correlated wave function methods as the least computationally involved one. This is the reason why numerous significant developments of the F12 approaches have been applied to the MP2 method, leading to different variants of MP2-F12. The general concept of the MP2-F12 approach is based on the augmentation of the conventional wave function with the explicitly correlated term for each pair of electrons:

$$|\Psi\rangle = t_{ab}^{ij}|\Psi_{ij}^{ab}\rangle + t_{kl}^{ij}F_{\alpha\beta}^{kl}|\Psi_{ij}^{\alpha\beta}\rangle \quad (2.47)$$

with

$$F_{\alpha\beta}^{kl} = \langle kl|\hat{F}_{12}\hat{Q}_{12}|\alpha\beta\rangle. \quad (2.48)$$

The  $i, j, k, l$  indicies are occupied orbitals;  $a, b$  are virtual orbitals;  $\alpha, \beta$  are functions from the complete orthonormal or RI basis.  $|\Psi_{ij}^{ab}\rangle$  is a doubly excited determinant,  $t_{ab}^{ij}$  and  $t_{kl}^{ij}$  are conventional and explicitly correlated amplitudes, respectively,  $\hat{F}_{12} \equiv f(r_{12})$  is a suitable short-range correlation factor.  $F_{\alpha\beta}^{kl}$  can be viewed as an internal contraction which projects the full space of doubly excited configurations  $|\Psi_{ij}^{\alpha\beta}\rangle$  to the small set of amplitudes  $t_{kl}^{ij}$ . The  $\hat{Q}_{12}$  operator ensures strong orthogonality of the explicitly correlated

term to the reference function, and can be expressed as:

$$\widehat{Q}_{12} = (1 - \widehat{Q}_1)(1 - \widehat{Q}_2)(1 - \widehat{V}_1\widehat{V}_2), \quad (2.49)$$

where  $\widehat{Q} = |i\rangle\langle i|$  and  $\widehat{V} = |a\rangle\langle a|$  are one-electron projection operators onto the occupied and unoccupied (virtual) spaces, respectively.

While in the early times of the R12 methods the correlation factor  $\widehat{F}_{12}$  was chosen to be linear, it has been shown that the Slater-type exponential correlation factor [65] drastically improves the accuracy of results. Several other forms of non-linear correlation factors, such as:  $r_{12}\exp(-\gamma r_{12})$ ,  $\operatorname{erfc}(\gamma r_{12})$ ,  $r_{12}\operatorname{erfc}(\gamma r_{12})$  have been tested by Tew and Klopper [66], showing superior results to the linear  $r_{12}$  one. Currently, the Slater-type geminal is usually approximated with a linear combination of Gaussian-type geminals:

$$e^{-\gamma r_{12}} \approx \sum_i^N c_i e^{-\alpha_i r_{12}^2}. \quad (2.50)$$

The exponent  $\gamma$  is a length-scale parameter that accounts for the size of the correlation hole, while  $c_i$  and  $\alpha_i$  are coefficients determined in a least-squares manner.

The final MP2-F12 energy is the sum of the standard MP2 energy and the explicitly correlated correction:

$$E_{MP2-F12} = E_{MP2} + E_{F12}. \quad (2.51)$$

The reader is referred to Refs. [1, 59] for the derivation of the working equations for the F12 correction. However, it needs to be emphasized that during the evaluation of the MP2-F12 energy, the set of intermediates ( $V$ ,  $X$ ,  $B$ ,  $C$ ) that occurs, gives rise to notorious



three- and four-electron integrals, as mentioned at the beginning of this section. In order to shed some light on this issue, let us consider the  $V$  intermediate as an example, whose matrix elements are given by [1, 50]:

$$\begin{aligned}
V_{ij}^{kl} &= \langle ij|r_{12}^{-1}\widehat{Q}_{12}f(r_{12})|kl\rangle \\
&= \langle ij|r_{12}^{-1}(1-\widehat{Q}_1)(1-\widehat{Q}_2)(1-\widehat{V}_1\widehat{V}_2)f(r_{12})|kl\rangle \\
&= \langle ij|r_{12}^{-1}f(r_{12})|kl\rangle + \sum_{mn}\langle ij|r_{12}^{-1}|mn\rangle\langle mn|f(r_{12})|kl\rangle \\
&\quad - \sum_{ab}\langle ij|r_{12}^{-1}|ab\rangle\langle ab|f_{12}|kl\rangle - \langle ij|r_{12}^{-1}\widehat{Q}_1f(r_{12})|kl\rangle \\
&\quad - \langle ij|r_{12}^{-1}\widehat{Q}_2f(r_{12})|kl\rangle
\end{aligned} \tag{2.52}$$

In the expression above, the first three terms in the final r.h.s only require evaluation of two-electron integrals, and although the correlation factor  $f(r_{12})$  appears, the complexity of the new integrals is the same as for the standard Coulomb integrals. The last two terms are problematic, yielding three-electron integrals:

$$\langle ij|r_{12}^{-1}\widehat{Q}_1f_{12}|kl\rangle = \sum_m\langle ijm|r_{12}^{-1}f(r_{23})|mlk\rangle \tag{2.53}$$

$$\langle ij|r_{12}^{-1}\widehat{Q}_2f_{12}|kl\rangle = \sum_m\langle ijm|r_{12}^{-1}f(r_{13})|kml\rangle. \tag{2.54}$$

The main strategy to deal with these expensive integrals is to insert the resolution of identity (RI) [56, 58]:

$$1 \approx \sum_{\alpha}|\alpha\rangle\langle\alpha|, \tag{2.55}$$

where  $\alpha$  is the RI basis that approximates the complete basis set. Once Eq. 2.55 is plugged into Eqs. 2.53, and 2.54, we get a desired product of two-electron integrals:

$$\sum_m \langle ijm | r_{12}^{-1} f(r_{23}) | mlk \rangle = \sum_{m\alpha} \langle ij | r_{12}^{-1} | m\alpha \rangle \langle m\alpha | f(r_{12}) | kl \rangle. \quad (2.56)$$

The MP2-F12 methods have been used to compute energies of closed-shell and open-shell systems [31,46,47] including weak intermolecular interaction energies [67, 68] as well as molecular properties [69, 70]. Many benchmark calculations have proven that the MP2-F12 calculations with triple-zeta basis sets produce better results than conventional MP2 in pentuple-zeta basis sets.

### Explicitly Correlated Coupled-Cluster Methods

The application of the F12 theory to the coupled cluster method turned out to be a much more complicated problem. While the complete CCSD-F12 amplitude equations have been derived and demonstrated [71, 72], they turned out to be too computationally demanding to be practical. As a result, many approximations to CCSD-F12 were developed. Generally, they are based on three ways of calculating F12 corrections for the basis set incompleteness error: before, during, or after evaluating the energies and amplitudes. The most common approach is to incorporate the F12 terms during the non-F12 calculations like in MP2-F12 [59]. Such an approach was subsequently employed to approximate frozen geminal coupled-cluster singles and doubles variants such as: CCSD(F12) [60, 61], CCSD-F12a [62, 63], CCSD-F12b [62, 63], and CCSD(F12\*) $\equiv$  CCSD-F12c [64]. A *posteriori* F12 correction is achieved based on the second-order perturbation theory referred to as CCSD-[2]R12/[2]F12 [73, 74, 75]. Also, it became feasible to calculate an *a priori* F12

correction where the Hamiltonian matrix elements of the parent method are dressed with explicit correlation beforehand. This technique is known as the canonical transcorrelated theory, and gave rise to F12-CCSD [76].

Moving on to the perturbative triples, the situation is very similar. The inclusion of explicitly correlated terms for the (T) correction has been developed [77], however, it is much more computationally demanding than conventional (T). The workaround is to compute the (T) correction using the conventional CCSD(T) formula equipped with converged CCSD-F12 singles and doubles amplitudes. Such an approach does not ensure an improvement of (T) by the F12 treatment, so that a scaling of the triples contribution is a common technique. The scaling factor may be taken as the ratio between the MP2-F12 and MP2 correlation energies like [63]:

$$\Delta E^{(T^{**})} = \Delta E^{(T)} \frac{E_{corr}^{MP2-F12}}{E_{corr}^{MP2}}, \quad (2.57)$$

where  $\Delta E^{(T)} = E^{CCSD(T)-F12} - E^{CCSD-F12}$ . Alternatively, the triples scaling factor can be chosen as the ratio of the correlation energies from CCSD-F12b (or CCSD-F12c) and conventional CCSD [78]:

$$\Delta E^{(T^{bb})} = \Delta E^{(T)} \frac{E_{corr}^{CCSD-F12b}}{E_{corr}^{CCSD}}. \quad (2.58)$$

Different CCSD(T)-F12 flavors have been extensively tested on molecular energies and properties [61, 64]. These studies confirm that explicitly correlated CCSD(T) at the triple-zeta set level can provide more accurate energies than conventional CCSD(T) at the quadruple-zeta level. Also, the performance of CCSD(T)-F12 has been benchmarked on

weak intermolecular interaction energies [79, 80, 81, 82, 83, 84] and excellent results are obtained for the valence-valence correlation.

### 2.3.7 Density Functional Theory

The quantum mechanical methods described in the previous sections are based on the electronic wavefunction that is a function of the coordinates of all electrons. This is the reason why these methods are inherently computationally expensive. An alternative approach is the density functional theory (DFT) [85], which attempts to solve the Schrödinger equation by replacing the complicated electron wave function of  $3N$  variables by the electron density distribution, that is a function of 3 spatial coordinates, defined as:

$$\rho(r) = N \sum_{\sigma_1=-\frac{1}{2}, \frac{1}{2}} \int d\tau_2 d\tau_3 \dots d\tau_N |\Psi(r, \sigma_1, r_2, \sigma_2, \dots, r_N, \sigma_N)|^2. \quad (2.59)$$

In this way, we get  $\rho$  by carrying out the integration of  $|\Psi|^2$  over the coordinates (space and spin) of all electrons except the one with coordinates  $r, \sigma_1$ ; in addition, we perform the summation over its spin coordinate ( $\sigma_1$ ). It is worth noting that the definition of  $\rho$  is independent of the label of the electron we do not integrate over. Therefore,  $\rho$  represents the density of the electron cloud carrying  $N$  electrons, and the integration over the whole space leads to the number of electrons:

$$\int \rho(r) d^3r = N. \quad (2.60)$$

Another important ingredient of DFT is the Hohenberg-Kohn theorem [86] which proved that the exact ground-state energy of a molecule is a functional of the above defined electronic density:

$$E_0 = E_{DFT}[\rho]. \quad (2.61)$$

The reader may draw a conclusion that DFT is an exact method. This is theoretically true, but the issue lies in the fact that no one knows the expression for the exact functional. However, the crucial point is that we can find the unique functional relationship between the electron density and the Hamiltonian for a given system, so that all the properties of the system can be parameterized through the electron density. Therefore, the energy can be expanded as:

$$E_0 = E[\rho] = T[\rho] + V_{ne}[\rho] + J[\rho] + E_{xc}[\rho], \quad (2.62)$$

where  $T[\rho]$  is the kinetic energy of the non-interacting electrons,  $V_{ne}[\rho]$  is the nuclear-electron interaction,  $J[\rho]$  is the total Coulomb interaction energy. The last term  $E_{xc}[\rho]$  stands for the exchange-correlation energy and its role is to encompass the correction to the kinetic energy deriving from the interacting nature of the electrons, and all non-classical corrections to the electron-electron repulsion energy. The exact form of the  $E_{xc}[\rho]$  functional is unknown, thus it became a subject of various approximations. The set of existing functionals can be assigned to rungs of “Jacob’s ladder” proposed by Perdew [87, 88], where each additional step is leading to higher accuracy. In this work, we will use several standard functionals, such as: local density approximation (LDA), generalized gradient approximation (GGA) functionals, and the hybrid XC functionals.

The popularity of the DFT methods skyrocketed in chemistry over the last two decades as a result of its favorable cost/accuracy ratio. Despite its wide range of applicability and attractive scalability ( $\mathcal{O}(N^4)$ ), this method cannot be termed as the ‘‘Holy Grail’’ of computational chemistry since it fails in describing the long-range electronic effects that result in the London dispersion forces. In order to overcome this limitation, numerous new approaches have been devised, allowing to combine the relatively low cost of DFT with, in most cases, costless additive terms that include dispersion in an empirical way. Following the schemes introduced in Refs. [3, 89], the dispersion treatment in DFT can be divided into four levels of approximation:

- **Ground level** - The set of methods that are devised to improve DFT accuracy in medium range, but do not take into account the correct long-range asymptotics of dispersion energy. The most popular examples are the Minnesota density functionals [90], and the dispersion-corrected atom-centered potentials (DCACPs) [91].
- **Level I** - Semi-empirical, pair-wise methods not taking into account the local chemical environment. These methods employ the generalized London dispersion expansion scaled by a damping function:

$$E_{disp} = - \sum_{A>B} f_{damp}(R_{AB}) \frac{C_6^{AB}}{R_{AB}^6}, \quad (2.63)$$

where  $R_{AB}$  is the interatomic distance,  $C_6^{AB}$  is a dispersion coefficient for atoms A and B which is independent of the molecular environment (the same for all pairs of atoms of the same types). The role of the damping function  $f_{damp}(R_{AB})$  is to

recover the correct behavior of the potential at short and medium interatomic distances, i.e. it avoids singularity problems and the double-counting of correlation at these distances. Examples of these methods are DFT-D and DFT-D2 proposed by Grimme [92, 93], which simply add the dispersion contribution *a posteriori* to the total DFT energy:

$$E_{DFT-D2} = E_{DFT} + E_{disp}. \quad (2.64)$$

- **Level II** - Approaches that add a dependence of the atom-atom asymptotic constants on the environment. A few strategies have been utilized to capture the environmental dependence of the van der Waals coefficients, all of which exploit the concept that the polarizability of an atom is proportional to its volume. Methods belonging to this group are: DFT-D3 [2], DFT-D4 [22], the exchange-hole dipole moment (XDM) method of Becke and Johnson [94, 95, 96], and the Tkatchenko-Scheffler (TS) method [97].
- **Level III** - Long-range, non-local density functionals. This approach incorporates the dispersion interactions into a typical local or semi-local exchange-correlation functional:

$$E_{xc} = E_x^{GGA} + E_c^{LDA} + E_c^{nl} \quad (2.65)$$

with the non-local correlation energy  $E_c^{nl}$  computed as:

$$E_c^{nl} = \int \int dr_1 dr_2 \rho(r_1) \phi(r_1, r_2) \rho(r_2). \quad (2.66)$$

The best known examples at this step are the van der Waals density functionals (vdW-DF, vdW-DF2) of Langreth, Lundqvist, and coworkers [98, 99], and the non-local functionals of Vydrov and Van Voorhis (VV09, VV10) [100, 101].

- **Level IV** - Methods which go beyond the pairwise additive approximation and add many-body dispersion terms. The classical examples at this step are the many-body dispersion (MBD) [102] and the random-phase approximation (RPA) [103].

## 2.4 Calculations of Noncovalent Interactions

We can distinguish two fundamental approaches to calculating the interaction energy of two given atoms or molecules: *supermolecular* and *perturbative*. In the former one, the interaction energy for a two-body system (A and B) is defined as the difference between the dimer's energy and the sum of isolated monomers' energies:

$$E_{int} = E_{AB} - E_A - E_B. \quad (2.67)$$

Among the most essential advantages of supermolecular calculations are their universality, conceptual simplicity and applicability at any distance between interacting molecules. Although the utilization of the above formula seems to be simple, we have to keep in mind that the interaction energy is typically 4-7 orders of magnitude smaller over the total energy of the dimer and monomers, and strong cancellation of errors is required to occur due to the subtraction in the above equation. Thus, the methodology of the calculation of interaction energy needs particular attention: for example, very small energy thresholds (order of  $10^{-10}$  hartree) are needed to recover the interaction energy with high accuracy



at very long intermonomer separations. Another serious drawback of the supermolecular method constitutes the basis set superposition error (BSSE), which is the nonphysical and artificial stabilization of the monomer energy in dimer calculations due to employing extra basis functions from the interacting partner. On top of this, the result of the supermolecular technique is just a single number representing the entire intermolecular interaction energy that gives no physical insight into the nature of the interaction. Therefore, an alternative method of calculating interaction energy has been proposed - the perturbation theory approach, e.g. SAPT, which provides a unique chance to better understand the details of the interactions.

## 2.5 Counterpoise Correction (CP)

The BSSE mentioned above may be present in all calculations that are carried out in finite basis sets and on more than one atom. The common procedure of removing this shortcoming is by computing all energies in the same dimer basis set. This technique is known as the *counterpoise correction* (CP) of Boys and Bernardi [104]:

$$E_{int} = E_{AB}^{AB} - E_A^{AB} - E_B^{AB} \quad (2.68)$$

The magnitude of the BSSE diminishes with the increase of the basis set and vanishes completely in the infinite basis.

## 2.6 Orbital and Auxiliary Basis Sets

A basis set is one of the key ingredients of quantum chemistry calculations, where the molecular orbitals are constructed from atomic orbitals. In section 2.2 we said that the one-electron molecular wavefunctions are expressed as linear combinations within a finite set of basis functions. The form of these functions is dictated by the necessity of the evaluation of non-trivial two-electron integrals. Therefore, in *ab initio* methods the Gaussian-type orbitals (GTOs) are utilized:

$$\Psi_{\zeta nlm}(r, \theta, \phi) = N x^l y^m z^n e^{-\zeta(\vec{r}-\vec{R}_A)^2}, \quad (2.69)$$

where the sum of  $l$ ,  $m$ , and  $n$  determines the type of orbital (s, p, d,...),  $N$  is a normalization constant, and  $\zeta$  is an exponent. Since these functions poorly describe the wave function near the nucleus, the combination of multiple GTOs with different exponents is created to form contracted orbitals:

$$\Phi_\mu = \sum_{i=1}^L d_{i\mu} \Psi_{i,\zeta_{i\mu}}. \quad (2.70)$$

Here,  $d_{i\mu}$  denotes the expansion coefficient of the primitive Gaussian function  $\Psi_i$  with an exponent  $\zeta_{i\mu}$ .

In this work, we will make extensive use of the Dunning correlation-consistent bases aug-cc-pVXZ $\equiv$ aXZ ( $X = D, T, Q, 5, 6$ ) [105, 106]. These correlation-consistent bases

were optimized for the systematic convergence of valence correlation energies with a constant  $X^{-3}$  rate. Following this convergence pattern, we can compute the CBS-limit correlation energy  $E_{\infty}^{corr}$  by extrapolating the results in two consecutive- $X$  basis sets  $E_{X-1}^{corr}$  and  $E_X^{corr}$ :

$$E_{\infty}^{corr} = E_X^{corr} + \frac{(1 - 1/X)^3}{1 - (1 - 1/X)^3} (E_X^{corr} - E_{X-1}^{corr}). \quad (2.71)$$

In addition to the orbital basis sets, the resolution of identity (RI) as well as density fitting (DF) techniques require auxiliary basis sets, denoted by a prefix -RI (also called -MP2FIT), and -JKFIT. They are specially optimized to represent quantities other than orbitals, for example products of occupied orbitals in the case of DF sets designed for the exchange integrals. Basis sets used in this dissertation are listed in Table 2.1.

Table 2.1: List of basis sets utilized in the dissertation.

aug-cc-pVXZ (X = D,T,Q,5,6)	Dunning’s family correlation consistent polarized valence X-tuple zeta basis sets [105, 106]. These are basis optimized for systematic convergence of correlation energies. aug- stands for the <i>augmentation</i> by additional diffuse functions such that anions, noncovalent interactions, and excited states can be described more accurately.
aug-cc-pCVXZ (X = D,T,Q,5,6)	Used for all-electron calculations describing valence, core-core, and core-valence correlation [105].
aug-cc-pCVXZ-DK (X = D,T,Q,5,6)	Used for relativistic effects [107].
aug-cc-pVXZ-JKFIT (X = D,T,Q,5,6)	Weigend’s family auxiliary basis sets [108]. These are basis appropriate for fitting ( <i>oo</i>  -type products.
aug-cc-pVXZ-MP2FIT ≡ aug-cc-pVXZ-RI (X = D,T,Q,5,6)	Weigend’s family auxiliary basis sets [109]. These are basis appropriate for fitting ( <i>ov</i>  -type products.

## Chapter 3

### Triple bonds and coupled-cluster convergence: CCSDTQ interaction energies for complexes involving CO and N<sub>2</sub>

Noncovalent interaction energies are strongly dependent on the level of electron correlation included in the calculations. Therefore, the “gold standard” of quantum chemistry, the coupled-cluster approach with single, double, and noniterative triple interactions (CCSD(T)) [19], has been the method of choice for obtaining accurate interaction energies between small systems. If both monomers are well described by a single reference formalism, the CCSD(T) interaction energies are typically accurate to within 1–2% as long as the calculations have converged to the complete basis set (CBS) limit. However, when spectroscopic ( $\sim 1 \text{ cm}^{-1}$ ) or better accuracy is needed, in addition to converging the CCSD(T) interaction energy to the CBS limit, one needs to consider the effects of electron excitations beyond the CCSD(T) level.

The multi-system studies of Refs. [110, 7, 39, 111, 112, 113] have revealed two classes of systems for which the post-CCSD(T) effects are particularly important. The first class contains systems with four valence electrons: He–He [114], H<sub>2</sub>–H<sub>2</sub> [115], and He–H<sub>2</sub> [116]. The post-CCSD(T) contribution for these systems often exceeds 3% of interaction energy, however, it mainly comes from  $\delta_T = \text{CCSDT} - \text{CCSD(T)}$ , that is, the

remaining quadruple excitations are modest. The second class comprises complexes involving triply bound systems, for which even  $\delta_Q = \text{CCSDTQ} - \text{CCSDT(Q)}$  constitutes a significant contribution. The importance of the  $\delta_Q$  interaction energy term was for the first time emphasized by Boese [113] while studying  $\text{CN}^- - \text{H}_2\text{O}$  as well as  $\text{HF} - \text{HCN}$ , and subsequently confirmed by Smith et al. for  $\text{N}_2 - \text{N}_2$  [111]. This importance can be explained by the fact that triply bound systems require a full description of the  $\pi \rightarrow \pi^*$  excitations, which can be achieved only by a method with quadruple excitations such as  $\text{CCSDT(Q)}$  or, preferably,  $\text{CCSDTQ}$ . The work of Ref. [117] on the  $\text{P}_2 - \text{P}_2$  and  $\text{PCCP} - \text{PCCP}$  complexes, performed at the  $\text{CCSDT(Q)}$  level, proves that the post- $\text{CCSD(T)}$  corrections are significant also for heavier atoms. Interestingly, the problems of the many-body perturbation theory and coupled-cluster expansions for interactions between triply bonded systems have been discovered much earlier. The landmark theoretical study on  $\text{CO} - \text{CO}$  by Rode et. al [118], showed large differences between the fourth-order Møller-Plesset perturbation theory (MP4) and  $\text{CCSD(T)}$  interaction energies for this system. These discrepancies were addressed using some MP5 contributions which are not included in  $\text{CCSD(T)}$ .

With the growth of computer power and advances in algorithms, we can revisit the conclusions of Ref. [118] by examining the convergence of the post- $\text{CCSD(T)}$  interaction energy contributions for the carbon monoxide complex. An extension of the  $\text{N}_2 - \text{N}_2$  calculations of Ref. [111] to even higher basis sets is also warranted to provide the most reliable post- $\text{CCSD(T)}$  effects for this challenging system. In this chapter, we are going to investigate nine characteristic points on the  $\text{CO} - \text{CO}$ ,  $\text{N}_2 - \text{N}_2$ , and  $\text{CO} - \text{N}_2$  potential energy surfaces with the highest accuracy possible, within  $1 \text{ cm}^{-1}$ . Some findings are presented in Appendices A and B [119].

### 3.1 Previous studies on CO–CO, N<sub>2</sub>–N<sub>2</sub>, and CO–N<sub>2</sub>

The CO–CO, N<sub>2</sub>–N<sub>2</sub>, and CO–N<sub>2</sub> complexes are of high importance for spectroscopists, thus they were a subject of a few potential energy surface studies. As stated above, the CO–CO complex turned out to be especially difficult for theoretical investigations using low-level electronic structure methods. The most accurate potential energy surface was reported by Dawes et al. [120] and allowed the precise reproduction of experimental rovibrational levels [120] and rotationally inelastic cross sections [121]. However, this accomplishment can be attributed to error cancellation between the post-CCSD(T) effects and the basis set incompleteness errors, and we will elaborate on this problem in Section 3.2.4.

Several ab initio N<sub>2</sub> – N<sub>2</sub> potential energy surfaces have been constructed in the literature [122, 123, 124, 125, 126, 127, 128, 129, 130] with the one by Hellmann [129] attaining the highest accuracy so far. Hellmann’s calculations were based on the CCSD(T) method using basis sets up to quintuple-zeta with bond functions. Subsequently, interaction energies were extrapolated to the CBS limit and supplemented with corrections for core-core and core-valence correlations, relativistic effects, and higher coupled-cluster levels up to CCSDT(Q) in the aug-cc-pVDZ basis set. Using such a level of theory, Hellmann reproduced the best experimental data for virial coefficients, viscosity, and thermal conductivity of a dilute nitrogen gas. Nevertheless, he scaled  $\delta_{T+(Q)}$  by a factor of 0.5 in order to match experimental results. He suggested that this scaling accounted for the basis set incompleteness effects of the  $\delta_{T+(Q)}/aDZ$  results and the missing contribution from full quadruple excitations.

Interestingly, for a long time there were only a couple of *ab initio* studies on the CO-N<sub>2</sub> complex [131, 132] performed at low levels of accuracy. Nevertheless, in 2018, three surfaces for this system were published, employing the following levels of theory: CCSD(T)-F12b/aQZ [133], CCSD(T)/aQZ+(3s2p1d) [134], and CCSD(T)/aQZ+(3s3p2d1f1g) [135], respectively. The potential proposed in Ref. [135] is in the best agreement with the experimental rovibrational level data.

### 3.2 Results and Discussion

The key step of our study is the geometry optimization which allows one to find the most stable structures on the potential energy surface, such as minima and transition states. Such structures are called stationary points, where all first derivatives of the energy with respect to geometrical coordinates are zero. Therefore, second derivatives need to be calculated in order to determine the character of a stationary point. The matrix of second derivatives is called Hessian and takes the form:

$$H_{ij} = \frac{\partial^2 U}{\partial q_i \partial q_j}. \quad (3.1)$$

When all eigenvalues of the Hessian matrix are positive, we are at a minimum. One negative eigenvalue indicates that we obtained a first-order saddle point. Maxima and other saddle points have two or more negative eigenvalues and we do not investigate them.

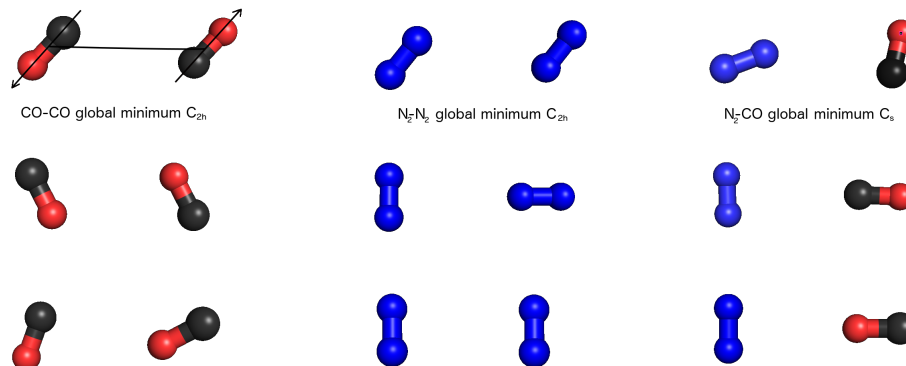
We performed the geometry optimization by minimizing the CCSD(T)-F12b/aug-cc-pV5Z interaction energy computed with the counterpoise (CP) correction for basis set superposition error [104]. The C–O and N–N bond lengths were optimized separately at



the CCSD(T)/aug-cc-pV5Z level. The resulting values of  $r_{\text{CO}} = 2.137$  bohr, and  $r_{\text{NN}} = 2.078$  bohr were kept in all calculations. For rigid monomers, the geometry of the CO–CO, N<sub>2</sub>–N<sub>2</sub>, and CO–N<sub>2</sub> complexes is defined by four variables:  $R$ , the distance between the centres of mass of monomers, and the angles  $\theta_A$ ,  $\theta_B$ , and  $\phi$ . The angles  $\theta_A$  and  $\theta_B$  are located between the vector  $\mathbf{R}$  joining the centres of mass of the monomers (from A to B, from CO to N<sub>2</sub> in the CO–N<sub>2</sub> case) and the vectors  $\mathbf{r}_A$  and  $\mathbf{r}_B$  pointing along the molecular axes of monomers A and B, respectively (from the C atom to the O atom in case of CO). The dihedral angle  $\phi$  between two planes specified by the vectors  $(\mathbf{R}, \mathbf{r}_A)$  and  $(\mathbf{R}, \mathbf{r}_B)$  ranges from  $-180^\circ$  to  $+180^\circ$ .

We have located three nonequivalent stationary points on the CO–CO and CO–N<sub>2</sub> potential energy surfaces and two on the N<sub>2</sub>–N<sub>2</sub> one. An additional, highly symmetric ( $D_{2h}$ ) N<sub>2</sub>–N<sub>2</sub> structure is just a radial minimum (a maximum in the angular directions), but we investigated it anyway. Importantly, each of the structures considered has at least  $C_s$  symmetry which is crucial for the feasibility of the post-CCSD(T) calculations. The resulting structures are presented in Fig. 3.1. The character of investigated points strongly depends on the level of theory utilized for the geometry optimization, e.g. the T-shaped and nearly T-shaped CO–N<sub>2</sub> structures are saddle points when the no-CP CCSD(T)/aQZ approach is utilized, whereas they are minima at the CP CCSD(T)/aQZ level. However, the optimizations performed at the CP and noCP CCSD(T)-F12b/a5Z levels revealed that in addition to the global minima for each system, there are two minima for the CO–CO system with  $C_{2h}$  and  $C_s$  symmetry, respectively. The remaining structures are the saddle points.

Figure 3.1: The stationary points on the CO–CO, N<sub>2</sub>–N<sub>2</sub>, and CO–N<sub>2</sub> potential energy surfaces considered in this work.



In order to attain the spectroscopic accuracy for the investigated systems, we use the following composite scheme to compute the total interaction energy:

$$E_{\text{int}} = E_{\text{int}}^{\text{CCSD(T)/CBS}} + \delta_{\text{T}} + \delta_{(\text{Q})} + \delta_{\text{Q}} + \delta_{\text{core}} + \delta_{\text{rel}}, \quad (3.2)$$

where the consecutive corrections to the frozen-core CCSD(T)/CBS interaction energy account for higher-order coupled-cluster excitations, core-core and core-valence correlation, and relativistic effects.

### 3.2.1 CCSD(T) interaction energies

It is of high importance to examine how well the frozen-core (FC) CCSD(T) interaction energy is converged to the CBS limit. Frozen-core means that only the valence electrons are correlated in the post-HF calculations. In this work, all interaction energies were calculated with the CP correction [104], and basis sets were selected from Dunning's

correlation-consistent sets  $cc\text{-}pVXZ\equiv XZ$  and  $aug\text{-}cc\text{-}pVXZ\equiv aXZ$  with  $X=D, T, Q, 5, 6$  [105, 106]. We tested various basis sets (with and without midbond) and different explicitly correlated CCSD(T)-F12 variants in addition to conventional CCSD(T). Tables 3.1, 3.2, and 3.3 present interaction energies at the minima for the CO–CO, N<sub>2</sub>–N<sub>2</sub>, and N<sub>2</sub>–CO complexes, respectively. The complete set of CCSD(T) and CCSD(T)-F12 interaction energies for the remaining six structures can be found in Appendix A (Tables SI–SVI).

In all cases, the interaction energy converges smoothly with respect to the increasing cardinal number of the basis set. The inclusion of midbond functions significantly speeds up the convergence, and we already get better results in  $aQZ\text{+}midbond$  than in  $a6Z$  without midbond functions. In the next step, we examined the performance of the F12 methods. These methods are designed to eliminate the issue with slow basis set convergence [50, 1, 51]. Due to technical aspects which were described in Chapter 2 (section on explicitly correlated methods), CCSD(T)-F12 lacks true F12 triple contributions. In this work, in order to approximate the explicitly correlated perturbative triples, the scaling technique was utilized based on Eq. 2.57. The double star notation in Eq. 2.57 denotes that we scale the dimer and monomer (T) terms by the same (dimer) factor. If the scaling factor is specified separately for each CP calculation, the resulting interaction energy is not guaranteed to be size consistent [79, 78]. The CCSD(T)-F12 explicitly correlated method in its various approximate variants has a remarkably beneficial influence on the accuracy of the  $aDZ$  and  $aTZ$  interaction energies compared to conventional CCSD(T) [79, 80, 81, 82, 83, 84]. This effect is less visible in larger basis sets. Without scaling, the F12a approach is superior to the less approximate F12b one, which is a consequence of error cancellation between

Table 3.1: CCSD(T) and CCSD(T)-F12 interaction energies (in  $\text{cm}^{-1}$ ) for the global minimum ( $C_{2h}$ ) geometry of the CO dimer, Fig. 3.1. The extrapolated value (rows “ext.”) in the  $X$  column is computed using interaction energies in bases  $a(X-1)Z$  and  $aXZ$ . The letter M in the basis set stands for the hydrogenic set of midbond functions from the same  $aXZ$  basis.

method	$X$				
	D	T	Q	5	6
CCSD(T)/ $aXZ$	-104.79	-119.64	-127.27	-130.38	-131.63
ext.		-127.67	-132.27	-133.13	-133.35
CCSD(T)/ $aXZM$	-116.31	-129.72	-132.03	-132.62	-132.83
ext.		-135.64	-133.45	-133.17	-133.11
CCSD(T)-F12a/ $aXZ$	-125.20	-130.75	-132.33	-132.88	-133.10
ext.		-133.20	-133.50	-133.43	-133.38
CCSD(T**)-F12a/ $aXZ$	-134.04	-134.27	-134.00	-133.78	-133.65
ext.		-134.50	-133.81	-133.53	-133.45
CCSD(T)-F12b/ $aXZ$	-119.05	-128.10	-131.01	-132.10	-132.58
ext.		-132.04	-133.16	-133.21	-133.22
CCSD(T**)-F12b/ $aXZ$	-127.88	-131.63	-132.68	-133.00	-133.13
ext.		-133.33	-133.46	-133.32	-133.29
CCSD(T)-F12a/ $aXZM$	-127.68	-133.17	-133.40	-133.30	
ext.		-135.41	-133.61	-133.21	
CCSD(T**)-F12a/ $aXZM$	-137.24	-136.83	-135.08	-134.20	
ext.		-136.59	-133.85	-133.29	
CCSD(T)-F12b/ $aXZM$	-122.12	-131.04	-132.49	-132.82	
ext.		-134.73	-133.60	-133.19	
CCSD(T**)-F12b/ $aXZM$	-131.68	-134.70	-134.17	-133.73	
ext.		-135.91	-133.84	-133.27	

the CCSD part and the triples part [83]. When the (T\*\*) scaling of triples is applied, the CCSD(T)-F12b results are improved, but the CCSD(T)-F12a ones are overestimated. The addition of midbond functions only slightly improves the CCSD(T)-F12 convergence for all variants. Since we utilized Dunning’s correlation consistent basis sets, the  $X^{-3}$  extrapolation technique was applied based on Eq. 2.71. The extrapolation clearly improves the

Table 3.2: CCSD(T) and CCSD(T)-F12 interaction energies (in  $\text{cm}^{-1}$ ) for the global minimum ( $C_{2h}$ ) geometry of the  $\text{N}_2$  dimer, Fig. 3.1. The extrapolated value (rows “ext.”) in the  $X$  column is computed using interaction energies in bases  $a(X-1)Z$  and  $aXZ$ . The letter M in the basis set stands for the hydrogenic set of midbond functions from the same  $aXZ$  basis.

method	$X$				
	D	T	Q	5	6
CCSD(T)/ $aXZ$	-80.50	-97.56	-102.68	-105.05	-106.59
ext.		-104.54	-106.50	-107.30	-108.64
CCSD(T)/ $aXZM$	-94.35	-105.47	-107.36	-107.70	-107.88
ext.		-109.97	-108.71	-108.09	-108.13
CCSD(T)-F12a/ $aXZ$	-109.45	-108.39	-107.68	-107.83	-108.01
ext.		-108.02	-107.25	-107.98	-108.26
CCSD(T <sup>**</sup> )-F12a/ $aXZ$	-116.64	-111.11	-108.95	-108.51	-108.43
ext.		-108.86	-107.47	-108.04	-108.32
CCSD(T)-F12b/ $aXZ$	-101.79	-105.50	-106.33	-107.06	-107.53
ext.		-107.15	-107.03	-107.81	-108.18
CCSD(T <sup>**</sup> )-F12b/ $aXZ$	-108.97	-108.22	-107.60	-107.75	-107.95
ext.		-107.99	-107.25	-107.88	-108.24
CCSD(T)-F12a/ $aXZM$	-105.80	-107.91	-108.43	-108.31	
ext.		-108.97	-108.80	-108.18	
CCSD(T <sup>**</sup> )-F12a/ $aXZM$	-113.59	-110.71	-109.71	-108.99	
ext.		-109.67	-108.97	-108.23	
CCSD(T)-F12b/ $aXZM$	-99.18	-105.72	-107.51	-107.83	
ext.		-108.65	-108.81	-108.16	
CCSD(T <sup>**</sup> )-F12b/ $aXZM$	-106.96	-108.52	-108.79	-108.51	
ext.		-109.35	-108.98	-108.21	

convergence of both CCSD(T) and CCSD(T)-F12 interaction energies for all structures. It is worth noting that the CBS extrapolation brings the four different CCSD(T)-F12 variants much closer together. The CCSD(T<sup>\*\*</sup>)-F12b/( $a5Z$ ,  $a6Z$ ) result has the lowest uncertainty, so it was selected as the leading FC term  $E_{\text{int}}^{\text{CCSD(T)}/\text{CBS}}$  for the total interaction energy, Eq. 3.2.

Table 3.3: CCSD(T) and CCSD(T)-F12 interaction energies (in  $\text{cm}^{-1}$ ) for the global minimum geometry of the CO–N<sub>2</sub> complex, Fig. 3.1. The extrapolated value (rows “ext.”) in the  $X$  column is computed using interaction energies in bases  $a(X-1)Z$  and  $aXZ$ . The letter  $M$  in the basis set stands for the hydrogenic set of midbond functions from the same  $aXZ$  basis.

method	$X$				
	D	T	Q	5	6
CCSD(T)/ $aXZ$	-90.82	-107.59	-113.85	-116.32	-117.60
ext.		-114.64	-118.18	-118.40	-119.32
CCSD(T)/ $aXZM$	-101.50	-115.90	-118.02	-118.51	-118.71
ext.		-120.59	-119.41	-118.96	-118.98
CCSD(T)-F12a/ $aXZ$	-116.04	-118.79	-118.58	-118.78	-118.93
ext.		-120.02	-118.50	-118.96	-119.13
CCSD(T <sup>**</sup> )-F12a/ $aXZ$	-123.27	-121.58	-119.88	-119.48	-119.36
ext.		-120.94	-118.73	-119.03	-119.19
CCSD(T)-F12b/ $aXZ$	-110.36	-116.43	-117.44	-118.12	-118.51
ext.		-119.07	-118.26	-118.81	-119.03
CCSD(T <sup>**</sup> )-F12b/ $aXZ$	-117.59	-119.22	-118.75	-118.82	-118.94
ext.		-119.99	-118.49	-118.88	-119.09
CCSD(T)-F12a/ $aXZM$	-115.44	-119.21	-119.30	-119.17	
ext.		-120.56	-119.38	-119.04	
CCSD(T <sup>**</sup> )-F12a/ $aXZM$	-123.27	-122.10	-120.62	-119.87	
ext.		-121.36	-119.56	-119.10	
CCSD(T)-F12b/ $aXZM$	-110.08	-117.31	-118.48	-118.74	
ext.		-120.10	-119.35	-119.02	
CCSD(T <sup>**</sup> )-F12b/ $aXZM$	-117.91	-120.19	-119.79	-119.44	
ext.		-120.90	-119.52	-119.08	

### 3.2.2 Higher-order Coupled-Cluster Corrections

The post-CCSD(T) corrections are the most expensive step since they require running the CCSDT, CCSDT(Q) and CCSDTQ methods, which scale like  $O(N^8)$ ,  $O(N^9)$ , and  $O(N^{10})$ , respectively. Thus, point group symmetry plays an important role in these calculations. For the  $C_{2h}$  and  $C_{2v}$  structures, including the CO–CO global minimum and the

$N_2-N_2$  stationary points, we were able to run CCSDT, CCSDT(Q), and CCSDTQ in bases as large as aQZ, aTZ, and aDZ, respectively. Due to the lower symmetry of CO- $N_2$  ( $C_s$ ), the CCSDTQ calculations were performed in smaller basis sets DZ and 6-31G\*(0.25) [136]. The particularly high  $D_{2h}$  symmetry of the  $N_2-N_2$  rectangular configuration allows for calculations in somewhat larger bases than for all other structures, specifically, CCSDT/5Z and CCSDT(Q)/QZ. Tables 3.4, 3.5, and 3.6 present the post-CCSD(T) interaction energy contributions for CO-CO,  $N_2-N_2$ , and  $N_2-CO$ , respectively. Table 3.4 shows that higher-order coupled-cluster corrections are especially significant for the carbon monoxide dimer.

Table 3.4: Post-CCSD(T) interaction energy contributions for the CO–CO dimer (in  $\text{cm}^{-1}$ ). The core and relativistic corrections used the aug-cc-pCVXZ and aug-cc-pCVXZ-DK bases, respectively.

basis	$E_{\text{int}}^{\text{CCSD(T)}}$	$\delta_{\text{T}}$	$\delta_{(\text{Q})}$	$\delta_{\text{Q}}$	$\delta_{\text{core}}$	$\delta_{\text{rel}}$
Global minimum ( $\text{C}_{2h}$ )						
6-31G*(0.25)	-105.79	-5.54	0.36	-1.25		
aDZ	-104.79	-2.91	-1.93	-0.67	-0.26	0.18
aTZ	-119.64	-1.99	-2.56		-0.46	0.18
aQZ	-127.27	-1.54			-0.53	0.19
a5Z	-130.38				-0.53	0.20
DZ	-61.99	-3.11	0.25	-1.01		
TZ	-86.33	-1.80	-1.17			
QZ	-107.24	-1.52				
Local minimum 1 ( $\text{C}_{2h}$ )						
6-31G*(0.25)	-85.61	8.28	-1.14	1.08		
aDZ	-83.24	5.38	-1.37	0.64	-0.22	0.20
aTZ	-110.22	6.06	-2.58		-0.11	0.20
aQZ	-117.37	6.14			0.14	0.20
a5Z	-120.83				0.20	0.20
DZ	-8.53	5.70	-0.88	0.98		
TZ	-52.80	5.71	-1.71			
QZ	-85.73	5.97				
Local minimum 2 ( $\text{C}_s$ )						
6-31G*(0.25)	-101.66	5.19	-1.85	0.81		
aDZ	-90.32	3.79	-2.34		-0.22	0.18
aTZ	-110.53	4.05	-3.08		-0.14	0.18
aQZ	-117.10	4.18			0.02	0.19
a5Z	-120.26				0.07	0.19
DZ	-37.50	3.89	-1.57	0.78		
TZ	-67.28	3.96	-2.29			
QZ	-91.47	4.13				



Table 3.5: Post-CCSD(T) interaction energy contributions for the  $N_2-N_2$  dimer (in  $cm^{-1}$ ). The core and relativistic corrections used the aug-cc-pCVXZ and aug-cc-pCVXZ-DK bases, respectively.

basis	$E_{int}^{CCSD(T)}$	$\delta_T$	$\delta_{(Q)}$	$\delta_Q$	$\delta_{core}$	$\delta_{rel}$
Global minimum ( $C_{2h}$ )						
6-31G*(0.25)	-86.16	2.39	-4.32	1.43		
aDZ	-80.50	2.74	-4.72	1.31	-0.20	0.09
aTZ	-97.56	3.49	-5.30		-0.24	0.12
aQZ	-102.68	3.73			-0.21	0.13
a5Z	-105.05				-0.19	0.13
DZ	-41.22	1.90	-2.80	0.86		
TZ	-62.86	3.09	-3.91			
QZ	-80.55	3.53				
Saddle point ( $C_{2v}$ )						
6-31G*(0.25)	-74.56	2.11	-4.20	1.11		
aDZ	-76.12	2.35	-4.21	1.13	-0.21	0.14
aTZ	-93.48	2.99	-4.77		-0.30	0.16
aQZ	-98.26	3.20			-0.27	0.17
a5Z	-100.05				-0.26	0.17
DZ	-39.88	1.74	-2.65	0.73		
TZ	-61.30	2.73	-3.59			
QZ	-77.67	3.06				
Rectangular configuration ( $D_{2h}$ )						
6-31G*(0.25)	-48.47	2.01	-3.34	1.46		
aDZ	-45.83	2.45	-3.82	1.19	-0.17	-0.14
aTZ	-67.63	3.50	-4.73		-0.05	-0.13
aQZ	-71.99	3.80			0.03	-0.12
a5Z	-74.92				0.06	-0.12
DZ	18.42	1.74	-2.15	0.91		
TZ	-19.88	2.94	-3.21			
QZ	-44.82	3.49	-4.06			
5Z	-58.11	3.76				

Table 3.6: Post-CCSD(T) interaction energy contributions for the CO–N<sub>2</sub> dimer (in cm<sup>-1</sup>). The core and relativistic corrections used the aug-cc-pCVXZ and aug-cc-pCVXZ-DK bases, respectively.

basis	$E_{\text{int}}^{\text{CCSD(T)}}$	$\delta_{\text{T}}$	$\delta_{(\text{Q})}$	$\delta_{\text{Q}}$	$\delta_{\text{core}}$	$\delta_{\text{rel}}$
Global minimum (C <sub>s</sub> )						
6-31G*(0.25)	-95.33	1.02	-2.46	0.78		
aDZ	-90.82	1.39	-3.33		-0.22	0.18
aTZ	-107.59	1.95	-3.94		-0.28	0.19
aQZ	-113.85	2.18			-0.25	0.20
a5Z	-116.32				-0.23	0.20
DZ	-57.07	1.20	-1.81	0.57		
TZ	-77.59	1.88	-2.80			
QZ	-94.92	2.11				
Near T-shaped Saddle point 1, C points towards N <sub>2</sub> (C <sub>s</sub> )						
6-31G*(0.25)	-78.43	2.76	-3.84	1.15		
aDZ	-84.79	2.66	-4.53		-0.23	0.16
aTZ	-97.73	3.02	-4.94		-0.38	0.17
aQZ	-102.87	3.20			-0.43	0.18
a5Z	-105.05				-0.43	0.18
DZ	-39.80	2.39	-3.01	0.91		
TZ	-61.69	2.95	-3.74			
QZ	-81.75	3.12				
T-shaped Saddle point 2, O points towards N <sub>2</sub> (C <sub>2v</sub> )						
6-31G*(0.25)	-79.96	-0.58	-0.83	-0.28		
aDZ	-76.14	0.32	-1.46	-0.20	-0.23	0.15
aTZ	-97.76	1.46	-2.19		-0.25	0.16
aQZ	-102.50	1.76			-0.12	0.17
a5Z	-105.00				-0.08	0.17
DZ	-24.91	-0.27	0.00	-0.38		
TZ	-53.91	1.02	-1.13			
QZ	-76.52	1.58				

For the global minimum,  $\delta_T$  and  $\delta_{(Q)}$  are of the same sign and add up to 3.0% of the CCSD(T)/CBS value while for the remaining two stationary points  $\delta_T$  and  $\delta_{(Q)}$  partially cancel each other. One needs to point out the importance of the full-quadruples correction  $\delta_Q$  which, in the largest basis set feasible, amounts to 0.5% of the CCSD(T)/CBS interaction energy, can be of either sign, and should not be neglected in calculations of spectroscopic accuracy.

Considering the  $N_2-N_2$  system,  $\delta_{(Q)}$  provides the biggest post-CCSD(T) contribution to total interaction energy for all three structures presented in Table 3.5. However, about two thirds of  $\delta_{(Q)}$  are cancelled by  $\delta_T$ . Again, we need to emphasize the importance of the full quadruples contribution which turns out to be even more significant than for the CO-CO complex, amounting to slightly over 1% of the CCSD(T)/CBS interaction energy [111]. In the case of the CO- $N_2$  complex,  $\delta_{(Q)}$  is the biggest post-CCSD(T) interaction energy contribution although we again observe some cancellation between  $\delta_T$  and  $\delta_{(Q)}$ . The  $\delta_Q$  value is still significant for this system, but varies in sign.

### 3.2.3 Core-core and Core-valence Correlation, Relativistic, and DBOC Effects

In order to obtain the highest-accuracy interaction energies possible, we also investigated the core-core and core-valence correlation correction  $\delta_{core}$ , as well as relativistic effects,  $\delta_{rel}$ . The  $\delta_{core}$  correction was computed as the difference between the all-electron (AE) and FC conventional (non-F12) CCSD(T) interaction energies. In this case, we utilized aug-cc-pCVXZ (aCXZ) [105] basis sets, which are Dunning-type sets specially designed for the correct treatment of core electrons. The relativistic effects were estimated employing the second-order Douglas-Kroll-Hess (DKH) Hamiltonian [137, 138] within the all-electron

conventional CCSD(T) method. For these calculations, we employed the aug-cc-pCVXZ [105] and aug-cc-pCVXZ-DK [107] basis sets. The results for these corrections are shown in Tables 3.4, 3.5, and 3.6. The core-core and core-valence corrections can be either sign, while  $\delta_{\text{rel}}$  is always positive. Interestingly,  $\delta_{\text{rel}}$  is highly consistent between different stationary points for the same complex. Nevertheless, both of these contributions are small and quickly convergent with the basis set. It means that the accuracy of our total interaction energies is limited almost exclusively by the accuracy of the post-CCSD(T) coupled-cluster contributions.

We have also assessed the importance of the diagonal Born-Oppenheimer (DBOC) interaction energy correction. The DBOC term is expected to be small as no ultralight atoms are present. Indeed, the estimate of the DBOC interaction energy correction computed at the CCSD/aQZ level [139] amounts to only  $-0.08 \text{ cm}^{-1}$  at the CO–CO global minimum. Therefore, the DBOC term is not considered in this work any further.

### 3.2.4 Total Interaction Energies

The best-estimate interaction energy  $E_{\text{int}}$  was computed based on Eq. 3.2. Here are some remarks on the most accurate estimate:

- the  $\delta_{\text{T}}$  and  $\delta_{(\text{Q})}$  corrections were extrapolated to the CBS limit using the  $X^{-3}$  scheme and the (aTZ,aQZ) bases for  $\delta_{\text{T}}$  and (aDZ,aTZ) for  $\delta_{(\text{Q})}$ ,
- the additional  $\delta_{\text{T}}/5\text{Z}$  and  $\delta_{(\text{Q})}/\text{QZ}$  results available for the  $D_{2h}$  structure of  $\text{N}_2\text{--N}_2$  do not lead to any more accurate extrapolated values so we did not use them in the final estimates,

- the  $\delta_Q$ ,  $\delta_{\text{core}}$ , and  $\delta_{\text{rel}}$  results were not extrapolated - the  $\delta_Q/\text{aDZ}$  value was used when available, otherwise we took  $\delta_Q/\text{DZ}$ .

The resulting total interaction energies are presented in tables 3.7, 3.8, and 3.9 along with the optimized geometries. Both interaction energies and geometries are compared to the literature values. The CO–CO results show that the effects beyond the FC CCSD(T) level constitute -3.3 – 3.8% of the CCSD(T)/CBS interaction energy for the three minima, making the global minimum deeper and the two local ones shallower. Interestingly, all three geometries of the  $\text{N}_2 - \text{N}_2$  complex, Table 3.8, exhibit a nearly complete cancellation of the post-CCSD(T) terms. As a result, the effects beyond the FC CCSD(T) level amount to only -0.4–0.6% of the CCSD(T)/CBS interaction energy. In the case of  $\text{N}_2\text{--CO}$ , the post-CCSD(T) interaction energy terms are somewhere between the CO–CO and  $\text{N}_2\text{--N}_2$  ones. The partial cancellation between  $\delta_T$  and  $\delta_{(Q)}$  results in the effects beyond the FC CCSD(T) level amounting to 0.6 – 1.1% of the CCSD(T)/CBS interaction energy.

Table 3.7: Geometrical parameters and interaction energies for the CO–CO complex, computed by us as explained in the text (upper part) and taken from literature (lower part). All distances, angles, and interaction energies are given in bohr, degrees, and  $\text{cm}^{-1}$ , respectively.  $E_{\text{int}}$  represents our best interaction energy estimate computed according to Eq. (3.2).

	Global Minimum ( $C_{2h}$ )		Local Minimum ( $C_{2h}$ )		Local Minimum ( $C_s$ )
$R$	8.20		6.86		7.43
$r_{CO}$	2.137		2.137		2.137
$\theta_A$	134.73		64.78		26.23
$\theta_B$	45.27		115.22		69.03
$\phi$	180		180		0
$E_{\text{int}}^{\text{CCSD(T)-F12b/a5Z}}$	-132.10		-123.88		-122.39
$E_{\text{int}}^{\text{CCSD(T)/CBS}}$	-133.29		-124.78		-123.37
$E_{\text{int}}$	-138.32		-120.64		-121.46
Reference	[121] <sup>a</sup>	[140] <sup>b</sup>	[121] <sup>a</sup>	[140] <sup>b</sup>	[121] <sup>a</sup>
$R$	8.18	8.20	6.86	6.95	-
$r_{CO}$	2.132	2.132	2.132	2.132	2.132
$\theta_A$	134.58	134.23	65.21	59.63	~40
$\theta_B$	45.42	45.77	114.79	120.37	~110
$E_{\text{int}}$	-135.14	-135.53	-119.55	-124.21	-121.06

<sup>a</sup> Interaction energy computed at the all-electron CCSD(T)-F12b level in the cc-pCVQZ-F12 basis.

<sup>b</sup> Interaction energy obtained using the CCSD(T)/aTZ+midbond level.

It needs to be stressed that the post-CCSD(T) effects may have a strong influence on some features of the potential energy surfaces, for example on the intermolecular rovibrational spectra. In particular, the relative energy differences between the three CO–CO minima indicate that the high-order terms may have strong impact on the resulting rovibrational levels as the low-energy rovibrational wave functions are strongly delocalized along a pathway passing through all three minima. To examine this effect in more detail, we calculated differences between the depths of stationary points of CO–CO at different levels of theory (Table 3.10).

Table 3.8: Geometrical parameters and interaction energies for the N<sub>2</sub>-N<sub>2</sub> complex, computed by us as explained in the text (upper part) and taken from literature (lower part). All distances, angles, and interaction energies are given in bohr, degrees, and cm<sup>-1</sup>, respectively.  $E_{\text{int}}$  represents our best interaction energy estimate computed according to Eq. (3.2).

	Global Minimum (C <sub>2h</sub> )	Saddle point (C <sub>2v</sub> )	Rectangle (D <sub>2h</sub> )
$R$	7.58	7.81	7.01
$r_{NN}$	2.078	2.078	2.078
$\theta_A$	49.60	90	90
$\theta_B$	130.40	0	90
$\phi$	180	0	0
$E_{\text{int}}^{\text{CCSD(T)-F12b/a5Z}}$	-107.06	-101.88	-77.70
$E_{\text{int}}^{\text{CCSD(T)/CBS}}$	-108.24	-102.63	-79.03
$E_{\text{int}}$	-108.64	-103.25	-78.68 <sup>a</sup>
Reference	[129] <sup>b</sup>	[126] <sup>c</sup>	
$R$	7.55	7.65	
$r_{NN}$	2.081	2.074	
$\theta_A$	50.08	45.00	
$\theta_B$	129.92	135.00	
$E_{\text{int}}$	-110.19	-119.34	

<sup>a</sup> Including an estimate of the perturbative pentuples contribution,  $\delta_{(P)}=0.31$  cm<sup>-1</sup> calculated in the DZ basis set.

<sup>b</sup> Interaction energy calculated up to the CCSD(T)/a5Z+midbond level and supplemented with corrections for core-core and core-valence correlation, relativistic effects, and higher coupled-cluster levels up to CCSDT(Q)/aDZ.

<sup>c</sup> Interaction energy obtained from symmetry-adapted perturbation theory with a [5s3p2d1f] basis set.

A very important observation is that the “gold standard” FC CCSD(T) approach at its CBS limit underestimates the difference between the minimum depths by a factor of 1.7 for the C<sub>s</sub> local-minimum structure and more than 2 for the C<sub>2h</sub> one. The “platinum standard” [119] FC CCSDT(Q)/CBS approach recovers only about 88% of the two differences, and the majority of the missing contribution is assigned to  $\delta_Q$ . For comparison, Table 3.10 also lists minimum depth differences obtained at lower levels of theory, MP2 and CCSD

Table 3.9: Geometrical parameters and interaction energies for the CO–N<sub>2</sub> complex, computed by us as explained in the text (upper part) and taken from literature (lower part). The dihedral angle  $\phi=0^0$  and all distances, angles, and interaction energies are given in bohr, degrees, and cm<sup>-1</sup>, respectively.  $E_{\text{int}}$  represents our best interaction energy estimate computed according to Eq. (3.2).

	Global Minimum ( $C_s$ )			Saddle point ( $C_s$ )	Saddle point ( $C_{2v}$ )
$R$	7.85			8.33	7.38
$r_{CO}$	2.137			2.137	2.137
$r_{NN}$	2.078			2.078	2.078
$\theta_{CO}$	109.13			177.65	0
$\theta_{N_2}$	163.42			92.29	90
$E_{\text{int}}^{\text{CCSD(T)-F12b/a5Z}}$	-118.12			-106.75	-107.13
$E_{\text{int}}^{\text{CCSD(T)/CBS}}$	-119.09			-107.69	-108.16
$E_{\text{int}}$	-120.40			-108.82	-108.78
Reference	[133] <sup>a</sup>	[134] <sup>b</sup>	[135] <sup>c</sup>	[133] <sup>a</sup>	[133] <sup>a</sup>
$R$	7.85	7.86	7.86	7.37	7.39
$r_{CO}$	2.081	2.137	2.132	2.081	2.081
$r_{NN}$	2.079	2.079	2.074	2.079	2.079
$\theta_{CO}$	107.0	109.4	111.34	180	0
$\theta_{N_2}$	166.0	162.8	159.70	90	90
$E_{\text{int}}$	-117.42	-117.35	-118.2	-105.56	-106.45

<sup>a</sup> Calculations performed at the CCSD(T)-F12b/aQZ level.

<sup>b</sup> Calculations performed at the CCSD(T)/aQZ+(3s2p1d) level.

<sup>c</sup> Calculations performed at the CCSD(T)/aQZ+(3s3p2d1f1g) level.

(both at the FC CBS limit). The complete set of MP2, MP2-F12, CCSD, and CCSD-F12 interaction energies for all nine structures is given in Appendix A. The below-CCSD(T) calculations result in qualitatively incorrect energy differences between the minima, which is in line with previous studies [118, 141, 142].

Another important feature of the total interaction energies in Tables 3.7 and 3.9 is the ordering of the stationary points on the CO–CO and CO–N<sub>2</sub> potential energy surfaces. In the CO–CO case, the  $C_{2h}$  structure is more favorable at the FC CCSD(T)/CBS level (by 1.4 cm<sup>-1</sup>), however, the inclusion of the post-CCSD(T) corrections reverses this ordering,



Table 3.10: Differences between the global ( $C_{2h}$ ) and local minima ( $C_{2h}$  and  $C_s$ ) well depths for the CO–CO complex calculated at different levels of theory. The MP2, CCSD, and CCSD(T) values were obtained from the MP2-F12/(a5Z,a6Z), CCSD-F12b/(a5Z,a6Z), and CCSD(T\*\*)-F12b/(a5Z,a6Z) extrapolations, respectively, and the higher-level corrections were computed in the basis sets specified in Sec. 3.2.1.

Theory level	$\Delta E(\text{cm}^{-1})$	
	$E_{\text{Global}} - E_{\text{Local}(C_{2h})}$	$E_{\text{Global}} - E_{\text{Local}(C_s)}$
MP2	45.65	43.62
CCSD	1.67	2.11
CCSD(T)	8.51	9.92
CCSDT	15.91	15.40
CCSDT(Q)	15.63	14.82
CCSDTQ	16.94	16.27
+core	17.67	16.87
+relativistic	17.68	16.86

with the  $C_s$  structure being now more favorable by  $0.8 \text{ cm}^{-1}$ . For CO–N<sub>2</sub>, the differences are even smaller: at the FC CCSD(T)/CBS level, the  $C_{2v}$  structure is deeper by less than  $0.5 \text{ cm}^{-1}$  than the  $C_s$  one, while at the highest theory level considered in this work, the two stationary points are virtually isoenergetic.

We have extended our calculations for CO–CO and computed interaction energies with different levels of theory along the pathway passing through the global and local minima [119] (Fig. 2 in Appendix B). The best estimate of the all electron CCSD(T)/CBS value was calculated as a sum of the FC CCSD(T\*\*)-F12b/(aQZ,a5Z) result and the CCSD(T)/aug-cc-pCV5Z correction for the core-core and core-valence correlation. We also included corrections from the higher-order CC excitations: CCSDT/aQZ and CCSDT(Q)/aTZ. Moreover, we estimated energies employing the level of theory from

Ref. [120], that is, all-electron non-CP corrected CCSD(T)-F12b with and without extrapolation from the cc-pCVXZ-F12 $\equiv$ CVXZ-F12 basis set family [143] with  $X=D,T,Q$ . Figure 2 (Appendix B) confirms that the post-CCSD(T) corrections are significant for this system, and consequently influence the shape of the minimum-energy pathway. Figure 3 in Appendix B clearly shows that the CCSD(T)/CBS level of theory is highly inaccurate for CO–CO. Interestingly, the results computed with the level selected in Ref. [120] are close to our CCSDT(Q) values, which is the effect of error cancellation between the basis set incompleteness effects at the CCSD(T) level and contributions from higher-order coupled-cluster excitations. Therefore, CO–CO is the epic example of a system for which we cannot neglect the interaction energy contributions beyond the CCSD(T)/CBS level.

### 3.3 Summary

We have observed high-order coupled-cluster interaction energy effects all the way through CCSDTQ to be significant for the CO–CO, N<sub>2</sub>–N<sub>2</sub>, and CO–N<sub>2</sub> complexes, which is in line with earlier investigations at lower levels of theory [118, 141, 120]. The  $\delta_{(Q)}$  term is always negative and its magnitude increases with the basis set size, amounting to 2.1–6.5% of the CCSD(T) interaction energy at the CBS limit. The  $\delta_T$  term can be of either sign, although most of the time it is positive (between –5.1 and 0.9% of the CCSD(T)/CBS interaction energy), canceling the  $\delta_{(Q)}$  contribution to a large extent. A notable exception is the CO–CO global minimum where  $\delta_T$  and  $\delta_{(Q)}$  are of the same sign and add up to 3.0% of the CCSD(T)/CBS value. The higher-order  $\delta_Q$  correction is smaller but still nonnegligible, amounting to between –1.5 and 0.5% of the CCSD(T)/CBS interaction energy. The core correlation and relativistic corrections are less significant.

As post-CCSD(T) calculations at the level presented here are not feasible for the entire potential energy surface, one cannot at present directly assess the importance of the  $\delta_T$ ,  $\delta_{(Q)}$ , and  $\delta_Q$  corrections on observables such as rovibrational transitions for all considered complexes. However, the differences between the CO–CO global and local minima well depths provide compelling indirect evidence for the critical influence of the post-CCSD(T) effects on the properties of this complex. The FC CCSD(T) approach at its CBS limit underestimates the difference between the minima by a factor of 1.7 for the  $C_s$  local-minimum structure and more than 2 for the  $C_{2h}$  one. Thus, even the CCSD(T)/CBS level of theory is not sufficient to map out the correct landscape of the potential energy surface in the region surrounding the minima.

It should be pointed out that the highly successful potentials of Refs. [120, 121, 129, 135] calculated at the “gold standard” CCSD(T)/CBS level for CO–CO, N<sub>2</sub>–N<sub>2</sub>, and CO–N<sub>2</sub> are strongly benefiting from a cancellation of the error from basis set incompleteness with the error from the lack of higher-order coupled-cluster corrections.

## Chapter 4

### Deducing the Optimal Damping Function for the D3 Dispersion Correction to Density Functional Theory

#### 4.1 Introduction

The standard semilocal density functional theory (DFT) does not describe long-range electron correlation effects, and hence it fails in the description of noncovalent interactions. The quest to incorporate dispersion interactions into DFT has been an active research area in computational chemistry [144, 145, 146, 147, 89] and many dispersion correction approaches have been exploited. Following the “stairway to heaven”, proposed by Klimeš and Michaelides, each step of the stairway introduces more robust but computationally more expensive correction schemes [89]. However, the most straightforward and effective way to include dispersion in a density functional calculation of interaction energy is the D3 atom-pairwise dispersion correction by Grimme [2]. The DFT+D method relies on supplementing the DFT energy by a dispersion contribution  $E_{disp}$  written as a sum of atom-atom terms:

$$E_{disp} = -\frac{1}{2} \sum_{A \neq B} \sum_{n=6,8,10,\dots} \frac{C_n^{AB}}{r_{AB}^n} f_{damp,n}(r_{AB}). \quad (4.1)$$

where the sum runs over all atom pairs in the system,  $C_n^{AB}$  denotes the averaged (isotropic)  $n$ th-order dispersion coefficient (orders  $n = 6, 8, 10, \dots$ ) for atom pair AB, and  $r_{AB}$  denotes their internuclear distance. Over the years, different expressions for the damping function have been investigated with the most popular being Chai-Head-Gordon (CHG) [148] and Becke-Johnson (BJ) [95] formulas (see section 4.2 for more details). One needs to point out that the original parameters of these damping functions were fitted to the training set containing 130 datapoints broken into 72 intermolecular interactions and 58 thermochemistry datapoints. A recent development of databases of noncovalent interactions opened up avenue for reoptimizing DFT-based approaches on a much larger scale. Smith et al. [4] showed that a refitting of original D3 damping parameters can significantly improve the overall accuracy of the DFT-D3 methods, however, the performance degradation at short range cannot fully be ameliorated by refitting. This research highlights limitations of the damping functions currently employed in the popular DFT+D approaches.

In our study, in order to eliminate constraints of the currently utilized DFT-D3 dispersion corrections, we propose and investigate new physically meaningful forms of damping functions, such as: 1) a linear combination of error functions, and 2) a piecewise-defined function. Their performance is compared with the -D3, -D3M, -D3(BJ), and -D3M(BJ) approaches. Moreover, the possibility of designing a damped dispersion function without higher than  $C_6$  dispersion coefficients is demonstrated.

## 4.2 Overview of Damping Functions Used in the DFT+D Approaches

The damping function  $f_{damp}$  is utilized to include charge-overlap effects beyond the multipole approximation (physical effects) and to prevent double counting of correlation at

short range (an unphysical effect). In the DFT-D3 method, there are two broadly utilized damping functions:

- Chai-Head-Gordon (CHG) [148]:

$$E_{\text{disp}}^{\text{D3}} = -\frac{1}{2} \sum_{A \neq B} \left( \frac{C_6^{AB}}{r_{AB}^6} \frac{1}{1 + 6(r_{AB}/(s_{r,6} R_0^{AB}) + R_0^{AB} \beta)^{-14}} + s_8 \frac{C_8^{AB}}{r_{AB}^8} \frac{1}{1 + 6(r_{AB}/R_0^{AB} + R_0^{AB} \beta)^{-16}} \right) \quad (4.2)$$

which has two optimized parameters  $s_8$ , and  $s_{r,6}$  (a third optional parameter  $\beta$  was introduced in Ref. [4]).

- Becke-Johnson (BJ) [95]:

$$E_{\text{disp}}^{\text{D3(BJ)}} = -\frac{1}{2} \sum_{A \neq B} \left( \frac{C_6^{AB}}{r_{AB}^6 + (\alpha_1 \cdot R_0^{AB} + \alpha_2)^6} + s_8 \frac{C_8^{AB}}{r_{AB}^8 + (\alpha_1 \cdot R_0^{AB} + \alpha_2)^8} \right) \quad (4.3)$$

containing three optimized parameters  $s_8$ ,  $\alpha_1$ , and  $\alpha_2$ .

The  $R_0^{AB}$  parameter is the cutoff radius for atom pair AB. The above damping functions with variables reoptimized on a broader database [4] are denoted by -D3M and -D3M(BJ).

An alternative damping function ‘‘C-Six-Only’’ (CSO) was introduced by Schröder et. al [149]. It simplifies the -D3(BJ) expression, and includes only the  $C_6$  dispersion coefficients while the eighth-order term is approximated by means of a sigmoidal interpolation function. Consequently, this approach reduces the number of fitted parameters to two ( $s_6$

and  $\alpha_1$ ). The -D3(CSO) dispersion correction is given by:

$$E_{\text{disp}}^{\text{D3(CSO)}} = -\frac{1}{2} \sum_{A \neq B} \frac{C_6}{r_{AB}^6 + (2.5^2)^6} \left[ s_6 + \frac{\alpha_1}{1 + \exp(R_{AB} - 2.5R_0^{AB})} \right]. \quad (4.4)$$

However, this scheme was trained only on the S66 database [150], which contains exclusively systems at equilibrium distances. It has been shown that the efficiency of DFT-D3(CSO) is not transferable to more balanced data sets [151].

Quite recently, Witte et al. in the paper titled: ‘‘Assessing DFT-D3 Damping Functions Across Widely Used Density Functionals: Can We Do Better?’’ proposed an ‘‘optimized power’’ damping function (DFT-D3(op)) [151]. The new scheme generalizes the standard -D3(BJ) one by adding a parameter whose role is to determine the rate at which the dispersion is switched on:

$$E_{\text{disp}}^{\text{D3(op)}} = -\frac{1}{2} \sum_{A \neq B} \left( \frac{C_6^{AB}}{r_{AB}^6} \frac{r_{AB}^\beta}{r_{AB}^\beta + (\alpha_1 \cdot R_0^{AB} + \alpha_2)^\beta} + s_8 \frac{C_8^{AB}}{r_{AB}^8} \frac{r_{AB}^{\beta+2}}{r_{AB}^{\beta+2} + (\alpha_1 \cdot R_0^{AB} + \alpha_2)^{\beta+2}} \right). \quad (4.5)$$

The damping parameters  $\alpha_1$ ,  $\alpha_2$ ,  $\beta$ , and  $s_8$  were optimized on 2475 noncovalent binding energies and isomerization energies. While the authors observed an improvement of DFT-D3(op) over the existing damping functions [151], the results seem to be biased, because of the used MUE statistical metric which, most likely, overemphasizes errors originating from water and ion-water clusters.

The question ‘‘Can we do better?’’ still stands.

### 4.3 Damping Function Development

The target of the DFT approach for noncovalent interactions is to reproduce CCSD(T)-quality results at different intermolecular distances. Therefore, in the damping function development, the choice of an appropriate unbiased dataset plays the key role; it has to be large, rich with diverse interaction types, and balanced [4, 25]. Moreover, the data should be split into a training set against which the parameters are optimized, and a validation set, allowing to assess whether the optimized parameters are transferable to complexes outside of the training set. To satisfy these requirements, we utilized the comprehensive dataset of noncovalent interactions collected by Smith et. al [4]. This database contains 8,299 structures split into training (1,526 points) and validation (6,773 points) sets. The nature of intermolecular interactions in the dataset can be inferred by the three SAPT components: electrostatics, induction, and dispersion, and they were visualized in the form of ternary diagrams (see Ref. [4]). Another significant aspect of this development is a proper selection of a statistical metric. Since the database covers a large range of interaction energies, the statistical technique has to allow all curves in the datasets to be treated equally, as well as to prevent from running into singularities at short range when the PES crosses the zero line or at long range where the interaction energy is very small. It has been shown [4, 25] that for performing overall statistics, mean capped unsigned relative error (MCURE) is particularly suitable metric:

$$\begin{aligned} \text{MCURE} &= 100\% \cdot \frac{1}{N} \sum_i^N \left( \frac{|E_i^{\text{int}} - E_i^{\text{int,ref}}|}{E_i^{\text{weight}}} \right) \\ E_i^{\text{weight}} &= \max\left\{ |E_i^{\text{int,ref}}|, \frac{\xi |E_i^{\text{int,ref-eq}}|}{z_i^3} \right\}, \end{aligned} \quad (4.6)$$



where  $\xi$  stands for the dimensionless parameter which controls the aggressiveness of the capping and  $z_i=R_i/R_{eq,i}$  is the dimensionless reduced distance. During calculations,  $\xi$  was set to 0.2 except for the SSI, BBI [152] data sets for which complete curves are not available and a simple cap of 0.5 kcal/mol was applied. Moreover, being in line with Ref. [4], we weighted each database identically, except for SSI, which always contributes  $\frac{1}{3}$  to the statistics. This approach was adopted to avoid an implicit weighting of the entire datasets and to preserve the relevance of the SSI dataset.

An alternative statistical metric appropriate for the development in this work is capped root mean square error (CRMSE):

$$\text{CRMSE} = \sqrt{\frac{1}{N} \sum_{i=1}^N \left( \frac{E_i^{int} - E_i^{int,ref}}{E_i^{weight}} \right)^2}. \quad (4.7)$$

It is chosen to assess the performance of damping functions with parameters fitted using the least squares method, since the sum of the squares of the residuals is minimized.

The standard DFT energies were computed in the QZVP basis set with the counterpoise correction (CP). The optimization of damping parameters was performed for eight density functionals B2PLYP [153], BLYP [154, 155], B3LYP [156, 157], LC- $\omega$ PBE [158], PBE0 [159, 160], PBE [161], BP86 [154, 162], and B97 [93].

#### 4.4 New Forms of Damping Functions

A damping function, whose purpose is to reproduce dispersion effects at short range, has to be a fairly arbitrary increasing function of the reduced distance with limits of 0 at short

range and 1 at long range. Therefore, our desired function  $f_{damp}(\rho)$  needs to satisfy the following conditions:

- $f_{damp}(\rho)$  is an increasing function of  $\rho$ ,
- $\lim_{\rho \rightarrow 0} f_{damp}(\rho) = 0$ ,
- $\lim_{\rho \rightarrow \infty} f_{damp}(\rho) = 1$  after proper normalization.

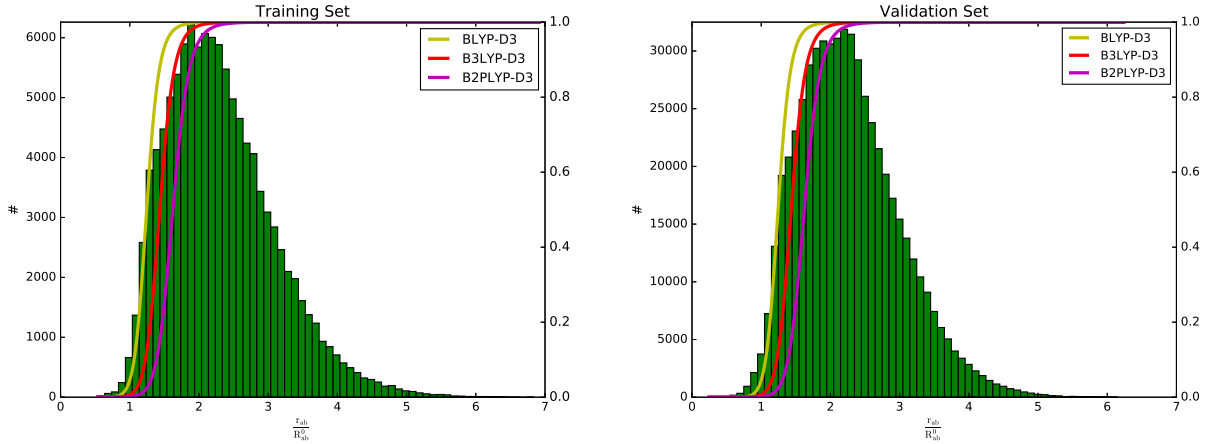
Here,  $\rho$  is defined as the “effective distance”, that is, the ratio of the interatomic distance and a cut-off radius for atom pair AB,  $\frac{r_{AB}}{R_0^{AB}}$ . The  $R_0^{AB}$  values come from the original -D3 work [2]. Such a definition of damping function ensures that the dispersion correction becomes zero or constant for small distances and has the proper asymptotic form for long distances. The resulting dispersion correction with a new damping function is expressed as:

$$E_{disp}^{new} = -\frac{1}{2} \sum_{A \neq B} \left( \frac{C_6^{AB}}{r_{AB}^6} f_{damp,6} \left( \frac{r_{AB}}{R_0^{AB}} \right) + \frac{C_8^{AB}}{r_{AB}^8} f_{damp,8} \left( \frac{r_{AB}}{R_0^{AB}} \right) \right) \quad (4.8)$$

Furthermore, we performed an investigation, at which range of intermolecular distances  $\frac{r_{AB}}{R_0^{AB}}$  the damping function varies the most. For this purpose, the numbers of occurrences of intermolecular  $\frac{r_{AB}}{R_0^{AB}}$  values were computed on the training and validation sets. Subsequently, utilizing that span of  $\frac{r_{AB}}{R_0^{AB}}$ , the functions which damp the  $C_6$  dispersion term in BLYP-D3, B3LYP-D3, and B2PLYP-D3 were examined. The findings illustrated in Fig. 4.1 indicate that our yet to be designed function should be switched on at the range between around 0.8 and 2.2 where the intra- and short intermolecular interactions play the

most important role. Moreover, histograms confirm that our datasets are appropriate for probing at these separations.

Figure 4.1: The number of occurrences of intermolecular  $\frac{r_{AB}}{R_0^{AB}}$  values in the training and validation sets. The functions that damp the  $C_6$  dispersion term in three DFT-D3 variants are also plotted.



#### 4.4.1 Damping Function Expressed by an Error Function

A natural choice of a function satisfying the above conditions is the error function (erf), which is defined as follows:

$$\text{erf}(x) = \frac{2}{\sqrt{\pi}} \int_0^x e^{-t^2} dt. \quad (4.9)$$

To provide enough flexibility to the damping function, we investigated a linear combination of shifted and scaled error functions:

$$f_{damp}(\rho) = \int_0^R \sum_i^n c_i e^{-\alpha_i(t-r_i)^2} dt, \quad (4.10)$$

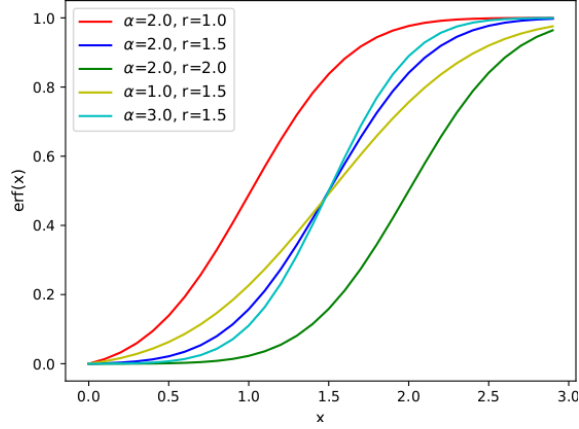


Figure 4.2: Error function curves with different values of  $\alpha_i$  and  $r_i$ .

where parameters  $\alpha_i$  and  $r_i$  correspond to the steepness and location of center of the function, respectively. Fig. 4.2 illustrates the dependence of the erf curve on these two variables.

#### 4.4.2 Piecewise-linear Function

Alternatively, one can define a damping function utilizing a piecewise linear function with parameters  $y_i$ , satisfying the following conditions:

$$\sum_{i=1}^n y_i \leq 1 \quad (4.11)$$

$$\forall_i y_i \geq 0 \quad (4.12)$$

$$f_{damp}(x) = \sum_{i=1}^k y_i + \frac{y_{k+1}}{x_{k+1} - x_k} (x - x_k), \quad (4.13)$$

where

$$x_k \leq x \leq x_{k+1} \quad k = 0, 1, \dots, n \quad (4.14)$$

The  $n$  variable denotes the number of parameters. Therefore, the previously estimated range of reduced intermolecular distances at which the damping function is supposed to work ( $\rho \in [0.8; 2.2]$ ), is split into  $k + 1$  equal intervals and we assume that  $f_{damp}$  increases linearly within each one. The  $k$  values of  $f_{damp}$  at the interval borders constitute the linear fitting parameters. In order to remove the limitation of the damping function, defined in this way, which depends solely on the “effective distance”, we introduced a new form of  $\rho$  with a scaling parameter:

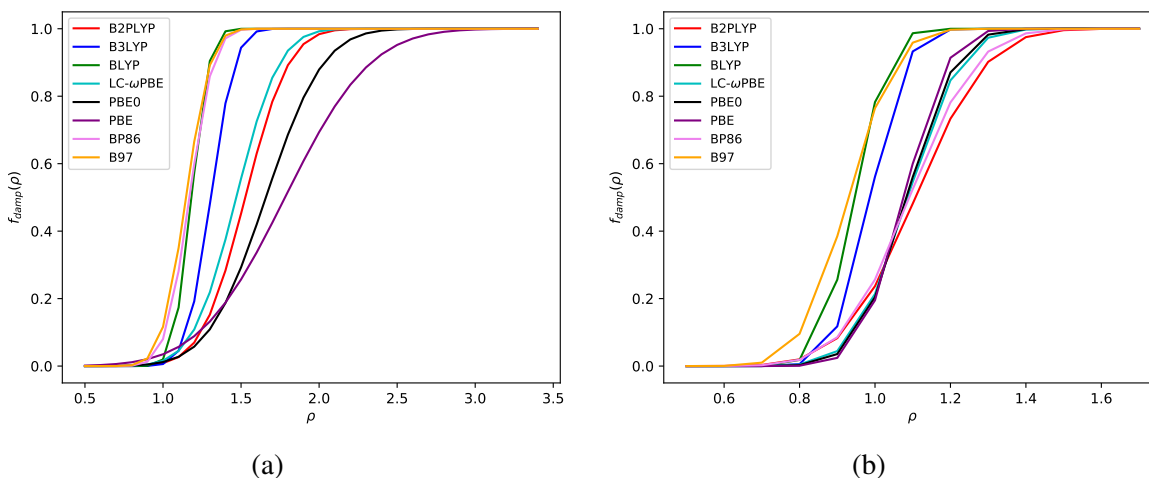
$$\rho = \frac{r_{AB}}{(R_0^{AB})^\gamma}. \quad (4.15)$$

## 4.5 Results and Discussion

We started our considerations by exploring the erf-based damping function. At the first stage, we took into account a single error function for each of the  $C_6$  and  $C_8$  dispersion terms including in total 4 nonlinear parameters. Subsequently, a linear combination of two error functions was applied for the  $C_6$  contribution (keeping only one for  $C_8$ ), which increases the number of parameters by 3. Additionally, in both cases, the influence of an empirical parameter  $s_8$  was examined.

Figure 4.3 (a) displays functions based on one erf term which damp the  $\frac{C_6}{R^6}$  dispersion part. One can observe that the damping functions for BLYP, B3LYP, B97, and BP86 functionals work at short and medium distances ( $\rho \in [0.6; 1.5]$ ), converging steeply to 0. Not surprisingly, short-range PBE0 and PBE functionals require adding dispersion at longer separations up to 2.5 and 2.8, respectively. Considering the damping functions for the  $C_8$  contribution of the multipolar expansion (Fig. 4.3 (b)), it is noticeable that dispersion is damped at smaller separations than for the  $C_6$  term. Functionals are split into

Figure 4.3: Damping functions based on one erf function for a)  $C_6$  and b)  $C_8$  terms in Eq. 4.10 with optimized parameters.



three distinctive groups: B3LYP, BLYP, B97 (converged to 1 at the distance of 1.2), LC- $\omega$ PBE, PBE0, PBE (converged to 1 at the distance of 1.4) and B2PLYP, BP86 (converged to 1 at the distance of 1.6). Furthermore, the functions are steeper than for the  $C_6$  part with the parameter  $\alpha$  (Eq. 4.10) up to 103 for BLYP. This effect is related to the fundamental fact that the  $C_8$  term of the dispersion energy increases faster at short range than the  $C_6$  one, thus it must be damped harder.

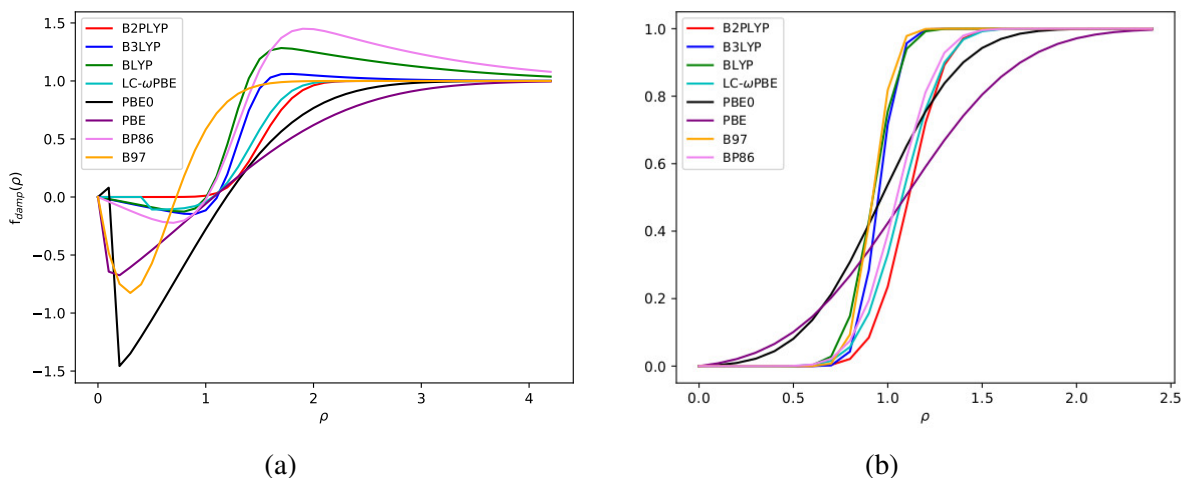
Figure 4.4 (a) depicts the behavior of the damping functions based on a linear combination of two error functions with the coefficient  $c_i$  not being constrained. The B3LYP, BLYP and BP86 functionals exhibit a hump beyond 1.0. It is caused by the fact that these functionals are highly repulsive, thus they need to be complemented with more than 100% of the asymptotic dispersion to match the benchmark interaction energy. It means that these functionals require “antidamping” to amplify the asymptotic dispersion effects

at medium range. An interesting effect is revealed at short distances where all density functionals (except B2PLYP) exhibit a hump below 0, indicating a need of subtracting dispersion at that range. However, results for PBE0 and PBE at the short range seem to be artificially set during optimization in favor of a better description of dispersion at long range. The inclusion or subtraction of an extra amount of dispersion seem to be in line with Ref. [163], suggesting that damping functions correct DFT functionals for effects unrelated to dispersion interactions.

In the case of the  $C_8$  contribution of multipole expansion (Fig. 4.4 (b)), like in the previous model, there are three distinguishable groups of damping functions. However, in this case, the PBE and PBE0 density functionals work at longer intermolecular separations. It is also noticeable that damping functions are less steep (except B2PLYP and BP86).

Figure 4.5 presents damping functions based on the piecewise linear approach with 6 constrained optimized parameters. Functionals B2LYP, PBE, PBE0, and BP86 show a very similar trend as functions increase up to 1.4 (1.2 and 1.6 in the case of B97 and PBE0, respectively) and, subsequently, they become constant. B2PLYP and LC- $\omega$ PBE reach the limit of 1 for  $\rho = 2.0$ , which is consistent with one erf-based damping function, while BP86 and B97 damp dispersion at longer separations, that is, up to  $\rho = 1.8$  and  $\rho = 2.2$ , respectively. It seems that the PBE0 and PBE functionals are forced to converge to 1 at  $\rho = 2.2$  because of our assumed condition of “effective distance”. When we remove constraints from the fitting parameters, damping functions reveal new features. Figure 4.10 shows piecewise damping functions for different functionals with 6 and 13 unconstrained coefficients. Interestingly, all functions smoothly increase up to  $\rho = 1.2$  or  $\rho = 1.4$ , and

Figure 4.4: Damping functions based on a linear combination of two erf functions a) the  $C_6$  term and one erf function for b)  $C_8$  term with optimized parameters.



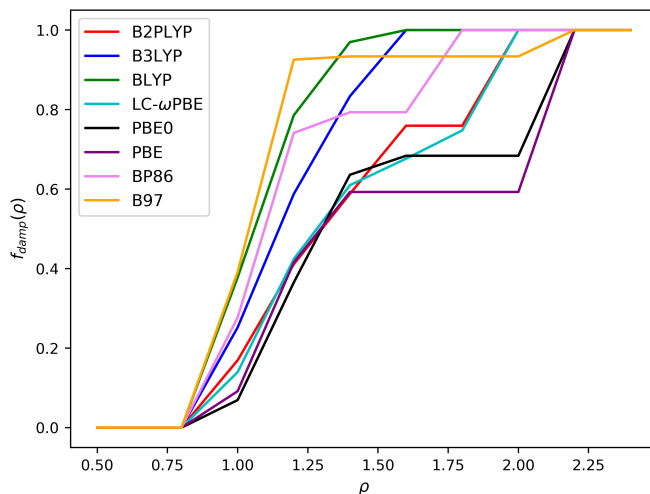
beyond this region, they display more erratic behavior. However, B2PLYP, LC- $\omega$ PBE, and BP86 functionals consistently require adding more dispersion at the region  $\rho \in [1.4; 2.2]$ .

#### 4.5.1 Performance of Erf-based Damping Functions

Fig. 4.6 shows the MCURE of functionals utilizing the new erf-based damping functions compared to DFT-D3 with original [148] and modified [4] damping parameters. The damping function with one erf term each for the  $C_6$  and  $C_8$  contributions improves results only over the standard -D3 approach. The combination of two error functions for the  $C_6$  term slightly reduces the error over the previous model for all considered functionals except LC- $\omega$ PBE. The largest improvement is noticeable for PBE0 and PBE for which MCURE was decreased by 2.2% and 2.0%, respectively, compared to the one erf-based damping function. The addition of a  $s_8$  factor, although it does not have any physical meaning,



Figure 4.5: The piecewise linear damping functions with 6 constrained parameters for different functionals.



makes functionals with new damping functions more efficient. The largest enhancement of performance was achieved for the damping expressed by a linear combination of two erf functions for  $C_6$ . While this model significantly reduces MCURE versus -D3 and -D3(BJ) (even by 10.4% for PBE with respect to PBE-D3), it provides only mild improvement over -D3M and -D3M(BJ) (largest reduction in error is 3.4% for B97 compared to B97-D3M). The best performer across the considered functionals and dispersion corrections is B2PLYP with any proposed erf-based damping function with the MCURE of 5.5 – 5.6 %.

#### 4.5.2 Performance of Piecewise Linear Damping Functions

Due to the fact that the piecewise linear damping function parameters were optimized utilizing the least squares method, the CRMSE statistical metric is chosen for the analysis herein.

Figure 4.6: The MCURE values for functionals utilizing the new erf-based damping function compared to DFT-D3 with original and modified damping parameters.

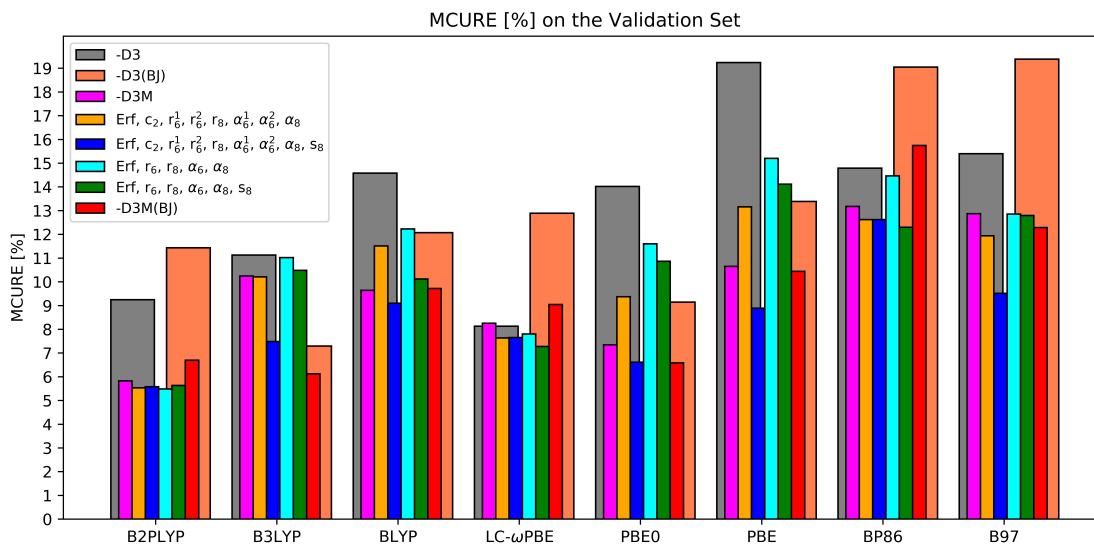


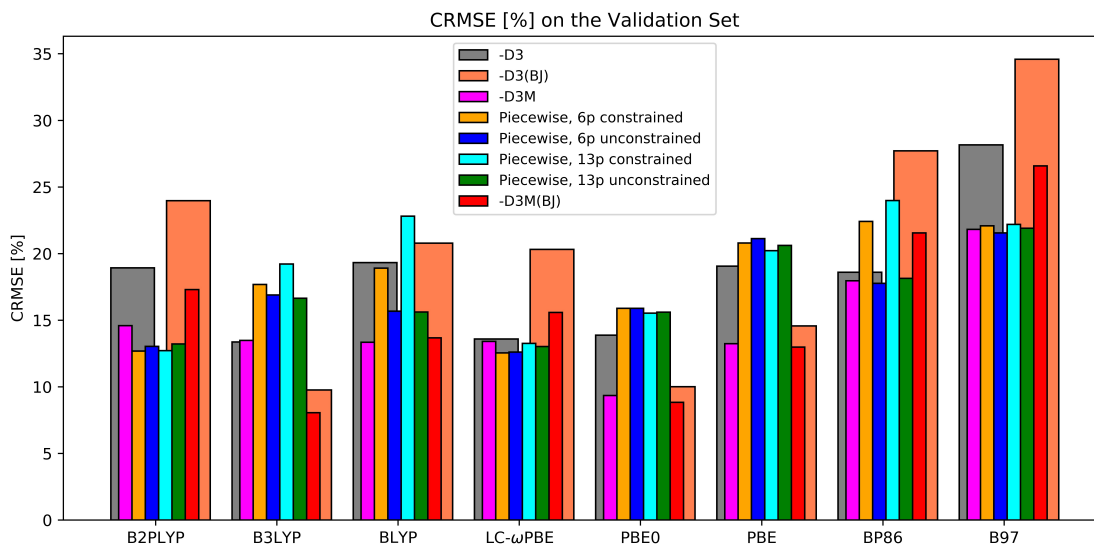
Figure 4.7 presents the CRMSE values for functionals employing a piecewise damping function with 6 and 13 constrained (with constraints in Eqs. 4.11 and 4.12) or unconstrained (free from constraints) coefficients. The variant with 6-parameter damping functions improves the results over the standard -D3 approach by 0.4–6.2% for four functionals, B2LYP, BLYP, LC- $\omega$ PBE, and B97. One can expect that the increase in the number of coefficients would reduce the error, however, the variant with a 13-parameter piecewise linear damping function works the worst (except PBE0 and PBE). This suggests that the number of constrained parameters becomes too large for optimizing the function in the range  $\rho \in [0.8, 2.2]$  leading to overfitting (note that all displayed CRMSE values are computed on the validation set, which is separate from the training set). Examining the piecewise-defined unconstrained counterparts, we can see that the 6-parameter option reduces the error for B3LYP, BLYP, BP86, and B97 over the constrained counterpart. The

largest improvement is visible for BP86, where the CRMSE is lowered by 4.6%. The analysis of the flavor with 13 unconstrained parameters shows the performance being comparable with the one containing 6 unconstrained parameters.

Additionally, the performance of damping functions with the reformulated “effective distance”  $\frac{r_{AB}}{(R_{AB}^0)^\gamma}$  was examined (Fig. 4.8). Adding an additional fitting parameter  $\gamma$  to a damping function with 6 unconstrained coefficients makes the DFT-D3 more accurate for B3LYP, BLYP, PBE0, and PBE by 5.1%, 2.2%, 2.5%, and 2.8% respectively. This sort of enhancement highlights the benefits of the modified “effective distance”. One can notice that when applying the same approach to piecewise linear damping with 13 unconstrained coefficients, we get similar errors.

It is of high importance to compare the results with -D3M and -D3M(BJ). Overall, the B2PLYP, LC- $\omega$ PBE, and BP86 functionals with the new piecewise damping functions with 6 and 13 constrained or unconstrained parameters, B97 with a damping function utilizing 6 unconstrained parameters, as well as B3LYP and BP86 with a damping function containing unconstrained parameters and including  $\gamma$  slightly beat the -D3M scheme. Comparing our approaches with -D3M(BJ), B2PLYP with any damping function, BLYP utilizing a damping function with 6 and 13 unconstrained parameters and including  $\gamma$ , as well as LC- $\omega$ PBE, BP86, and B97 with a damping which depends on 6 and 13 constrained or unconstrained parameters (with and without the parameter  $\gamma$ ) work better.

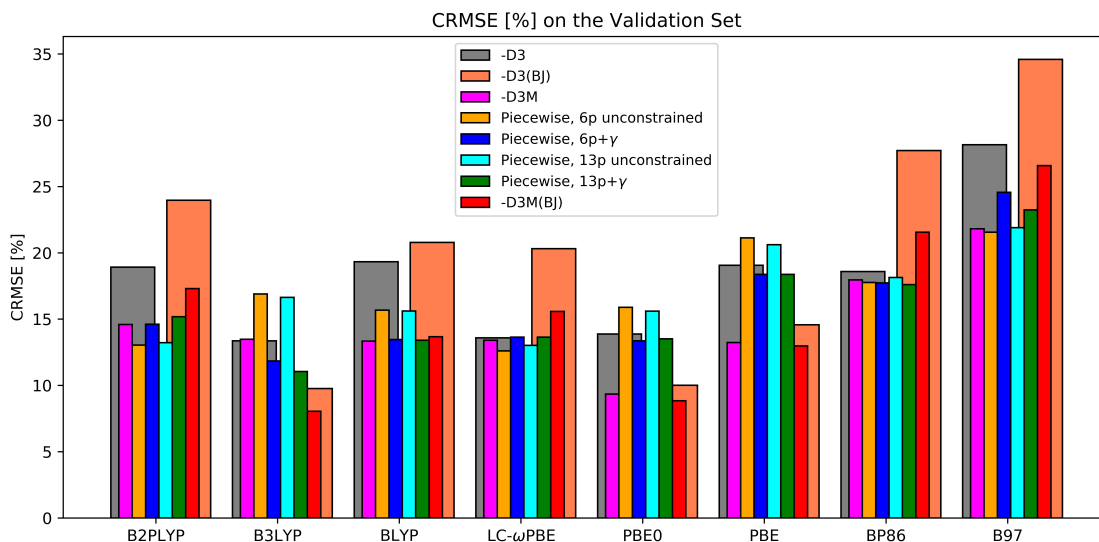
Figure 4.7: The CRMSE values of density functionals with the piecewise linear damping function utilizing 6 and 13 constrained and unconstrained damping parameters with the  $C_6$  and  $C_8$  coefficients, compared to DFT-D3 with original [2, 3] and modified damping parameters [4].



### 4.5.3 Dispersion expressions with $C_6$ only

A very important question arises if we can design a damped dispersion expression which includes only the  $C_6$  term of the multipole expansion in analogy to the -D3(CSO) method of Ref. [149]. The piecewise-defined damping function with unconstrained parameters adds more dispersion when it exceeds the limit of 1. Being in line with this observation, the idea of incorporating the  $C_8$  part into the  $C_6$  one as an extra dispersion contribution above 100% of the  $C_6$  term seems to be reasonable. For this development, the “reduced distance” was extended from 2.2 to 3.0. This region was split into equal distances with the interval of 0.2 and 0.1, giving rise to 10 and 21 parameters, respectively. The damping coefficients which were fitted assuming only a  $C_6$  term are presented in Table 4.7.

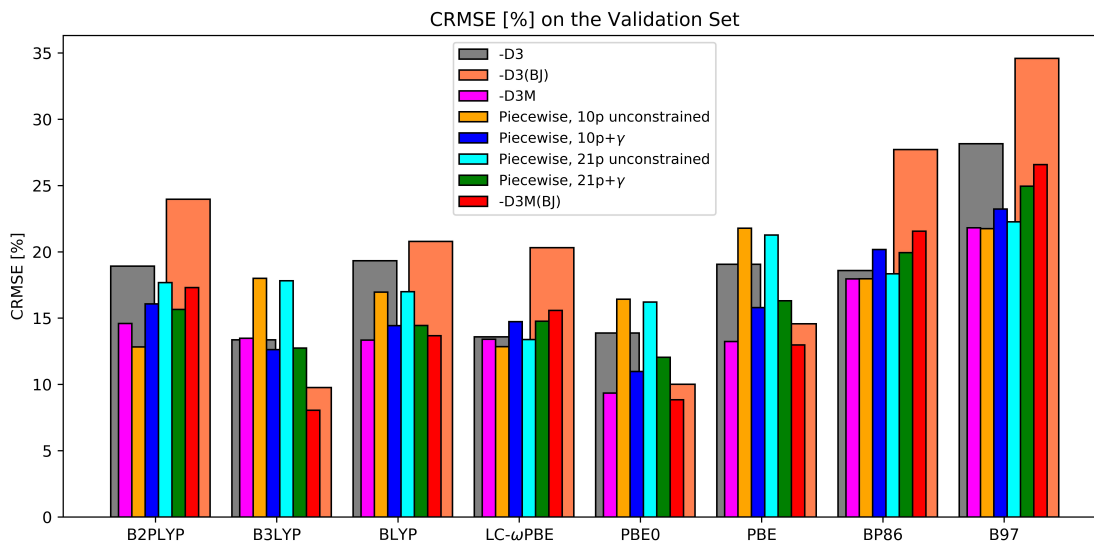
Figure 4.8: The CRMSE values of density functionals with the piecewise linear damping function utilizing 6 and 13 unconstrained damping parameters with the  $C_6$  and  $C_8$  coefficients, compared to DFT-D3 with original [2, 3] and modified damping parameters [4]. The additional parameter  $\gamma$  was introduced to reformulate the “effective distance” (Eq. 4.15).



The performance of our new  $C_6$ -based dispersion expression for different functionals is shown in Fig. 4.9. There is no substantial difference between the options with 10 and 21 unconstrained parameters, the largest variation amounts to 4.9% for B2PLYP. One can notice that the  $C_6$ -only function beats the standard -D3 approach for five functionals B2PLYP, BLYP, LC- $\omega$ PBE, BP86, and B97. The introduction of the parameter  $\gamma$  for an “effective distance” substantially lowers the error for B3LYP, BLYP, PBE0, and PBE functionals with piecewise linear damping by 5.3%, 2.5%, 4.4% and 5.5%, respectively. Generally, only the B2PLYP, BP86, B97 and LC- $\omega$ PBE functionals with the  $C_6$ -based dispersion expression containing 10 unconstrained parameters exhibit comparable or slightly

better performance over -D3M and -D3M(BJ). Among these variants, B2PLYP with our new damping function is the best choice, leading to the CRMSE of 12.8%.

Figure 4.9: The CRMSE values of density functionals with the  $C_6$ -based damping function utilizing 10 and 21 unconstrained parameters with and without  $\gamma$  compared to DFT-D3 with original [2, 3] and modified [4] damping parameters.



## 4.6 Summary

New forms of damping functions examined in this work shed some light on the current limitations of the DFT-D3 method. The overall performance is not improved without including empirical parameters. One issue that can be addressed is that the van der Waals coefficients  $C_6$  and  $C_8$  as well as the cut off radii  $R_0^{AB}$  may not be precise enough in the -D3 approach. One way is to examine -D4 [22] which may lead to some improvement. Another constraint, most likely, comes from short-range intermolecular interactions. It is assumed that the existing functionals reproduce the dispersion energies at separations

smaller than van der Waals minimum, where exchange effects occur. However, this statement was questioned in Ref. [163], proving that the DFT contribution at this region behaves unphysically and comes mostly from non-exchange-correlation terms. Therefore, damping functions may correct DFT functionals at small separations for effects unrelated to dispersion interactions.

Figure 4.10: The piecewise linear damping functions with 6 constrained, and 6 and 13 unconstrained parameters for different functionals.

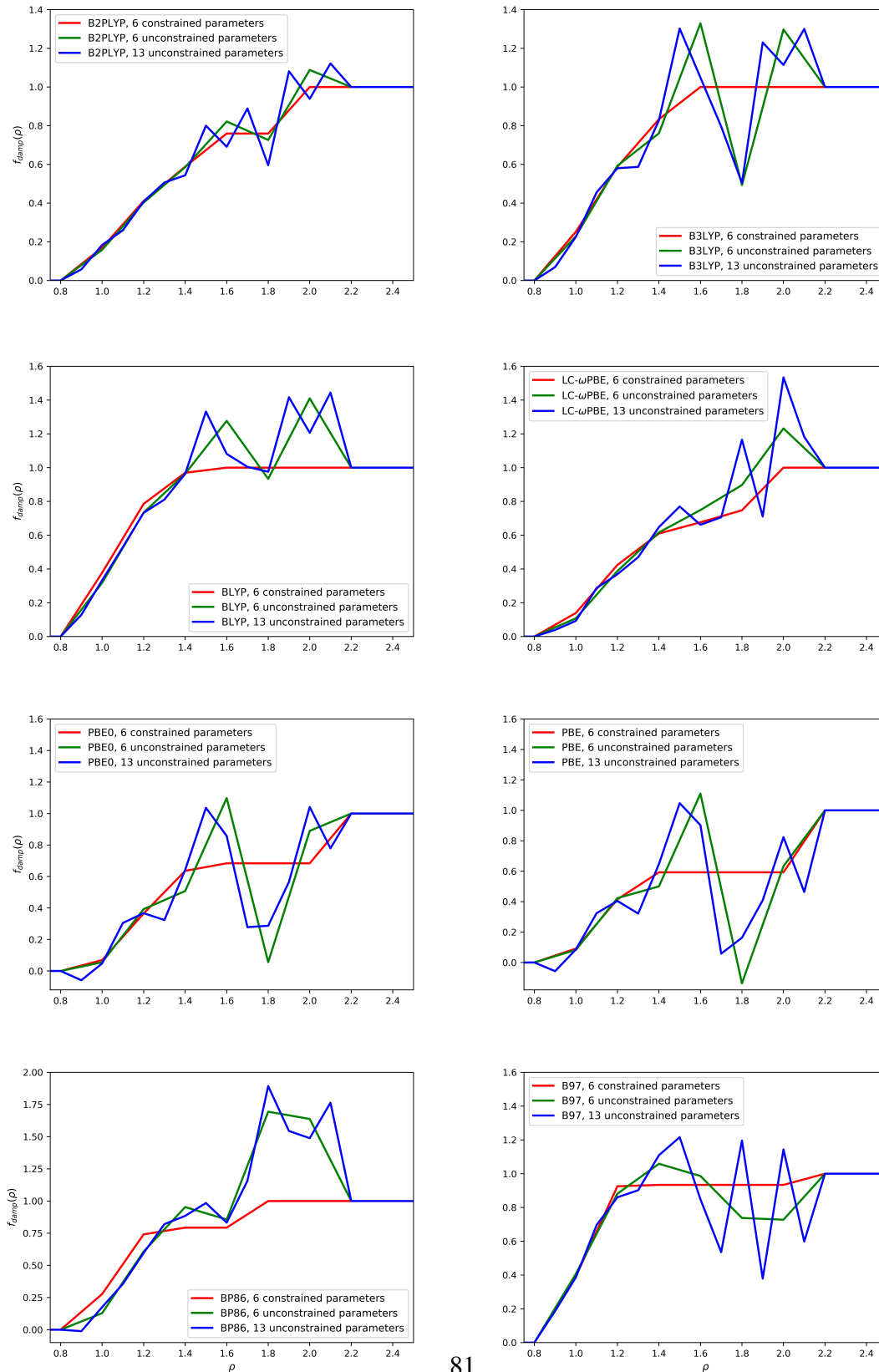




Figure 4.11: The piecewise linear damping functions with 10 and 21 unconstrained parameters including only the  $C_6$  coefficient for different functionals.

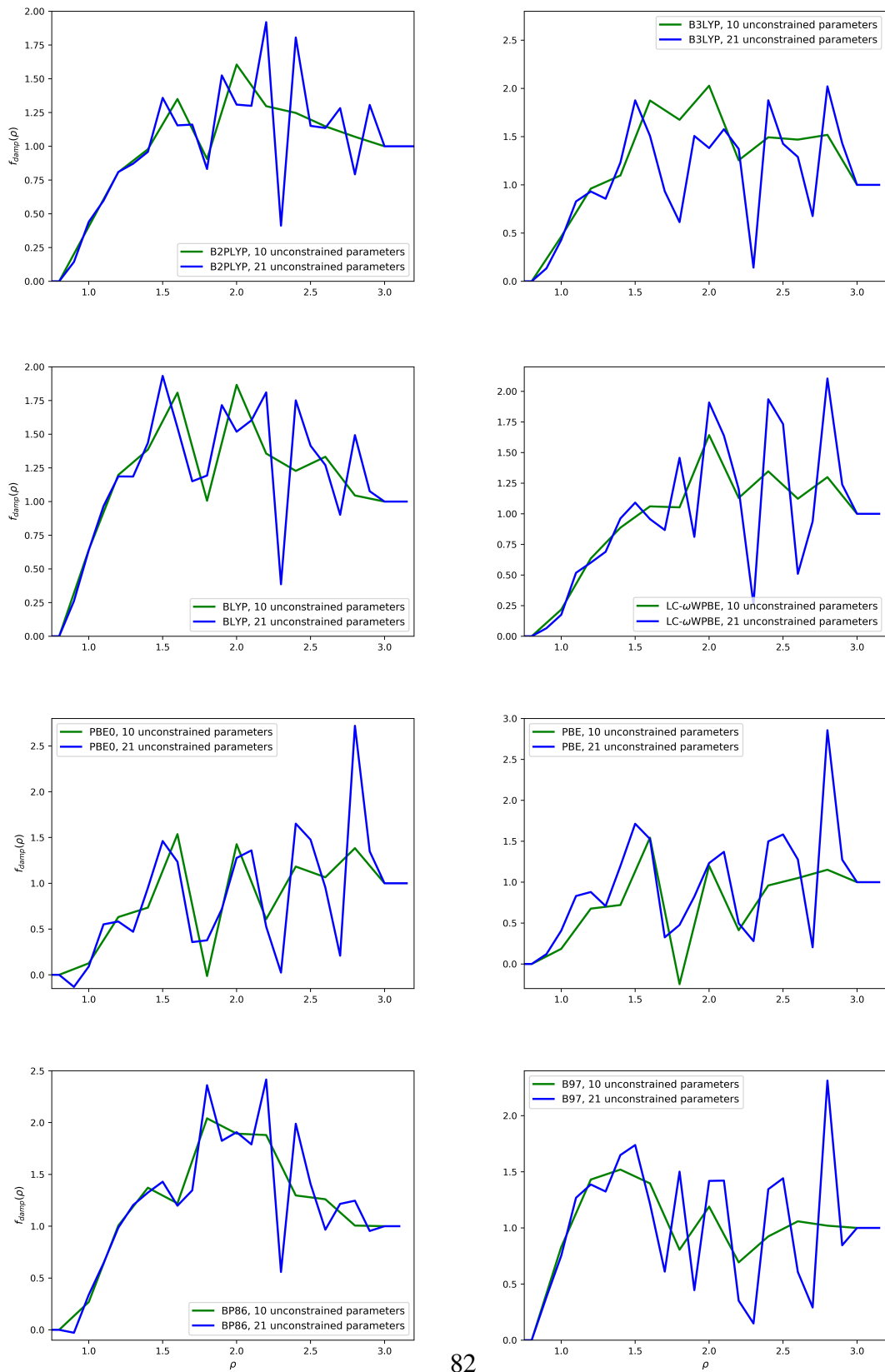


Table 4.1: Damping parameters for one erf each for  $C_6$  and  $C_9$  with and without an  $s_8$  factor.

Functional	$r_6$	$\alpha_6$	$r_8$	$\alpha_8$	$s_8$
B2PLYP	1.866582	1.684730	1.137208	21.686197	1.00
B3LYP	1.306256	33.599776	0.988453	89.993645	1.00
BLYP	1.183630	63.083942	0.945624	103.230487	1.00
LC- $\omega$ PBE	1.469472	10.507580	1.087307	41.284480	1.00
PBE0	1.659007	5.891349	1.084484	47.795724	1.00
PBE	1.781773	2.687986	1.077260	61.899548	1.00
BP86	1.169869	34.207224	1.091382	25.611600	1.00
B97	1.147321	32.844310	0.928864	51.449159	1.00
B2PLYP	2.505793	0.797034	1.301573	8.586300	2.070765
B3LYP	1.450523	44.025552	1.065208	35.501576	1.620762
BLYP	1.423536	50.028595	1.068853	25.651516	2.139820
LC- $\omega$ PBE	1.732073	5.038505	1.203817	16.160668	1.898549
PBE0	2.096682	2.730473	1.214011	15.910099	1.935984
PBE	2.507019	2.684443	1.290434	11.169536	2.678109
BP86	1.644719	56.737909	1.231064	14.500408	3.404418
B97	1.121316	50.464587	0.906327	60.591637	0.894742

Table 4.2: Damping parameters for a combination of error functions with and without the  $s_8$  factor. The parameter  $c_2$  is calculated as a difference  $1 - c_1$ .

Functional	$c_1$	$r_6^1$	$\alpha_6^1$	$r_6^2$	$\alpha_6^2$	$r_8$	$\alpha_8$	$s_8$
B2PLYP	0.705333	1.401292	15.197685	1.590710	7.780365	1.110165	21.360566	1.00
B3LYP	1.334847	0.000000	0.266747	1.291166	16.322195	0.949853	65.305952	1.00
BLYP	1.604436	0.856120	0.134526	1.239993	13.378103	0.920214	37.470008	1.00
LC- $\omega$ PBE	1.108337	0.440680	14180.17	1.417117	6.969897	1.076256	16.382199	1.00
PBE0	2.723303	0.148795	887.714156	0.734163	0.686625	0.966904	4.399108	1.00
PBE	1.805770	0.011584	137.821963	0.862079	0.373696	1.083771	21.699223	1.00
BP86	2.196850	0.247185	0.103772	1.288230	5.535931	1.047790	16.892313	1.00
B97	0.894888	46.985549	17.212141	1.112861	73.947161	0.918271	61.932123	1.00
B2PLYP	1.318265	0.399528	3342645370.00	1.505126	0.182459	1.252432	8.184294	1.576447
B3LYP	5.975438	0.551237	0.893058	1.070866	1.643820	0.998452	5.257360	2.343029
BLYP	3.595532	0.419587	0.643154	1.140520	6.322250	0.758205	13.463902	1.336507
LC- $\omega$ PBE	1.104331	0.442172	9135618.92	1.422617	6.990888	1.076789	17.366851	1.008604
PBE0	1.820802	0.068504	268.460009	2.127954	0.313017	1.361481	3.179071	4.572269
PBE	2.061108	0.071688	210.412562	1.887941	0.083885	1.368015	2.714350	5.326970
BP86	2.776212	0.696318	0.323739	1.258248	5.217628	1.036104	6.220659	1.333364
B97	0.406009	889.116629	852.312265	1.409013	30.925313	1.079037	19.593670	2.763571

Table 4.3: Parameters for the piecewise linear damping function with 6 constrained coefficients.

Functional	$x_1$	$x_2$	$x_3$	$x_4$	$x_5$	$x_6$
B2PLYP	0.16941088	0.24154535	0.17711725	0.17132775	0.00000000	0.24059877
B3LYP	0.25218753	0.33547078	0.24587331	0.16646838	0.00000000	0.00000000
BLYP	0.37779603	0.40784296	0.18399495	0.03036606	0.00000000	0.00000000
LC- $\omega$ PBE	0.13961128	0.28424411	0.18599323	0.06663257	0.07099198	0.25252683
PBE0	0.06936568	0.29577189	0.27085380	0.04781445	0.00000000	0.00000000
PBE	0.09164946	0.32359812	0.17750103	0.00000000	0.00000000	0.00000000
BP86	0.27707430	0.46413474	0.05202975	0.00000000	0.20676121	0.00000000
B97	0.39194187	0.53361805	0.00811184	0.00000000	0.00000000	0.00000000

85

Table 4.4: Parameters for the piecewise linear damping function with 6 unconstrained coefficients.

Functional	$x_1$	$x_2$	$x_3$	$x_4$	$x_5$	$x_6$
B2PLYP	0.15829277	0.24432155	0.18304458	0.23611784	-0.09540873	0.36181346
B3LYP	0.22895080	0.36401577	0.16772643	0.56861551	-0.83595882	0.80408399
BLYP	0.31791893	0.41612900	0.22986939	0.31304389	-0.34342615	0.47663543
LC- $\omega$ PBE	0.10801363	0.27966791	0.22876414	0.13252137	0.14815767	0.33512406
PBE0	0.05548419	0.33735481	0.11488429	0.59013149	-1.04172065	0.83353122
PBE	0.08344948	0.33977673	0.07166136	0.60570497	-1.24470090	0.94194603
BP86	0.12854639	0.47899050	0.34581031	-0.09682196	0.83797688	-0.05651160
B97	0.40739365	0.47436553	0.17703637	-0.07234849	-0.24861782	-0.01015243

Table 4.5: Parameters for the piecewise linear damping function with 13 constrained coefficients.

Functional	$x_1$	$x_2$	$x_3$	$x_4$	$x_5$	$x_6$	$x_7$	$x_8$	$x_9$	$x_{10}$	$x_{11}$	$x_{12}$	$x_{13}$
B2PLYP	0.06429131	0.13614682	0.07454092	0.14853114	0.08548999	0.02205095	0.20396055	0.00000000	0.00000000	0.00000000	0.08853393	0.17645438	0.00000000
B3LYP	0.08982046	0.18407081	0.21900355	0.10755862	0.00033300	0.32114026	0.00001938	0.00000000	0.00000000	0.00000000	0.00000000	0.00000000	0.07805392
BLYP	0.19014087	0.25902423	0.20881257	0.17034859	0.00005965	0.06634095	0.00007559	0.00000000	0.00000000	0.00000000	0.00000000	0.00000000	0.10519754
LC- $\omega$ PBE	0.06653342	0.07210648	0.21118135	0.06847704	0.06354530	0.12194734	0.02629237	0.00000000	0.00000000	0.16258981	0.00000000	0.20732689	0.00000000
PBE0	0.00000000	0.01301626	0.30328225	0.03501447	0.02717943	0.31996044	0.00000000	0.00000000	0.00000000	0.00000000	0.00000000	0.00000000	0.00000000
PBE	0.00000000	0.05485458	0.29025070	0.03122119	0.09073007	0.13495254	0.00000000	0.00000000	0.00000000	0.00000000	0.00000000	0.00000000	0.00000000
BP86	0.15176850	0.18798927	0.18889450	0.16886615	0.08263086	0.00001576	0.00000000	0.00000000	0.09197314	0.12786183	0.00000000	0.00000000	0.00000000
B97	0.19748868	0.17033055	0.33425513	0.19454702	0.03762589	0.00000000	0.00000000	0.00000000	0.00000000	0.00000000	0.00000000	0.00000000	0.00000000

Table 4.6: Parameters for the piecewise linear damping function with 13 unconstrained coefficients.

Functional	$x_1$	$x_2$	$x_3$	$x_4$	$x_5$	$x_6$	$x_7$	$x_8$	$x_9$	$x_{10}$	$x_{11}$	$x_{12}$	$x_{13}$
B2PLYP	0.05767625	0.12582551	0.07635599	0.14852891	0.09795883	0.03728072	0.25650337	-0.10886243	0.19753556	-0.293054	0.48546372	-0.14205791	0.18260217
B3LYP	0.06933628	0.15637789	0.23008939	0.1244838	0.00677868	0.24087121	0.47444569	-0.25396264	-0.25288994	-0.29137757	0.72622138	-0.11632913	0.1859393
BLYP	0.12844305	0.20489025	0.1967506	0.2026687	0.07825167	0.15212343	0.36857341	-0.25012147	-0.0769155	-0.02876479	0.44060289	-0.21001795	0.23752265
LC- $\omega$ PBE	0.0388252	0.05409468	0.19463233	0.08125945	0.10101882	0.17786647	0.12224254	-0.10811667	0.04418998	0.45939447	-0.45463191	0.82350838	-0.35213272
PBE0	-0.05870051	0.10665535	0.25720357	0.0619239	-0.04368324	0.31887391	0.39384409	-0.17848368	-0.57932358	0.00904219	0.27869829	0.47551513	-0.26274576
PBE	-0.0569015	0.1426698	0.23857073	0.07996164	-0.08261424	0.32527708	0.40006142	-0.144603	-0.84400924	0.10440291	0.24623935	0.41498145	-0.36061069
BP86	-0.01117617	0.18681577	0.18000463	0.24139417	0.22351377	0.06410871	0.10009718	-0.15245138	0.32539167	0.73527133	-0.34848947	-0.05586361	0.27578472
B97	0.18720856	0.19964496	0.30946061	0.16408925	0.04144085	0.20730105	0.10705101	-0.36798049	-0.31260816	0.66040323	-0.81666022	0.76451515	-0.54519976

Table 4.7: Parameters for the  $C_6$  only piecewise linear damping function with 10 unconstrained coefficients and the  $\gamma$  parameter.

Functional	$x_1$	$x_2$	$x_3$	$x_4$	$x_5$	$x_6$	$x_7$	$x_8$	$x_9$	$x_{10}$	$\gamma$
B2PLYP	-0.11121771	0.17331595	0.4001504	0.30515398	0.17239784	0.06668061	0.28629747	-0.35013786	0.45388105	0.30594072	0.8
B3LYP	-0.28606485	0.26448874	-0.04985634	0.04881965	0.37452362	0.2693773	0.2951304	0.11313722	0.04244094	0.69263795	0.6
BLYP	0.01841217	0.08889524	0.57293187	0.51805387	0.01100087	0.37989423	0.11472881	-0.72937956	0.81787939	0.14034528	0.8
LC- $\omega$ PBE	-0.02939794	0.01424245	0.29176289	0.34025753	0.04612828	0.40294835	-0.14954121	0.37295086	-0.12328295	0.60706797	0.8
PBE0	-0.38584738	0.28988485	-0.03000787	-0.06342905	0.22465796	0.23115779	0.28764829	0.09299354	-0.05679849	0.61702228	0.6
PBE	-0.42802334	0.40939025	-0.09640167	-0.11610378	0.33095373	0.14235683	0.36572615	0.07926824	-0.16870372	0.61921725	0.6
BP86	-0.13823254	0.52771795	0.63047039	0.22542824	-0.02803315	0.52848637	0.20395422	0.24123384	-0.58606663	-0.1163615	0.9
B97	-0.03504169	0.29736679	-0.07740566	0.5545346	0.62406324	0.04709331	-0.31079134	0.98769333	-0.85916007	-0.22208095	0.7

## Chapter 5

### Explicitly Correlated Dispersion and Exchange Dispersion Energies in Symmetry-Adapted Perturbation Theory

One of the greatest, very often overlooked, advantages of energy decomposition methods such as SAPT, is that various perturbation corrections can be studied separately, and consequently calculated in different basis sets. Therefore, it is possible to reach a CBS limit of a particular correction independently from others. This opens up an avenue for a development of improved second-order dispersion  $E_{\text{disp}}^{(20)}$  and exchange dispersion  $E_{\text{exch-disp}}^{(20)}$  energies in SAPT, since they are, in contrast to other corrections, notably slowly convergent with respect to the basis set size. The requirement of utilizing large correlation-consistent basis sets augmented with diffuse functions to saturate the dispersion energy contribution precludes its calculation for large molecular systems. The common strategies to circumnavigate this problem in SAPT are CBS extrapolation [44, 45] and midbond functions [46, 47, 48] (or both). However, it is worth investigating if the F12 techniques [50, 1, 51], which are successfully used in supermolecular calculations, can also improve the basis set convergence of dispersion in SAPT0.

Until quite recently, explicitly correlated methods in SAPT were applied only to the helium dimer. For this complex, the  $E_{\text{disp}}^{(20)}$ ,  $E_{\text{exch-disp}}^{(20)}$ , and  $E_{\text{disp}}^{(21)}$  corrections, have been

derived and computed employing a Gaussian-type geminal (GTG) basis [164, 114, 165], resulting in a very accurate potential. However, due to a large number of nonlinear parameters in primitive basis functions, as well as the evaluation of complicated three- and four-electron integrals, the GTG-based SAPT is not suitable for complexes larger than the helium dimer. The first indirect combination of SAPT and explicitly correlated F12 methods, termed SAPT-F12(MP2), was introduced by Frey et. al [26]. The SAPT-F12(MP2) variant appends the  $\Delta$ F12 correction to the second-order dispersion and exchange dispersion energies. This correction is calculated based on a proper selection of the double excitations out of a local MP2-F12 calculation. A more rigorous F12 approach to  $E_{\text{disp}}^{(20)}$  was proposed by Przybytek [166]. Although Ref. [166] presents the technical details of derivation of  $E_{\text{disp}}^{(20)}$ -F12 with fully optimized-amplitudes, this variant, because of a steep computational scaling ( $O(N^8)$ ), has relatively little practical significance. Independently, we have [6] presented a derivation and implementation of  $E_{\text{disp}}^{(20)}$ -F12 as well as  $E_{\text{exch-disp}}^{(20)}$ -F12, the latter obtained for the first time. Additionally, in Ref. [6] fully optimized, EBC, optimized diagonal, and fixed-amplitude Ansätze were explored, leading to the deduction of the most accurate and the most computationally efficient flavor. The  $E_{\text{disp}}^{(20)}$ -F12,  $E_{\text{exch-disp}}^{(20)}$ -F12, and  $E_{\text{disp}}^{(20)}$ -F12+ $E_{\text{exch-disp}}^{(20)}$ -F12 corrections with various F12 Ansätze were compared with the approximate SAPT-F12(MP2) method. This chapter summarizes the work in Appendix C [6]. It also presents the first application of the density fitting techniques in the explicitly correlated dispersion and exchange dispersion methods, resulting in DF- $E_{\text{disp}}^{(20)}$ -F12 and DF- $E_{\text{exch-disp}}^{(20)}$ -F12.



## 5.1 F12 Dispersion Energy

In SAPT0, based on the RS perturbation theory, the second-order correction is expressed as:

$$\begin{aligned}
 E^{(20)} = & \sum_{m \neq 0} \frac{|\langle \phi_{\text{HF}}^{\text{A}} \phi_{\text{HF}}^{\text{B}} | V | \phi_{\text{m}}^{\text{A}} \phi_{\text{HF}}^{\text{B}} \rangle|^2}{E_{\text{A}}^0 - E_{\text{A}}^m} + \sum_{n \neq 0} \frac{|\langle \phi_{\text{HF}}^{\text{A}} \phi_{\text{HF}}^{\text{B}} | V | \phi_{\text{HF}}^{\text{A}} \phi_{\text{n}}^{\text{B}} \rangle|^2}{E_{\text{B}}^0 - E_{\text{B}}^n} \\
 & + \sum_{m \neq 0} \sum_{n \neq 0} \frac{|\langle \phi_{\text{HF}}^{\text{A}} \phi_{\text{HF}}^{\text{B}} | V | \phi_{\text{m}}^{\text{A}} \phi_{\text{n}}^{\text{B}} \rangle|^2}{E_{\text{A}}^0 + E_{\text{B}}^0 - E_{\text{A}}^m - E_{\text{B}}^n}, \tag{5.1}
 \end{aligned}$$

where the the sums on the right hand side denote  $E_{\text{ind}, \text{B} \rightarrow \text{A}}^{(20)}$ ,  $E_{\text{ind}, \text{A} \rightarrow \text{B}}^{(20)}$ , and  $E_{\text{disp}}^{(20)}$ , respectively.  $\phi_{\text{m}}^{\text{A}}$  and  $\phi_{\text{n}}^{\text{B}}$  are excited eigenfunctions of the Fock operator for monomer A,  $F^{\text{A}}$ , and B,  $F^{\text{B}}$ , respectively. The related first-order wave function reads:

$$\begin{aligned}
 \Psi^{(10)} = & \sum_{m \neq 0} \frac{\langle \phi_{\text{m}}^{\text{A}} \phi_{\text{HF}}^{\text{B}} | V | \phi_{\text{HF}}^{\text{A}} \phi_{\text{HF}}^{\text{B}} \rangle}{E_{\text{A}}^0 - E_{\text{A}}^m} |\phi_{\text{m}}^{\text{A}} \phi_{\text{HF}}^{\text{B}} \rangle + \sum_{n \neq 0} \frac{\langle \phi_{\text{HF}}^{\text{A}} \phi_{\text{n}}^{\text{B}} | V | \phi_{\text{HF}}^{\text{A}} \phi_{\text{HF}}^{\text{B}} \rangle}{E_{\text{B}}^0 - E_{\text{B}}^n} |\phi_{\text{HF}}^{\text{A}} \phi_{\text{n}}^{\text{B}} \rangle \\
 & + \sum_{m \neq 0} \sum_{n \neq 0} \frac{\langle \phi_{\text{m}}^{\text{A}} \phi_{\text{n}}^{\text{B}} | V | \phi_{\text{HF}}^{\text{A}} \phi_{\text{HF}}^{\text{B}} \rangle}{E_{\text{A}}^0 + E_{\text{B}}^0 - E_{\text{A}}^m - E_{\text{B}}^n} |\phi_{\text{m}}^{\text{A}} \phi_{\text{n}}^{\text{B}} \rangle \tag{5.2}
 \end{aligned}$$

It should be noted that  $\phi_{\text{m}}^{\text{A}}$  depends on the coordinates of electrons 1, 2, ...,  $N_{\text{A}}$  assigned to monomer A and  $\phi_{\text{n}}^{\text{B}}$  depends on the coordinates of electrons  $N_{\text{A}} + 1, N_{\text{A}} + 2, \dots, N_{\text{A}} + N_{\text{B}}$  assigned to monomer B.

In order to isolate induction and dispersion effects, the  $\mathcal{Q}_{\text{A}}$  and  $\mathcal{Q}_{\text{B}}$  operators are defined, which project out the ground state for a a given monomer:

$$\mathcal{Q}_{\text{A}} = 1 - |\phi_{\text{HF}}^{\text{A}} \rangle \langle \phi_{\text{HF}}^{\text{A}}| \quad \mathcal{Q}_{\text{B}} = 1 - |\phi_{\text{HF}}^{\text{B}} \rangle \langle \phi_{\text{HF}}^{\text{B}}|. \tag{5.3}$$

The operators  $\mathcal{Q}_A$  and  $\mathcal{Q}_B$  have the following features: 1) they are Hermitian, 2) they are idempotent, e.g.  $(\mathcal{Q}_A)^2 = \mathcal{Q}_A$ , and 3) they commute, i.e.  $[\mathcal{Q}_A, \mathcal{Q}_B] = 0$ . Applying the product of projection operators for monomer A and B, that is  $\mathcal{Q}_A \mathcal{Q}_B$ , to Eq. 5.2, the desirable dispersion wave function is obtained:

$$\mathcal{Q}_A \mathcal{Q}_B \Psi^{(10)} = \Psi_{\text{disp}}^{(10)}. \quad (5.4)$$

Alternatively,  $E_{\text{disp}}^{(20)}$ -F12 can be obtained variationally by minimizing the ‘‘dispersion only’’ Hylleraas functional [167] to determine the dispersion wave function ( $\mathcal{Q}_A \mathcal{Q}_B \Psi^{(10)}$ ):

$$\begin{aligned} J_{\text{disp}}[\chi] = & \langle \chi | \mathcal{Q}_A \mathcal{Q}_B (F^A + F^B - E_A^0 - E_B^0) \mathcal{Q}_A \mathcal{Q}_B | \chi \rangle \\ & + \langle \chi | \mathcal{Q}_A \mathcal{Q}_B (V - E_{\text{elst}}^{(10)} | \phi_{\text{HF}}^A \phi_{\text{HF}}^B \rangle + \langle \phi_{\text{HF}}^A \phi_{\text{HF}}^B | (V - E_{\text{elst}}^{(10)}) \mathcal{Q}_A \mathcal{Q}_B | \chi \rangle, \end{aligned} \quad (5.5)$$

Table 5.1: Orbital spaces used in this work.

Orbital space	Monomer A	Monomer B
Occupied orbitals	$i, k, m, o$	$j, l, n, v$
Virtual orbitals	$a$	$b$
Any molecular orbitals	$r$	$s$
Complementary auxiliary orbitals	$x$	$y$
Complete orthonormal or RI basis	$\alpha$	$\beta$

The philosophy of the variational principle was also utilized to derive the expression for  $E_{\text{disp}}^{(20)}$ -F12. One can choose an arbitrary function and minimize the Hylleraas functional which will provide the energy value larger or equal to the exact  $E_{\text{disp}}^{(20)}$ . In our case,

following the MP2-F12 approach [59] (see Eq. 2.47), a trial function is defined as:

$$\chi = T_{ab}^{ij}|\Phi_{ij}^{ab}\rangle + T_{kl}^{ij}\mathcal{F}_{\alpha\beta}^{kl}|\Phi_{ij}^{\alpha\beta}\rangle \quad (5.6)$$

with unknown dispersion amplitudes  $T_{ab}^{ij}$  and explicitly correlated amplitudes  $T_{kl}^{ij}$ . Since it is computationally unfeasible to create all excitations from the occupied to the complete spaces ( $i \rightarrow \alpha$  and  $j \rightarrow \beta$ ), the formally complete space is reached via a set of  $T_{kl}^{ij}$  coefficients and a suitable internal contraction:

$$\mathcal{F}_{\alpha\beta}^{kl} = \langle kl|\hat{F}_{12}\hat{Q}_{12}|\alpha\beta\rangle. \quad (5.7)$$

In line with the established explicitly correlated methods for supermolecular calculations, as well as Przybytek's recommendations [166], the  $\hat{F}_{12} \equiv F(r_{12})$  correlation factor is expressed in a standard exponential  $\exp(-\beta r_{12})$  form herein. The role of the projection operator  $\hat{Q}_{12}$  is to force strong orthogonality between the reference dispersion wavefunction and the explicitly correlated one. In the current work, the Ansatz 3 (analogs of 2.49) is utilized for  $\hat{Q}_{12}$ :

$$\hat{Q}_{12} = \left(1_1 - \sum_i |i\rangle\langle i|_1\right) \left(1_2 - \sum_j |j\rangle\langle j|_2\right) \left(1_{12} - \sum_{ab} |ab\rangle\langle ab|_{12}\right). \quad (5.8)$$

In contrast to Eq. 2.49, the above formula contains the subscripts clarifying which electron coordinates are affected by a given part of the projector. The advantage of applying Ansatz 3 is that it leads to some simplifications when we derive a formula for  $E_{\text{disp}}^{(20)}$ -F12, since  $\hat{Q}_{12}|ab\rangle = 0$ , and consequently the matrix elements  $\mathcal{F}_{ab}^{kl}$  are zero.

Now, inserting Eq. 5.6 into Eq. 5.5 and performing some mathematical operations (see Appendix C for the full derivation), we obtain the final formula for  $J_{\text{disp}}[\chi]$  [6]:

$$\begin{aligned}
J_{\text{disp}}[\chi] &= 4T_{ij}^{ab}T_{ab}^{ij}(\epsilon_a^A + \epsilon_b^B - \epsilon_i^A - \epsilon_j^B) + 8T_{ab}^{ij}K_{ij}^{ab} \\
&+ 4T_{ij}^{kl}T_{k'l'}^{ij}B_{kl,k'l'} - 4(\epsilon_i^A + \epsilon_j^B)T_{ij}^{kl}T_{k'l'}^{ij}X_{kl,k'l'} + 8T_{ij}^{kl}V_{kl}^{ij} \\
&+ 8T_{ij}^{ab}T_{kl}^{ij}C_{ab}^{kl}
\end{aligned} \tag{5.9}$$

with the set of matrix intermediates fully analogous to these defined in the MP2-F12(3C) method [59]:

$$K_{ij}^{ab} = \langle ab|r_{12}^{-1}|ij\rangle \tag{5.10}$$

$$V_{kl}^{ij} = \langle ij|r_{12}^{-1}\widehat{Q}_{12}\widehat{F}_{12}|kl\rangle \tag{5.11}$$

$$B_{kl,k'l'} = \langle kl|\widehat{F}_{12}\widehat{Q}_{12}(\widehat{f}_{A1} + \widehat{f}_{B2})\widehat{Q}_{12}\widehat{F}_{12}|k'l'\rangle \tag{5.12}$$

$$X_{kl,k'l'} = \langle kl|\widehat{F}_{12}\widehat{Q}_{12}\widehat{F}_{12}|k'l'\rangle \tag{5.13}$$

$$C_{ab}^{kl} = \langle kl|\widehat{F}_{12}\widehat{Q}_{12}(\widehat{f}_{A1} + \widehat{f}_{B2})|ab\rangle \tag{5.14}$$

The evaluation of the above intermediate matrices leads to many three- and four-electron integrals. The way to deal with them is the same as in the MP2-F12(3C) approach (see section 2.3.6 for more details) as long as the Fock operator for the right monomer is applied each time.

In the next step, we need to calculate the amplitudes  $T_{ij}^{ab}$  and  $T_{ij}^{kl}$  that minimize Eq. (5.9). To do so, the partial derivatives of Eq. 5.9 with respect to amplitudes are taken:

$$\frac{\partial J_{\text{disp}}}{\partial T_{ij}^{ab}} = 8T_{ij}^{ab}(\epsilon_a^A + \epsilon_b^B - \epsilon_i^A - \epsilon_j^B) + 8K_{ij}^{ab} + 8 \sum_{kl} T_{kl}^{ij} C_{ab}^{kl} = 0 \quad (5.15)$$

$$\frac{\partial J_{\text{disp}}}{\partial T_{ij}^{kl}} = 8 \sum_{k'l'} T_{ij}^{k'l'} B_{kl,k'l'} - 8(\epsilon_i^A + \epsilon_j^B) \sum_{k'l'} T_{ij}^{k'l'} X_{kl,k'l'} + 8V_{kl}^{ij} + 8 \sum_{ab} T_{ij}^{ab} C_{ab}^{kl} = 0 \quad (5.16)$$

One can notice that Eqs. 5.15 and 5.16 are coupled which means that the solutions for  $T_{ij}^{ab}$  and  $T_{ij}^{kl}$  depend on each other. When both gradients are set to zero, we obtain a system of linear equations for each pair of occupied orbitals (i,j). Then, Eq. 5.15 is solved for  $T_{ij}^{ab}$  and subsequently the result is inserted into Eq. 5.16:

$$T_{ij}^{ab} = \frac{K_{ij}^{ab} + \sum_{kl} T_{kl}^{ij} C_{ab}^{kl}}{\epsilon_i^A + \epsilon_j^B - \epsilon_a^A - \epsilon_b^B} \quad (5.17)$$

$$\begin{aligned} & \sum_{k'l'} T_{ij}^{k'l'} \left[ B_{kl,k'l'} - (\epsilon_i^A + \epsilon_j^B) X_{kl,k'l'} + \sum_{ab} \frac{C_{ab}^{k'l'} C_{ab}^{kl}}{\epsilon_i^A + \epsilon_j^B - \epsilon_a^A - \epsilon_b^B} \right] \\ &= -V_{kl}^{ij} - \sum_{ab} \frac{K_{ij}^{ab} C_{ab}^{kl}}{\epsilon_i^A + \epsilon_j^B - \epsilon_a^A - \epsilon_b^B}. \end{aligned} \quad (5.18)$$

This procedure allows one to determine fully optimized amplitudes, which will be denoted as FULL in this work. Once we plug the optimized amplitudes into Eq. 5.9, a simplified formula for  $E_{\text{disp}}^{(20)}$ -F12 is obtained:

$$E_{\text{disp}}^{(20)}\text{-F12} = 4T_{ab}^{ij} K_{ij}^{ab} + 4T_{ij}^{kl} V_{kl}^{ij}. \quad (5.19)$$

Unfortunately, the computational cost of  $E_{\text{disp}}^{(20)}$ -F12 with fully optimized amplitudes is very unfavorable, since the number of operations needed to be performed is  $o_A^3 v_A o_B^3 v_B$ , leading to overall scaling of  $O(N^8)$ . This variant is 3 orders of  $N$  more expensive than the standard second-order dispersion energy  $E_{\text{disp}}^{(20)}$ , so that it cannot be competitive for practical calculations. It needs to be stressed that the standard  $E_{\text{disp}}^{(20)}$  computation scales like  $O(N^5)$ , and the newly developed  $E_{\text{disp}}^{(20)}$ -F12 should not be much more computationally expensive than the parent method. Therefore, in order to reduce the computational scaling, we have [6] proposed and tested three simplified *Ansätze*, described below.

**EBC Ansatz.** This variant utilizes the extended Brillouin condition (EBC), saying that the virtual orbitals are not improved by the complementary auxiliary basis functions. Therefore, matrix elements  $(f^A)_x^a$  and  $(f^A)_a^x$  are zero. As a result,  $C_{ab}^{kl} = 0$ , so that Eqs. 5.15 and 5.16 become decoupled and Eq. 5.18 takes the form:

$$\sum_{k'l'} (T^{\text{EBC}})_{ij}^{k'l'} \left[ B_{kl,k'l'} - (\epsilon_i^A + \epsilon_j^B) X_{kl,k'l'} \right] = -V_{kl}^{ij}. \quad (5.20)$$

The above equation is the most expensive step in the EBC approximation. The noniterative way of solving a system of linear equations leads to the scaling of  $o_A^4 o_B^4$ , which is again  $O(N^8)$ . However, it can be computed cheaper in the iterative way of solving the systems of equations (a single iteration is simply a matrix-vector multiplication) which brings the overall scaling down to  $o_A^3 o_B^3$  or  $O(N^6)$ .

**Optimized Diagonal Ansatz (ODA).** This approach assumes that the amplitudes  $T_{ij}^{kl}$  are diagonal, that is:

$$T_{ij}^{kl} = T_{ij}^{ij} \delta_{ik} \delta_{jl}. \quad (5.21)$$

This condition simplifies Eqs. 5.17–5.18, and consequently there is no need to solve the system of linear equations. The amplitudes are computed in  $o_A v_A o_B v_B$  operations, so that the intermediates Eqs. of 5.10–5.14 constitute the limiting factor, as they are computed in  $O(N^5)$  operations.

**Fixed-Amplitude Ansatz (FIX).** This approximation assumes that all explicitly correlated amplitudes are diagonal and equal to a constant parameter  $T_{ij}^{ij} = \lambda$ . The Hylleraas functional  $J_{\text{disp}}[\chi]$ , Eq. 5.9, is quadratic in  $\lambda$ , thus we only need to find a minimum of this quadratic equation. We have [6] found that the optimal  $\lambda$  values are in the range 0.3–0.6. The limiting factor of the FIX approximation boils down to the computation of the intermediate matrices. Thus, the overall scaling of this approach is also  $O(N^5)$ .

## 5.2 F12 Exchange Dispersion Energy

In SAPT, two variants allowing to compute the second-order exchange dispersion energy  $E_{\text{exch-disp}}^{(20)}$  have been proposed: 1) the conventional expression derived using density matrices [168], and 2) the less popular, expression derived using the second-quantized form of the single exchange operator [169]. Since the latter formalism requires fewer different integrals, it will be employed herein. The  $E_{\text{exch-disp}}^{(20)}$  contribution expressed in the second-quantization formalism takes the form [170]:

$$\begin{aligned}
E_{\text{exch-disp}}^{(20)} = & 2T_{ab}^{ij} \left[ -K_{ij}^{a'b'} S_{a'}^b S_{b'}^a + K_{i'j}^{ab'} S_i^b S_{b'}^{i'} - 2K_{ij}^{ab'} S_{i'}^b S_{b'}^{i'} \right. \\
& + K_{ij'}^{a'b} S_j^a S_{a'}^{j'} - 2K_{ij}^{a'b} S_j^a S_{a'}^{j'} - K_{i'j'}^{ab} S_i^b S_j^{i'} \\
& + 2K_{ij'}^{ab} S_{i'}^b S_j^{i'} + 2K_{i'j}^{ab} S_i^b S_{j'}^{i'} - 2(\omega_B)_i^a S_{i'}^b S_j^{i'} \\
& \left. + (\omega_B)_{i'}^a S_i^b S_{j'}^{i'} - (\omega_B)_i^{a'} S_{a'}^b S_j^a - 2(\omega_A)_j^b S_j^a S_i^{j'} \right]
\end{aligned}$$

$$+(\omega_A)_{j'}^b S_j^a S_i^{j'} - (\omega_A)_j^{b'} S_i^b S_{b'}^a] \quad (5.22)$$

where  $S_j^i = \langle i|j \rangle$  is the overlap integral and  $(\omega_B)_i^a$  is the matrix element of the electrostatic potential of monomer B, that is,

$$(\omega_B)_i^a = \langle a|v_B|i \rangle + 2K_{ij}^{aj} \quad (5.23)$$

and  $v_B$  is the nuclear potential of molecule B. The  $(\omega_A)_j^b$  matrix elements are defined in a similar way. It needs to be emphasized that the amplitudes  $T_{ab}^{ij}$  in Eq. 5.22 are taken from the dispersion energy calculations.

In the next step, we want to obtain the expression for  $E_{\text{exch-disp}}^{(20)}$ -F12. To do so, the F12 Ansatz is defined as follows:

$$T_{\gamma\delta}^{ij} |\Phi_{ij}^{\gamma\delta}\rangle \longrightarrow T_{ab}^{ij} |\Phi_{ij}^{ab}\rangle + T_{kl}^{ij} \mathcal{F}_{\alpha\beta}^{kl} |\Phi_{ij}^{\alpha\beta}\rangle \quad (5.24)$$

where both  $T_{ab}^{ij}$  and  $T_{kl}^{ij}$  are determined in the previous  $E_{\text{disp}}^{(20)}$ -F12 calculation. The above Ansatz allows one to perform calculations in the formally complete one-electron basis  $|\alpha\rangle$  for monomer A and  $|\beta\rangle$  for monomer B. According to the generalized Brillouin condition (GBC), the complementary auxiliary functions do not improve the  $i$  and  $j$  occupied orbitals, so that they are unchanged in the F12 approach. However, the virtual  $a, b$  orbitals are replaced by larger spaces  $\gamma, \delta$  (un-occupied orbitals) on A and B, respectively. This means that the index  $\gamma$  runs over  $a$  and  $x$ , and the index  $\delta$  runs over  $b$  and  $y \equiv x$ .

As  $E_{\text{exch-disp}}^{(20)}$  is not a variational quantity, analogously to CCSD(T)-F12, we substitute the Ansatz given in Eq. 5.24 into Eq. 5.22 and perform some simplifications (see



Appendix C for the full derivation). The resulting formula for the F12 correction to the second-order exchange-dispersion energy [6] is given by:

$$\begin{aligned}
\delta E_{\text{exch-disp}}^{(20)\text{-F12}} = & 2T_{kl}^{ij} [F_{xb}^{kl} K_{i'j}^{xb'} S_i^b S_{b'}^{i'} - 2F_{xb}^{kl} K_{ij}^{xb'} S_{i'}^b S_{b'}^{i'} + F_{ay}^{kl} K_{i'j'}^{a'y} S_j^a S_{a'}^{j'} - 2F_{ay}^{kl} K_{ij}^{a'y} S_{j'}^a S_{a'}^{j'} \\
& - 2F_{xb}^{kl} (\omega_B)_i^x S_{i'}^b S_j^{i'} + F_{xb}^{kl} (\omega_B)_{i'}^x S_i^b S_j^{i'} - F_{ay}^{kl} (\omega_B)_i^y S_j^a \\
& - 2F_{ay}^{kl} (\omega_A)_j^y S_{j'}^a S_i^{j'} + F_{ay}^{kl} (\omega_A)_{j'}^y S_j^a S_i^{j'} - F_{xb}^{kl} (\omega_A)_j^x S_i^b \\
& - \langle kl | \hat{F}_{12} r_{12}^{-1} | i' j' \rangle S_i^{j'} S_j^{i'} + 2 \langle kl | \hat{F}_{12} r_{12}^{-1} | i j' \rangle S_{i'}^{j'} S_j^{i'} + 2 \langle kl | \hat{F}_{12} r_{12}^{-1} | i' j \rangle S_i^{j'} S_{j'}^{i'} \\
& - \langle lk | \hat{F}_{12} r_{12}^{-1} | i j \rangle + F_{i'j'}^{lk} K_{ij}^{i'j'} + F_{aj'}^{lk} K_{ij}^{aj'} + F_{i'b}^{lk} K_{ij}^{i'b} + F_{xj'}^{lk} K_{ij}^{xj'} + F_{i'y}^{lk} K_{ij}^{i'y} \\
& + F_{xn}^{kl} K_{ij}^{ax} S_a^n + F_{my}^{kl} K_{ij}^{yb} S_b^m + F_{rs}^{kl} K_{ij}^{ab} S_a^s S_b^r \\
& + F_{xn}^{kl} K_{i'j'}^{xn} S_i^{j'} S_j^{i'} + F_{my}^{kl} K_{i'j'}^{my} S_i^{j'} S_j^{i'} + F_{rs}^{kl} K_{i'j'}^{rs} S_i^{j'} S_j^{i'} \\
& - 2F_{xn}^{kl} K_{ij'}^{xn} S_{i'}^{j'} S_j^{i'} - 2F_{my}^{kl} K_{ij'}^{my} S_{i'}^{j'} S_j^{i'} - 2F_{rs}^{kl} K_{ij'}^{rs} S_{i'}^{j'} S_j^{i'} \\
& - 2F_{xn}^{kl} K_{i'j}^{xn} S_i^{j'} S_{j'}^{i'} - 2F_{my}^{kl} K_{i'j}^{my} S_i^{j'} S_{j'}^{i'} - 2F_{rs}^{kl} K_{i'j}^{rs} S_i^{j'} S_{j'}^{i'}. \tag{5.25}
\end{aligned}$$

Therefore, the F12 second-order exchange dispersion energy is given by:

$$E_{\text{exch-disp}}^{(20)\text{-F12}} = E_{\text{exch-disp}}^{(20)} + \delta E_{\text{exch-disp}}^{(20)\text{-F12}}, \tag{5.26}$$

that is a sum of the conventional  $E_{\text{exch-disp}}^{(20)}$ , Eq. 5.22 and the F12 correction expressed by Eq. 5.25.

### 5.3 SAPT-F12(MP2)

As it was mentioned before, the SAPT-F12(MP2) method [26] computes the  $\Delta$ F12 correction as a by-product of the local MP2-F12 calculation where only intermolecular double

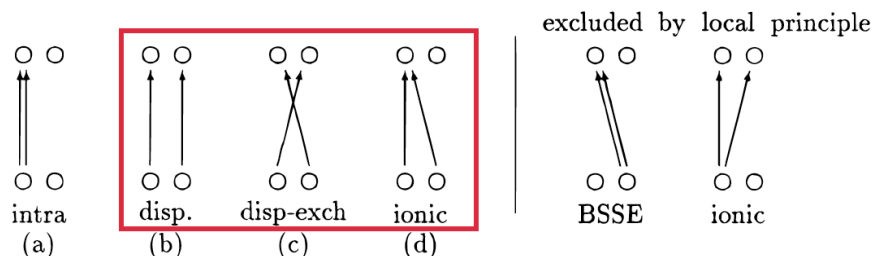


Figure 5.1: Schematic representation of double excitations in the local MP2 method. The figure comes from Ref. [5].

excitation contributions to the energy are taken into account. In the original work [26], this correction is added to the standard second-order dispersion energy  $E_{\text{disp}}^{(20)}$ . However, considering all possible electron excitations in the local MP2 method (see Fig. 5.1), most likely,  $\Delta\text{F12}$  contains the correction to both  $E_{\text{disp}}^{(20)}$  and  $E_{\text{exch-disp}}^{(20)}$ .

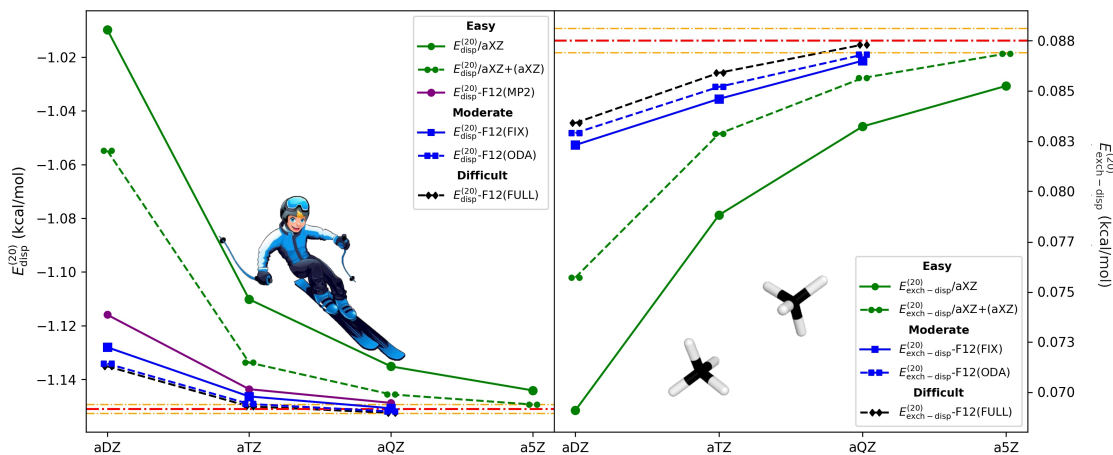
#### 5.4 Test Systems

The first test systems considered were five weakly interacting dimers: He–He, Ne–Ne, Ar–Ar, H<sub>2</sub>O–H<sub>2</sub>O, and CH<sub>4</sub>–CH<sub>4</sub> at their minimum separations. The exhaustive calculations were performed using basis sets up to a5Z combined with auxiliary sets up to a5Z-RI (a6Z and a6Z-RI for the helium dimer). The basis sets with one lower cardinal number, that is aQZ and aQZ-RI, were utilized for the CH<sub>4</sub>–CH<sub>4</sub> complex, due to the code limitations. Tables 2–10 in Appendix C present the  $E_{\text{disp}}^{(20)}$ -F12 and  $E_{\text{exch-disp}}^{(20)}$ -F12 values calculated with the FIX, ODA, EBC, FULL, and F12(MP2) Ansätze. All these results were compared to the benchmark values computed utilizing the conventional approach in the a6Z orbital basis set augmented with the hydrogenic a6Z midbond set, a6Z+(a6Z), except the helium dimer, for which the Gaussian-type geminal (GTG) benchmark is available [165].

It is important to verify if the explicitly correlated second-order energy satisfies the variational principle (energies should be above the benchmark when  $X$  is increased). It turned out that the  $E_{\text{disp}}^{(20)}$ -F12 energies obtained in the aXZ/aXZ-RI basis sets do not obey that condition for all rare gas dimers. An additional examination of this issue revealed that such an effect results from a very slow convergence of the energy with the auxiliary basis. The same basis set convergence behavior was observed for  $E_{\text{exch-disp}}^{(20)}$ -F12, however, the second-order exchange-dispersion energy is not a variational quantity, so we are not guaranteed an improvement of results while enlarging the basis set. Moreover, for noble gas dimers, the  $E_{\text{disp}}^{(20)}$ -F12 energies in the aDZ orbital basis sets are not converged with respect to the RI basis even in the largest applied a5Z-RI level (a6Z-RI for He–He), as shown in Tables 1–3 (Appendix C). It is worth emphasizing, that for the He–He dimer all  $E_{\text{disp}}^{(20)}$ -F12(FULL)/aDZ energies are below the benchmark value. Thus, we constructed a larger auxiliary basis, a (17s15p13d11f9g7h5i) set [6] and tested it with  $E_{\text{disp}}^{(20)}$ -F12(FULL)/aDZ for this system. In this case, the resulting energy was -0.0332 kcal/mol, which is above the variational limit. Therefore, the final conclusion is that the slow convergence of noble gas dimer interaction energies can be linked with the auxiliary basis sets not being properly optimized for dispersion energy calculations [6]. Such an issue is not observed for the H<sub>2</sub>O–H<sub>2</sub>O and CH<sub>4</sub>–CH<sub>4</sub> complexes, for which the  $E_{\text{disp}}^{(20)}$ -F12 and  $E_{\text{exch-disp}}^{(20)}$ -F12 energies converge quickly with the RI basis.

From the technical point of view, when performing tests on the initial systems, we encountered some convergence problems in the full optimization of dispersion amplitudes. They are caused by the fact that the systems of linear equations defined by Eqs. 5.15–5.16

Figure 5.2: Convergence of  $E_{\text{disp}}^{(20)}$ -F12 and  $E_{\text{exch-disp}}^{(20)}$ -F12 as a function of basis set for the  $\text{CH}_4$ - $\text{CH}_4$  complex. This Figure was adapted from [6].



are quite ill-conditioned. Therefore, the  $E_{\text{disp}}^{(20)}$ -F12(FULL) contribution was substituted by  $E_{\text{disp}}^{(20)}$ -F12(ODA) for each pair of orbitals (i,j) whenever numerical issues occurred.

In terms of the performance,  $E_{\text{disp}}^{(20)}$ -F12 and  $E_{\text{exch-disp}}^{(20)}$ -F12 phenomenally speed up the basis set convergence over the conventional approaches. As an example, Fig. 5.2 depicts the basis set convergence for  $E_{\text{disp}}^{(20)}$ -F12 and  $E_{\text{exch-disp}}^{(20)}$ -F12 with various Ansätze for  $\text{CH}_4$ - $\text{CH}_4$ .

The explicitly correlated values obtained in the aDZ basis set are as good as standard dispersion energy with added two (for  $E_{\text{disp}}^{(20)}$ -F12) or more than one (for  $E_{\text{exch-disp}}^{(20)}$ -F12) shell of basis functions. However, there is a noticeable trend of overestimating the CBS energies in the aDZ/aDZ-RI basis set combination which was observed for all noble gases. This is a consequence of an incomplete error cancellation between the orbital and auxiliary basis sets truncations [6]. Thus, the aDZ/aDZ-RI basis set is not recommended for studies of rare gas dimers. One should notice a phenomenal performance of  $E_{\text{disp}}^{(20)}$ -F12 and  $E_{\text{exch-disp}}^{(20)}$ -F12 in the aTZ and aQZ bases, respectively. Generally, energies are close

to the benchmark or even better, depending on the Ansatz utilized in the calculations. It is undisputed that  $E_{\text{disp}}^{(20)}$ -F12 and  $E_{\text{exch-disp}}^{(20)}$ -F12 combined with the FULL Ansatz produce the most accurate results. Nevertheless, the ODA variant works nearly as well as the FULL one. The  $E_{\text{disp}}^{(20)}$ -F12 correction with the EBC Ansatz provides somewhat less accurate values than the ODA Ansatz, but it is opposite for  $E_{\text{exch-disp}}^{(20)}$ -F12. Therefore, the crucial step was to analyze  $E_{\text{disp}}^{(20)}$ -F12 +  $E_{\text{exch-disp}}^{(20)}$ -F12 since a sum of the second-order dispersion and exchange dispersion energies is a target for improvement in SAPT0. It turned out, that, overall, the EBC Ansatz is inferior to the optimized diagonal Ansatz and at the same time leads to more expensive calculations. Based on these observations, the EBC Ansatz was discarded from further tests. Although the FIX Ansatz is the worst performer, even this approach distinctly enhances the performance compared to the standard  $E_{\text{disp}}^{(20)}$ -F12 and  $E_{\text{exch-disp}}^{(20)}$ -F12. As it comes to  $E_{\text{disp}}^{(20)}$ -F12(MP2), generally, it improves the dispersion energy, and the results are converged in the aTZ basis set (see Tables 1–5 in Appendix C).

## 5.5 Tests on the A24 Database

After the first successful tests, we decided to examine the performance of the explicitly correlated second-order dispersion and exchange dispersion energies on the A24 database [7], using up to aTZ/aTZ-RI basis sets. Overall,  $E_{\text{disp}}^{(20)}$ -F12 computed with the FULL and ODA Ansätze exhibits a very fast basis set convergence going from aDZ to aTZ (see Figures 1, 2, S1, and S2 (Supporting Information) in Appendix C). These explicitly correlated variants provide energies converged to the benchmark level in aTZ/aTZ-RI or even earlier, e.g. for the NH<sub>3</sub>–H<sub>2</sub>O complex. However, there are two systems containing the argon atom which show slightly slower convergence (Ar–CH<sub>4</sub> and Ar–C<sub>2</sub>H<sub>4</sub>). The FULL Ansatz consistently

leads to convergence than the ODA one, however, this enhancement is really minor. The performance of  $E_{\text{disp}}^{(20)}$ -F12 combined with the FIX Ansatz clearly shows a slower convergence. This flavor combined with the aTZ basis set provides energies converging to the level of  $E_{\text{disp}}^{(20)}/\text{aQZ}+(\text{aQZ})$  for most systems, except Ar-CH<sub>4</sub> and Ar-C<sub>2</sub>H<sub>4</sub>, for which the accuracy is equivalent to aTZ+(aTZ). Considering the  $E_{\text{disp}}^{(20)}$ -F12(MP2) variant, the basis set convergence seems to be more erratic. Nevertheless, two groups of systems showing the same convergence pattern can be distinguished: 1) complexes containing at least one polar monomer, for which  $E_{\text{disp}}^{(20)}$ -F12(MP2) produces energies close to the CBS limit, 2) nonpolar molecules, for which  $E_{\text{disp}}^{(20)}$ -F12(MP2) is the worst variant among all considered explicitly correlated Ansätze.

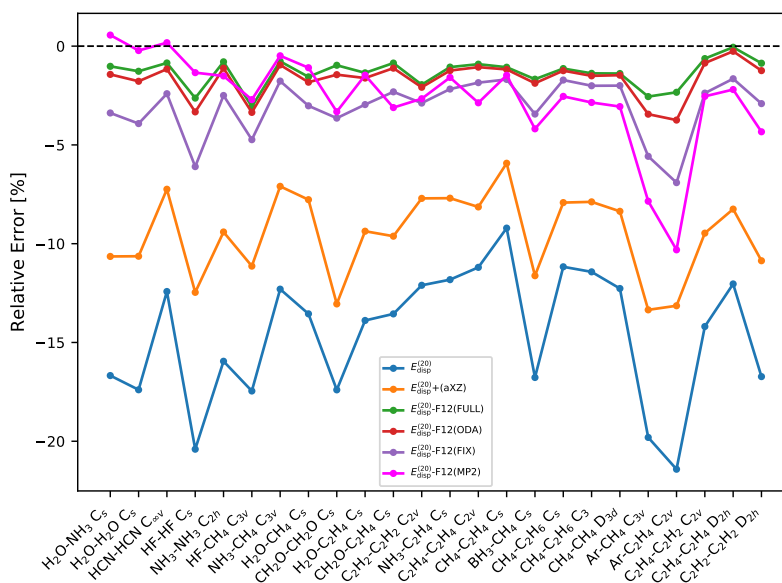
Analyzing, the  $E_{\text{exch-disp}}^{(20)}$ -F12 energies, we also noticed an accelerated basis set convergence while going from aDZ to aTZ, converging from below to the benchmark level. The FIX Ansatz is the worst performer showing only a little improvement of  $E_{\text{exch-disp}}^{(20)}$ -F12/aTZ over the conventional  $E_{\text{exch-disp}}^{(20)}/\text{aQZ}$ . In the case of  $E_{\text{exch-disp}}^{(20)}$ -F12/aDZ with the FULL and ODA Ansätze, energies are converged close to the point of conventional  $E_{\text{exch-disp}}^{(20)}/\text{aTZ}+(\text{aTZ})$ . In the aTZ basis set, the FULL and ODA amplitudes work either as well or better than  $E_{\text{exch-disp}}^{(20)}/\text{a5Z}$ .

It is of great importance to examine the basis set convergence of the sum of  $E_{\text{disp}}^{(20)}$ -F12 and  $E_{\text{exch-disp}}^{(20)}$ -F12. Again, we observed a really impressive basis set convergence for the FULL and ODA variants, as illustrated in Figures S5 and S6 in the Supporting Information of Appendix C. The sum  $E_{\text{disp}}^{(20)}$ -F12 +  $E_{\text{exch-disp}}^{(20)}$ -F12 computed in the aTZ basis is converged to the benchmark level or even lower with two exceptions of the Ar-CH<sub>4</sub> and Ar-C<sub>2</sub>H<sub>4</sub> complexes. The FIX Ansatz in the aTZ basis improves results over the

conventional  $E_{\text{disp}}^{(20)}$ -F12 +  $E_{\text{exch-disp}}^{(20)}$ -F12 sum in the aTZ+(aTZ) basis sets. Interestingly, one can notice that the  $E_{\text{disp}}^{(20)}$  +  $E_{\text{exch-disp}}^{(20)}$  with added -F12(MP2) correction computed in the aDZ or aTZ basis, generally, leads to overestimated results.

To show a larger picture of the performance of the newly developed F12-corrected dispersion, the relative errors with respect to the benchmark  $E_{\text{disp}}^{(20)}$ ,  $E_{\text{exch-disp}}^{(20)}$ , and  $E_{\text{disp}}^{(20)}$  +  $E_{\text{exch-disp}}^{(20)}$  data were calculated. The performance of our explicitly correlated methods is remarkable even in the aDZ basis set, as illustrated in Fig. 5.3. The  $E_{\text{disp}}^{(20)}$ -F12 result with

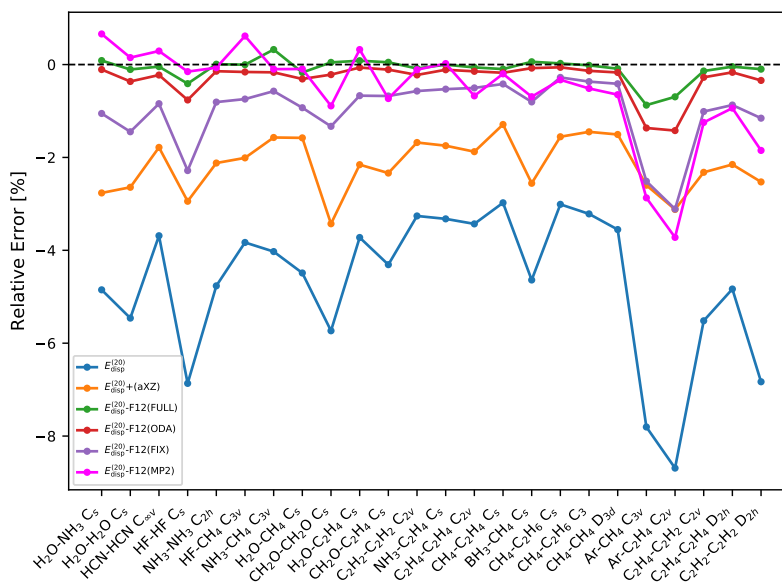
Figure 5.3: Relative errors on the A24 database [7] for  $E_{\text{disp}}^{(20)}$ -F12 computed with the aDZ/aTZ-RI basis sets. This Figure was adapted from Ref. [6].



the FULL Ansatz stands out from all examined variants, providing a maximum error of -3.1% for HF-CH<sub>4</sub>/aDZ. However,  $E_{\text{disp}}^{(20)}$ -F12 computed with ODA shows a very comparable performance leading to the largest error of -3.7% for Ar-C<sub>2</sub>H<sub>4</sub>. The fixed-amplitude Ansatz is the least accurate in the family of the SAPT-F12 approaches, with the maximum

error of -6.7% for Ar-C<sub>2</sub>H<sub>4</sub>. As it comes to SAPT-F12(MP2), this approach works well for polar complexes, but the performance degradation is noticeable for nonpolar ones. Moving on to the aTZ/aTZ-RI level,  $E_{\text{disp}}^{(20)}$ -F12 with both the FULL and ODA Ansätze provide a radical improvement over the standard  $E_{\text{disp}}^{(20)}$  (see Fig. 5.4) with mean unsigned relative errors (MUREs) values of 0.2 and 0.3%, respectively. Although the FIX and -F12(MP2)

Figure 5.4: Relative errors on the A24 database [7] for  $E_{\text{disp}}^{(20)}$ -F12 computed with the aTZ/aTZ-RI basis sets. Figure was adopted from Ref. [6].

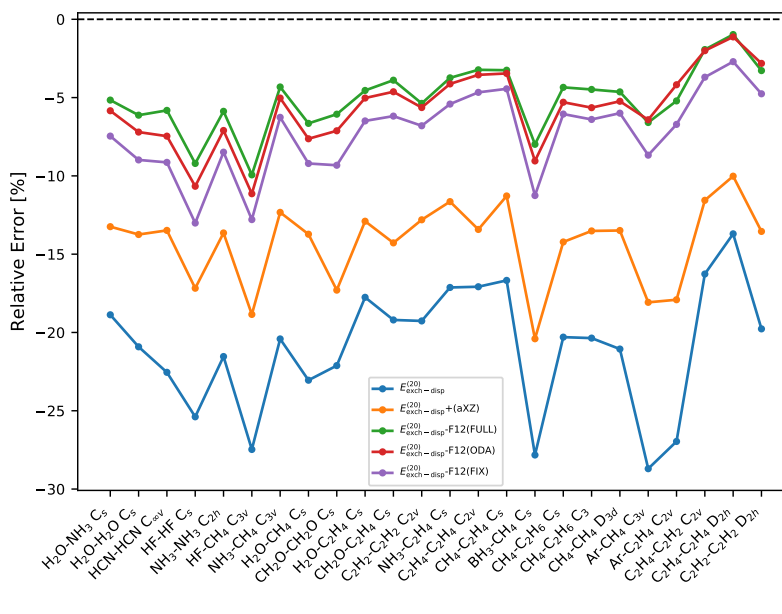


flavors are not that accurate, they still bring improvement over the standard second-order dispersion energy, leading to MURE values of 1.0 and 0.7%, respectively. Interestingly, the largest errors observed in our tests originate from complexes containing the argon atom. This trend confirms our conclusions highlighted in section 5.4, that the auxiliary basis sets for noble gas dimers are not optimized properly for dispersion calculations.



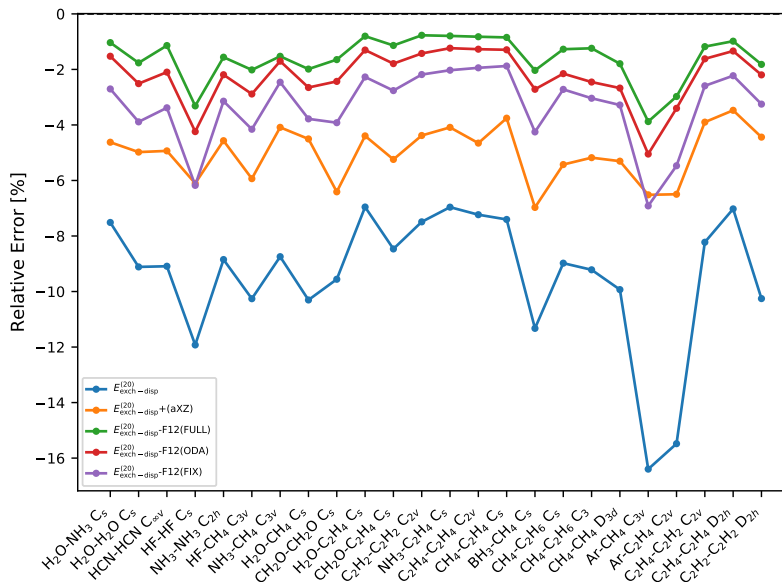
Analyzing the statistics for  $E_{\text{exch-disp}}^{(20)}$ -F12 in the aDZ/aTZ-RI basis sets (Fig. 5.5), all F12 variants lead to a very comparable performance and bring the improvement over the conventional  $E_{\text{exch-disp}}^{(20)}$ . Fig. 5.6 shows that an additional gain in the accuracy is obtained in the aTZ/aTZ-RI basis level (the largest error of -6.9% is reported for the FIX Ansatz).

Figure 5.5: Relative errors on the A24 database [7] for  $E_{\text{exch-disp}}^{(20)}$ -F12 computed with the aDZ/aTZ-RI basis sets.



In Fig. 5.7 we present the total sum  $E_{\text{disp}}^{(20)}$ -F12+ $E_{\text{exch-disp}}^{(20)}$ -F12 calculated in the aTZ/aTZ-RI basis sets. Again, the ODA flavor works as well as the FULL one. It is a very exciting observation since the former Ansatz is computationally much cheaper. The FIX Ansatz is the least accurate, but it can still be utilized to improve results over the standard SAPT0 dispersion. The -F12(MP2) variant, in most cases, overestimates the total results.

Figure 5.6: Relative errors on the A24 database [7] for  $E_{\text{exch-disp}}^{(20)}$ -F12 computed with the aTZ/aTZ-RI basis sets.



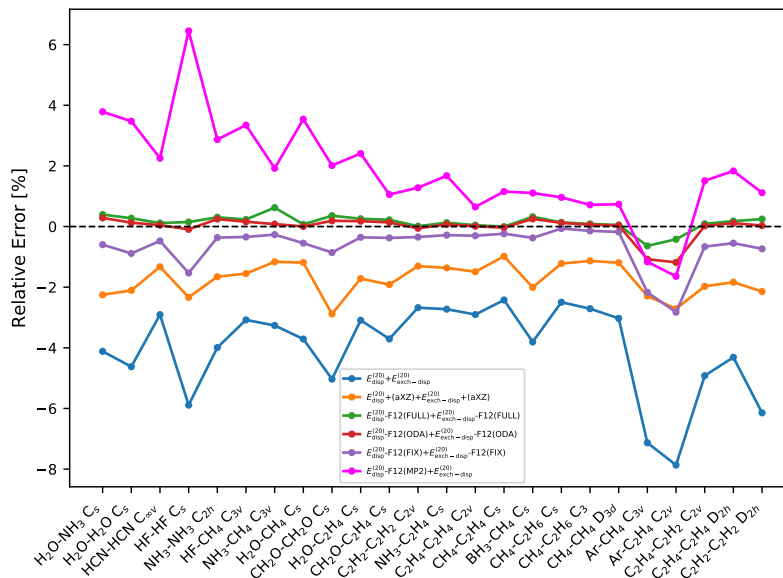
## 5.6 Density-Fitting Approximation in SAPT-F12

The bottleneck of the implementation of the  $E_{\text{disp}}^{(20)}$ -F12 and  $E_{\text{exch-disp}}^{(20)}$ -F12 methods is the integral evaluation and Fock matrix construction for the most computationally demanding step  $O(N^2 N_{aux}^2)$ , where  $N$  is the number of one-electron basis functions and  $N_{aux}$  stands for the number of auxiliary functions. In order to remove this limitation, and to speed up calculations, the density-fitting (DF) approximation [27, 28, 29] was applied.

Using the density-fitting technique, the two-electron repulsion integrals (ERI) are represented as follows:

$$K_{\lambda\rho}^{\mu\nu} \approx (\mu\nu|A)[J^{-1}]_{AB}(B|\lambda\gamma) \quad (5.27)$$

Figure 5.7: Relative errors on the A24 database [7] for the sum  $E_{\text{disp}}^{(20)} - \text{F12} + E_{\text{exch-disp}}^{(20)} - \text{F12}$  computed with the aTZ/aTZ-RI basis sets.



where the Coulomb metric  $J_{AB}$  and the three center integrals are defined as:

$$J_{AB} = \int A(r_1) \frac{1}{r_{12}} B(r_2) d^3 r_1 d^3 r_2 \quad (5.28)$$

$$(B|\lambda\sigma) = \int B(r_1) \frac{1}{r_{12}} \lambda(r_2) \sigma(r_2) d^3 r_1 d^3 r_2, \quad (5.29)$$

where  $\mu, \nu, \lambda, \rho$  are AO functions,  $A$  and  $B$  are the functions from the DF basis (which is in general different from the RI basis).

In our new F12-corrected dispersion energies, in addition to two-electron repulsion integrals, we need to fit four types of explicitly correlated integrals containing the operator:  $\hat{F}_{12}$ ,  $\hat{F}_{12}^2$ ,  $\hat{F}_{12} r_{12}^{-1}$ , and  $[[\hat{F}_{12}, \hat{t}_1 + \hat{t}_2], \hat{F}_{12}]$ . The last operator contains the commutator

between the correlation factor and the sum of kinetic energy operators for monomer A and B, respectively.

This set of integrals has to be evaluated employing density fitted formulas which are explicitly *robust* [29, 171]:

$$(pq|\hat{v}_{12}|rs)_{robust} \approx (\tilde{p}\tilde{q}|\hat{v}_{12}|rs) + (pq|\hat{v}_{12}|\tilde{r}\tilde{s}) - (\tilde{p}\tilde{q}|\hat{v}_{12}|\tilde{r}\tilde{s}). \quad (5.30)$$

The integrals are approximated by expanding each orbital product density in an auxiliary density fitting basis set, that is  $|pq\rangle \approx |\tilde{p}\tilde{q}\rangle$ . The  $\hat{v}_{12}$  operator in the above formula is a 2-electron operator, e.g.  $\hat{F}_{12}$ . This approach fulfils the condition that  $(pq|\hat{v}_{12}|rs) - (pq|\hat{v}_{12}|rs)_{robust}$  is quadratic in the fitting error. In order to find fitting coefficients, we minimize the residual:

$$\Delta_{pq}^w = (pq - \tilde{p}\tilde{q}|\hat{w}_{12}|pq - \tilde{p}\tilde{q}). \quad (5.31)$$

One can choose that  $\hat{w}_{12} = \hat{v}_{12}$ , but it is not recommended since additional charge constraints have to be assumed [29]. Therefore, the  $\hat{w}_{12} = r_{12}^{-1}$  weight factor is utilized from now on.

Applying the DF and robust DF formalism to the  $V$ ,  $X$ ,  $B$  and  $C$  intermediate matrices of Eqs. 5.10–5.14, we obtain:

$$\text{Notation :} \quad (5.32)$$

$$J_{AB} = (A|r_{12}^{-1}|B)$$

$$F_{AB} = (A|\hat{F}_{12}|B)$$

$$\begin{aligned}
K_{AB}^F &= (A|\widehat{F}_{12}r_{12}^{-1}|B) \\
F_{AB}^2 &= (A|\widehat{F}_{12}^2|B) \\
U_{AB}^F &= (A|[[\widehat{F}_{12}, \widehat{t}_1 + \widehat{t}_2], \widehat{f}_{12}]|B) \\
J_{ij}^A &= (A|r_{12}^{-1}|ij) \\
F_{ij}^A &= (A|\widehat{F}_{12}|ij) \\
K_{A,ij}^F &= (A|\widehat{F}_{12}r_{12}^{-1}|ij) \\
F_{A,ij}^2 &= (A|\widehat{F}_{12}^2|ij) \\
U_{A,ij}^F &= (A|[[\widehat{F}_{12}, \widehat{t}_1 + \widehat{t}_2], \widehat{f}_{12}]|ij) \\
D_{ij}^A &= [\mathbf{J}^{-1}]_{AB}(B|r_{12}^{-1}|ij)
\end{aligned}$$

$$\begin{aligned}
V_{kl}^{ij} &\approx D_{ik}^A K_{A,jl}^F + K_{A,ik}^F D_{jl}^A - D_{ik}^A K_{AB}^F D_{jl}^B \\
&- J_{ir}^A D_{js}^A (D_{kr}^C F_{ls}^C + F_{kr}^C D_{ls}^C - D_{kr}^C F_{CD} D_{ls}^D) \\
&- J_{ix}^A D_{jn}^A (D_{kx}^C F_{ln}^C + F_{kx}^C D_{ln}^C - D_{kx}^C F_{CD} D_{ln}^D) \\
&- J_{im}^A D_{jx}^A (D_{km}^C F_{lx}^C + F_{km}^C D_{lx}^C - D_{km}^C F_{CD} D_{lx}^D) \tag{5.33}
\end{aligned}$$

$$\begin{aligned}
X_{mn}^{kl} &\approx D_{km}^A F_{A,ln}^2 + F_{A,km}^2 D_{ln}^A - D_{km}^A F_{AB}^2 D_{ln}^B \\
&- (D_{kr}^A F_{ls}^A + F_{kr}^A D_{ls}^A - D_{kr}^A F_{AB} D_{ls}^B)(D_{mr}^C F_{ns}^C + F_{mr}^C D_{ns}^C - D_{mr}^C F_{CD} D_{ns}^D) \\
&- (D_{kx}^A F_{lv}^A + F_{kx}^A D_{lv}^A - D_{kx}^A F_{AB} D_{lv}^B)(D_{mx}^C F_{nv}^C + F_{mx}^C D_{nv}^C - D_{mx}^C F_{CD} D_{nv}^D) \\
&- (D_{ko}^A F_{lx}^A + F_{ko}^A D_{lx}^A - D_{ko}^A F_{AB} D_{lx}^B)(D_{mo}^C F_{nx}^C + F_{mo}^C D_{nx}^C - D_{mo}^C F_{CD} D_{nx}^D) \tag{5.34}
\end{aligned}$$

$$\begin{aligned}
C_{ab}^{kl} &= f_{ax}F_{xb}^{kl} + F_{ax}^{kl}f_{xb} \\
&\approx f_{ax}(D_{kx}^A F_{lb}^A + F_{kx}^A D_{lb}^A - D_{kx}^A F_{AB} D_{lb}^B) \\
&+ (D_{ka}^A F_{lx}^A + F_{ka}^A D_{lx}^A - D_{ka}^A F_{AB} D_{lx}^B) f_{xb}
\end{aligned} \tag{5.35}$$

$$\begin{aligned}
B_{kl,mn} &\approx D_{km}^A U_{A,ln}^F + U_{A,km}^F D_{ln}^A - D_{km}^A U_{AB}^F D_{ln}^B \\
&+ (D_{xm}^A (f_{xk} + k_{xk}) + D_{rm}^A (f_{rk} + k_{rk})) F_{A,ln}^2 \\
&+ (F_{A,xm}^2 (f_{xk} + k_{xk}) + F_{A,rm}^2 (f_{rk} + k_{rk})) D_{ln}^A \\
&- (D_{xm}^A (f_{xk} + k_{xk}) + D_{rm}^A (f_{rk} + k_{rk})) F_{AB}^2 D_{ln}^B \\
&+ D_{km}^A (F_{A,xn}^2 (f_{xl} + k_{xl}) + F_{A,sn}^2 (f_{sl} + k_{sl})) \\
&+ F_{A,km}^2 (D_{xn}^A (f_{xl} + k_{xl}) + D_{sn}^A (f_{sl} + k_{sl})) \\
&- D_{km}^A F_{AB}^2 (D_{xn}^B (f_{xl} + f_{xl}) + D_{sn}^B (f_{sl} + k_{sl})) \\
&- (D_{kr}^A k_{rx} + D_{kx'}^A k_{x'x}) F_{lb}^A (D_{mx}^C F_{nb}^C + F_{mx}^C D_{nb}^C - D_{mx}^C F_{CD} D_{nb}^D) \\
&- (F_{kr}^A k_{rx} + F_{kx'}^A k_{x'x}) D_{lb}^A (D_{mx}^C F_{nb}^C + F_{mx}^C D_{nb}^C - D_{mx}^C F_{CD} D_{nb}^D) \\
&+ (D_{kr}^A k_{rx} + D_{kx'}^A k_{x'x}) F_{AB} D_{lb}^B (D_{mx}^C F_{nb}^C + F_{mx}^C D_{nb}^C - D_{mx}^C F_{CD} D_{nb}^D) \\
&- D_{kx}^A (F_{ls}^A k_{sb} + F_{lx'}^A k_{x'b}) (D_{mx}^C F_{nb}^C + F_{mx}^C D_{nb}^C - D_{mx}^C F_{CD} D_{nb}^D) \\
&- F_{kx}^A (D_{ls}^A k_{sb} + D_{lx'}^A k_{x'b}) (D_{mx}^C F_{nb}^C + F_{mx}^C D_{nb}^C - D_{mx}^C F_{CD} D_{nb}^D) \\
&+ D_{kx}^A F_{AB} (D_{ls}^B k_{sb} + D_{lx'}^B k_{x'b}) (D_{mx}^C F_{nb}^C + F_{mx}^C D_{nb}^C - D_{mx}^C F_{CD} D_{nb}^D) \\
&- (D_{kr}^A k_{ra} + D_{kx'}^A k_{x'a}) F_{lx}^A (D_{ma}^C F_{nx}^C + F_{ma}^C D_{nx}^C - D_{ma}^C F_{CD} D_{nx}^D)
\end{aligned}$$

$$\begin{aligned}
& - (F_{kr}^A k_{ra} + F_{kx'}^A k_{x'a}) D_{lx}^A (D_{ma}^C F_{nx}^C + F_{ma}^C D_{nx}^C - D_{ma}^C F_{CD} D_{nx}^D) \\
& + (D_{kr}^A k_{ra} + D_{kx'}^A k_{x'a}) F_{AB} D_{lx}^B (D_{ma}^C F_{nx}^C + F_{ma}^C D_{nx}^C - D_{ma}^C F_{CD} D_{nx}^D) \\
& - D_{ka}^A (F_{ls}^A k_{sx} + F_{lx'}^A k_{x'x}) (D_{ma}^C F_{nx}^C + F_{ma}^C D_{nx}^C - D_{ma}^C F_{CD} D_{nx}^D) \\
& - F_{ka}^A (D_{ls}^A k_{sx} + D_{lx'}^A k_{x'x}) (D_{ma}^C F_{nx}^C + F_{ma}^C D_{nx}^C - D_{ma}^C F_{CD} D_{nx}^D) \\
& + D_{ka}^A F_{AB} (D_{ls}^B k_{sx} + D_{lx'}^B k_{x'x}) (D_{ma}^C F_{nx}^C + F_{ma}^C D_{nx}^C - D_{ma}^C F_{CD} D_{nx}^D) \\
& - (D_{kr}^A k_{rx} + D_{kx'}^A k_{x'x}) F_{ly}^A (D_{mx}^C F_{ny}^C + F_{mx}^C D_{ny}^C - D_{mx}^C F_{CD} D_{ny}^D) \\
& - (F_{kr}^A k_{rx} + F_{kx'}^A k_{x'x}) D_{ly}^A (D_{mx}^C F_{ny}^C + F_{mx}^C D_{ny}^C - D_{mx}^C F_{CD} D_{ny}^D) \\
& + (D_{kr}^A k_{rx} + D_{kx'}^A k_{x'x}) F_{AB} D_{ly}^B (D_{mx}^C F_{ny}^C + F_{mx}^C D_{ny}^C - D_{mx}^C F_{CD} D_{ny}^D) \\
& - D_{kx}^A (F_{ls}^A k_{sy} + F_{lx'}^A k_{x'y}) (D_{mx}^C F_{ny}^C + F_{mx}^C D_{ny}^C - D_{mx}^C F_{CD} D_{ny}^D) \\
& - F_{kx}^A (D_{ls}^A k_{sy} + D_{lx'}^A k_{x'y}) (D_{mx}^C F_{ny}^C + F_{mx}^C D_{ny}^C - D_{mx}^C F_{CD} D_{ny}^D) \\
& + D_{kx}^A F_{AB} (D_{ls}^B k_{sy} + D_{lx'}^B k_{x'y}) (D_{mx}^C F_{ny}^C + F_{mx}^C D_{ny}^C - D_{mx}^C F_{CD} D_{ny}^D) \\
& - (D_{kr'}^A (f_{r'r} + k_{r'r}) + D_{kx}^A (f_{xr} + k_{xr})) \\
& \quad \times F_{ls}^A (D_{mr}^C F_{ns}^C + F_{mr}^C D_{ns}^C - D_{mr}^C F_{CD} D_{ns}^{CD}) \\
& - (F_{kr'}^A (f_{r'r} + k_{r'r}) + F_{kx}^A (f_{xr} + k_{xr})) \\
& \quad \times D_{ls}^A (D_{mr}^C F_{ns}^C + F_{mr}^C D_{ns}^C - D_{mr}^C F_{CD} D_{ns}^{CD}) \\
& + (D_{kr'}^A (f_{r'r} + k_{r'r}) + D_{kx}^A (f_{xr} + k_{xr})) \\
& \quad \times F_{AB} D_{ls}^B (D_{mr}^C F_{ns}^C + F_{mr}^C D_{ns}^C - D_{mr}^C F_{CD} D_{ns}^{CD}) \\
& - (D_{kr}^A (f_{rx} + k_{rx}) + D_{kx'}^A (f_{x'x} + k_{x'x})) \\
& \quad \times F_{lv}^A (D_{mx}^C F_{nv}^C + F_{mx}^C D_{nv}^C - D_{mx}^C F_{CD} D_{nv}^D) \\
& - (F_{kr}^A (f_{rx} + k_{rx}) + F_{kx'}^A (f_{x'x} + k_{x'x})) \\
& \quad \times D_{lv}^A (D_{mx}^C F_{nv}^C + F_{mx}^C D_{nv}^C - D_{mx}^C F_{CD} D_{nv}^D)
\end{aligned}$$

$$\begin{aligned}
& + (D_{kr}^A(f_{rx} + k_{rx}) + D_{kx'}^A(f_{x'x} + k_{x'x})) \\
& \quad \times F_{AB}D_{lv}^B(D_{mx}^C F_{nv}^C + F_{mx}^C D_{nv}^C - D_{mx}^C F_{CD}D_{nv}^D) \\
& - (D_{kr}^A(f_{ro} + k_{ro}) + D_{kx}^A(f_{xo} + k_{xo})) \\
& \quad \times F_{lx}^A(D_{mo}^C F_{nx}^C + F_{mo}^C D_{nx}^C - D_{mo}^C F_{CD}D_{nx}^D) \\
& - (F_{kr}^A(f_{ro} + k_{ro}) + F_{kx}^A(f_{xo} + k_{xo}))D_{lx}^A \\
& \quad \times (D_{mo}^C F_{nx}^C + F_{mo}^C D_{nx}^C - D_{mo}^C F_{CD}D_{nx}^D) \\
& + (D_{kr}^A(f_{ro} + k_{ro}) + D_{kx}^A(f_{xo} + k_{xo})) \\
& \quad \times F_{AB}D_{lx}^B(D_{mo}^C F_{nx}^C + F_{mo}^C D_{nx}^C - D_{mo}^C F_{CD}D_{nx}^D) \\
& - D_{kr}^A(F_{ls'}^A(f_{s's} + k_{s's}) + F_{lx}^A(f_{xs} + k_{xs})) \\
& \quad \times (D_{mr}^C F_{ns}^C + F_{mr}^C D_{ns}^C - D_{mr}^C F_{CD}D_{ns}^D) \\
& - F_{kr}^A(D_{ls'}^A(f_{s's} + k_{s's}) + D_{lx}^A(f_{xs} + k_{xs})) \\
& \quad \times (D_{mr}^C F_{ns}^C + F_{mr}^C D_{ns}^C - D_{mr}^C F_{CD}D_{ns}^D) \\
& + D_{kr}^A F_{AB}(D_{ls'}^B(f_{s's} + k_{s's}) + D_{lx}^B(f_{xs} + k_{xs})) \\
& \quad \times (D_{mr}^C F_{ns}^C + F_{mr}^C D_{ns}^C - D_{mr}^C F_{CD}D_{ns}^D) \\
& - D_{kx}^A(F_{ls}^A(f_{sv} + k_{sv}) + F_{lx}^A(f_{xv} + k_{xv})) \\
& \quad \times (D_{mx}^C F_{nv}^C + F_{mx}^C D_{nv}^C - D_{mx}^C F_{CD}D_{nv}^D) \\
& - F_{kx}^A(D_{ls}^A(f_{sv} + k_{sv}) + D_{lx}^A(f_{xv} + k_{xv})) \\
& \quad \times (D_{mx}^C F_{nv}^C + F_{mx}^C D_{nv}^C - D_{mx}^C F_{CD}D_{nv}^D) \\
& + D_{kx}^A F_{AB}(D_{ls}^B(f_{sv} + k_{sv}) + D_{lx}^B(f_{xv} + k_{xv})) \\
& \quad \times (D_{mx}^C F_{nv}^C + F_{mx}^C D_{nv}^C - D_{mx}^C F_{CD}D_{nv}^D) \\
& - D_{ko}^A(F_{ls}^A(f_{sx} + k_{sx}) + F_{lx'}^A(f_{x'x} + k_{x'x}))
\end{aligned}$$



$$\begin{aligned}
& \times (D_{mo}^C F_{nx}^C + F_{mo}^C D_{nx}^C - D_{mo}^C F_{CD} D_{nx}^D) \\
- & F_{ko}^A (D_{ls}^A (f_{sx} + k_{sx}) + D_{lx'}^A (f_{x'x} + k_{x'x})) \\
& \times (D_{mo}^C F_{nx}^C + F_{mo}^C D_{nx}^C - D_{mo}^C F_{CD} D_{nx}^D) \\
+ & D_{ko}^A F_{AB} (D_{ls}^B (f_{sx} + k_{sx}) + D_{lx'}^B (f_{x'x} + k_{x'x})) \\
& \times (D_{mo}^C F_{nx}^C + F_{mo}^C D_{nx}^C - D_{mo}^C F_{CD} D_{nx}^D) \\
- & (D_{ka}^A F_{lb}^A + F_{ka}^A D_{lb}^A - D_{ka}^A F_{AB} D_{lb}^B) f_{ax} (D_{mx}^C F_{nb}^C + F_{mx}^C D_{nb}^C - D_{mx}^C F_{CD} D_{nb}^D) \\
- & (D_{ka}^A F_{lb}^A + F_{ka}^A D_{lb}^A - D_{ka}^A F_{AB} D_{lb}^B) (D_{ma}^C F_{nx}^C + F_{ma}^C D_{nx}^C - D_{ma}^C F_{CD} D_{nx}^D) f_{xb}
\end{aligned} \tag{5.36}$$

Note that in the above formulas  $f_{kx}$  and  $k_{kx}$  are matrix elements of the Fock and exchange operators computed in various bases.

The density-fitted explicitly correlated second-order exchange-dispersion energy, DF- $E_{\text{exch-disp}}^{(20)}$ -F12, is expressed as follows:

$$\begin{aligned}
E_{\text{exch-disp}}^{(20)}\text{-F12} &= 2T_{kl}^{ij} [(D_{kx}^A F_{lb}^A + F_{kx}^A D_{lb}^A - D_{kx}^A F_{AB} D_{lb}^B) J_{xi}^C D_{b'j}^C S_i^b S_{b'}^{i'} \\
&- 2(D_{kx}^A F_{lb}^A + F_{kx}^A D_{lb}^A - D_{kx}^A F_{AB} D_{lb}^B) J_{xi}^C D_{b'j}^C S_i^b S_{b'}^{i'} \\
&+ (D_{ka}^A F_{ly}^A + F_{ka}^A D_{ly}^A - D_{ka}^A F_{AB} D_{ly}^B) J_{a'i}^C D_{yj}^C S_j^a S_{a'}^{j'} \\
&- 2(D_{ka}^A F_{ly}^A + F_{ka}^A D_{ly}^A - D_{ka}^A F_{AB} D_{ly}^B) J_{a'i}^C D_{yj}^C S_j^a S_{a'}^{j'} \\
&- 2(D_{kx}^A F_{lb}^A + F_{kx}^A D_{lb}^A - D_{kx}^A F_{AB} D_{lb}^B) ((V_B)_i^x + 2J_{xi}^C D_{vv}^C) S_i^b S_j^{i'} \\
&+ (D_{kx}^A F_{lb}^A + F_{kx}^A D_{lb}^A - D_{kx}^A F_{AB} D_{lb}^B) ((V_B)_{i'}^x + 2J_{xi}^C D_{vv}^C) S_i^b S_j^{i'} \\
&- (D_{ka}^A F_{ly}^A + F_{ka}^A D_{ly}^A - D_{ka}^A F_{AB} D_{ly}^B) ((V_B)_i^y + 2J_{yi}^C D_{vv}^C) S_j^a \\
&- 2(D_{ka}^A F_{ly}^A + F_{ka}^A D_{ly}^A - D_{ka}^A F_{AB} D_{ly}^B) ((V_A)_j^y + 2J_{oo}^C D_{yj}^C) S_j^a S_i^{j'}
\end{aligned}$$

$$\begin{aligned}
& + (D_{ka}^A F_{ly}^A + F_{ka}^A D_{ly}^A - D_{ka}^A F_{AB} D_{ly}^B)((V_A)_{j'}^y + 2J_{oo}^C D_{yj'}^C) S_j^a S_i^{j'} \\
& - (D_{kx}^A F_{lb}^A + F_{kx}^A D_{lb}^A - D_{kx}^A F_{AB} D_{lb}^B)((V_A)_j^x + 2J_{oo}^C D_{xj}^C) S_i^b \\
& - (D_{ki'}^A K_{A,lj'}^F + K_{A,ki'}^F D_{lj'}^A - D_{ki'}^A K_{AB}^F D_{lj'}^B) S_i^{j'} S_j^{i'} \\
& + 2(D_{ki}^A K_{A,lj'}^F + K_{A,ki}^F D_{lj'}^A - D_{ki}^A K_{AB}^F D_{lj'}^B) S_i^{j'} S_j^{i'} \\
& + 2(D_{ki'}^A K_{A,lj}^F + K_{A,ki'}^F D_{lj}^A - D_{ki'}^A K_{AB}^F D_{lj}^B) S_i^{j'} S_j^{i'} \\
& - (D_{li}^A K_{A,kj}^F + K_{A,li}^F D_{kj}^A - D_{li}^A K_{AB}^F D_{kj}^B) \\
& + (D_{li'}^A F_{kj'}^A + F_{li'}^A D_{kj'}^A - D_{li'}^A F_{AB} D_{kj'}^B) J_{i'i}^C D_{j'j}^C \\
& + (D_{la}^A F_{kj'}^A + F_{la}^A D_{kj'}^A - D_{la}^A F_{AB} D_{kj'}^B) J_{ai}^C D_{j'j}^C \\
& + (D_{li'}^A F_{kb}^A + F_{li'}^A D_{kb}^A - D_{li'}^A F_{AB} D_{kb}^B) J_{i'i}^C D_{bj}^C \\
& + (D_{lx}^A F_{kj'}^A + F_{lx}^A D_{kj'}^A - D_{lx}^A F_{AB} D_{kj'}^B) J_{xi}^C D_{j'j}^C \\
& + (D_{li'}^A F_{ky}^A + F_{li'}^A D_{ky}^A - D_{li'}^A F_{AB} D_{ky}^B) J_{i'i}^C D_{yj}^C \\
& + (D_{kx}^A F_{ln}^A + F_{kx}^A D_{ln}^A - D_{kx}^A F_{AB} D_{ln}^B) J_{ai}^C D_{xj}^C S_a^n \\
& + (D_{km}^A F_{ly}^A + F_{km}^A D_{ly}^A - D_{km}^A F_{AB} D_{ly}^B) J_{yi}^C D_{bj}^C S_b^m \\
& + (D_{kr}^A F_{ls}^A + F_{kr}^A D_{ls}^A - D_{kr}^A F_{AB} D_{ls}^B) J_{ai}^C D_{bj}^C S_a^s S_b^r \\
& + (D_{kx}^A F_{ln}^A + F_{kx}^A D_{ln}^A - D_{kx}^A F_{AB} D_{ln}^B) J_{xi'}^C D_{nj'}^C S_i^{j'} S_j^{i'} \\
& + (D_{km}^A F_{ly}^A + F_{km}^A D_{ly}^A - D_{km}^A F_{AB} D_{ly}^B) J_{mi'}^C D_{yj'}^C S_i^{j'} S_j^{i'} \\
& + (D_{kr}^A F_{ls}^A + F_{kr}^A D_{ls}^A - D_{kr}^A F_{AB} D_{ls}^B) J_{ri'}^C D_{sj'}^C S_i^{j'} S_j^{i'} \\
& - 2(D_{kx}^A F_{ln}^A + F_{kx}^A D_{ln}^A - D_{kx}^A F_{AB} D_{ln}^B) J_{xi}^C D_{nj'}^C S_i^{j'} S_j^{i'} \\
& - 2(D_{km}^A F_{ly}^A + F_{km}^A D_{ly}^A - D_{km}^A F_{AB} D_{ly}^B) J_{mi}^C D_{yj'}^C S_i^{j'} S_j^{i'} \\
& - 2(D_{kr}^A F_{ls}^A + F_{kr}^A D_{ls}^A - D_{kr}^A F_{AB} D_{ls}^B) J_{ri}^C D_{sj'}^C S_i^{j'} S_j^{i'} \\
& - 2(D_{kx}^A F_{ln}^A + F_{kx}^A D_{ln}^A - D_{kx}^A F_{AB} D_{ln}^B) J_{xi'}^C D_{nj}^C S_i^{j'} S_j^{i'}
\end{aligned}$$

$$\begin{aligned}
& - 2(D_{km}^A F_{ly}^A + F_{km}^A D_{ly}^A - D_{km}^A F_{AB} D_{ly}^B) J_{mi}^C D_{yj}^C S_i^{j'} S_{j'}^{i'} \\
& - 2(D_{kr}^A F_{ls}^A + F_{kr}^A D_{ls}^A - D_{kr}^A F_{AB} D_{ls}^B) J_{ri}^C D_{sj}^C S_i^{j'} S_{j'}^{i'} \quad (5.37)
\end{aligned}$$

The DF- $E_{\text{disp}}^{(20)}$ -F12(ODA) and DF- $E_{\text{exch-disp}}^{(20)}$ -F12(ODA) algorithms have been implemented in the PSI4NUMPY framework [172]. Although the optimization of the code is currently in progress, the DF approach dramatically improves the performance over the non-DF variant (see Table 5.2).

Table 5.2: The calculation times (in s) for the DF and non-DF  $E_{\text{disp}}^{(20)}$ -F12(ODA)+ $E_{\text{exch-disp}}^{(20)}$ -F12(ODA) corrections performed on the Hopper Supercomputer at Auburn University using 1 core. The results do not include the time for SCF calculations.

basis	non-DF	DF
	H <sub>2</sub> O–H <sub>2</sub> O	
aDZ/aDZ-RI	759.04	20.03
aTZ/aTZ-RI	4393.62	72.18
aQZ/aQZ-RI	34758.14	348.12
a5Z/a5Z-RI	688424.07	1278.98
	CH <sub>4</sub> –CH <sub>4</sub>	
aDZ/aDZ-RI	2798.12	43.58
aTZ/aTZ-RI	20057.72	191.44
aQZ/aQZ-RI	478924.25	914.21
a5Z/a5Z-RI	no result	4199.16

## 5.7 Summary

In this work, we presented and tested a novel development in SAPT, that is SAPT-F12. The F12 techniques significantly boost the basis sets convergence of the SAPT dispersion and exchange dispersion energy, resulting in the F12 calculations in an  $X$ -tuple zeta basis about as accurate as conventional calculations in bases with cardinal numbers  $(X + 2)$  for

$E_{\text{disp}}^{(20)}$  and either  $(X + 1)$  or  $(X + 2)$  for  $E_{\text{exch-disp}}^{(20)}$ . We also succeeded in finding an approximation, Optimized Diagonal Ansatz (ODA), which is computationally very efficient (scales like  $O(N^5)$ ), free from numerical issues, and leading to the accuracy comparable to the fully optimized-amplitude approach. Moreover, the density-fitted explicitly correlated dispersion and exchange dispersion methods were presented for the first time, bringing excellent performance. However, it should be noted that the DF- $E_{\text{disp}}^{(20)}$ -F12(ODA) and DF- $E_{\text{exch-disp}}^{(20)}$ -F12(ODA) implementations are not yet optimal and further work is underway to reduce the cost of these methods.

## Chapter 6

### Conclusions

In this work, in an attempt to compute high-accuracy interaction energies of triply bound systems, the characteristic points on the CO–CO, N<sub>2</sub>–N<sub>2</sub>, and CO–N<sub>2</sub> potential energy surfaces were studied. At the frozen core CCSD(T) level, the basis space was saturated utilizing a combination of midbond functions, basis set extrapolation, and explicit correlation. In order to ensure the spectroscopic accuracy, the post-CCSD(T) corrections, relativistic effects, and core-core and core-valence correlations were included. The importance of higher-orders of coupled cluster theory, which may have a critical impact on the shape of the potential energy surface, was highlighted for triply bound systems.

The new forms of damping functions for the DFT-D3 approach were presented. The models were designed based on a linear combination of error functions and a piecewise-linear function. We also explored the possibility of constructing a damped dispersion function without higher than  $C_6$  dispersion coefficients. The testing of new damping functions showed that they were unable to improve the performance over the -D3M and -D3M(BJ) variants without including an empirical  $s_8$  factor. One limitation of DFT-D3 may originate from the van der Waals coefficients  $C_6$  and  $C_8$  as well as the cutoff radius  $R_0^{AB}$  not being

sufficiently precise. However, it seems that the currently utilized damping functions in the DFT-D3 method are unable to reproduce effects at the short range which may be missing in the DFT functionals.

The explicitly correlated dispersion and exchange dispersion energies,  $E_{\text{disp}}^{(20)}$ -F12 and  $E_{\text{exch-disp}}^{(20)}$ -F12, were derived and implemented within the PSI4NUMPY framework. The most efficient and accurate approximation, Optimized Diagonal Ansatz (ODA), was proposed. The DF algorithm was applied to the explicitly correlated dispersion and exchange dispersion corrections, DF- $E_{\text{disp}}^{(20)}$ -F12(ODA) and DF- $E_{\text{exch-disp}}^{(20)}$ -F12(ODA), resulting in a remarkable speedup. This step is crucial to extend the SAPT-F12 calculations to medium and large systems.

## 6.1 Future and Outlook

There are many directions to continue the development of SAPT-F12. In the first step, the DF- $E_{\text{disp}}^{(20)}$ -F12(ODA) and DF- $E_{\text{exch-disp}}^{(20)}$ -F12(ODA) implementation will be ported to the public version of the PSI4 quantum chemistry program [173]. There is also ongoing massively parallel implementation of F12 dispersion in LS-Dalton [174]. Another direction is to apply the F12 formalism to the intramolecular  $E_{\text{disp}}^{(21)}$  correlation contribution and higher-order dispersion corrections.

## Bibliography

- [1] C. Hättig, W. Klopper, A. Köhn, and D. P. Tew, *Chem. Rev.* **112**, 4 (2012).
- [2] S. Grimme, J. Antony, S. Ehrlich, and H. Krieg, *J. Chem. Phys.* **132**, 154104 (2010).
- [3] S. Grimme, S. Ehrlich, and L. Goerigk, *J. Comput. Chem.* **32**, 1456 (2011).
- [4] D. G. A. Smith, L. A. Burns, K. Patkowski, and C. D. Sherrill, *J. Phys. Chem. Lett.* **7**, 2197 (2016).
- [5] M. Schütz, G. Rauhut, and H.-J. Werner, *J. Phys. Chem. A* **102**, 5997 (1998).
- [6] M. Kodrycka, C. Holzer, W. Klopper, and K. Patkowski, *J. Chem. Theory Comput.* **15**, 5965 (2019).
- [7] J. Řezáč and P. Hobza, *J. Chem. Theory Comput.* **9**, 2151 (2013).
- [8] M. Dubecký, M. Lubos, and P. Jurečka, *Chem. Rev.* **116**, 5188 (2016).
- [9] R. Sure and S. Grimme, *J. Chem. Theory Comput.* **11**, 3785 (2015).
- [10] R. Eisenschitz and F. London, *Eur. Phys. J. A* **60**, 491 (1930).
- [11] F. London, *Trans. Faraday Soc.* **33** (1937).
- [12] S. Grimme, C. Mück-Lichtenfeld, and J. Antony, *Phys. Chem. Chem. Phys.* **10**, 3327 (2008).
- [13] K. Autumn, M. Sitti, Y. A. Liang, A. M. Peattie, W. R. Hansen, S. Sponberg, T. W. Kenny, R. Fearing, J. N. Israelachvili, and R. J. Full, *Proc. Natl. Acad. Sci. U.S. A.* **99**, 12252 (2002).

- [14] S. Kotochigova, *New J. Phys.* **12**, 073041 (2010).
- [15] S. Hanlon, *Biochem. Biophys. Res. Commun.* **23**, 861 (1966).
- [16] M. D. Wodrich, C. S. Wannere, Y. Mo, P. D. Jarowski, K. N. Houk, and P. R. Schleyer, *Chem. Eur. J.* **13**, 7731 (2007).
- [17] P. R. Schreiner, L. V. Chernish, P. A. Gunchenko, E. Y. Tikhonchuk, H. Hausmann, M. Serafin, S. Schlecht, J. E. P. Dahl, R. M. K. Carlson, and A. A. Fokin, *Nature* **477**, 308 (2011).
- [18] J. P. Wagner and P. R. Schreiner, *Angew. Chem. Int. Ed.* **54**, 12274 (2015).
- [19] K. Raghavachari, G. W. Trucks, J. A. Pople, and M. Head-Gordon, *Chem. Phys. Lett.* **157**, 479 (1989).
- [20] B. Jeziorski, R. Moszyński, and K. Szalewicz, *Chem. Rev.* **94**, 1887 (1994).
- [21] K. Szalewicz, *WIREs Comput. Mol. Sci.* **2**, 254 (2012).
- [22] E. Caldeweyher, C. Bannwarth, and S. Grimme, *J. Chem. Phys.* **147**, 034112 (2017).
- [23] A. S. Christensen, T. Kubař, Q. Cui, and M. Elstner, *Chem. Rev.* **116**, 5301 (2016).
- [24] J. O. Behler, *J. Chem. Phys.* **145**, 219901 (2016).
- [25] K. Patkowski, in *Annual Reports in Computational Chemistry*, edited by D. A. Dixon (Elsevier, Amsterdam, 2017), vol. 13, pp. 3–91.
- [26] J. A. Frey, C. Holzer, W. Klopper, and S. Leutwyler, *Chem. Rev.* **116**, 5614 (2016).
- [27] B. I. Dunlap, *Phys. Chem. Chem. Phys.* **2**, 2113 (2000).
- [28] H.-J. Werner, F. R. Manby, and P. J. Knowles, *J. Chem. Phys.* **118**, 8149 (2003).
- [29] F. R. Manby, *J. Chem. Phys.* **119**, 4607 (2003).
- [30] E. Schrödinger, In *Collected Papers on Wave Mechanics* **79(4)**, 361 (1926).
- [31] E. Schrödinger, Chelsea Publishing Company: New York, N.Y, Translated from the second German edition ed. (1978).
- [32] M. Born and R. Oppenheimer, *Ann. Phys.* **389**, 457 (1927).
- [33] F. D. Pacati and S. Boffi, *Phys. Rev. C* **2**, 1205 (1970).



- [34] C. C. Roothaan, *Rev. Mod. Phys.* **23**(2), 61 (1951).
- [35] A. Szabo and N. Ostlund, *Modern Quantum Chemistry: Introduction to Advanced Electronic Structure Theory* (McGraw-Hill: New York, 1989).
- [36] J. Čížek, *J. Chem. Phys.* **45**, 4256 (1966).
- [37] J. Čížek and J. Paldus, *Int. J. Quantum Chem.* **5**, 359 (1971).
- [38] A. Bartelt, J. D. Close, F. Federmann, K. Hoffmann, N. Quaas, and J. P. Toennies, *Z. Phys. D* **39**, 1 (1997).
- [39] L. Šimová, J. Řezáč, and P. Hobza, *J. Chem. Theory Comput.* **9**, 3420 (2013).
- [40] J. O. Hirschfelder, *Chem. Phys. Lett.* **1**, 343 (1967).
- [41] E. G. Hohenstein and C. D. Sherrill, *J. Chem. Phys.* **133**, 014101 (2010).
- [42] T. Caves and M. Karplus, *J. Chem. Phys.* **50**, 3649 (1969).
- [43] T. M. Parker, L. A. Burns, R. M. Parrish, A. G. Ryno, and C. D. Sherrill, *J. Chem. Phys.* **140**, 094106 (2014).
- [44] T. Helgaker, W. Klopper, H. Koch, and J. Noga, *J. Chem. Phys.* **106**, 9639 (1997).
- [45] A. Halkier, T. Helgaker, P. Jørgensen, W. Klopper, H. Koch, J. Olsen, and A. K. Wilson, *Chem. Phys. Lett.* **286**, 243 (1998).
- [46] F.-M. Tao and W. Klemperer, *J. Chem. Phys.* **99**, 5976 (1993).
- [47] H. L. Williams, E. M. Mas, K. Szalewicz, and B. Jeziorski, *J. Chem. Phys.* **103**, 7374 (1995).
- [48] F.-M. Tao, *Int. Rev. Phys. Chem.* **20**, 617 (2001).
- [49] T. Kato, *Commun. Pure Appl. Math.* **10**, 151 (1957).
- [50] L. Kong, F. A. Bischoff, and E. F. Valeev, *Chem. Rev.* **112**, 75 (2012).
- [51] A. Grüneis, S. Hirata, Y. Ohnishi, and S. Ten-no, *J. Chem. Phys.* **146**, 080901 (2017).
- [52] T. Shiozaki and H.-J. Werner, *J. Chem. Phys.* **133**, 141103 (2010).

- [53] S. Kedžuch, O. Demel, J. Pittner, S. Ten-no, and J. Noga, Chem. Phys. Lett. **511**, 418 (2011).
- [54] E. A. Hylleraas, Z. Phys. **54**, 347 (1929).
- [55] W. Kutzelnigg, Theor. Chim. Acta **68**, 445 (1985).
- [56] W. Kutzelnigg and W. Klopper, J. Chem. Phys. **94**, 1985 (1991).
- [57] W. Klopper and W. Kutzelnigg, J. Chem. Phys. **94**, 2020 (1991).
- [58] W. Klopper and C. C. M. Samson, J. Chem. Phys. **116**, 6397 (2002).
- [59] H.-J. Werner, T. B. Adler, and F. R. Manby, J. Chem. Phys. **126**, 164102 (2007).
- [60] H. Fliegl, W. Klopper, and C. Hättig, J. Chem. Phys. **122**, 084107 (2005).
- [61] D. P. Tew, W. Klopper, C. Neiss, and C. Hättig, Phys. Chem. Chem. Phys. **9**, 1921 (2007).
- [62] T. B. Adler, G. Knizia, and H.-J. Werner, J. Chem. Phys. **127**, 221106 (2007).
- [63] G. Knizia, T. B. Adler, and H.-J. Werner, J. Chem. Phys. **130**, 054104 (2009).
- [64] C. Hättig, D. P. Tew, and A. Köhn, J. Chem. Phys. **132**, 231102 (2010).
- [65] S. Ten-no, Chem. Phys. Lett. **398**, 56 (2004).
- [66] D. P. Tew and W. Klopper, J. Chem. Phys. **123**, 074101 (2005).
- [67] D. P. Tew and W. Klopper, J. Chem. Phys. **125**, 094302 (2006).
- [68] O. Marchetti and H.-J. Werner, Phys. Chem. Chem. Phys. **10**, 3400 (2008).
- [69] E. Kordel, C. Villani, and W. Klopper, J. Chem. Phys. **122**, 214306 (2005).
- [70] E. Kordel, C. Villani, and W. Klopper, Mol. Phys. **105**, 2565 (2007).
- [71] T. Shiozaki, M. Kamiya, S. Hirata, and E. F. Valeev, J. Chem. Phys. **129**, 071101 (2008).
- [72] A. Köhn, G. W. Richings, and D. P. Tew, J. Chem. Phys. **129**, 201103 (2008).
- [73] E. F. Valeev, Phys. Chem. Chem. Phys. **10**, 106 (2008).

- [74] M. Torheyden and E. F. Valeev, *Phys. Chem. Chem. Phys.* **10**, 3410 (2008).
- [75] M. Torheyden and E. F. Valeev, *J. Chem. Phys.* **131**, 171103 (2009).
- [76] T. Yanai and T. Shiozaki, *J. Chem. Phys.* **136**, 084107 (2012).
- [77] A. Köhn, *J. Chem. Phys.* **130**, 131101 (2009).
- [78] M. S. Marshall and C. D. Sherrill, *J. Chem. Theory Comput.* **7**, 3978 (2011).
- [79] O. Marchetti and H.-J. Werner, *J. Phys. Chem. A* **113**, 11580 (2009).
- [80] K. M. de Lange and J. R. Lane, *J. Chem. Phys.* **134**, 034301 (2011).
- [81] J. D. McMahon and J. R. Lane, *J. Chem. Phys.* **135**, 154309 (2011).
- [82] K. Patkowski, *J. Chem. Phys.* **137**, 034103 (2012).
- [83] N. N. Dutta and K. Patkowski, *J. Chem. Theory Comput.* **14**, 3053 (2018).
- [84] D. A. Sirianni, L. A. Burns, and C. D. Sherrill, *J. Chem. Theory Comput.* **13**, 86 (2017).
- [85] Y. W. Robert G. Parr, *Density Functional Theory of Atoms and Molecules* (Oxford University Press, New York, 1989).
- [86] P. Hohenberg and W. Kohn, *Phys. Rev.* **136**, B864 (1964).
- [87] J. P. Perdew and K. Schmidt, *AIP Conference Proceedings* **577**, 1 (2001).
- [88] J. P. Perdew, A. Ruzsinszky, J. Tao, V. N. Staroverov, G. E. Scuseria, and G. I. Csonka, *J. Chem. Phys.* **123**, 062201 (2005).
- [89] J. Klimeš and A. Michaelides, *J. Chem. Phys.* **137**, 120901 (2012).
- [90] Y. Zhao and D. G. Truhlar, *J. Chem. Theory Comput.* **3**, 289 (2007).
- [91] O. A. von Lilienfeld, I. Tavernelli, U. Rothlisberger, and D. Sebastiani, *Phys. Rev. Lett.* **93**, 153004 (2004).
- [92] S. Grimme, *J. Comput. Chem.* **25**, 1463 (2004).
- [93] S. Grimme, *J. Comput. Chem.* **27**, 1787 (2006).
- [94] A. D. Becke and E. R. Johnson, *J. Chem. Phys.* **122**, 154104 (2005).

- [95] E. R. Johnson and A. D. Becke, *J. Chem. Phys.* **123**, 024101 (2005).
- [96] A. D. Becke and E. R. Johnson, *J. Chem. Phys.* **127**, 124108 (2007).
- [97] A. Tkatchenko and M. Scheffler, *Phys. Rev. Lett.* **102**, 073005 (2009).
- [98] M. Dion, H. Rydberg, E. Schröder, D. C. Langreth, and B. I. Lundqvist, *Phys. Rev. Lett.* **92**, 246401 (2004).
- [99] K. Lee, E. D. Murray, L. Kong, B. I. Lundqvist, and D. C. Langreth, *Phys. Rev. B* **82**, 081101 (2010).
- [100] O. A. Vydrov and T. Van Voorhis, *Phys. Rev. Lett.* **103**, 063004 (2009).
- [101] O. A. Vydrov and T. Van Voorhis, *J. Chem. Phys.* **133**, 244103 (2010).
- [102] A. Tkatchenko, R. A. DiStasio, Jr., R. Car, and M. Scheffler, *Phys. Rev. Lett.* **108**, 236402 (2012).
- [103] F. Furche, *Phys. Rev. B* **64**, 195120 (2001).
- [104] S. F. Boys and F. Bernardi, *Mol. Phys.* **19**, 553 (1970).
- [105] D. E. Woon and T. H. Dunning Jr., *J. Chem. Phys.* **103**, 4572 (1995).
- [106] R. A. Kendall, T. H. Dunning Jr., and R. J. Harrison, *J. Chem. Phys.* **96**, 6796 (1992).
- [107] W. A. de Jong, R. J. Harrison, and D. A. Dixon, *J. Chem. Phys.* **114**, 48 (2001).
- [108] F. Weigend, A. Köhn, and C. Hättig, *J. Chem. Phys.* **116**, 3175 (2002).
- [109] F. Weigend, *Phys. Chem. Chem. Phys.* **4**, 4285 (2002).
- [110] J. Řezáč, L. Šimová, and P. Hobza, *J. Chem. Theory Comput.* **9**, 364 (2013).
- [111] D. G. A. Smith, P. Jankowski, M. Slawik, H. A. Witek, and K. Patkowski, *J. Chem. Theory Comput.* **10**, 3140 (2014).
- [112] J. Řezáč, M. Dubecký, P. Jurečka, and P. Hobza, *Phys. Chem. Chem. Phys.* **17**, 19268 (2015).
- [113] A. D. Boese, *J. Chem. Theory Comput.* **9**, 4403 (2013).

- [114] T. Korona, H. L. Williams, R. Bukowski, B. Jeziorski, and K. Szalewicz, *J. Chem. Phys.* **106**, 5109 (1997).
- [115] K. Patkowski, W. Cencek, P. Jankowski, K. Szalewicz, J. B. Mehl, G. Garberoglio, and A. H. Harvey, *J. Chem. Phys.* **129**, 094304 (2008).
- [116] B. W. Bakr, D. G. A. Smith, and K. Patkowski, *J. Chem. Phys.* **139**, 144305 (2013).
- [117] E. V. Dornshuld and G. S. Tschumper, *J. Chem. Theory Comput.* **12**, 1534 (2016).
- [118] M. Rode, J. Sadlej, R. Moszyński, P. E. S. Wormer, and A. van der Avoird, *Chem. Phys. Lett.* **314**, 326 (1999).
- [119] M. Kodrycka and K. Patkowski, *J. Chem. Phys.* **151**, 070901 (2019).
- [120] R. Dawes, X. Wang, and T. Carrington, Jr., *J. Phys. Chem. A* **117**, 7612 (2013).
- [121] S. A. Ndengué, R. Dawes, and F. Gatti, *J. Phys. Chem. A* **119**, 7712 (2015).
- [122] A. van der Avoird, P. E. S. Wormer, and A. P. J. Jansen, *J. Chem. Phys.* **84**, 1629 (1986).
- [123] J. R. Stallcop and H. Partridge, *Chem. Phys. Lett.* **281**, 212 (1997).
- [124] K. Leonhard and U. K. Deiters, *Mol. Phys.* **100**, 2571 (2002).
- [125] M. H. Karimi-Jafari, A. Maghari, and S. Shahbazian, *Chem. Phys.* **314**, 249 (2005).
- [126] L. Gomez, B. Bussery-Honvault, T. Cauchy, M. Bartolomei, D. Cappelletti, and F. Pirani, *Chem. Phys. Lett.* **445**, 99 (2007).
- [127] P. Strąk and S. Krukowski, *J. Chem. Phys.* **126**, 194501 (2007).
- [128] M. H. Karimi-Jafari and M. Ashouri, *Phys. Chem. Chem. Phys.* **13**, 9887 (2011).
- [129] R. Hellmann, *Mol. Phys.* **111**, 387 (2013).
- [130] L. Pacifici, M. Verdicchio, N. Faginas Lago, A. Lombardi, and A. Costantini, *J. Comput. Chem.* **34**, 2668 (2013).
- [131] J. Fišer and R. Polák, *Chem. Phys. Lett.* **360**, 565 (2002).
- [132] M. H. Karimi-Jafari, A. Maghari, and A. Farjamnia, *J. Phys. Chem. A* **115**, 1143 (2011).

- [133] J.-M. Liu, Y. Zhai, X.-L. Zhang, and H. Li, *Phys. Chem. Chem. Phys.* **20**, 2036 (2018).
- [134] L. A. Surin, I. V. Tarabukin, S. Schlemmer, Y. N. Kalugina, and A. van der Avoird, *J. Chem. Phys.* **148**, 044313 (2018).
- [135] H. Cybulski, C. Henriksen, R. Dawes, X.-G. Wang, N. Bora, G. Avila, T. Carrington, and B. Fernández, *Phys. Chem. Chem. Phys.* **20**, 12624 (2018).
- [136] J. G. C. M. van Duijneveldt-van de Rijdt and F. B. van Duijneveldt, *J. Mol. Struct. (Theochem)* **6**, 185 (1982).
- [137] M. Douglas and N. M. Kroll, *Ann. Phys.* **82**, 89 (1974).
- [138] B. A. Hess, *Phys. Rev. A* **33**, 3742 (1986).
- [139] J. Gauss, A. Tajti, M. Kállay, J. F. Stanton, and P. G. Szalay, *J. Chem. Phys.* **125**, 144111 (2006).
- [140] G. W. M. Vissers, P. E. S. Wormer, and A. van der Avoird, *Phys. Chem. Chem. Phys.* **5**, 4767 (2003).
- [141] T. B. Pedersen, B. Fernández, and H. Koch, *Chem. Phys. Lett.* **334**, 419 (2001).
- [142] M. Rode, J. Sadlej, R. Moszyński, P. E. S. Wormer, and A. van der Avoird, *Chem. Phys. Lett.* **334**, 424 (2001).
- [143] J. G. Hill, S. Mazumder, and K. A. Peterson, *J. Chem. Phys.* **132**, 054108 (2010).
- [144] E. R. Johnson, I. D. Mackie, and G. A. DiLabio, *J. Phys. Org. Chem.* **22**, 1127 (2009).
- [145] A. Tkatchenko, L. Romaner, O. T. Hofmann, E. Zojer, C. Ambrosch-Draxl, and M. Scheffler, *MRS Bull.* **35**, 435 (2010).
- [146] L. A. Burns, A. Vazquez-Mayagoitia, B. G. Sumpter, and C. D. Sherrill, *J. Chem. Phys.* **134**, 084107 (2011).
- [147] S. Grimme, *WIREs Comput. Mol. Sci.* **1**, 211 (2011).
- [148] J.-D. Chai and M. Head-Gordon, *Phys. Chem. Chem. Phys.* **10**, 6615 (2008).
- [149] H. Schröder, A. Creon, and T. Schwabe, *J. Chem. Theory Comput.* **11**, 3163 (2015).

- [150] J. Řezáč, K. E. Riley, and P. Hobza, *J. Chem. Theory Comput.* **7**, 2427 (2011).
- [151] J. Witte, N. Mardirossian, J. B. Neaton, and M. Head-Gordon, *J. Chem. Theory Comput.* **13**, 2043 (2017).
- [152] L. A. Burns, J. C. Faver, Z. Zheng, M. S. Marshall, D. G. A. Smith, K. Vanommeslaeghe, A. D. MacKerell, Jr., K. M. Merz, Jr., and C. D. Sherrill, *J. Chem. Phys.* **147**, 161727 (2017).
- [153] S. Grimme, *J. Chem. Phys.* **124**, 034108 (2006).
- [154] A. D. Becke, *Phys. Rev. A* **38**, 3098 (1988).
- [155] C. Lee, W. Yang, and R. G. Parr, *Phys. Rev. B* **37**, 785 (1988).
- [156] A. D. Becke, *J. Chem. Phys.* **98**, 5648 (1993).
- [157] P. J. Stephens, F. J. Devlin, C. F. Chabalowski, and M. J. Frisch, *J. Phys. Chem.* **98**, 11623 (1994).
- [158] O. A. Vydrov and G. E. Scuseria, *J. Chem. Phys.* **125**, 234109 (2006).
- [159] C. Adamo and V. Barone, *J. Chem. Phys.* **110**, 6158 (1999).
- [160] M. Ernzerhof and G. E. Scuseria, *J. Chem. Phys.* **110**, 5029 (1999).
- [161] J. P. Perdew, K. Burke, and M. Ernzerhof, *Phys. Rev. Lett.* **77**, 3865 (1996).
- [162] J. P. Perdew, *Phys. Rev. B* **33**, 8822 (1986).
- [163] M. Shahbaz and K. Szalewicz, *Phys. Rev. Lett.* **121**, 113402 (2018).
- [164] K. Szalewicz and B. Jeziorski, *Mol. Phys.* **38**, 191 (1979).
- [165] M. Jeziorska, W. Cencek, K. Patkowski, B. Jeziorski, and K. Szalewicz, *J. Chem. Phys.* **127**, 124303 (2007).
- [166] M. Przybytek, *J. Chem. Theory Comput.* **14**, 5105 (2018).
- [167] B. Jeziorski and M. C. van Hemert, *Mol. Phys.* **31**, 713 (1976).
- [168] R. Moszyński, B. Jeziorski, S. Rybak, K. Szalewicz, and H. L. Williams, *J. Chem. Phys.* **100**, 5080 (1994).
- [169] R. Moszyński, B. Jeziorski, and K. Szalewicz, *J. Chem. Phys.* **100**, 1312 (1994).

- [170] K. Patkowski and K. Szalewicz, *J. Chem. Phys.* **127**, 164103 (2007).
- [171] J. C. Womack and F. R. Manby, *J. Chem. Phys.* **140**, 044118 (2014).
- [172] D. G. A. Smith, L. A. Burns, D. A. Sirianni, D. R. Nascimento, A. Kumar, A. M. James, J. B. Schriber, T. Zhang, B. Zhang, A. S. Abbott, et al., *J. Chem. Theory Comput.* **14**, 3504 (2018).
- [173] R. M. Parrish, L. A. Burns, D. G. A. Smith, A. C. Simmonett, A. E. DePrince, III, E. G. Hohenstein, U. Bozkaya, A. Y. Sokolov, R. Di Remigio, R. M. Richard, et al., *J. Chem. Theory Comput.* **13**, 3185 (2017).
- [174] LS-DALTON, *a linear-scaling molecular electronic structure program, Release Dalton2016, 2016*, <http://daltonprogram.org>.



## **Appendices**

## **Appendix A**

**Triple bonds and coupled-cluster convergence: CCSDTQ interaction energies for complexes involving CO and N<sub>2</sub>**

**Supporting Information for**  
**Triple bonds and coupled-cluster convergence: CCSDTQ**  
**interaction energies for complexes involving CO and N<sub>2</sub>**

TABLE SI: Interaction energy (in  $\text{cm}^{-1}$ ) of different CCSD(T)/CCSD(T)-F12 variants and basis sets for the  $C_{2h}$  local minimum of the CO dimer.

method	X				
	D	T	Q	5	6
CCSD(T)/aXZ	-83.24	-110.22	-117.37	-120.83	-122.77
ext.		-121.99	-123.64	-124.36	-125.32
CCSD(T)/aXZM	-103.59	-119.63	-123.28	-124.11	-124.49
ext.		-126.11	-125.99	-125.00	-125.00
CCSD(T)-F12a/aXZ	-128.35	-130.13	-125.10	-124.91	-124.89
ext.		-130.50	-121.49	-124.68	-124.80
CCSD(T <sup>**</sup> )-F12a/aXZ	-135.77	-133.04	-126.46	-125.65	-125.35
ext.		-131.50	-121.72	-124.76	-124.87
CCSD(T)-F12b/aXZ	-118.48	-126.42	-123.28	-123.88	-124.26
ext.		-129.38	-121.05	-124.48	-124.72
CCSD(T <sup>**</sup> )-F12b/aXZ	-125.90	-129.33	-124.64	-124.62	-124.71
ext.		-130.39	-121.28	-124.56	-124.78
CCSD(T)-F12a/aXZM	-120.33	-125.04	-125.50	-125.34	
ext.		-126.94	-125.75	-125.16	
CCSD(T <sup>**</sup> )-F12a/aXZM	-128.75	-128.07	-126.88	-126.08	
ext.		-127.69	-125.92	-125.22	
CCSD(T)-F12b/aXZM	-112.49	-122.38	-124.29	-124.69	
ext.		-126.45	-125.60	-125.09	
CCSD(T <sup>**</sup> )-F12b/aXZM	-120.92	-125.41	-125.67	-125.43	
ext.		-127.20	-125.77	-125.15	

The extrapolated value (rows ext.) in the X column is computed using interaction energies in bases a(X-1)Z and aXZ.

TABLE III: Interaction energy (in  $\text{cm}^{-1}$ ) of different CCSD(T)/CCSD(T)-F12 variants and basis sets for the  $C_s$  local minimum of the CO dimer.

method	X				
	D	T	Q	5	6
CCSD(T)/aXZ	-90.32	-110.53	-117.10	-120.26	-121.70
ext.		-119.69	-122.43	-123.03	-123.62
CCSD(T)/aXZM	-102.62	-119.04	-121.95	-122.63	-122.91
ext.		-124.29	-123.83	-123.25	-123.28
CCSD(T)-F12a/aXZ	-120.57	-124.48	-123.03	-123.13	-123.27
ext.		-126.01	-122.02	-123.18	-123.42
CCSD(T <sup>**</sup> )-F12a/aXZ	-127.87	-127.31	-124.35	-123.84	-123.71
ext.		-126.95	-122.25	-123.26	-123.48
CCSD(T)-F12b/aXZ	-114.05	-121.87	-121.73	-122.39	-122.80
ext.		-125.04	-121.69	-123.02	-123.32
CCSD(T <sup>**</sup> )-F12b/aXZ	-121.35	-124.69	-123.05	-123.10	-123.23
ext.		-125.98	-121.91	-123.09	-123.37
CCSD(T)-F12a/aXZM	-120.21	-123.68	-123.73	-123.59	
ext.		-124.87	-123.69	-123.43	
CCSD(T <sup>**</sup> )-F12a/aXZM	-128.30	-126.62	-125.06	-124.30	
ext.		-125.65	-123.85	-123.49	
CCSD(T)-F12b/aXZM	-114.21	-121.56	-122.76	-123.07	
ext.		-124.39	-123.56	-123.38	
CCSD(T <sup>**</sup> )-F12b/aXZM	-122.30	-124.50	-124.09	-123.78	
ext.		-125.16	-123.72	-123.44	

The extrapolated value (rows ext.) in the X column is computed using interaction energies in bases a(X-1)Z and aXZ.

TABLE SIII: Interaction energy (in  $\text{cm}^{-1}$ ) of different CCSD(T)/CCSD(T)-F12 variants and basis sets for the  $C_{2v}$  T-shape saddle point of the  $\text{N}_2$  dimer.

method	X				
	D	T	Q	5	6
CCSD(T)/aXZ	-76.12	-93.48	-98.26	-100.05	-101.33
ext.		-99.91	-101.71	-101.96	-103.06
CCSD(T)/aXZM	-91.82	-100.59	-102.06	-102.35	-102.50
ext.		-104.08	-103.24	-102.69	-102.70
CCSD(T)-F12a/aXZ	-109.09	-103.21	-102.36	-102.59	-102.62
ext.		-100.31	-101.68	-102.86	-102.64
CCSD(T <sup>**</sup> )-F12a/aXZ	-115.39	-105.61	-103.48	-103.20	-102.99
ext.		-101.07	-101.87	-102.91	-102.69
CCSD(T)-F12b/aXZ	-101.80	-100.44	-101.11	-101.88	-102.18
ext.		-99.44	-101.56	-102.69	-102.58
CCSD(T <sup>**</sup> )-F12b/aXZ	-108.10	-102.84	-102.24	-102.48	-102.55
ext.		-100.20	-101.75	-102.75	-102.63
CCSD(T)-F12a/aXZM	-100.67	-102.49	-103.03	-102.90	
ext.		-103.29	-103.39	-102.76	
CCSD(T <sup>**</sup> )-F12a/aXZM	-107.53	-104.96	-104.15	-103.50	
ext.		-103.91	-103.54	-102.80	
CCSD(T)-F12b/aXZM	-94.57	-100.44	-102.17	-102.44	
ext.		-102.95	-103.40	-102.73	
CCSD(T <sup>**</sup> )-F12b/aXZM	-101.43	-102.91	-103.29	-103.04	
ext.		-103.57	-103.55	-102.78	

The extrapolated value (rows ext.) in the X column is computed using interaction energies in bases a(X-1)Z and aXZ.

TABLE SIV: Interaction energy (in  $\text{cm}^{-1}$ ) of different CCSD(T)/CCSD(T)-F12 variants and basis sets for the  $D_{2h}$  configuration of the  $\text{N}_2$  dimer.

method	X=				
	D	T	Q	5	6
CCSD(T)/aXZ	-45.83	-67.63	-71.99	-74.92	-76.93
ext.		-77.11	-76.17	-77.82	-79.60
CCSD(T)/aXZM	-60.34	-75.13	-77.58	-78.42	-78.73
ext.		-81.23	-79.46	-79.27	-79.14
CCSD(T)-F12a/aXZ	-84.65	-81.77	-78.94	-78.70	-78.86
ext.		-80.28	-77.24	-78.52	-79.03
CCSD(T <sup>**</sup> )-F12a/aXZ	-91.43	-84.39	-80.16	-79.36	-79.27
ext.		-81.14	-77.46	-78.58	-79.09
CCSD(T)-F12b/aXZ	-74.90	-78.12	-77.20	-77.70	-78.25
ext.		-79.20	-76.91	-78.29	-78.97
CCSD(T <sup>**</sup> )-F12b/aXZ	-81.68	-80.73	-78.43	-78.36	-78.66
ext.		-80.05	-77.12	-78.36	-79.03
CCSD(T)-F12a/aXZM	-76.99	-78.95	-79.24	-79.22	-79.17
ext.		-79.94	-79.53	-79.22	-79.09
CCSD(T <sup>**</sup> )-F12a/aXZM	-84.55	-81.67	-80.48	-79.89	-79.58
ext.		-80.61	-79.71	-79.28	-79.15
CCSD(T)-F12b/aXZM	-69.51	-76.54	-78.22	-78.69	-78.86
ext.		-79.66	-79.53	-79.21	-79.08
CCSD(T <sup>**</sup> )-F12b/aXZM	-77.06	-79.25	-79.47	-79.36	-79.27
ext.		-80.34	-79.71	-79.26	-79.14

The extrapolated value (rows ext.) in the  $X$  column is computed using interaction energies in bases  $a(X-1)Z$  and  $aXZ$ .

TABLE SV: Interaction energy (in  $\text{cm}^{-1}$ ) of different CCSD(T)/CCSD(T)-F12 variants and basis sets for the  $C_s$  near T-shape saddle point of the CO–N<sub>2</sub> complex.

method	X				
	D	T	Q	5	6
CCSD(T)/aXZ	-84.79	-97.73	-102.87	-105.05	-106.30
ext.		-102.98	-106.18	-107.41	-108.02
CCSD(T)/aXZM	-99.3	-106.18	-107.12	-107.39	-107.51
ext.		-109.58	-108.12	-107.73	-107.70
CCSD(T)-F12a/aXZ	-116.34	-107.07	-107.11	-107.61	-107.67
ext.		-103.18	-106.89	-108.09	-107.75
CCSD(T <sup>**</sup> )-F12a/aXZ	-123.26	-109.75	-108.36	-108.29	-108.08
ext.		-104.07	-107.11	-108.16	-107.80
CCSD(T)-F12b/aXZ	-108.08	-103.84	-105.60	-106.75	-107.12
ext.		-102.07	-106.64	-107.91	-107.64
CCSD(T <sup>**</sup> )-F12b/aXZ	-115.0	-106.52	-106.86	-107.43	-107.54
ext.		-102.96	-106.86	-107.98	-107.69
CCSD(T)-F12a/aXZM	-105.37	-108.01	-108.04	-107.93	
ext.		-108.83	-108.02	-107.79	
CCSD(T <sup>**</sup> )-F12a/aXZM	-112.85	-110.77	-109.31	-108.61	
ext.		-109.61	-108.20	-107.85	
CCSD(T)-F12b/aXZM	-98.36	-105.57	-107.00	-107.38	
ext.		-108.31	-108.00	-107.75	
CCSD(T <sup>**</sup> )-F12b/aXZM	-105.83	-108.33	-108.27	-108.06	
ext.		-109.08	-108.18	-107.81	

The extrapolated value (rows ext.) in the X column is computed using interaction energies in bases a(X-1)Z and aXZ.



TABLE SVI: Interaction energy (in  $\text{cm}^{-1}$ ) of different CCSD(T)/CCSD(T)-F12 variants and basis sets for the  $C_{2v}$  T-shape saddle point of the CO–N<sub>2</sub> complex.

method	X				
	D	T	Q	5	6
CCSD(T)/aXZ	-76.14	-97.76	-102.50	-105.00	-106.51
ext.		-105.92	-106.57	-107.72	-108.51
CCSD(T)/aXZM	-92.59	-104.76	-107.04	-107.55	-107.78
ext.		-109.75	-108.84	-108.14	-108.09
CCSD(T)-F12a/aXZ	-129.47	-110.06	-107.73	-107.87	-108.00
ext.		-101.49	-105.85	-108.01	-108.15
CCSD(T <sup>**</sup> )-F12a/aXZ	-135.28	-112.36	-108.80	-108.45	-108.35
ext.		-102.31	-106.04	-108.07	-108.20
CCSD(T)-F12b/aXZ	-121.23	-107.11	-106.40	-107.13	-107.55
ext.		-100.76	-105.72	-107.88	-108.11
CCSD(T <sup>**</sup> )-F12b/aXZ	-127.03	-109.41	-107.48	-107.71	-107.91
ext.		-101.58	-105.90	-107.94	-108.16
CCSD(T)-F12a/aXZM	-104.33	-107.79	-108.40	-108.32	
ext.		-109.11	-108.76	-108.21	
CCSD(T <sup>**</sup> )-F12a/aXZM	-110.81	-110.16	-109.48	-108.90	
ext.		-109.76	-108.91	-108.26	
CCSD(T)-F12b/aXZM	-97.98	-105.71	-107.50	-107.84	
ext.		-108.83	-108.73	-108.16	
CCSD(T <sup>**</sup> )-F12b/aXZM	-104.46	-108.09	-108.59	-108.42	
ext.		-109.48	-108.88	-108.21	

The extrapolated value (rows ext.) in the X column is computed using interaction energies in bases a(X-1)Z and aXZ.

TABLE SVII: Interaction energy (in  $\text{cm}^{-1}$ ) of different MP2/MP2-F12 and CCSD/CCSD-F12 variants and basis sets for the global minimum geometry of the CO dimer.

method	X				
	D	T	Q	5	6
MP2/aXZ	-129.10	-141.76	-149.15	-152.52	-153.97
ext.		-148.87	-153.97	-155.55	-155.97
MP2/aXZM	-138.29	-151.09	-154.11	-155.12	-155.53
ext.		-156.75	-156.04	-156.11	-156.09
MP2-F12/aXZ	-152.15	-154.51	-155.30	-155.72	-155.92
ext.		-155.63	-155.89	-156.13	-156.17
MP2-F12/aXZM	-151.90	-155.58	-155.95	-156.06	
ext.		-157.06	-156.27	-156.18	
CCSD/aXZ	-76.08	-85.56	-91.40	-93.83	-94.78
ext.		-91.34	-95.09	-95.88	-96.09
CCSD/aXZM	-85.14	-94.03	-95.34	-95.66	-95.77
ext.		-98.04	-96.04	-95.93	-95.90
CCSD-F12a/aXZ	-97.44	-97.06	-96.64	-96.45	-96.33
ext.		-97.02	-96.35	-96.22	-96.15
CCSD-F12b/aXZ	-91.28	-94.42	-95.33	-95.67	-95.82
ext.		-95.86	-96.01	-96.01	-95.99
CCSD-F12a/aXZM	-97.37	-97.81	-96.85	-96.41	
ext.		-97.93	-96.20	-95.96	
CCSD-F12b/aXZM	-91.81	-95.68	-95.94	-95.94	
ext.		-97.24	-96.18	-95.94	

The extrapolated value (rows ext.) in the X column is computed using interaction energies in bases a(X-1)Z and aXZ.

TABLE SVIII: Interaction energy (in  $\text{cm}^{-1}$ ) of different MP2/MP2-F12 and CCSD/CCSD-F12 variants and basis sets for the  $C_{2h}$  local minimum of the CO dimer.

method	X				
	D	T	Q	5	6
MP2/aXZ	-69.56	-94.51	-101.79	-105.56	-107.77
ext.		-105.43	-108.17	-109.40	-110.71
MP2/aXZM	-86.95	-103.25	-107.74	-109.06	-109.74
ext.		-109.84	-111.07	-110.45	-110.66
MP2-F12/aXZ	-114.66	-116.20	-110.86	-110.55	-110.57
ext.		-116.46	-107.03	-110.20	-110.53
MP2-F12/aXZM	-103.89	-109.63	-110.66	-110.77	
ext.		-111.95	-111.33	-110.87	
CCSD/aXZ	-60.08	-82.33	-88.16	-91.07	-92.72
ext.		-92.10	-93.47	-94.01	-94.89
CCSD/aXZM	-76.81	-90.12	-93.16	-93.83	-94.16
ext.		-95.46	-95.43	-94.54	-94.60
CCSD-F12a/aXZ	-105.08	-102.45	-96.06	-95.27	-94.93
ext.		-100.97	-91.45	-94.40	-94.40
CCSD-F12b/aXZ	-95.21	-98.74	-94.24	-94.23	-94.30
ext.		-99.85	-91.01	-94.20	-94.32
CCSD-F12a/aXZM	-93.60	-95.75	-95.53	-95.15	
ext.		-96.56	-95.28	-94.74	
CCSD-F12b/aXZM	-85.77	-93.09	-94.32	-94.50	
ext.		-96.07	-95.13	-94.67	

The extrapolated value (rows ext.) in the X column is computed using interaction energies in bases a(X-1)Z and aXZ.

TABLE SIX: Interaction energy (in  $\text{cm}^{-1}$ ) of different MP2/MP2-F12 and CCSD/CCSD-F12 variants and basis sets for the  $C_s$  local minimum of the CO dimer.

method	X				
	D	T	Q	5	6
MP2/aXZ	-80.88	-99.04	-105.36	-108.66	-110.30
ext.		-107.33	-110.52	-111.57	-112.48
MP2/aXZM	-90.89	-106.58	-110.00	-111.13	-111.68
ext.		-111.52	-112.25	-112.22	-112.43
MP2-F12/aXZ	-111.55	-114.21	-112.26	-112.20	-112.37
ext.		-115.21	-110.90	-112.08	-112.55
MP2-F12/aXZM	-109.63	-112.16	-112.39	-112.48	
ext.		-112.96	-112.49	-112.57	
CCSD/aXZ	-67.01	-83.30	-88.63	-91.32	-92.54
ext.		-90.80	-93.06	-93.61	-94.14
CCSD/aXZM	-76.45	-90.33	-92.74	-93.30	-93.54
ext.		-94.50	-94.25	-93.79	-93.87
CCSD-F12a/aXZ	-97.66	-97.51	-94.73	-94.31	-94.19
ext.		-97.34	-92.75	-93.81	-93.98
CCSD-F12b/aXZ	-91.14	-94.90	-93.43	-93.56	-93.71
ext.		-96.37	-92.41	-93.65	-93.88
CCSD-F12a/aXZM	-94.56	-95.26	-94.67	-94.35	
ext.		-95.29	-94.18	-94.00	
CCSD-F12b/aXZM	-88.56	-93.14	-93.70	-93.83	
ext.		-94.81	-94.05	-93.95	

The extrapolated value (rows ext.) in the X column is computed using interaction energies in bases a(X-1)Z and aXZ.

TABLE SX: Interaction energy (in  $\text{cm}^{-1}$ ) of different MP2/MP2-F12 and CCSD/CCSD-F12 variants and basis sets for the global minimum geometry of the  $\text{N}_2$  dimer.

method	X				
	D	T	Q	5	6
MP2/aXZ	-108.79	-125.92	-131.45	-134.18	-135.93
ext.		-132.94	-135.55	-136.80	-138.29
MP2/aXZM	-120.04	-133.51	-136.23	-137.04	-137.46
ext.		-139.00	-138.20	-137.91	-138.03
MP2-F12/aXZ	-139.79	-138.41	-137.46	-137.62	-137.83
ext.		-137.91	-136.86	-137.77	-138.12
MP2-F12/aXZM	-133.73	-137.10	-137.88	-137.99	
ext.		-138.70	-138.44	-138.11	
CCSD/aXZ	-56.19	-68.98	-72.87	-74.76	-76.00
ext.		-74.17	-75.79	-76.50	-77.65
CCSD/aXZM	-67.59	-75.65	-76.79	-76.95	-77.06
ext.		-78.86	-77.60	-77.14	-77.22
CCSD-F12a/aXZ	-85.50	-80.08	-78.01	-77.62	-77.49
ext.		-77.89	-76.59	-77.19	-77.30
CCSD-F12b/aXZ	-77.83	-77.20	-76.67	-76.85	-77.01
ext.		-77.01	-76.37	-77.03	-77.22
CCSD-F12a/aXZM	-79.58	-78.38	-78.01	-77.64	
ext.		-78.04	-77.73	-77.24	
CCSD-F12b/aXZM	-72.96	-76.19	-77.09	-77.16	
ext.		-77.72	-77.74	-77.22	

The extrapolated value (rows ext.) in the X column is computed using interaction energies in bases  $a(X-1)Z$  and  $aXZ$ .

TABLE SXI: Interaction energy (in  $\text{cm}^{-1}$ ) of different MP2/MP2-F12 and CCSD/CCSD-F12 variants and basis sets for the  $C_{2v}$  T-shape saddle point of the  $\text{N}_2$  dimer.

method	X				
	D	T	Q	5	6
MP2/aXZ	-100.46	-117.53	-122.69	-124.79	-126.27
ext.		-123.83	-126.42	-127.02	-128.27
MP2/aXZM	-113.30	-124.29	-126.50	-127.23	-127.60
ext.		-128.71	-128.22	-128.03	-128.12
MP2-F12/aXZ	-135.22	-128.82	-127.71	-127.94	-127.98
ext.		-125.70	-126.84	-128.19	-128.01
MP2-F12/aXZM	-124.31	-127.27	-128.02	-128.12	
ext.		-128.56	-128.54	-128.21	
CCSD/aXZ	-54.92	-68.26	-71.92	-73.29	-74.33
ext.		-72.99	-74.56	-74.77	-75.72
CCSD/aXZM	-68.21	-74.30	-75.09	-75.20	-75.29
ext.		-76.65	-75.77	-75.36	-75.42
CCSD-F12a/aXZ	-88.11	-78.22	-76.14	-75.92	-75.67
ext.		-73.63	-74.58	-75.69	-75.32
CCSD-F12b/aXZ	-80.82	-75.45	-74.90	-75.20	-75.23
ext.		-72.76	-74.45	-75.53	-75.26
CCSD-F12a/aXZM	-77.57	-76.45	-76.19	-75.83	
ext.		-76.01	-75.97	-75.45	
CCSD-F12b/aXZM	-71.47	-74.40	-75.33	-75.37	
ext.		-75.67	-75.98	-75.42	

The extrapolated value (rows ext.) in the X column is computed using interaction energies in bases  $a(X-1)Z$  and  $aXZ$ .

TABLE SXII: Interaction energy (in  $\text{cm}^{-1}$ ) of different MP2/MP2-F12 and CCSD/CCSD-F12 variants and basis sets for the  $D_{2h}$  configuration of the  $\text{N}_2$  dimer.

method	X=				
	D	T	Q	5	6
MP2/aXZ	-81.26	-103.52	-108.22	-111.57	-113.89
ext.		-113.19	-112.65	-114.91	-116.99
MP2/aXZM	-93.35	-111.19	-114.29	-115.54	-116.07
ext.		-118.57	-116.64	-116.81	-116.79
MP2-F12/aXZ	-121.14	-119.53	-116.38	-116.17	-116.40
ext.		-118.59	-114.45	-116.02	-116.66
MP2-F12/aXZM	-111.22	-115.96	-116.50	-116.68	-116.77
ext.		-118.12	-116.98	-116.89	-116.89
CCSD/aXZ	-23.76	-40.36	-43.31	-45.65	-47.28
ext.		-47.64	-46.47	-47.93	-49.42
CCSD/aXZM	-34.98	-46.38	-47.94	-48.53	-48.75
ext.		-51.05	-49.17	-49.10	-49.04
CCSD-F12a/aXZ	-62.07	-54.59	-50.32	-49.47	-49.24
ext.		-51.17	-47.57	-48.65	-48.88
CCSD-F12b/aXZ	-52.32	-50.94	-48.58	-48.47	-48.64
ext.		-50.08	-47.24	-48.42	-48.82
CCSD-F12a/aXZM	-51.54	-50.34	-49.69	-49.39	-49.23
ext.		-49.99	-49.31	-49.08	-49.01
CCSD-F12b/aXZM	-44.05	-47.92	-48.68	-48.86	-48.92
ext.		-49.71	-49.31	-49.06	-49.00

The extrapolated value (rows ext.) in the  $X$  column is computed using interaction energies in bases  $a(X-1)Z$  and  $aXZ$ .

TABLE SXIII: Interaction energy (in  $\text{cm}^{-1}$ ) of different MP2/MP2-F12 and CCSD/CCSD-F12 variants and basis sets for the global minimum geometry of the CO–N<sub>2</sub> complex.

	X				
MP2/aXZ	-105.68	-121.30	-127.44	-130.08	-131.51
ext.		-127.87	-131.68	-132.33	-133.43
MP2/aXZM	-114.09	-128.79	-131.50	-132.39	-132.81
ext.		-133.61	-133.32	-133.27	-133.37
MP2-F12/aXZ	-132.40	-133.88	-133.06	-133.13	-133.25
ext.		-134.59	-132.54	-133.18	-133.41
MP2-F12/aXZM	-129.84	-133.14	-133.31	-133.36	
ext.		-134.28	-133.46	-133.42	
CCSD/aXZ	-66.68	-79.43	-84.42	-86.46	-87.50
ext.		-84.79	-87.82	-88.09	-88.88
CCSD/aXZM	-75.14	-86.48	-87.95	-88.26	-88.41
ext.		-89.88	-88.86	-88.54	-88.59
CCSD-F12a/aXZ	-92.63	-90.99	-89.33	-89.02	-88.90
ext.		-90.38	-88.19	-88.68	-88.71
CCSD-F12b/aXZ	-86.95	-88.63	-88.19	-88.36	-88.48
ext.		-89.42	-87.95	-88.52	-88.62
CCSD-F12a/aXZM	-89.87	-90.13	-89.39	-89.02	
ext.		-89.99	-88.87	-88.63	
CCSD-F12b/aXZM	-84.51	-88.22	-88.56	-88.59	
ext.		-89.54	-88.83	-88.61	

The extrapolated value (rows ext.) in the X column is computed using interaction energies in bases a(X-1)Z and aXZ.



TABLE SXIV: Interaction energy (in  $\text{cm}^{-1}$ ) of different MP2/MP2-F12 and CCSD/CCSD-F12 variants and basis sets for the  $C_s$  near T-shape saddle point of the CO-N<sub>2</sub> complex.

method	X				
	D	T	Q	5	6
MP2/aXZ	-97.39	-110.83	-116.89	-119.52	-121.06
ext.		-116.28	-120.87	-122.36	-123.18
MP2/aXZM	-109.93	-119.24	-121.33	-122.15	-122.55
ext.		-123.67	-123.18	-123.06	-123.13
MP2F12/aXZ	-132.61	-122.24	-122.31	-122.83	-122.95
ext.		-117.89	-122.12	-123.33	-123.12
MP2-F12/aXZM	-119.40	-122.57	-122.99	-123.12	
ext.		-123.61	-123.25	-123.24	
CCSD/aXZ	-62.01	-70.92	-74.84	-76.49	-77.48
ext.		-74.47	-77.26	-78.29	-78.83
CCSD/aXZM	-74.36	-78.13	-78.35	-78.42	-78.47
ext.		-80.22	-78.83	-78.55	-78.56
CCSD-F12a/aXZ	-94.16	-80.55	-79.22	-79.13	-78.90
ext.		-74.84	-78.00	-78.99	-78.58
CCSD-F12b/aXZ	-85.95	-77.35	-77.73	-78.28	-78.36
ext.		-73.73	-77.76	-78.81	-78.47
CCSD-F12a/aXZM	-81.11	-80.28	-79.43	-79.05	
ext.		-79.64	-78.77	-78.63	
CCSD-F12b/aXZM	-74.14	-77.85	-78.40	-78.50	
ext.		-79.13	-78.75	-78.59	

The extrapolated value (rows ext.) in the X column is computed using interaction energies in bases a(X-1)Z and aXZ.

TABLE SXV: Interaction energy (in  $\text{cm}^{-1}$ ) of different MP2/MP2-F12 and CCSD/CCSD-F12 variants and basis sets for the  $C_{2v}$  T-shape saddle point of the CO-N<sub>2</sub> complex.

method	X				
	D	T	Q	5	6
MP2/aXZ	-97.28	-110.84	-116.95	-119.60	-121.16
ext.		-116.34	-120.97	-122.46	-123.29
MP2/aXZM	-109.87	-119.3	-121.42	-122.25	-122.66
ext.		-123.78	-123.28	-123.17	-123.24
MP2F12/aXZ	-132.61	-122.33	-122.42	-122.94	-123.06
ext.		-118.01	-122.23	-123.45	-123.24
MP2-F12/aXZM	-119.48	-122.67	-123.10	-123.23	
ext.		-123.72	-123.37	-123.35	
CCSD/aXZ	-61.68	-70.69	-74.64	-76.31	-77.30
ext.		-74.28	-77.09	-78.13	-78.66
CCSD/aXZM	-74.08	-77.93	-78.18	-78.25	-78.31
ext.		-80.07	-78.67	-78.38	-78.39
CCSD-F12a/aXZ	-93.92	-80.39	-79.06	-78.97	-78.74
ext.		-74.70	-77.84	-78.84	-78.42
CCSD-F12b/aXZ	-85.66	-77.16	-77.55	-78.11	-78.19
ext.		-73.59	-77.60	-78.65	-78.31
CCSD-F12a/aXZM	-80.95	-80.13	-79.27	-78.89	
ext.		-79.48	-78.61	-78.46	
CCSD-F12b/aXZM	-73.94	-77.68	-78.23	-78.33	
ext.		-78.96	-78.59	-78.42	

The extrapolated value (rows ext.) in the X column is computed using interaction energies in bases a(X-1)Z and aXZ.

## **Appendix B**

### **A Platinum, gold, and silver standards of intermolecular interaction energy calculations**


# Platinum, gold, and silver standards of intermolecular interaction energy calculations

Cite as: J. Chem. Phys. **151**, 070901 (2019); <https://doi.org/10.1063/1.5116151>

Submitted: 21 June 2019 . Accepted: 16 July 2019 . Published Online: 15 August 2019

Monika Kodrycka , and Konrad Patkowski 

## COLLECTIONS

 This paper was selected as Featured



View Online



Export Citation



CrossMark

The Journal  
of Chemical Physics

Submit Today

The Emerging Investigators Special Collection and Awards  
Recognizing the excellent work of early career researchers!



# Platinum, gold, and silver standards of intermolecular interaction energy calculations

Cite as: J. Chem. Phys. 151, 070901 (2019); doi: 10.1063/1.5116151

Submitted: 21 June 2019 • Accepted: 16 July 2019 •

Published Online: 15 August 2019



View Online



Export Citation



CrossMark

Monika Kodrycka  and Konrad Patkowski<sup>a)</sup> 

## AFFILIATIONS

Department of Chemistry and Biochemistry, Auburn University, Auburn, Alabama 36849, USA

<sup>a)</sup> Author to whom correspondence should be addressed: [patkowski@auburn.edu](mailto:patkowski@auburn.edu)

## ABSTRACT

High-accuracy noncovalent interaction energies are indispensable as data points for potential energy surfaces and as benchmark values for improving and testing more approximate approaches. The preferred algorithm (the *gold standard*) for computing these energies has been the coupled-cluster method with singles, doubles, and perturbative triples [CCSD(T)] converged to the complete basis set (CBS) limit. However, gold-standard calculations are expensive as correlated interaction energies converge slowly with the basis set size, and establishing the CBS limit to better than 0.05 kcal/mol typically requires a CCSD(T) calculation in a basis set of at least triple-zeta quality. If an even higher accuracy is required (for example, for the assignment of complicated high-resolution spectra), establishing a superior *platinum standard* requires both a precisely converged CCSD(T)/CBS limit and the corrections for the core correlation, relativistic effects, and higher-order coupled-cluster terms at least through the perturbative quadruple excitations. On the other hand, if a triple-zeta CCSD(T) calculation is not feasible but a double-zeta one is, it is worthwhile to look for a *silver standard* that provides the most accurate and consistent approximation to the gold standard at a reduced computational cost. We review the recent developments aimed at (i) increasing the breadth and diversity of the available collection of gold-standard benchmark interaction energies, (ii) evaluating the best computational strategies for platinum-standard calculations and producing beyond-CCSD(T) potential energy surfaces for spectroscopic and scattering applications of the highest precision, and (iii) improving the accuracy of the silver-standard, double-zeta-level CCSD(T)/CBS estimates through the use of explicit correlation and midbond basis functions. We also outline the remaining challenges in the accurate *ab initio* calculations of noncovalent interaction energies.

Published under license by AIP Publishing. <https://doi.org/10.1063/1.5116151>

## I. INTRODUCTION

A reliable description of intermolecular interactions is essential for a large variety of problems in chemistry, physics, biology, and materials science. Weak interactions between gas molecules give rise to deviations from ideal gas law, which can be quantified, e.g., via second and higher virial coefficients. The latter coefficients can be used, for example, to establish a connection between pressure, temperature, and the speed of sound in a gas that can be employed to construct a new temperature standard.<sup>1</sup> Weak interactions with a background gas result in broadening and shifting of spectral lines, and a combination of accurate measurements and calculations is required to advance the description of spectral line shapes beyond the conventional convolution of Lorentzian and Gaussian pictures.<sup>2</sup> The intermolecular rovibrational bound states give rise to rich (and

hard to assign) infrared and microwave spectra,<sup>3</sup> while the unbound states determine cross sections for elastic and inelastic scattering processes essential for astrophysical modeling.<sup>4</sup> A delicate balance of two-, three-, and higher-body interactions determines the stability of molecular clusters,<sup>5</sup> the structure and polymorphism of molecular crystals,<sup>6</sup> and the thermodynamical properties of liquids.<sup>7</sup> Noncovalent interactions are an important factor in catalysis as they can preferentially stabilize the transition state for a desired reaction.<sup>8</sup> Interactions within layered materials<sup>9</sup> and between adsorbate molecules and surfaces or porous media<sup>10</sup> are crucial for the performance of modern materials in a variety of applications ranging from semiconductors to carbon capture. Last but not least, weak interactions stabilize the structures of proteins and nucleic acids and bind substrates (as well as inhibitors) to the active sites of enzymes.<sup>11</sup> Thus, it is not a surprise that the field of intermolecular interactions has

continually attracted widespread interest from experimentalists and theorists alike.

From the computational perspective, the necessary prerequisite to determining spectra, scattering cross sections, and many other quantities of experimental interest is the generation (in whole or in part) of the *potential energy surface* (PES), that is, a function that expresses the energy of the complex in terms of the internal and relative geometries of its constituent molecules. This energy is a sum of the energies of individual molecules (monomers), including the energetic penalty incurred when the monomers adapt their geometric configurations in the complex instead of their individually optimized structures, and the actual interaction energy. The construction of a PES involves three steps: establishing a grid of configurations that span the surface, interaction energy calculations for each grid point, and a fitting or interpolation of an analytical function that provides a reasonable PES approximation in between the computed grid points as well as at larger intermolecular separations. Recently, significant advances have been made on optimizing the selection of grid points,<sup>12</sup> making the fitting more robust,<sup>13</sup> and automating the whole process of PES construction;<sup>14,15</sup> however, the vast majority of computer time still needs to be spent on the middle step, that is, electronic structure calculations on each configuration from the grid. While the individual interaction energies can be computed directly via symmetry-adapted perturbation theory (SAPT),<sup>16</sup> it is more common to obtain these values via subtraction of monomer energies from the total energy of the complex, within the so-called supermolecular framework. In such a case, the accuracy of interaction energy hinges on a cancellation of errors (which arise due to the use of an approximate electronic structure theory and an incomplete basis set) between the quantities that are subtracted. Obviously, this cancellation is much easier if the individual errors are small to begin with: this is one of the reasons why intermolecular interaction energies place particularly high demands on the accuracy of the underlying electronic structure theory. The other reason is the van der Waals dispersion forces which arise entirely out of electron correlation and thus require a high-level account of the correlation energy.

Except for few-electron complexes where full configuration interaction (FCI) calculations are possible, the most successful strategy for computing accurate correlated interaction energies has been the coupled-cluster (CC) approach.<sup>17</sup> In particular, the coupled-cluster variant with single, double, and perturbative triple excitations [CCSD(T)]<sup>18</sup> has been termed the *gold standard* of electronic structure theory as it provides consistently accurate interaction energies for closed-shell complexes. In fact, due to favorable error cancellation, CCSD(T) typically performs in this context just as well as the variant with full iterative triples, CCSDT.<sup>19</sup> It should be noted that, when the interacting molecules cannot be qualitatively described by individual determinants, single-reference CC methods in general, and perturbative variants such as CCSD(T) in particular, are unable to provide reliable interaction energies. In such a case, computing a high-accuracy PES is a much more difficult task, and multireference electronic structure methods of benchmark quality are still under active development—see, e.g., a recent perspective for a review.<sup>20</sup> It might be noted in passing that the CC methods have the attractive property that the extent of multireference character for a problematic system can be inferred from examining the cluster amplitudes. In this perspective, we will be concerned with single-reference

complexes so that CCSD(T) is indeed a reliable gold standard *as long as the results are converged to the complete basis set limit* (CBS).

Computing a gold standard CCSD(T)/CBS interaction energy is an expensive task due to both an unfavorable  $N^7$  computational scaling of CCSD(T) with the system size and a slow basis set convergence of correlated interaction energies. The scaling can be reduced by exploiting spatial locality of electron correlation; however, the errors of the local approximation sometimes exceed the accuracy one would expect from the gold standard interaction energies.<sup>21</sup> Nevertheless, local CCSD(T) variants are undergoing constant improvement<sup>22–25</sup> and are on the verge of becoming a reliable source of benchmark-quality gold standard estimates. The basis set convergence of CCSD(T) interaction energies can be improved by a number of techniques—see Ref. 26 for a recent review. These techniques can be used separately or in combination and include the composite MP2/CBS+ $\delta$ [CCSD(T)] treatment {where the easier-to-compute CBS limit of the second-order Møller-Plesset perturbation theory (MP2) is augmented with a  $\delta$ [CCSD(T)] = CCSD(T)–MP2 correction computed in a moderate basis set}, CBS extrapolations, midbond functions, and various variants of the explicitly correlated CCSD(T)-F12 approach.<sup>27,28</sup> Even with these enhancements, one typically cannot avoid performing a CCSD(T) calculation in at least a partially augmented triple-zeta basis set: otherwise, the basis set truncation errors overwhelm the intrinsic errors of the CCSD(T) approach.

The gold standard CCSD(T)/CBS estimates are a centerpiece of the field of accurate *ab initio* studies of weakly interacting complexes and a centerpiece of this perspective. In addition to numerous investigations of PESs for individual systems of experimental interest, the gold standard calculations have led to the establishment of benchmark noncovalent databases that compile accurate interaction energy values for a diverse selection of complexes and configurations. The available noncovalent databases have been recently reviewed in Refs. 26 and 29: the most widely employed sets include the S22<sup>30</sup> and S66<sup>31</sup> databases of the Hobza group. In the last couple of years, benchmark databases have grown larger and more diverse in order to meet the growing demands of the community as various more approximate (but much less computationally demanding) approaches are formulated and tested against high-accuracy *ab initio* data. Such approximate but efficient techniques may be based on density functional theory (DFT),<sup>32</sup> semiempirical methods,<sup>33</sup> or machine learning (ML).<sup>34</sup> At the same time, one frequently needs to go either above or slightly below the gold standard. For example, using PESs to reproduce and interpret high-resolution spectroscopic data might call for interaction energies beyond the CCSD(T)/CBS level. Thus, it has been worthwhile to establish a *platinum standard* of interaction energy calculations of subspectroscopic accuracy. On the other hand, for larger complexes, a CCSD(T) calculation in a triple-zeta basis set, required by the gold standard, might be unaffordable and one needs to resort to CCSD(T)/CBS estimates that only require a CCSD(T) calculation in a double-zeta basis set or even estimates that do not require a CCSD(T) calculation at all. For this purpose, *silver*, *bronze*, and even *pewter standards* of interaction energy calculations have been designated,<sup>35</sup> with the goal of providing the most accurate approximations to the gold standard at a given (significantly reduced) level of computational complexity.

The aim of this perspective is to describe the current state of the art for the entire family of “precious metals” standards of intermolecular interaction energies. Therefore, after a brief introduction to the methodology of interaction energy calculations in Sec. II, we continue by reviewing recent progress in gold-standard calculations, with emphasis on the development of diverse and balanced benchmark databases and accurate PESs for systems of experimental interest, in Sec. III. We then move on to calculations of even higher accuracy, illustrating some important applications of platinum-standard interaction energies in Sec. IV. Finally, in Sec. V, we review the establishment and refinement of the silver-standard level of theory as a cost-effective alternative to the gold standard. In all cases, we try to focus on the current directions of research as well as the remaining challenges that will likely be addressed in the near future. As the accuracy of more approximate approaches (for example, those based on DFT) has been steadily improving,<sup>36,37</sup> the bronze and pewter standards do not provide benchmark interaction energies with sufficient precision to evaluate the best performers. Therefore, the primary focus of this perspective is the levels of accuracy from the silver standard onward.

## II. METHODOLOGY

For a given complex A–B, the interaction energy calculation at the silver, gold, or platinum level requires three CCSD(T) runs<sup>18</sup> combined within the supermolecular framework<sup>38</sup>

$$E_{\text{int}}^{\text{CCSD(T)}} = E_{\text{A-B}}^{\text{CCSD(T)}} - E_{\text{A}}^{\text{CCSD(T)}} - E_{\text{B}}^{\text{CCSD(T)}}. \quad (1)$$

The energies for the individual subsystems A and B are evaluated at their geometries adopted in the complex, which might not be the same as the optimal geometries for isolated monomers. The energetic penalty of distorting A and B to their geometries in the complex, called the *deformation energy*,<sup>39</sup> can (and often should) be included separately; however, in this perspective, we will focus on the computation of the interaction energy proper, that is, Eq. (1) [which can be used with CCSD(T) or with any other electronic structure method, for example, MP2]. The typical choice of basis sets used to perform the CCSD(T) computations is the correlation-consistent cc-pVXZ family of Dunning and coworkers,<sup>40</sup> enhanced with diffuse functions to form the completely augmented aug-cc-pVXZ  $\equiv$  aXZ sets<sup>41</sup> or the partially augmented “calendar” bases such as jun-cc-pVXZ.<sup>42</sup> In order to achieve a cancellation of most of the electronic structure and basis set errors between the quantities subtracted in Eq. (1) and obtain an interaction energy that goes to zero at large A–B separations, the basis functions centered on molecule A have to be the same in the calculations of  $E_{\text{A-B}}^{\text{CCSD(T)}}$  and  $E_{\text{A}}^{\text{CCSD(T)}}$ , and those centered on B have to be the same in the calculations of  $E_{\text{A-B}}^{\text{CCSD(T)}}$  and  $E_{\text{B}}^{\text{CCSD(T)}}$  [note that another possible issue that would break the correct long-range limit could be the use of a size-inconsistent approach, such as a truncated configuration interaction method, in place of CCSD(T)]. However, if the  $E_{\text{A}}^{\text{CCSD(T)}}$  and  $E_{\text{B}}^{\text{CCSD(T)}}$  calculations contain only the subsystem’s own basis functions, another problem appears: the description of, say, A is more complete in  $E_{\text{A-B}}^{\text{CCSD(T)}}$  than in  $E_{\text{A}}^{\text{CCSD(T)}}$ , thanks to the additional flexibility afforded by the basis functions centered on the other subsystem. This inconsistency is called the *basis set*

*superposition error (BSSE)*, and the most popular remedy for it is the counterpoise (CP) correction of Boys and Bernardi.<sup>43</sup> In the CP-corrected supermolecular framework, all three quantities in Eq. (1) are computed in the full basis set of the complex, that is, the calculation of  $E_{\text{A}}^{\text{CCSD(T)}}$  includes *ghost basis functions* centered at the locations of B’s nuclei in the complex and vice versa. As the basis set is enlarged, the CP-corrected and uncorrected interaction energies [the latter obtained from Eq. (1) with the calculations of  $E_{\text{A}}^{\text{CCSD(T)}}$  and  $E_{\text{B}}^{\text{CCSD(T)}}$  utilizing only the basis set of the subsystem] typically bracket the CBS value of  $E_{\text{int}}^{\text{CCSD(T)}}$ , converging there from below (CP-uncorrected) and above (CP-corrected). This behavior has two consequences. First, some authors have argued that the CP scheme overcorrects the true BSSE<sup>44</sup> and the merits of the counterpoise correction were a hot topic in the literature some time ago. Second, a “half-corrected” scheme, that is, the arithmetic mean of the CP-corrected and uncorrected interaction energies,<sup>45,46</sup> might sometimes be more accurate than either variant alone. On the practical side, an extensive comparison of CCSD(T)/CBS estimates obtained from CP-corrected, uncorrected, and half-corrected calculations was performed by Burns *et al.*,<sup>47</sup> concluding that the averaged scheme avoids the worst errors incurred by either variant alone; however, in most cases, the fully corrected and half-corrected approaches perform similarly well and either one can be recommended. As the fully CP-corrected interaction energy calculations are currently the most prevalent, throughout the rest of this perspective, all computations will be assumed CP-corrected unless explicitly stated otherwise. Another point that, in our opinion, tips the scales toward the fully CP-corrected approach is that it is the only one compatible with the addition of extra basis functions centered on the intermolecular bond.<sup>48</sup>

For the gold and silver standard accuracy, an approximation to CCSD(T)/CBS is all that is needed, and it is normally sufficient to perform the CCSD(T) calculations of Eq. (1) within the frozen core approximation, where only the valence electrons are correlated. However, going beyond the gold-standard level of theory requires a concerted effort as several neglected contributions might be of comparable size: the core-core and core-valence correlation, the coupled-cluster excitations beyond CCSD(T), the relativistic effects, and sometimes even the quantum electrodynamics (QED) term. At the same time, residual errors of the leading, frozen-core CCSD(T)/CBS term tend to be comparable to the corrections mentioned above, and the generation of a PES beyond the gold standard of accuracy requires *both a further refinement of the CCSD(T)/CBS estimate and the inclusion of terms beyond the frozen-core CCSD(T) level*.

If one sets out to compute, say, a double zeta-level CCSD(T) interaction energy, there are many variants to choose from, and all of them are of comparable computational complexity. One can opt for conventional CCSD(T) or for any variant of explicitly correlated CCSD(T), such as the CCSD(T)-F12a, CCSD(T)-F12b,<sup>49,50</sup> or CCSD(F12\*) (T)  $\equiv$  CCSD(T)-F12c<sup>51</sup> approximations. The triples contribution in an F12 calculation can be included as-is or scaled to approximately account for the lack of explicit correlation in (T). The scaling factor is commonly taken as the ratio of MP2-F12 and MP2 correlation energies,<sup>50</sup> and when the ratio obtained for the dimer is also used in monomer calculations to maintain size consistency,<sup>52</sup> such an approach is denoted (T\*\*).<sup>53</sup> Alternatively,

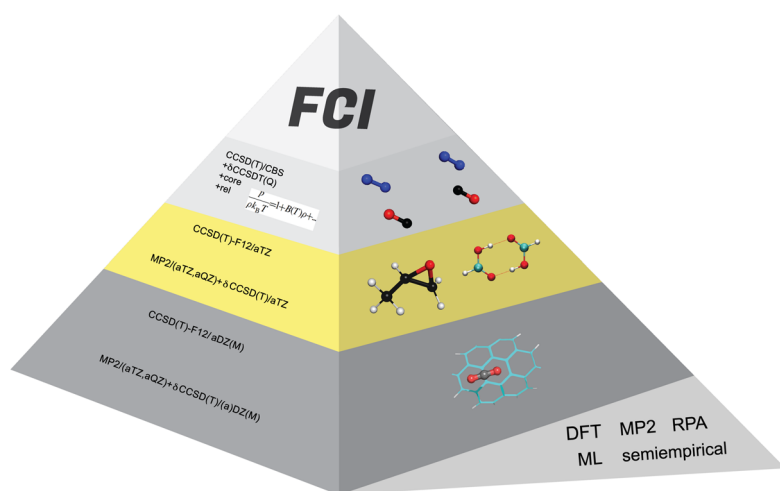


FIG. 1. Summary of the silver, gold, and platinum standards described in this perspective, providing successive approximations to the FCI/CBS interaction energy.

the triples scaling factor can be chosen as the ratio of the correlation energies from CCSD-F12b (or CCSD-F12c) and conventional CCSD.<sup>54</sup> Instead of the standard aDZ basis set, one might opt for the cc-pVDZ-F12 set specifically developed for F12 calculations<sup>55</sup> or even its aug-cc-pVDZ-F12 counterpart with additional diffuse functions added.<sup>56</sup> The atom-centered basis set might be supplemented by midbond functions. Basis set superposition error might be alleviated by the CP correction, but uncorrected or half-corrected calculations are also possible. Finally, for any choice described above, one might perform a simple CCSD(T) calculation or a composite MP2/CBS+ $\delta$ [CCSD(T)] one, with the MP2/CBS limit established with either conventional MP2 or MP2-F12, with or without a complete basis set extrapolation. Thus, a “double zeta-level CCSD(T) interaction energy” might mean many different things, and we need to be precise when defining the actual theory and basis set level designated by the precious-metal standard. This issue becomes even more pronounced in the case of the gold standard which is colloquially known as simply CCSD(T)/CBS. Sections III–V of this perspective will review the research that established what it means to converge the CCSD(T) interaction energy to the CBS limit sufficiently well to be accepted as the gold (or silver) standard, and what precise combinations of CCSD(T)/CCSD(T)-F12 variants, basis sets, and other details mentioned above are the most effective in achieving the required accuracy at an optimal computational cost. Here, we just summarize the recommendations that have been established and give the most important examples of precise theory and basis set levels that have been deemed worthy of a platinum/gold/silver standard designation. These examples as well as representative applications of precious-metal standards described in this work are summarized in Fig. 1.

The most common precise designation of the gold standard CCSD(T)/CBS approximation<sup>35</sup> is MP2/(aTZ,aQZ)+ $\delta$ [CCSD(T)]/aTZ, where the notation (aXZ, aYZ) signifies that the two sets have been employed in the standard  $X^{-3}$  extrapolation of the correlation energy contribution.<sup>57,58</sup> The Hartree-Fock part of the MP2 interaction energy is usually quite well converged in the aQZ basis and no extrapolation is performed for this part. A platinum-standard

calculation needs to extend the coupled-cluster level at least to CCSDT(Q),<sup>59</sup> that is, include full triple and perturbative quadruple excitations on top of CCSD(T). In addition, the leading frozen-core CCSD(T) term has to be converged to CBS even tighter than for the gold standard, and corrections for the core-core and core-valence correlation, relativistic effects, and possibly even terms neglected in the Born-Oppenheimer approximation<sup>60</sup> need to be included. Such a composite designation of the platinum standard is inspired by the high-accuracy composite approaches to thermochemistry, such as HEAT (high accuracy extrapolated *ab initio* thermochemistry),<sup>61</sup> the Weizmann-n (Wn) family of methods,<sup>62</sup> the Feller-Peterson-Dixon algorithm,<sup>63</sup> and the correlation consistent composite approach (ccCA).<sup>64</sup> The silver standard has been designated in Ref. 35 as the DW-CCSD(T<sup>\*\*</sup>)-F12/aDZ level, employing the dispersion-weighted combination of CCSD(T<sup>\*\*</sup>)-F12a and CCSD(T<sup>\*\*</sup>)-F12b proposed in Ref. 53. Several other possible silver standards using double-zeta basis sets with midbond functions will be introduced in Sec. V.

### III. THE GOLD STANDARD—CCSD(T) AT THE COMPLETE BASIS SET LIMIT

#### A. Designation of the gold standard

We envision the gold standard of interaction energy calculations to be suitable for *all benchmarking applications*, where the quality of, e.g., DFT or ML approaches is assessed, and *most PES applications*, where the experimental spectroscopic, scattering, or thermophysical data are to be recovered from the *ab initio* PES. At present, the strictest challenge to the former requirement arises from the recent combinatorially optimized density functionals such as  $\omega$ B97M-V,<sup>65</sup> which attains a root mean standard deviation of 0.18 kcal/mol on an extensive set of (comparatively) “easy” dimers.<sup>37</sup> The severity of the latter requirement obviously varies, and many latest high-resolution spectroscopic and scattering experiments necessitate going beyond the gold standard of theory, as will be illustrated



in detail in Sec. IV. Overall, it is clear that the successful gold standard needs to be accurate, on the average, to well below 0.1 kcal/mol: one would actually prefer the errors to stay within 0.05 kcal/mol even for (most) outliers. At this level of precision, it is quite nontrivial to even assess the performance of a gold standard candidate—we need something better than gold standard for reference! It would be highly desirable to obtain such a reference from experiment, but it is immensely difficult.<sup>66</sup> Interaction energies are not directly measurable, and other experimental quantities such as spectra or cross sections require further calculations (such as solving the nuclear Schrödinger equation) beyond the PES construction (which brings about other sources of uncertainty besides the interaction energy itself) and always probe more than a single geometry on the PES. Thus, our best option to assess potential gold-standard candidates is by comparison to even higher-level *ab initio* interaction energies and, as of right now, there is exactly one benchmark database that has sufficient accuracy to serve as a reference: A24.<sup>67,68</sup>

The current best-estimate A24 interaction energies contain the frozen-core CCSD(T)/CBS term extrapolated from the aQZ and a5Z bases (a5Z and a6Z for selected systems)<sup>47</sup> enhanced by the corrections for core correlation, relativistic effects, and an estimate of the higher-order coupled-cluster terms from the CCSDT(Q)<sup>59</sup> calculations. Thus, these energies are sufficiently accurate to both judge the performance of the CCSD(T)/CBS treatment and evaluate various approximations to this CBS limit. Note that while the gold standard level is often referred to simply as CCSD(T)/CBS, its practical realization requires a particular, sufficiently precise, way to estimate the CBS limit using finite-basis calculations. In fact, the screening of potential gold-standard candidates should be performed in reference to a precise CCSD(T)/CBS estimate (such as the one computed in Ref. 47 and adopted in Ref. 68) with the higher-level corrections omitted to keep the candidate and the reference on an equal footing. For the A24 database, such a screening was performed in Ref. 69 for conventional CCSD(T) and CCSD(T)-F12, and Ref. 70 extended this screening to bases with midbond functions. The results of Ref. 69 show that the CCSD(T) estimates that require only aDZ-level coupled-cluster calculations are quite accurate on the average {with the mean unsigned error (MUE) of only 0.03 kcal/mol for MP2/(aTZ,aQZ)+ $\delta$ [CCSD(T)]/aDZ}; however, individual errors extend all the way from -0.1 to 0.1 kcal/mol, so this level of theory cannot be recommended as an unambiguous gold standard. In contrast, in the aTZ basis sets, both straight-up F12 calculations [e.g., CCSD(T<sup>\*\*</sup>)-F12b/aTZ<sup>49,50</sup>] and composite conventional ones [e.g., MP2/(aTZ,aQZ)+ $\delta$ [CCSD(T)]/aTZ, the originally designated gold standard from Ref. 35] are capable of bringing the MUE down to 0.01 kcal/mol, with all results within 0.05 kcal/mol of the CBS reference. Therefore, any of these variants can be adopted as the gold standard.

We will review the strategies for improving gold-standard interaction energies, and the applications for which such improvement is crucial, in Sec. IV, and the most accurate double-zeta-level approximations to the gold standard in Sec. V. For now, we go back to the two primary areas of gold-standard applications stated at the beginning of this section: the construction of benchmark noncovalent databases and the generation of accurate PESs for individual complexes. Both areas have witnessed an enormous progress in recent years, and it is worthwhile to summarize the most significant new developments.

## B. Benchmark noncovalent databases

We have established how to calculate a gold-standard interaction energy for an individual structure of an intermolecular complex. Now, we have to consider how to select the structures and complexes that make up a noncovalent database suitable for benchmarking applications, that is, sufficiently *diverse* and *balanced*. While the early benchmark databases such as the widely popular S22 set<sup>30</sup> were composed of a handful of (mostly organic) dimers in their respective van der Waals minimum geometries, it was realized soon afterward that the off-minimum radial and angular configurations, including long-range (nearly asymptotic) and short-range (repulsive) ones, are just as important as the minimum structures. In fact, when constructing a dataset, it is not even crucial to precisely pin down the optimal geometry of the complex (unless the geometry itself serves as a reference<sup>71-73</sup>), as an adequate coverage of different PES regions is much more important than having a single point at the actual minimum configuration. As a result, most of the newer databases contain also off-minimum configurations (radially displaced, angularly displaced, or both). A way to achieve the ultimate configurational diversity is to pick the entire set of grid points used to construct an *ab initio* PES for a given system, or the full set of configurations that are attained in actual systems (such as the entire set of amino acid sidechain-sidechain contacts found in the Protein Data Bank<sup>74</sup>). Beyond the geometries of a single system, it is imperative to build a database out of complexes with different interaction types. One particularly useful way of elucidating the physical origins of interaction and classifying systems into interaction types is symmetry-adapted perturbation theory (SAPT).<sup>16,75,76</sup> The relative importance of three possible attractive SAPT components, electrostatics, induction, and dispersion, can be displayed and analyzed by means of ternary diagrams<sup>35,77</sup> so that the relative coverage of the diagram is a measure of the database diversity. It might be noted in passing that the presence of very different interaction strengths (both between different complexes and between different radial configurations of the same system) makes it nontrivial to select a suitable statistical measure to quantify the agreement of an approximate approach with the benchmark values. The commonly used mean unsigned error (MUE), also termed mean absolute deviation (MAD), is not a good description of structures with very different interaction energies, and the mean unsigned relative error (MURE) runs into a problem around the points where the PES crosses zero as small absolute errors can lead to very large relative errors in this case. Several improved metrics have been proposed,<sup>78-81</sup> and the reader is referred to Ref. 26 for a more detailed discussion of the database diversity and performance assessment. Overall, several highly diverse benchmark databases have been constructed in recent years<sup>37,81,82</sup> by combining (and sometimes extending) smaller sets available in the literature: each of these composite datasets contains more than 1000 accurate interaction energies. An even larger dataset, with 247 560 interaction energies, has been created in order to improve the MP2 theory with neural network-optimized spin component scaling;<sup>83</sup> however, this set can hardly be called balanced as nearly half of the structures involve a water molecule as one of the subsystems.

In parallel to the improvements in the database scope and diversity, the accuracy of some older benchmark interaction energies has undergone improvement as well. At the beginning of this decade, quite a bit of effort was directed into refining the original S22

benchmark data<sup>30</sup> as some of them were obtained at the MP2/(cc-pVTZ,cc-pVQZ)+ $\delta$ [CCSD(T)]/cc-pVDZ level that, as we will see in Sec. V, is not even up to the silver standard of accuracy. The currently established benchmark values compiled in Ref. 84, termed S22B, have been computed<sup>84–87</sup> at several different levels of basis set saturation: importantly, the  $\delta$ [CCSD(T)] term has been obtained in at least the aTZ basis set for all 22 systems. The differences between the refined S22B values and the original benchmark range up to nearly 0.7 kcal/mol, confirming that the original data of Ref. 30 were not up to current benchmark standards. Besides the S22 set, several other popular databases such as S66x8<sup>31</sup> and WATER27<sup>88</sup> have been recently refined using explicitly correlated coupled-cluster calculations;<sup>54,89–91</sup> see Sec. V for more details. It should be stressed that, according to our theory level classification, the existing benchmark databases are split into gold-standard and silver-standard data. In fact, complete gold-standard calculations would be too costly for some of the largest databases such as the amino acid sidechain-sidechain interactions (SSI) set of Ref. 74. The bare minimum that can be considered as silver-standard benchmark accuracy is the inclusion of the CCSD(T) interaction energy in at least a partially augmented double-zeta basis, in either stand-alone CCSD(T)-F12 calculation or the composite MP2/CBS+ $\delta$ [CCSD(T)] one (Sec. V will examine the optimal strategies for computing silver-standard interaction energies). While the silver-standard accuracy is sufficient for current applications of the benchmark datasets, some potential upgrades to gold-standard accuracy might be pursued in the future. Overall, in our opinion, the existing collection of benchmark noncovalent databases is sufficiently accurate and sufficiently broad for the assessment and development of new DFT, wavefunction, semiempirical, and machine-learning approaches for *ground-state closed-shell complexes involving small and medium-sized molecules composed of light atoms*; however, the extensions to open-shell systems, excited states, heavy atoms, and large systems still require significant progress. The most notable applications of benchmark noncovalent databases have been reviewed, e.g., in Refs. 26, 29, and 36; see also Refs. 37 and 92.

### C. Accurate potential energy surfaces

The other key application of gold-standard interaction energies is the development of spectroscopically accurate PESs for individual systems of interest. While going beyond CCSD(T)/CBS is sometimes necessary for the highest accuracy (some relevant examples will be discussed in Sec. IV), there exists a large class of complexes (roughly speaking, those containing 2–6 nonhydrogen atoms) for which post-CCSD(T) calculations on the entire set of PES grid points are not feasible; however, the CCSD(T)/aTZ or even CCSD(T)/aQZ calculations (with or without F12 and/or midbond functions) can be carried out with relative ease and used to generate all data points. With the recent progress in the automated PES generation<sup>14,15</sup> and the improved understanding of the CBS convergence of finite-basis CCSD(T) interaction energies (brought about by many developments reviewed in this perspective), the construction of gold-standard PESs is nowadays close to a routine task. Thus, *ab initio* electronic structure theory has happily delivered on the numerous requests for accurate intermolecular PESs, with applications to spectroscopy, scattering, virial coefficients, viscosities, and condensed phase properties. In the rest of this

section, we will review a few of these PESs. Their selection is motivated only by their subjective appeal to us, and the list is far from complete.

The particular significance of interaction potentials for water stems from both its special role in sustaining life and its unusual physical properties in the liquid (such as the density maximum at 4 °C). While an accurate description of any condensed phase requires at least the three-body potential (that is, the account of nonadditive interactions in molecular trimers) in addition to the two-body one,<sup>6</sup> water is a particularly demanding case where the three-body interactions are unusually significant and even the four-body ones are not entirely negligible.<sup>93</sup> Therefore, both two-body and three-body potentials for water have attracted widespread attention. While reaching this point required many years of development by multiple research groups, *ab initio* potentials for (H<sub>2</sub>O)<sub>2</sub><sup>94</sup> and (H<sub>2</sub>O)<sub>3</sub><sup>95</sup> are now available at the gold-standard level of theory including all internal degrees of freedom for the water molecules. The two-body potential<sup>94</sup> was built from 42 508 interaction energies computed at the CCSD(T)/(aTZ+(3s3p2d1f),aQZ+(3s3p2d1f)) level, where the additional (3s3p2d1f) basis functions are centered on the midbond. The three-body potential<sup>95</sup> employed 12 347 trimer interaction energies obtained with CCSD(T)/aTZ+(3s3p2d1f). These potentials have been successful at reproducing a range of experimental quantities, from strictly dimer data such as the vibration-rotation-tunneling spectrum<sup>96</sup> and the second virial coefficient<sup>97</sup> to the structure and energetics of small water clusters<sup>5,98,99</sup> to properties of liquid water such as density and radial distribution functions.<sup>100</sup> Several other CCSD(T)-level PESs for water have been introduced<sup>101–103</sup>—see Ref. 104 for a review.

At the beginning of this century, a strong driving force for the generation of *ab initio* PESs was the spectroscopy of molecules embedded in superfluid helium nanodroplets.<sup>105</sup> Many molecules were investigated in this way, and carbonyl sulfide (OCS) has been one of the most popular as it is quite rigid, linear (so the spectra are simple), and polar (so it is a strong chromophore in both microwave and infrared regions). One of the first experiments compared the infrared spectrum of OCS in <sup>4</sup>He and <sup>3</sup>He nanodroplets, with the sharp rotational lines in the former environment confirming its superfluid nature.<sup>106</sup> Early on, it seemed that the gold-standard level of theory is not absolutely necessary for the He-OCS interaction since the fourth-order Møller-Plesset perturbation theory MP4/aTZ+(3s3p2d) potential has proven quite successful at reproducing experimental vibrational shifts in He<sub>n</sub>-OCS clusters with  $n = 1, \dots, 8$ .<sup>107</sup> Later, a gold-standard four-dimensional He-OCS PES has been constructed by Li and Ma<sup>108</sup> employing the CCSD(T)/aQZ+(3s3p2d1f1g) theory and basis set combination, resulting in substantially improved agreement with experimental microwave and infrared transitions relative to the potential of Ref. 107. Helium is not the only important interacting partner for OCS: the availability of high-resolution infrared<sup>109</sup> and microwave<sup>110</sup> spectra of OCS in *para*- and *ortho*-hydrogen clusters prompted the development of a six-dimensional H<sub>2</sub>-OCS PES at the gold-standard CCSD(T)-F12a/aTZ level.<sup>111</sup> The (OCS)<sub>2</sub> homodimer is also of significant interest to spectroscopy, and the interplay of its polar and nonpolar minima has been elucidated with the help of a CCSD(T)-F12b/cc-pVTZ-F12 potential energy surface.<sup>112</sup>

Another source of demand for high-level PESs is the astrophysical community, where accurate scattering cross sections are required to understand and model the rates of collisional processes occurring in various interstellar objects.<sup>113</sup> One of the collisional partners is usually helium or H<sub>2</sub>, but the other partner can be selected from the long and ever-growing list of molecules detected in interstellar media. An important and unusual (from the perspective of Earth) class of such systems are linear carbon chains, both unsubstituted and capped at one end by hydrogen or another atom. The astrophysical applications have prompted the creation of several high-accuracy PESs involving such chains. The linear tricarbon (C<sub>3</sub>) molecule is an important member of this class, and in the past, our group has contributed to the development of a new He–C<sub>3</sub> potential that was employed to compute rate coefficients for the rotational excitation and deexcitation of C<sub>3</sub> by helium<sup>114</sup> [the underlying PES actually went beyond the gold standard and contained contributions from coupled-cluster excitations beyond CCSD(T)]. More recently, Walker *et al.* have constructed rigid C<sub>6</sub>H<sup>−</sup>–H<sub>2</sub> and C<sub>6</sub>H<sup>−</sup>–He potential surfaces at the gold-standard CCSD(T<sup>\*</sup>)-F12b/cc-pVTZ-F12 level.<sup>115</sup> Interestingly, the long and highly anisotropic C<sub>6</sub>H<sup>−</sup> anion interacts very differently with helium and hydrogen, leading to strongly different rotationally inelastic cross sections. We mention in passing another interesting astrophysically motivated PES, the very recent CCSD(T)-F12b/(cc-pVTZ-F12,cc-pVQZ-F12) potential for a helium atom interacting with a propylene oxide molecule.<sup>116</sup> Propylene oxide is the first chiral organic molecule detected in the interstellar space,<sup>117</sup> and the measurement and modeling of its spectral and collisional properties might shed some light onto the (likely extraterrestrial) origins of the homochirality of life.<sup>118,119</sup>

We conclude this section by mentioning a few of the largest systems for which gold-standard (or close) PESs have been constructed. The sizes of these complexes illustrate the current computational capabilities for running a large number of triple-zeta CCSD(T) calculations and manipulating the resulting data (for example, fitting an analytical PES expression). For CCSD(T) calculations with the full aTZ basis set on all atoms, the largest system with a PES is probably the ethane dimer, for which the MP2/(aQZ,a5Z)+δ[CCSD(T)]/(aDZ,aTZ) potential has been developed by Hellmann<sup>120</sup> and used to compute the second virial coefficient and some transport properties of dilute ethane gas. In the partially augmented haTZ basis (with diffuse basis functions on nonhydrogen atoms only), one should mention the CCSD(T)-F12a PES for the formic acid dimer by Qu and Bowman.<sup>121</sup> While this surface does not extend to all possible geometries, it is sufficiently broad to cover not only all normal modes of the complex but also the entire pathway for the concerted double proton tunneling between the HCOOH molecules. Quite surprisingly, the largest atom-molecule system with a gold-standard PES comes from a 10-year old paper on the benzene-argon complex,<sup>122</sup> with the *ab initio* data obtained at the CCSD(T)/aTZ+(3s3p2d1f1g) level. The interaction energies turned out to be very similar to those obtained in an earlier CCSD(T)/aDZ+(3s3p2d1f1g) study;<sup>123</sup> therefore, subsequent PES calculations on complexes between a rare gas atom and an aromatic molecule tend to use the aDZ basis supplemented by bond functions.<sup>124,125</sup> To our knowledge, no gold-standard PESs for interactions between two aromatic molecules exist; however, all symmetry-nonequivalent close dimers

in the benzene crystal have been studied at the CCSD(T)-F12a/aTZ level.<sup>126</sup>

## IV. THE PLATINUM STANDARD—WHEN CCSD(T) IS NOT ENOUGH

### A. What is a good platinum standard?

Even the gold-standard CCSD(T)/CBS interaction energies are not always accurate enough to interpret high-resolution spectra or scattering cross sections. However, as already mentioned, going beyond the gold standard requires a simultaneous further refinement of the CCSD(T)/CBS leading term and the inclusion of corrections beyond the frozen-core CCSD(T) level. As far as the former improvement is concerned, one needs to go to basis sets of augmented quintuple-zeta (or even sextuple-zeta) quality, combined with CBS extrapolation, the F12 approach, and/or midbond functions. The best strategy for pinpointing an ultra-precise CBS estimate is actually an interesting question. While explicit correlation is so effective in improving small- and medium-basis estimates, conventional CCSD(T) calculations in the largest possible bases are sometimes superior to the CCSD(T)-F12 calculations in the largest basis sets available at that level.<sup>127,128</sup> The primary reason for this somewhat unexpected observation is the residual inaccuracies of the a/b/c approximations to full CCSD(T)-F12. Overall, the accuracy of both CCSD(T) and CCSD(T)-F12 is strongly enhanced by the presence of bond functions, and ultra-precise CBS estimates might need ultra-large midbond sets. Below, we focus on the additional contributions past the CBS limit of the frozen-core CCSD(T) interaction energy.

The interaction energy contribution arising from the correlation of core electrons is easy to compute as the difference between the all-electron and frozen-core CCSD(T) values, obtained in a basis set that includes compact functions optimized for core correlation, such as the aug-cc-pCVXZ and aug-cc-pwCVXZ sequences of Dunning and co-workers.<sup>129</sup> The relativistic correction can be approximated at the scalar one-electron level using the second-order Douglas-Kroll-Hess Hamiltonian<sup>130</sup> or, more recently, the spin-free exact two-component theory in the one-electron approximation (SFX2C-1e or X2C for short).<sup>131</sup> However, the two-electron relativistic interaction energy corrections, such as the spin(own)-orbit term, might also be nonnegligible.<sup>132</sup> The effects of higher-order coupled-cluster excitations might be the most difficult to compute due to the steep computational scaling increase with every excitation level included. Overall, there are two strategies for computing post-CCSD(T) interaction energy terms: full-configuration-interaction (FCI) calculations for few-electron systems and coupled-cluster calculations with full triples (CCSDT), perturbative quadruples [CCSDT(Q)], or even full quadruples (CCSDTQ) for systems where FCI is not feasible. For the latter strategy, it is important to identify the theory level that provides consistent improvement over the gold-standard CCSD(T) calculation—a level that can be recommended as the “platinum standard” for computing interaction energies of subspectroscopic accuracy.

The importance of the CCSDT, CCSDT(Q), and CCSDTQ interaction energy corrections was first studied on individual systems, mainly rare gas dimers.<sup>133,134</sup> The first systematic study of these

corrections over a range of systems (including the newly established A24 database of 24 small complexes<sup>67</sup>) was performed by Hobza and co-workers.<sup>19,135</sup> By comparison with interaction energies computed with the full inclusion of pentuple excitations (CCSDTQP) or with FCI for the smallest systems, Šimová *et al.* showed<sup>19</sup> that the inclusion of full noniterative triples does not provide a systematic improvement over CCSD(T). In order to reach a “platinum standard” level of electron correlation, one needs to include connected quadruple excitations. Fortunately, the perturbative treatment of quadruples via the CCSDT(Q) approach<sup>59</sup> provides an excellent approximation to full iterative CCSDTQ results. Thus, CCSDT(Q) [more precisely, the composite CCSD(T)/CBS+ $\delta_{T+(Q)}$  treatment] is a good candidate for the platinum standard level of theory, but what basis sets are appropriate for computing the very expensive  $\delta_{T+(Q)}$  = CCSDT(Q)–CCSD(T) correction?

In the benchmark studies of the Hobza group,<sup>19,67,135</sup> the post-CCSD(T) corrections were computed using very small bases 6-31G\*(0.25) and 6-31G\*\*(0.25,0.15) (with the numbers in parentheses indicating the altered exponents of the polarization functions relative to 6-31G\*\*)—only a limited subset of complexes employed the somewhat larger aDZ basis. However, the  $\delta_{T+(Q)}$  correction, just like the  $\delta[\text{CCSD(T)}]$  one,<sup>84,136</sup> strongly varies with the basis set and requires at least the aTZ basis to obtain a reasonably saturated value. This behavior of  $\delta_{T+(Q)}$  was established by one of us and co-workers<sup>137</sup> on a set of 21 small weakly bound complexes. Relative to the benchmark  $\delta_{T+(Q)}$  values computed in basis sets aTZ and larger, the 6-31G\*\*(0.25,0.15) estimates were off by 80% on average, showing that it is almost as bad to neglect the post-CCSD(T) contribution altogether as to calculate it in such a small basis set! The aDZ results were better but still far from converged, deviating by an average 35% from the  $\delta_{T+(Q)}$  benchmark. In view of this observation, the earlier CCSDT(Q) benchmarks of the Hobza group were subsequently refined<sup>68</sup> by including the  $\delta_{T+(Q)}/\text{aDZ}$  estimate. The resulting improved A24 database remains the only set of benchmark interaction energies for diverse systems computed at the platinum standard level of theory, and this database has become a keystone for high-accuracy studies of intermolecular interactions including the further refinement of the gold standard.<sup>69</sup>

## B. Ultra-accurate calculations for four-electron complexes

Having made recommendations on how to compute platinum-standard interaction energies for small complexes, we now turn to several important examples where attaining accuracy beyond the gold standard is critical for experimental or fundamental reasons. We first examine the simplest systems which have four electrons total, namely, the He–He, He–H<sub>2</sub>, and H<sub>2</sub>–H<sub>2</sub> complexes. In this case, CCSDTQ is equivalent to FCI and is feasible in at least a moderate basis set.

The helium dimer poses the most stringent demands for the accuracy of the pair potential as its second virial coefficients (density, acoustic, and dielectric) are necessary for the most accurate measurements of the thermodynamic temperature and, consequently, for the development of an improved temperature (and pressure) standard.<sup>1</sup> These measurements utilize constant-volume, acoustic, and dielectric-constant gas thermometers filled with helium, and

the nonideality effects of the gas need to be known to extrapolate to zero pressure (note that these effects are particularly minor for helium as the virial coefficients are small in the first place). Indeed, the current best available pair potential for helium,<sup>138</sup> the culmination of a long-term series of ever-improving descriptions of this interaction,<sup>139–145</sup> exhibits millikelvin (nanohartree) accuracy, with the total interaction energy at the near-minimum separation of 5.6 bohrs amounting to  $-10.995\,57 \pm 0.000\,20$  K. Attaining this accuracy has only been possible by going beyond one-electron basis sets and computing the nonrelativistic potential variationally (that is, at the FCI level) in a four-electron explicitly correlated Gaussian basis. Moreover, the relativistic, quantum electrodynamic, and adiabatic corrections were carefully determined and included in the potential.

The accuracy of the best available He–He interaction energies is truly remarkable, and it cannot at present be matched for any other weakly interacting system, including the seemingly similar four-electron complexes He–H<sub>2</sub> and H<sub>2</sub>–H<sub>2</sub>. There are three reasons why the latter systems, especially the hydrogen dimer, are much more difficult than He–He: the dimensionality of the problem (the fully flexible He–He, He–H<sub>2</sub>, and H<sub>2</sub>–H<sub>2</sub> PESs are 1D, 3D, and 6D, respectively), the number of required centers for basis functions, and the point-group symmetry of the problem (which simplifies the He–He calculations significantly while a general H<sub>2</sub>–H<sub>2</sub> configuration may have no symmetry elements at all). Consequently, the uncertainties for the best available He–H<sub>2</sub> and H<sub>2</sub>–H<sub>2</sub> potentials, while still impressively low, cannot match the He–He potential uncertainty. Specifically, the interaction energies at the van der Waals minima amount to  $-15.870 \pm 0.065$  K for He–H<sub>2</sub><sup>146</sup> and  $-56.96 \pm 0.16$  K for H<sub>2</sub>–H<sub>2</sub>.<sup>147</sup> The potentials of Refs. 146 and 147 were obtained using large one-electron Gaussian basis sets with all excitation levels up to FCI taken into account. At the respective minimum configurations, these higher-level excitations contribute about  $-0.57$  and  $-1.8$  K [beyond gold standard, FCI–CCSD(T)] or  $-0.005$  and  $-0.044$  K [beyond platinum standard, FCI–CCSDT(Q)] for He–H<sub>2</sub> and H<sub>2</sub>–H<sub>2</sub>, respectively. The two potentials have been employed in fully quantum calculations of the second virial coefficient including the effects of monomer flexibility.<sup>148,149</sup> While the flexibility effects are not entirely negligible and the quantum treatment is the only one appropriate below about 50 K, overall, the second virial coefficients are only moderately sensitive to the interaction potential. Some more demanding applications of these PESs include scattering cross sections,<sup>150</sup> bound state properties, and the pressure broadening and shifting effects on the line shapes of Raman transitions in H<sub>2</sub>. The quest for a precise description of the spectral line shapes has already prompted an extension of the original He–H<sub>2</sub> potential<sup>146</sup> to a substantially larger range of H–H vibrations, which has a noticeable effect on the computed pressure broadening and shifting coefficients.<sup>151</sup> In conjunction with the ongoing improvement in the spectral resolution of the experimental H<sub>2</sub> transitions, the “platinum-standard” theoretical PES of Refs. 146 and 151 is expected to enable a fundamentally new description of spectral line shapes beyond the commonly used Voigt profile (the convolution of Lorentzian and Gaussian shapes).<sup>2,152</sup>

The same He–H<sub>2</sub> complex poses a significant and exciting challenge to *ab initio* quantum chemistry also in the excited state, where experimental rate coefficients<sup>153,154</sup> for the Penning ionization  $\text{He}(2^3S)+\text{H}_2 \rightarrow \text{He} + \text{H}_2^+ + e^-$  are precise enough to pinpoint

inaccuracies even in the platinum-standard calculation. While the inclusion of a post-CCSD(T) correction from FCI/aQZ clearly improved the CCSD(T)/CBS description of rate coefficients, some discrepancies remain at low collision energies. In Ref. 154, these discrepancies were resolved by an *ad hoc* scaling of the correlation energy by a factor of 1.004; however, a purely *ab initio* description of the experimentally observed low-energy resonances has not yet been achieved.

### C. Applications of the CCSDT(Q)-level platinum standard

We now move on to somewhat larger complexes where a FCI calculation is not feasible, but the interaction energy accuracy beyond the gold-standard level can be achieved by including higher-order coupled-cluster corrections. In many cases, the existing spectroscopic data are sufficiently precise to confirm the advantage of a post-CCSD(T) treatment over the CCSD(T) one or at least to pinpoint the residual inaccuracies in the CCSD(T)/CBS estimates. Our first example of this kind is the H<sub>2</sub>-CO complex which has been thoroughly studied with both theory and experiment. The high-resolution infrared spectrum of this system is rich in features and strongly depends on the nuclear spin coupling in the H<sub>2</sub> monomer. While the infrared spectrum of *para*-H<sub>2</sub>-CO has been measured and assigned a long time ago,<sup>155</sup> the assignment of the more complex *ortho*-H<sub>2</sub>-CO spectrum, also recorded in Ref. 155, provided a challenge that took more than a decade to overcome. Importantly, an older H<sub>2</sub>-CO potential computed at the CCSD(T)/CBS level of theory<sup>156</sup> had insufficient accuracy to explain the congested spectrum, so a platinum-standard PES was necessary. In fact, H<sub>2</sub>-CO was one of the first complexes for which the importance of post-CCSD(T) corrections was demonstrated as the CCSDT(Q) calculations at the two minimum geometries gave substantial (and unequal) corrections beyond CCSD(T).<sup>157</sup> Accordingly, a new PES was constructed in Ref. 3 using the CCSD(T)/CBS+ $\delta_{T+(Q)}/aDZ$  level of theory, with an estimated accuracy within 0.5 cm<sup>-1</sup> around the van der Waals minimum. This platinum-standard PES led to an impressive agreement with the experimental high-resolution *ortho*-H<sub>2</sub>-CO spectrum, with the discrepancies in infrared transition energies not exceeding 0.06 cm<sup>-1</sup>, so that a complete assignment of the spectral lines was finally possible. The same PES was also highly successful in the reproduction of experimental microwave spectra,<sup>158</sup> scattering cross sections,<sup>159</sup> and second virial coefficients.<sup>160</sup> More recently, a similar inclusion of the  $\delta_{T+(Q)}/aDZ$  interaction energy term significantly improved the He-HCN potential,<sup>161</sup> reducing the deviations of rovibrational energy levels from experimental values<sup>162</sup> by a factor of five.

In some cases, the calculation of a PES at a level of theory higher than CCSD(T) is not feasible, but high-resolution experimental data indicate that the accuracy of the CCSD(T)/CBS treatment might not be sufficient. A prime example is the combined experimental-theoretical study of low-energy resonances in the H<sub>2</sub>-NO interaction.<sup>163</sup> Two CCSD(T)-level NO-H<sub>2</sub> potentials are available,<sup>164,165</sup> differing in the details of how the CBS limit has been established. The experimental integral cross sections at near-resonance collision energies<sup>163</sup> were sufficiently precise to favor the CCSD(T)-F12a/aTZ+(3s3p2d2f1g1h) potential of Ref. 165 over the conventional CCSD(T) potential extrapolated from the (aTZ,aQZ) bases.<sup>164</sup>

However, as stated in Ref. 163, this does not mean that the former CCSD(T)/CBS estimate is more accurate than the latter: quite likely, the opposite is true. However, the slight deviation of the Ref. 165 potential from the CBS values of Ref. 164 might be compensating for the lack of interaction energy terms beyond CCSD(T). Thus, it would be worthwhile to construct a CCSDT(Q)-level H<sub>2</sub>-NO PES to resolve the remaining differences. This is, however, a very formidable task, due in no small part to the open-shell, orbitally degenerate character of NO and the necessity to compute two PESs for the two diabatic states of the complex.

A careful reader has noticed by now that all many-electron examples presented so far involve a molecule with a triple bond (CO, HCN, NO). This is not a coincidence. Interactions of triply bonded molecules are notoriously difficult to describe with low levels of electron correlation. A simple (and crude) justification of this behavior is the importance of  $\pi \rightarrow \pi^*$  excitations for the electronic structure of the interacting molecule: for a triple bond, a full description of the  $\pi \rightarrow \pi^*$  states requires a method with quadruple excitations such as CCSDT(Q) or, preferably, full CCSDTQ. Therefore, complexes involving triply bonded monomers typically come out as the worst offenders in database-level benchmarks of coupled-cluster interaction energies: notable examples are the HF-HCN and H<sub>2</sub>O-CN<sup>-</sup> systems among 16 hydrogen-bonded complexes investigated by Boese<sup>166</sup> and the two N<sub>2</sub>-N<sub>2</sub> structures among the 21 complexes examined in Ref. 137. Interactions involving triply bonded molecules require extra care at all stages of the calculation: not only the  $\delta_T = \text{CCSDT}-\text{CCSD(T)}$  and  $\delta_{(Q)} = \text{CCSDT(Q)}-\text{CCSDT}$  differences constitute up to several percent of interaction energy each but even the  $\delta_Q = \text{CCSDTQ}-\text{CCSDT(Q)}$  contribution might alter the final result by another percent or so.<sup>137</sup> Moreover, the pioneering CCSDT(Q) investigations on the P<sub>2</sub>-P<sub>2</sub> and PCCP-PCCP complexes<sup>167</sup> suggest that the importance of post-CCSD(T) corrections does not diminish as heavier atoms are present.

The complexes of two triply bonded molecules present quite a range of different behaviors of the post-CCSD(T) corrections. For the N<sub>2</sub>-N<sub>2</sub> system, the CCSDT-CCSD(T) and CCSDT(Q)-CCSDT effects are substantial but cancel each other to a large extent. At the near van der Waals minimum geometry, the CCSD(T)/CBS interaction energy amounts to -108.2 cm<sup>-1</sup>, while the  $\delta_T/aQZ$ ,  $\delta_{(Q)}/aTZ$ , and  $\delta_Q/aDZ$  corrections are 3.7, -5.3, and 1.3 cm<sup>-1</sup>, respectively. This cancellation of higher-order effects appears to hold throughout the entire N<sub>2</sub>-N<sub>2</sub> PES: a highly accurate, CCSD(T)/CBS+ $\delta_{T+(Q)}/aDZ$  potential (including also core correlation and relativistic effects) was constructed by Hellmann<sup>168</sup> and it successfully reproduced the best experimental data for virial coefficients, viscosity, and thermal conductivity of a dilute nitrogen gas. Hellmann observed that his  $\delta_{T+(Q)}$  correction for different angular configurations was similar in magnitude, but opposite in sign, to the correction for full triples only, illustrating the (partial but consistent) cancellation. Hellmann also found that his recovery of experimental second virial coefficient data was improved when the  $\delta_{T+(Q)}$  contribution was scaled by a factor of 0.5. This scaling likely implicitly accounts for both the basis set incompleteness effects of the  $\delta_{T+(Q)}/aDZ$  value and the contribution from full quadruple excitations.

For a long time, the isoelectronic CO-N<sub>2</sub> complex was computationally investigated only at lower levels of accuracy. However, in 2018, three CCSD(T)/CBS level surfaces for this system were

published.<sup>169–171</sup> The precise theory level for the *ab initio* grid points ranged from CCSD(T)-F12b/aQZ<sup>169</sup> to CCSD(T)/aQZ+(3s2p1d)<sup>170</sup> to CCSD(T)/aQZ+(3s3p2d1f1g).<sup>171</sup> These small differences in the CCSD(T)/CBS estimates resulted in differences of below 0.01 bohr for the minimum intermolecular separation, up to 7° in the angles of CO and N<sub>2</sub> with respect to the center-of-mass axis and up to 0.8 cm<sup>-1</sup> (out of about 118 cm<sup>-1</sup>) in the minimum interaction energies. The potential of Ref. 171, a tiny bit deeper than the other two, was observed to provide the best agreement with the experimental rovibrational level data, suggesting that a properly selected “gold-standard” estimate might be adequate for CO–N<sub>2</sub>. However, our calculations at the van der Waals minimum geometry indicate that  $\delta_T/aQZ$ ,  $\delta_{(Q)}/aTZ$ , and  $\delta_Q/cc-pVDZ$  contribute 2.2, -3.9, and 0.6 cm<sup>-1</sup>, respectively, to the interaction energy. Thus, CCSD(T) calculations require some error cancellation between basis set incompleteness effects and the higher-order terms to produce a spectroscopically accurate representation of the CO–N<sub>2</sub> surface.

The CO–CO complex happens to be especially difficult for low-level electronic structure methods. It was observed already in 1999 that CCSD(T) is not accurate for this system as it misses important fifth-order interaction terms.<sup>172</sup> Nevertheless, the CCSD(T)-level potential developed by Dawes *et al.*<sup>173</sup> was successful at accurately reproducing experimental rovibrational levels<sup>173</sup> as well as rotationally inelastic cross sections.<sup>174</sup> However, the success of this potential is a consequence of picking a specific, reasonably accurate but not converged, CCSD(T)/CBS estimate so that the basis set incompleteness errors partially cancel the post-CCSD(T) effects. Dawes *et al.* chose the all-electron CCSD(T)-F12b approach without the counterpoise correction extrapolated from the cc-pCVXZ-F12  $\equiv$  CVXZ-F12<sup>175</sup> basis set family with  $X = D, T, Q$ . The different CO–CO minima are connected by a pathway with very minimal barriers so that even the lowest rovibrational states of this complex extend over all of them. Thus, the precise landscape of the minimum-energy pathway, in particular, the difference between the minimum depths, has a large influence on the computed spectroscopic data.

The dependence of the CO–CO interaction energy along the minimum-energy pathway on the theory level is presented in Fig. 2 [the calculations in this figure used a slightly different C–O bond length (2.137 bohrs) than Ref. 173 (2.132 bohrs)]. In addition to the CCSD(T)-F12b/CVXZ-F12 levels employed in Ref. 173,  $X = D, T, Q$ , we present our best estimate of the all-electron CCSD(T)/CBS limit, computed by combining the frozen-core CCSD(T<sup>\*\*</sup>)-F12b/(aQZ,a5Z) value with the CCSD(T)/aug-cc-pCV5Z correction for the core-core and core-valence correlation. Note that the standard  $X^{-3}$  extrapolation used above, while not exactly optimal for explicitly correlated calculations,<sup>176</sup> is certainly better than no extrapolation at all (and it was employed for some variants of the PES in Ref. 173). Furthermore, we add the corrections for full triples (from CCSDT/aQZ) and perturbative quadruples [from CCSDT(Q)/aTZ]. The large discrepancies between different theory and basis set levels in Fig. 2 indicate the inherent difficulty of this complex: the lowest level shown, CCSD(T)-F12b/CVDZ-F12, predicts a saddle point in the global minimum location! One can see that the post-CCSD(T) effects are large and drastically alter the landscape of the minimum-energy pathway. While the  $\delta_{(Q)}$  term is fairly constant, deepening the surface by 2.1–3.4 cm<sup>-1</sup>, the  $\delta_T$

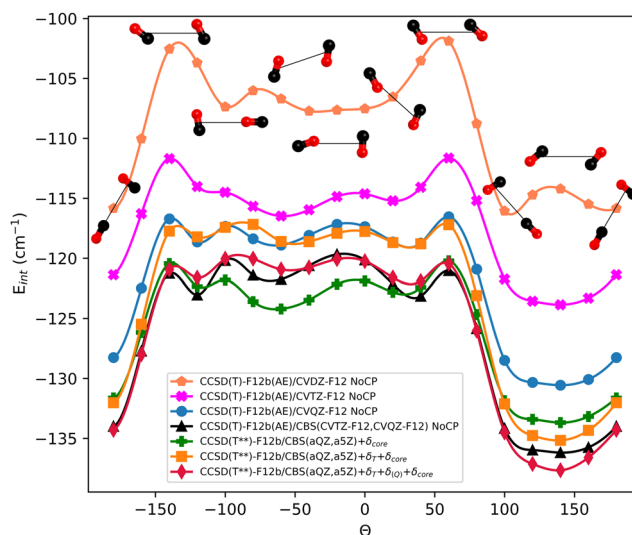


**FIG. 2.** CO–CO interaction energies along the pathway passing through the global and local minima of the complex, computed at various levels of theory. The angle  $\Theta$  is the angle of one of the CO molecules with respect to the line joining the centers of masses; all other intermolecular degrees of freedom are optimized [at the counterpoise-corrected CCSD(T)-F12b/aTZ level] for each  $\Theta$  to stay on the minimum energy pathway. All results have been computed in the present work. The results marked in black are similar (but not identical) to the data points of the best-performing PES of Ref. 173—our calculations use a slightly different C–O bond length and a different CBS extrapolation scheme.

contribution is quite erratic, ranging all the way from -1.9 to 6.4 cm<sup>-1</sup>. Thus, the two leading post-CCSD(T) effects can both amplify each other (like in the global minimum) or partially cancel out (like in the local minima). This behavior is illustrated in Fig. 3 which presents the differences between lower levels of theory and our benchmark CCSDT(Q)-level interaction energies. The (very computationally demanding) full CCSDTQ/aDZ calculations were performed for two high-symmetry minima, and even the  $\delta_Q$  correction turned out to be nonnegligible, amounting to -0.7 cm<sup>-1</sup> for the global minimum and 0.6 cm<sup>-1</sup> for the local one [thus, even the platinum standard CCSDT(Q)/CBS approach underestimates the difference between the two minima by more than 1 cm<sup>-1</sup>]. Figure 3 shows that the CCSD(T)/CBS gold standard description of the CO–CO potential valley, enhanced only by the core correlation, is highly inaccurate. However, the level of theory selected in Ref. 173 is consistently close to our CCSDT(Q)-level results thanks to an error cancellation between the basis set incompleteness effects at the CCSD(T) level and the contribution from higher-order coupled-cluster excitations. Thus, the potential of Ref. 173 owes its very good performance to a clever selection of a CCSD(T)/CBS estimate that facilitates this error cancellation. The large discrepancies shown in Figs. 2 and 3 are clearly not typical and result from a particularly unfortunate combination of a large magnitude of the post-CCSD(T) terms and their variations in sign. We present this worst-case scenario to serve as a cautionary tale against automatically neglecting the interaction energy contributions beyond the gold standard.

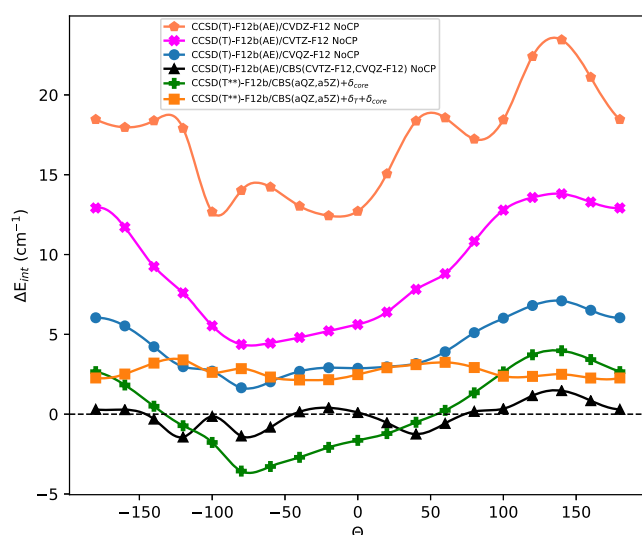


FIG. 3. Differences between lower levels of theory and our best platinum-standard CCSD(T)-level estimate (the red diamonds in Fig. 2) for the CO-CO minimum interaction energy pathway depicted in Fig. 2.

## V. THE SILVER STANDARD—WHEN CCSD(T)/ATZ IS NOT AN OPTION

### A. Approximations to the gold standard

We have postulated in Sec. III that the gold-standard precision in the determination of the CCSD(T)/CBS limit requires, one way or another, a CCSD(T) calculation in a basis set of triple-zeta quality and size. When such a calculation is available, a suitable CCSD(T)/CBS estimate can be generated in several ways including the explicitly correlated approach [for example, CCSD(T<sup>\*\*</sup>)-F12b/aTZ], the composite treatment [for example, MP2/(aQZ,a5Z)+δ[CCSD(T)]/aTZ], or a combination of both. It should be noted, however, that a CBS extrapolation involving a double- and triple-zeta basis set {for example, CCSD(T)/(aDZ,aTZ) or MP2/(aQZ,a5Z)+δ[CCSD(T)]/(aDZ,aTZ)} is typically inferior to plain aTZ as the information from the small aDZ basis set does more harm than good.<sup>84</sup>

Unfortunately, for a large class of medium-sized systems, CCSD(T)/aDZ is feasible but CCSD(T)/aTZ is not. In such a case, the precision attained by a CBS limit estimate involving only aDZ-level CCSD(T) [or CCSD(T)-F12] calculations might not be up to the gold-standard requirements. Nevertheless, it is highly useful to establish a level of theory and basis set that can be termed “silver standard,” that is, it is feasible when CCSD(T)/aDZ is feasible, reasonably accurate, and free from particularly bad outliers as long as the underlying complexes are entirely single reference. A silver-standard benchmark calculation is accurate enough for many practical purposes, including the refinement of more approximate methods based on DFT, semiempirical approaches, or machine learning. Therefore, there is a large market for accurate silver-standard benchmark interaction energies and it is worthwhile to examine the best options to utilize CCSD(T)/aDZ-level results in the determination of benchmark values.

The selection of approximate electronic structure methods that do the best job at recovering gold-standard interaction energy benchmarks was thoroughly studied by Burns *et al.*<sup>35</sup> In this work, which should be credited for coining the terms “silver standard” and “bronze standard,” the benchmark level of theory was chosen as MP2/(aTZ,aQZ)+δ[CCSD(T)]/aTZ. Relative to this realization of the gold standard, 394 different combinations of theory level and basis set were tested on a dataset of 345 weak interaction energies. Among the methods that require some aDZ-level CCSD(T) calculation, the best performer (the “silver standard”) was found to be the DW-CCSD(T<sup>\*\*</sup>)-F12/aDZ dispersion-weighted approach.<sup>53</sup> The silver-standard interaction energies deviated by an average of 0.05 kcal/mol from the gold-standard values, indicating a very acceptable and consistent accuracy. Burns *et al.*<sup>35</sup> went on to propose also a “bronze standard” MP2C-F12/aDZ model chemistry, based on the “coupled MP2” (MP2C) approach of Hesselmann,<sup>177</sup> that leads to an average error of 0.16 kcal/mol and is significantly cheaper than even a double-zeta CCSD(T) calculation. One should note, however, that the 0.16 kcal/mol accuracy is only marginally better than the one afforded (on similar weakly interacting systems) by the most modern variants of density functional theory.<sup>37</sup> Therefore, the bronze standard may not be accurate enough for an important class of applications, the benchmarking and refinement of DFT-based approaches to weak interactions, and we will focus exclusively on the silver standard from now on.

### B. Double-zeta CCSD(T) interaction energies

As we have already stated in Sec. II, a “double zeta-level CCSD(T) interaction energy” might mean many different things. Therefore, a thorough assessment of the performance of different possible variants is worthwhile. A careful study of the influence of the F12 variant and basis set on the quality of the CCSD(T)-F12 interaction energies was published by Sirianni *et al.*<sup>69</sup> The authors examined in detail the A24<sup>67</sup> and S22<sup>30</sup> noncovalent databases and compared the performance of different CCSD(T)-F12 approximations as well as of the aXZ and cc-pVXZ-F12 basis set families. Probably the most interesting finding of Ref. 69 was the clearly inferior performance of the cc-pVXZ-F12 sequence compared to the standard aXZ one (the same phenomenon was observed earlier for a much smaller class of systems<sup>127,128</sup>). The underperformance of CCSD(T)-F12/cc-pVXZ-F12 interaction energies might be somewhat surprising—contrary to what the basis set name suggests, for atoms other than H and He, the cc-pVXZ-F12 set has more functions than the aXZ one at the same X. It has been argued<sup>69</sup> that the high-angular-momentum exponents of the cc-pVXZ-F12 sets, optimized for molecular correlation energies, are not diffuse enough for noncovalent interaction energy computations. Our criticism of the cc-pVXZ-F12 basis sets in the context of interaction energy calculations is not meant to discredit a series of recent benchmark interaction energy reevaluations<sup>54,89–91</sup> for the S66x8,<sup>31</sup> WATER27,<sup>88</sup> and X40x10<sup>178</sup> databases using a combination of MP2-F12/CBS and the CCSD-MP2 and CCSD(T)-CCSD corrections calculated using either the F12 approach with cc-pVXZ-F12 basis sets or the conventional approach with heavy-augmented cc-pVXZ bases. The benchmark interaction energies computed in this way are clearly superior to the original estimates due to the sheer power of the F12 approach and a careful selection of the CCSD-F12 variant, the (T) estimate,

and the treatment of the counterpoise correction. However, it is quite likely that similarly accurate (or better) CCSD(T)/CBS estimates could have been obtained at a reduced computational cost should the authors of Refs. 54 and 89–91 have chosen the standard aXZ basis set family instead of the cc-pVXZ-F12 one.

As far as the aXZ basis sets are concerned, Sirianni *et al.*<sup>69</sup> found that the CCSD(T<sup>\*\*</sup>)-F12b and CCSD(F12<sup>\*</sup>)(T<sup>\*\*</sup>) variants exhibited very similar (and impressive) performance on both the A24 and S22 databases. The performance of CCSD(T<sup>\*\*</sup>)-F12a is more erratic—it happens to be the best aDZ-level variant for A24 but the worst one for S22. For the latter dataset, the highest aDZ-level accuracy was attained by the DW-CCSD(T<sup>\*\*</sup>)-F12 combination.<sup>53</sup> As DW-CCSD(T<sup>\*\*</sup>)-F12/aDZ performed also respectably well on the A24 dataset, its designation as the silver standard<sup>35</sup> was confirmed in Ref. 69. Overall, the combination of the F12 approach, aXZ basis sets, and the counterpoise correction emerged as the best strategy to converge to the CBS limit, especially at the silver-standard level requiring only double-zeta coupled-cluster calculations.

### C. The role of midbond functions

The authors of Ref. 69 did not consider one more technique that has proven successful in accurately recovering weak interaction energies—the addition of midbond functions. Such functions increase the basis set size only slightly as one additional basis function center is added to all the atomic centers in the complex (one may note in passing that the placement of more than one midbond center, or even the determination whether more than one center is needed, has not been investigated so far, but some initial tests have been carried out for a “cloud” of off-center Gaussians surrounding the complex<sup>179,180</sup>). As a result, for molecules of the size targeted by the silver standard, an aDZ+(bond) calculation is significantly cheaper than an aTZ one. The use of midbond functions has initially been popularized by Tao,<sup>181,182</sup> who designed standard midbond sets such as (3s3p2d) and established, through tests on very simple complexes, that neither the precise location of the midbond center nor the precise midbond exponents have a significant influence on the accuracy of the resulting interaction energies. Thus, present-day calculations involving midbond functions typically use either one of the standard midbond sets (independent of the atom-centered basis set) or a hydrogenic aXZ basis with the cardinal number *X* that varies together with the cardinal number of the atom-centered set. The latter choice somewhat simplifies calculations that require density-fitting and/or resolution-of-identity basis sets [such as MP2-F12 and CCSD(T)-F12] as the required auxiliary bases are readily available for aXZ. In contrast, for standard midbond sets, only one auxiliary basis has been constructed and tested.<sup>183</sup> While the use of bond functions requires a dimer basis set in all calculations (in other words, the counterpoise correction must be included), there is nothing wrong with combining midbond functions with CBS extrapolation<sup>184</sup> and/or the F12 approach.<sup>127</sup> Thus, it is worthwhile to check if the inclusion of bond functions in aDZ-level CCSD(T) and/or CCSD(T)-F12 calculations can lead to an improved silver standard of interaction energy. A recent study from our group<sup>70</sup> has shown that the answer is yes.

In order to build directly on the findings of Ref. 69, Ref. 70 examined the same A24<sup>87</sup> and S22<sup>30</sup> databases. The performance of CCSD(T), CCSD(T)-F12a, and CCSD(T)-F12b (with or without the scaling of triples) has been compared between midbond-less aXZ bases and the same atom-centered aXZ sets augmented by a constant [(3s3p2d) and (3s3p2d2f)] or variable (hydrogenic aXZ) set of functions centered on the intermolecular bond. The one-step CCSD(T) approaches were compared to the composite MP2/CBS+ $\delta$ [CCSD(T)] ones, and the partially augmented basis sets (from the “calendar” family: jul-cc-pVXZ, jun-cc-pVXZ, ...<sup>42</sup>) were investigated together with the fully augmented aXZ ones. As far as the F12 variant is concerned, an interesting observation was made that confirmed earlier findings for a more limited class of systems:<sup>80,185</sup> the CCSD-F12a variant, which is more approximate (contains fewer diagrams) than CCSD-F12b,<sup>49,50</sup> performs best when combined with unscaled triples (which can be viewed as more approximate than scaled triples—even if the scaling is imperfect, it is almost certainly better than no scaling at all). An exception to this observation are the data in the smallest aDZ basis when CCSD(T<sup>\*\*</sup>)-F12a accidentally happens to be the best one. The CCSD-F12b variant, in turn, performs best when a scaled (T<sup>\*\*</sup>) contribution is added to it. This suggests that while the CCSD(T<sup>\*\*</sup>)-F12b [or CCSD(F12<sup>\*</sup>)(T<sup>\*\*</sup>)] combination provides “the right answer for the right reason,” the CCSD(T)-F12a approach benefits from an (accidental but quite systematic) error cancellation between the CCSD part and the triples part. By comparing against separate CCSD/CBS and (T)/CBS benchmarks for the A24 database, the authors of Ref. 70 showed that this is indeed the case, especially for larger basis sets and when the milder, CCSD-based scaling<sup>54</sup> is used for the triples contribution instead of the MP2-based one.

The addition of midbond functions improved the accuracy of all variants considered in Ref. 70 except for CCSD(T<sup>\*\*</sup>)-F12a. In the case of conventional CCSD(T) and of CCSD(T)-F12b with unscaled and CCSD-scaled triples, the improvement increased systematically as the midbond basis set was enlarged, while for CCSD(T)-F12a and CCSD(T<sup>\*\*</sup>)-F12b, the ordering of results with different midbonds was more erratic. It was observed that the combination of midbond functions and CCSD(T)-F12b with CCSD-scaled triples was the least reliant on error cancellation between the CCSD part and the triples part and thus likely to provide the most consistent performance for systems outside of the investigated databases. Moreover, the combination of midbond functions and the composite MP2/CBS+ $\delta$ [CCSD(T)] treatment is still capable of providing accurate results when some or all diffuse functions are removed from the atom-centered part of the basis set. In fact, the cheapest variant that delivered an average accuracy within 0.1 kcal/mol for both databases was MP2/CBS+ $\delta$ [CCSD(T)]/cc-pVDZ+(3s3p2d2f), where the only diffuse functions present were those centered on the midbond. The switch from  $\delta$ [CCSD(T)] to a suitably chosen variant of  $\delta$ [CCSD(T)-F12] decreased the errors further, and considering both the accuracy and the computational cost, the authors of Ref. 70 went ahead to propose three new silver standards. The aforementioned MP2/CBS+ $\delta$ [CCSD(T)]/cc-pVDZ+(3s3p2d2f) level was designated the “silver-minus” one as it is significantly cheaper than the established DW-CCSD(T<sup>\*\*</sup>)-F12/aDZ silver standard<sup>35</sup> but only slightly less accurate. The newly designated “silver” level, MP2/CBS+ $\delta$ [CCSD(T)-F12a]/jun-cc-pVDZ+(3s3p2d2f), is both a



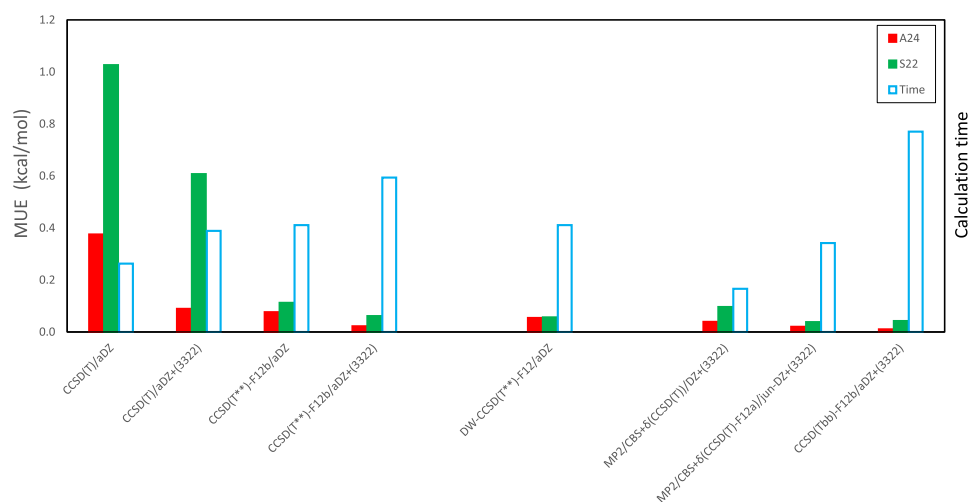


**FIG. 4.** The accuracy (MUE values on the A24 and S22 databases) and computational efficiency (relative timings for the parallel-displaced benzene dimer) of different CCSD(T)/CBS approximations that require only double-zeta coupled-cluster calculations. The original silver standard of Ref. 35 and the new “silver-minus,” “silver,” and “silver-plus” standards introduced in Ref. 70 are included. (3322) is a shorthand notation for the (3s3p2d2f) set of midbond functions. Reprinted with permission from Dutta and Patkowski, *J. Chem. Theory Comput.* **14**, 3053–3070 (2018). Copyright 2018 American Chemical Society.

little more accurate and a little more efficient than the silver standard of Ref. 35. Finally, the “silver-plus” level, CCSD(T)bb-F12b/aDZ + (3s3p2d2f), where (Tbb) denotes the CCSD-F12b-based scaling of triples,<sup>54</sup> is somewhat more expensive than the original silver standard but provides much higher accuracy. The performance of different silver-standard variants considered in Ref. 70 is summarized in Fig. 4.

In Ref. 70, substantial improvement to the double-zeta-level CCSD(T)/CBS estimates was achieved with standard, off-the-shelf sets of midbond functions. It remains to be seen whether additional gains in the accuracy can be attained by optimizing the exponents of midbond functions and/or their precise placement in the interaction region. As the original work of Tao<sup>182</sup> suggested this is not the case, little effort has been made in the literature to design improved midbond sets. However, a recent work by Shaw and Hill<sup>186</sup> has challenged this paradigm. These authors optimized compact sets of bond functions at the MP2 and CCSD(T) levels for several noble gas dimers, alkali metal dimers, and small molecular complexes investigated in Ref. 128. Shaw and Hill concluded that while the commonly used intermolecular midpoints were close to the optimal location for the midbond center, the dependence of the interaction energy on the midbond exponents was quite considerable, and the optimization made their compact midbond sets highly competitive with larger unoptimized sets (on the negative side, the optimized exponents did not appear to be transferable between different systems). The findings of Ref. 186 suggest that there is still room for improvement of the silver standard by choosing carefully optimized midbond sets instead of the unoptimized ones. We expect this direction of research to be pursued in the near future, together with an extension of the silver-standard performance studies to larger and more diverse databases including off-minimum intermolecular separations.

## VI. CONCLUDING REMARKS

We have presented the current state of the art in the calculations of accurate interaction energies in small- and medium-sized

complexes. This state of the art is quite impressive—there exists an established gold standard that is typically accurate to several hundredths of a kcal/mol and capable of producing PESs that reproduce experimental observables for all but the highest-resolution spectroscopic and scattering measurements. Moreover, this gold standard can be either further improved if even higher accuracy is required or relaxed to provide interaction energies of near-gold-standard accuracy at a significantly reduced computational cost. Thus, the gold standard, realized in practice by MP2/(aTZ,aQZ)+δ[CCSD(T)]/aTZ or a similar calculation, is supported by the higher-accuracy platinum standard, composed of an accurate frozen-core CCSD(T)/CBS estimate plus corrections for higher-level coupled-cluster excitations through CCSDT(Q), the correlation of core electrons, and relativistic effects. On the other side, the gold standard is accompanied by the silver one, with average interaction energy errors still well below 0.1 kcal/mol attained using only a double-zeta CCSD(T) calculation. The accuracy of CCSD(T)/aDZ is strongly improved by the explicitly correlated CCSD(T)-F12 approach, the composite MP2/CBS+δ[CCSD(T)] treatment, the addition of midbond functions, or, preferably, by a combination of at least two of these enhancements.<sup>69,70</sup> Thus, at this point, we have a very clear understanding of how to attain a given level of accuracy for a small closed-shell complex, and given the recent advances in the automatic generation of the entire PES,<sup>14,15</sup> the development of new gold-standard-level potentials for complexes of experimental interest is now close to routine. Moreover, with significant computational effort required to compute CCSDT(Q) interaction energies, one can produce an even more accurate platinum-standard PES that is capable of resolving the intricacies of complicated spectra and locating resonances in elastic and inelastic cross sections.

Impressive progress has also been made in the construction of gold- and silver-standard benchmark noncovalent databases, both in terms of the accuracy of the individual data points and the breadth and diversity of the entire dataset. As a result, the newest composite databases involve at least  $10^3$  CCSD(T) interaction energies: in one case,<sup>83</sup> the number of data points is over  $10^5$ ! This increase in

the amount of available high-accuracy data is particularly helpful for developing machine-learning approaches which are notoriously data-intensive. Interestingly, while nearly all gold-standard PESs for individual complexes have been obtained in bases with midbond functions (cf. Sec. III), very few numbers included in noncovalent databases have been computed with midbonds. There is no good algorithmic reason for this: it is likely that the awareness of the benefits of midbonds in the benchmarking community is lower than in the PES community. One relatively unexplored issue of adding midbond functions is the dependence of the accuracy improvement on the size of the complex: it is quite intuitive that the addition of a single midbond center will provide more benefit for an atom-atom complex, where the midbond constitutes 1/3 of the basis function centers, than, say, for a coronene dimer where the midbond is just 1 out of 73 centers. For a stacked structure of the latter system, it is likely that more than one midbond center is required for a good coverage of the large contact area between the molecules. However, the best practices of placing multiple midbond centers, or even deciding whether more than one center is needed, are yet to be explored.

Contrary to the situation for closed-shell systems, the existing benchmark data for open-shell noncovalent complexes are quite scarce. A few small datasets for interactions involving radicals have been constructed using high-level calculations,<sup>187–189</sup> but each set is composed of fairly similar systems and none of them contain off-minimum configurations. Thus, substantial progress is required to assess the accuracy of approximate approaches for open-shell interactions on an equal footing with the closed-shell ones, and we expect new extended open-shell databases to appear in the near future. Another direction of current and future progress is the extension of benchmark datasets beyond just interaction energies. Indeed, there already exist pilot benchmark studies of noncovalent geometries,<sup>72,73</sup> and a recent database of CCSD(T)-level dipole moments<sup>190</sup> includes some noncovalent complexes in addition to single molecules. However, more variety in the benchmark data for each of these kinds would be desirable as would a benchmark dataset of harmonic vibrational frequencies in some noncovalent complexes. Actually, there is some evidence that these frequencies are even more sensitive to the theory level than interaction energies: some MP2 normal modes for water clusters are very far off the benchmark CCSD(T) values.<sup>191</sup> Finally, several current applications including the construction of first-principles-based force fields<sup>192,193</sup> and physics-based machine learning of noncovalent interaction energies<sup>194</sup> strongly benefit from an accurate physical energy decomposition, that is, a partitioning of the overall interaction energy into well-defined terms of different physical origins. Such a partitioning can be provided by SAPT,<sup>16</sup> and in recent years, the accuracy of different-level SAPT decompositions has been thoroughly tested,<sup>195</sup> including the generation of a small set of benchmark SAPT data for the highest-accuracy, coupled-cluster treatment of intramolecular electron correlation.<sup>196</sup>

Perhaps the most pressing issue in the accurate calculations of noncovalent interaction energies is an extension of the benchmark methodology to larger systems. This specific issue has been the subject of a recent perspective by Al-Hamdani and Tkatchenko;<sup>197</sup> here, we will just mention a few obstacles that lie ahead. There currently exist two small benchmark datasets of large intermolecular complexes: L7<sup>198</sup> and S12L.<sup>199,200</sup> The reference energies for the S12L

set were obtained by (approximately) back-correcting experimental association free energies for effects such as harmonic zero-point energy, entropy, and solvent influence. The L7 reference interaction energies were computed *ab initio*, using MP2/CBS plus a correction for higher-level correlation obtained from the quadratic configuration interaction method with singles, doubles, and perturbative triples [QCISD(T)] in a very small 6-31G\*(0.25) basis set. Thus, both reference data are not fully up to even the silver standard discussed in Sec. V. Several other high-level calculations have been performed for partial or whole L7 and S12L datasets,<sup>21,201,202</sup> including domain-based local pair natural orbital CCSD(T) [DLPNO-CCSD(T)]<sup>203</sup> and diffusion Monte Carlo (DMC).<sup>204</sup> However, those high-level results differ from the original reference energies and from each other by several kcal/mol,<sup>197</sup> indicating that the accuracy with which the L7 and S12L interaction energies are known is significantly inferior to the precious metals standards discussed in this perspective. The challenges facing such accurate calculations are not limited to the computational cost: one has to also minimize the residual errors of the local CCSD(T) approximation (or, alternatively, the fixed-node errors in DMC), and for some important classes of complexes (for example, those involving large polycyclic aromatic hydrocarbons), even full CCSD(T) might be inaccurate due to the emerging multireference character. Thus, the accurate *ab initio* treatment of larger complexes still leaves a lot to be desired, and we expect continuous improvement of large benchmarks in the near future.

## ACKNOWLEDGMENTS

This work was supported by the U.S. National Science Foundation CAREER Award No. CHE-1351978.

## REFERENCES

- M. R. Moldover, W. L. Tew, and H. W. Yoon, *Nat. Phys.* **12**, 7 (2016).
- J.-M. Hartmann, H. Tran, R. Armante, C. Boulet, A. Campargue, F. Forget, L. Gianfrani, I. Gordon, S. Guerlet, M. Gustafsson *et al.*, *J. Quant. Spectrosc. Radiat. Transfer* **213**, 178 (2018).
- P. Jankowski, A. R. W. McKellar, and K. Szalewicz, *Science* **336**, 1147 (2012).
- B. Yang, P. Zhang, X. Wang, P. C. Stancil, J. M. Bowman, N. Balakrishnan, and R. C. Forrey, *Nat. Commun.* **6**, 6629 (2015).
- Y. Wang, V. Babin, J. M. Bowman, and F. Paesani, *J. Am. Chem. Soc.* **134**, 11116 (2012).
- G. J. O. Beran, *Chem. Rev.* **116**, 5567 (2016).
- P. Wernet, D. Nordlund, U. Bergmann, M. Cavalleri, M. Odelius, H. Ogasawara, L. Å. Näslund, T. K. Hirsch, L. Ojamäe, P. Glatzel *et al.*, *Science* **304**, 995 (2004).
- R. R. Knowles and E. N. Jacobsen, *Proc. Natl. Acad. Sci. U. S. A.* **107**, 20678 (2010).
- A. K. Geim and I. V. Grigorieva, *Nature* **499**, 419 (2013).
- S. O. Odoh, C. J. Cramer, D. G. Truhlar, and L. Gagliardi, *Chem. Rev.* **115**, 6051 (2015).
- A. S. Mahadevi and G. N. Sastry, *Chem. Rev.* **116**, 2775 (2016).
- J. Cui and R. V. Krems, *J. Phys. B: At. Mol. Opt. Phys.* **49**, 224001 (2016).
- C. Qu, Q. Yu, B. L. Van Hoozen, Jr., J. M. Bowman, and R. A. Vargas-Hernández, *J. Chem. Theory Comput.* **14**, 3381 (2018).
- M. P. Metz, K. Piszczatowski, and K. Szalewicz, *J. Chem. Theory Comput.* **12**, 5895 (2016).
- E. Quintas-Sánchez and R. Dawes, *J. Chem. Inf. Model.* **59**, 262 (2019).
- B. Jeziorski, R. Moszyński, and K. Szalewicz, *Chem. Rev.* **94**, 1887 (1994).
- R. J. Bartlett and M. Musiał, *Rev. Mod. Phys.* **79**, 291 (2007).

- <sup>18</sup>K. Raghavachari, G. W. Trucks, J. A. Pople, and M. Head-Gordon, *Chem. Phys. Lett.* **157**, 479 (1989).
- <sup>19</sup>L. Šimová, J. Řezáč, and P. Hobza, *J. Chem. Theory Comput.* **9**, 3420 (2013).
- <sup>20</sup>F. A. Evangelista, *J. Chem. Phys.* **149**, 030901 (2018).
- <sup>21</sup>F. Pavošević, C. Peng, P. Pinski, C. Riplinger, F. Neese, and E. F. Valeev, *J. Chem. Phys.* **146**, 174108 (2017).
- <sup>22</sup>G. Schmitz and C. Hättig, *J. Chem. Theory Comput.* **13**, 2623 (2017).
- <sup>23</sup>Y. Guo, C. Riplinger, U. Becker, D. G. Liakos, Y. Minenkov, L. Cavallo, and F. Neese, *J. Chem. Phys.* **148**, 011101 (2018).
- <sup>24</sup>Q. Ma and H.-J. Werner, *Wiley Interdiscip. Rev.: Comput. Mol. Sci.* **8**, e1371 (2018).
- <sup>25</sup>P. R. Nagy, G. Samu, and M. Kállay, *J. Chem. Theory Comput.* **14**, 4193 (2018).
- <sup>26</sup>K. Patkowski, in *Annual Reports in Computational Chemistry*, edited by D. A. Dixon (Elsevier, Amsterdam, 2017), Vol. 13, pp. 3–91.
- <sup>27</sup>C. Hättig, W. Klopper, A. Köhn, and D. P. Tew, *Chem. Rev.* **112**, 4 (2012).
- <sup>28</sup>L. Kong, F. A. Bischoff, and E. F. Valeev, *Chem. Rev.* **112**, 75 (2012).
- <sup>29</sup>J. Řezáč and P. Hobza, *Chem. Rev.* **116**, 5038 (2016).
- <sup>30</sup>P. Jurečka, J. Šponer, J. Černý, and P. Hobza, *Phys. Chem. Chem. Phys.* **8**, 1985 (2006).
- <sup>31</sup>J. Řezáč, K. E. Riley, and P. Hobza, *J. Chem. Theory Comput.* **7**, 2427 (2011).
- <sup>32</sup>E. Caldeweyher, C. Bannwarth, and S. Grimme, *J. Chem. Phys.* **147**, 034112 (2017).
- <sup>33</sup>A. S. Christensen, T. Kubař, Q. Cui, and M. Elstner, *Chem. Rev.* **116**, 5301 (2016).
- <sup>34</sup>J. Behler, *J. Chem. Phys.* **145**, 170901 (2016).
- <sup>35</sup>L. A. Burns, M. S. Marshall, and C. D. Sherrill, *J. Chem. Phys.* **141**, 234111 (2014).
- <sup>36</sup>S. Grimme, A. Hansen, J. G. Brandenburg, and C. Bannwarth, *Chem. Rev.* **116**, 5105 (2016).
- <sup>37</sup>N. Mardirossian and M. Head-Gordon, *Mol. Phys.* **115**, 2315 (2017).
- <sup>38</sup>G. Chałasiński and M. M. Szczyński, *Chem. Rev.* **100**, 4227 (2000).
- <sup>39</sup>B. Santra, A. Michaelides, and M. Scheffler, *J. Chem. Phys.* **131**, 124509 (2009).
- <sup>40</sup>T. H. Dunning, Jr., *J. Chem. Phys.* **90**, 1007 (1989).
- <sup>41</sup>R. A. Kendall, T. H. Dunning, Jr., and R. J. Harrison, *J. Chem. Phys.* **96**, 6796 (1992).
- <sup>42</sup>E. Papajak, J. Zheng, X. Xu, H. R. Leverentz, and D. G. Truhlar, *J. Chem. Theory Comput.* **7**, 3027 (2011).
- <sup>43</sup>S. F. Boys and F. Bernardi, *Mol. Phys.* **19**, 553 (1970).
- <sup>44</sup>I. Mayer and A. Vibók, *Int. J. Quantum Chem.* **40**, 139 (1991).
- <sup>45</sup>J. Kim, S. Lee, S. J. Cho, B. J. Mhin, and K. S. Kim, *J. Chem. Phys.* **102**, 839 (1995).
- <sup>46</sup>A. Halkier, W. Klopper, T. Helgaker, P. Jørgensen, and P. R. Taylor, *J. Chem. Phys.* **111**, 9157 (1999).
- <sup>47</sup>L. A. Burns, M. S. Marshall, and C. D. Sherrill, *J. Chem. Theory Comput.* **10**, 49 (2014).
- <sup>48</sup>F.-M. Tao, *J. Chem. Phys.* **98**, 2481 (1993).
- <sup>49</sup>T. B. Adler, G. Knizia, and H.-J. Werner, *J. Chem. Phys.* **127**, 221106 (2007).
- <sup>50</sup>G. Knizia, T. B. Adler, and H.-J. Werner, *J. Chem. Phys.* **130**, 054104 (2009).
- <sup>51</sup>C. Hättig, D. P. Tew, and A. Köhn, *J. Chem. Phys.* **132**, 231102 (2010).
- <sup>52</sup>O. Marchetti and H.-J. Werner, *J. Phys. Chem. A* **113**, 11580 (2009).
- <sup>53</sup>M. S. Marshall and C. D. Sherrill, *J. Chem. Theory Comput.* **7**, 3978 (2011).
- <sup>54</sup>B. Brauer, M. K. Kesharwani, S. Kozuch, and J. M. L. Martin, *Phys. Chem. Chem. Phys.* **18**, 20905 (2016).
- <sup>55</sup>K. A. Peterson, T. B. Adler, and H.-J. Werner, *J. Chem. Phys.* **128**, 084102 (2008).
- <sup>56</sup>N. Sylvetsky, M. K. Kesharwani, and J. M. L. Martin, *J. Chem. Phys.* **147**, 134106 (2017).
- <sup>57</sup>T. Helgaker, W. Klopper, H. Koch, and J. Noga, *J. Chem. Phys.* **106**, 9639 (1997).
- <sup>58</sup>A. Halkier, T. Helgaker, P. Jørgensen, W. Klopper, H. Koch, J. Olsen, and A. K. Wilson, *Chem. Phys. Lett.* **286**, 243 (1998).
- <sup>59</sup>Y. J. Bomble, J. F. Stanton, M. Kállay, and J. Gauss, *J. Chem. Phys.* **123**, 054101 (2005).
- <sup>60</sup>J. Gauss, A. Tajti, M. Kállay, J. F. Stanton, and P. G. Szalay, *J. Chem. Phys.* **125**, 144111 (2006).
- <sup>61</sup>A. Tajti, P. G. Szalay, A. G. Császár, M. Kállay, J. Gauss, E. F. Valeev, B. A. Flowers, J. Vázquez, and J. F. Stanton, *J. Chem. Phys.* **121**, 11599 (2004).
- <sup>62</sup>A. Karton, E. Rabinovich, J. M. L. Martin, and B. Ruscic, *J. Chem. Phys.* **125**, 144108 (2006).
- <sup>63</sup>D. Feller, K. A. Peterson, and D. A. Dixon, *J. Chem. Phys.* **129**, 204105 (2008).
- <sup>64</sup>N. J. DeYonker, T. R. Cundari, and A. K. Wilson, *J. Chem. Phys.* **124**, 114104 (2006).
- <sup>65</sup>N. Mardirossian and M. Head-Gordon, *J. Chem. Phys.* **144**, 214110 (2016).
- <sup>66</sup>R. A. Mata and M. A. Suhm, *Angew. Chem., Int. Ed.* **56**, 11011 (2017).
- <sup>67</sup>J. Řezáč and P. Hobza, *J. Chem. Theory Comput.* **9**, 2151 (2013).
- <sup>68</sup>J. Řezáč, M. Dubecký, P. Jurečka, and P. Hobza, *Phys. Chem. Chem. Phys.* **17**, 19268 (2015).
- <sup>69</sup>D. A. Sirianni, L. A. Burns, and C. D. Sherrill, *J. Chem. Theory Comput.* **13**, 86 (2017).
- <sup>70</sup>N. N. Dutta and K. Patkowski, *J. Chem. Theory Comput.* **14**, 3053 (2018).
- <sup>71</sup>J. R. Lane, *J. Chem. Theory Comput.* **9**, 316 (2013).
- <sup>72</sup>J. Witte, M. Goldey, J. B. Neaton, and M. Head-Gordon, *J. Chem. Theory Comput.* **11**, 1481 (2015).
- <sup>73</sup>D. A. Sirianni, A. Alenaizan, D. L. Cheney, and C. D. Sherrill, *J. Chem. Theory Comput.* **14**, 3004 (2018).
- <sup>74</sup>L. A. Burns, J. C. Faver, Z. Zheng, M. S. Marshall, D. G. A. Smith, K. Vanommeslaeghe, A. D. MacKerell, Jr., K. M. Merz, Jr., and C. D. Sherrill, *J. Chem. Phys.* **147**, 161727 (2017).
- <sup>75</sup>K. Szalewicz, K. Patkowski, and B. Jeziorski, *Struct. Bonding* **116**, 43 (2005).
- <sup>76</sup>E. G. Hohenstein and C. D. Sherrill, *Wiley Interdiscip. Rev.: Comput. Mol. Sci.* **2**, 304 (2012).
- <sup>77</sup>N. J. Singh, S. K. Min, D. Y. Kim, and K. S. Kim, *J. Chem. Theory Comput.* **5**, 515 (2009).
- <sup>78</sup>L. A. Burns, A. Vazquez-Mayagoitia, B. G. Sumpter, and C. D. Sherrill, *J. Chem. Phys.* **134**, 084107 (2011).
- <sup>79</sup>R. Podeszwa and K. Szalewicz, *J. Chem. Phys.* **136**, 161102 (2012).
- <sup>80</sup>D. G. A. Smith and K. Patkowski, *J. Phys. Chem. C* **119**, 4934 (2015).
- <sup>81</sup>D. G. A. Smith, L. A. Burns, K. Patkowski, and C. D. Sherrill, *J. Phys. Chem. Lett.* **7**, 2197 (2016).
- <sup>82</sup>S. T. Schneebeli, A. D. Bochevarov, and R. A. Friesner, *J. Chem. Theory Comput.* **7**, 658 (2011).
- <sup>83</sup>R. T. McGibbon, A. G. Taube, A. G. Donchev, K. Siva, F. Hernández, C. Hargus, K.-H. Law, J. L. Klepeis, and D. E. Shaw, *J. Chem. Phys.* **147**, 161725 (2017).
- <sup>84</sup>M. S. Marshall, L. A. Burns, and C. D. Sherrill, *J. Chem. Phys.* **135**, 194102 (2011).
- <sup>85</sup>O. Marchetti and H.-J. Werner, *Phys. Chem. Chem. Phys.* **10**, 3400 (2008).
- <sup>86</sup>R. Podeszwa, K. Patkowski, and K. Szalewicz, *Phys. Chem. Chem. Phys.* **12**, 5974 (2010).
- <sup>87</sup>T. Takatani, E. G. Hohenstein, M. Malagoli, M. S. Marshall, and C. D. Sherrill, *J. Chem. Phys.* **132**, 144104 (2010).
- <sup>88</sup>V. S. Bryantsev, M. S. Diallo, A. C. T. van Duin, and W. A. Goddard III, *J. Chem. Theory Comput.* **5**, 1016 (2009).
- <sup>89</sup>D. Manna, M. K. Kesharwani, N. Sylvetsky, and J. M. L. Martin, *J. Chem. Theory Comput.* **13**, 3136 (2017).
- <sup>90</sup>M. K. Kesharwani, D. Manna, N. Sylvetsky, and J. M. L. Martin, *J. Phys. Chem. A* **122**, 2184 (2018).
- <sup>91</sup>M. K. Kesharwani, A. Karton, N. Sylvetsky, and J. M. L. Martin, *Aust. J. Chem.* **71**, 238 (2018).
- <sup>92</sup>L. Goerigk, A. Hansen, C. Bauer, S. Ehrlich, A. Najibi, and S. Grimme, *Phys. Chem. Chem. Phys.* **19**, 32184 (2017).
- <sup>93</sup>U. Góra, R. Podeszwa, W. Cencek, and K. Szalewicz, *J. Chem. Phys.* **135**, 224102 (2011).
- <sup>94</sup>V. Babin, C. Leforestier, and F. Paesani, *J. Chem. Theory Comput.* **9**, 5395 (2013).
- <sup>95</sup>V. Babin, G. R. Medders, and F. Paesani, *J. Chem. Theory Comput.* **10**, 1599 (2014).

- <sup>96</sup>F. N. Keutsch, L. B. Braly, M. G. Brown, H. A. Harker, P. B. Petersen, C. Leforestier, and R. J. Saykally, *J. Chem. Phys.* **119**, 8927 (2003).
- <sup>97</sup>A. H. Harvey and E. W. Lemmon, *J. Phys. Chem. Ref. Data* **33**, 369 (2004).
- <sup>98</sup>B. Temelso, K. A. Archer, and G. C. Shields, *J. Phys. Chem. A* **115**, 12034 (2011).
- <sup>99</sup>C. Pérez, M. T. Muckle, D. P. Zaleski, N. A. Seifert, B. Temelso, G. C. Shields, Z. Kisiel, and B. H. Pate, *Science* **336**, 897 (2012).
- <sup>100</sup>G. R. Medders, V. Babin, and F. Paesani, *J. Chem. Theory Comput.* **10**, 2906 (2014).
- <sup>101</sup>R. Bukowski, K. Szalewicz, G. C. Groenenboom, and A. van der Avoird, *Science* **315**, 1249 (2007).
- <sup>102</sup>W. Cencek, K. Szalewicz, C. Leforestier, R. van Harreveld, and A. van der Avoird, *Phys. Chem. Chem. Phys.* **10**, 4716 (2008).
- <sup>103</sup>Y. Wang, B. C. Shepler, B. J. Braams, and J. M. Bowman, *J. Chem. Phys.* **131**, 054511 (2009).
- <sup>104</sup>G. A. Cisneros, K. T. Wikfeldt, L. Ojamäe, J. Lu, Y. Xu, H. Torabifard, A. P. Bartók, G. Csányi, V. Molinero, and F. Paesani, *Chem. Rev.* **116**, 7501 (2016).
- <sup>105</sup>K. Szalewicz, *Int. Rev. Phys. Chem.* **27**, 273 (2008).
- <sup>106</sup>S. Grebenev, J. P. Toennies, and A. F. Vilesov, *Science* **279**, 2083 (1998).
- <sup>107</sup>F. Paesani and K. B. Whaley, *J. Chem. Phys.* **121**, 4180 (2004).
- <sup>108</sup>H. Li and Y.-T. Ma, *J. Chem. Phys.* **137**, 234310 (2012).
- <sup>109</sup>J. Tang and A. R. W. McKellar, *J. Chem. Phys.* **121**, 3087 (2004).
- <sup>110</sup>J. M. Michaud and W. Jäger, *J. Chem. Phys.* **129**, 144311 (2008).
- <sup>111</sup>J.-M. Liu, Y. Zhai, and H. Li, *J. Chem. Phys.* **147**, 044313 (2017).
- <sup>112</sup>J. Brown, X.-G. Wang, R. Dawes, and T. Carrington, Jr., *J. Chem. Phys.* **136**, 134306 (2012).
- <sup>113</sup>M.-L. Dubernet, M. H. Alexander, Y. A. Ba, N. Balakrishnan, C. Balança, C. Ceccarelli, J. Cernicharo, F. Daniel, F. Dayou, M. Doronin *et al.*, *Astron. Astrophys.* **553**, A50 (2013).
- <sup>114</sup>D. G. A. Smith, K. Patkowski, D. Trinh, N. Balakrishnan, T.-G. Lee, R. C. Forrey, B. H. Yang, and P. C. Stancil, *J. Phys. Chem. A* **118**, 6351 (2014).
- <sup>115</sup>K. M. Walker, F. Dumouchel, F. Lique, and R. Dawes, *J. Chem. Phys.* **145**, 024314 (2016).
- <sup>116</sup>A. Faure, P. J. Dagdigian, C. Rist, R. Dawes, E. Quintas-Sánchez, F. Lique, and M. Hochlaf, *ACS Earth Space Chem.* **3**, 964 (2019).
- <sup>117</sup>B. A. McGuire, P. B. Carroll, R. A. Loomis, I. A. Finneran, P. R. Jewell, A. J. Remijan, and G. A. Blake, *Science* **352**, 1449 (2016).
- <sup>118</sup>J. R. Cronin and S. Pizzarello, *Science* **275**, 951 (1997).
- <sup>119</sup>J. Bailey, A. Chrysostomou, J. H. Hough, T. M. Gledhill, A. McCall, S. Clark, F. Ménard, and M. Tamura, *Science* **281**, 672 (1998).
- <sup>120</sup>R. Hellmann, *J. Chem. Eng. Data* **63**, 470 (2018).
- <sup>121</sup>C. Qu and J. M. Bowman, *Phys. Chem. Chem. Phys.* **18**, 24835 (2016).
- <sup>122</sup>S. Bouzón Capelo, B. Fernández, H. Koch, and P. M. Felker, *J. Phys. Chem. A* **113**, 5212 (2009).
- <sup>123</sup>H. Koch, B. Fernández, and J. Makarewicz, *J. Chem. Phys.* **111**, 198 (1999).
- <sup>124</sup>H. Cybulski, B. Fernández, C. Henriksen, and P. M. Felker, *J. Chem. Phys.* **137**, 074305 (2012).
- <sup>125</sup>J. Makarewicz and L. Shirkov, *J. Chem. Phys.* **150**, 074301 (2019).
- <sup>126</sup>J. Yang, W. Hu, D. Usvyat, D. Matthews, M. Schütz, and G. K. Chan, *Science* **345**, 640 (2014).
- <sup>127</sup>K. Patkowski, *J. Chem. Phys.* **137**, 034103 (2012).
- <sup>128</sup>K. Patkowski, *J. Chem. Phys.* **138**, 154101 (2013).
- <sup>129</sup>K. A. Peterson and T. H. Dunning, Jr., *J. Chem. Phys.* **117**, 10548 (2002).
- <sup>130</sup>M. Douglas and N. M. Kroll, *Ann. Phys.* **82**, 89 (1974).
- <sup>131</sup>D. Cremer, W. Zou, and M. Filatov, *Wiley Interdiscip. Rev.: Comput. Mol. Sci.* **4**, 436 (2014).
- <sup>132</sup>B. Jäger, R. Hellmann, E. Bich, and E. Vogel, *J. Chem. Phys.* **144**, 114304 (2016).
- <sup>133</sup>R. Hellmann, E. Bich, and E. Vogel, *Mol. Phys.* **106**, 133 (2008).
- <sup>134</sup>K. Patkowski and K. Szalewicz, *J. Chem. Phys.* **133**, 094304 (2010).
- <sup>135</sup>J. Řezáč, L. Šimová, and P. Hobza, *J. Chem. Theory Comput.* **9**, 364 (2013).
- <sup>136</sup>B. Temelso, C. R. Renner, and G. C. Shields, *J. Chem. Theory Comput.* **11**, 1439 (2015).
- <sup>137</sup>D. G. A. Smith, P. Jankowski, M. Slawik, H. A. Witek, and K. Patkowski, *J. Chem. Theory Comput.* **10**, 3140 (2014).
- <sup>138</sup>M. Przybytek, W. Cencek, B. Jeziorski, and K. Szalewicz, *Phys. Rev. Lett.* **119**, 123401 (2017).
- <sup>139</sup>T. Korona, H. L. Williams, R. Bukowski, B. Jeziorski, and K. Szalewicz, *J. Chem. Phys.* **106**, 5109 (1997).
- <sup>140</sup>W. Cencek, M. Jeziorska, R. Bukowski, M. Jaszuński, B. Jeziorski, and K. Szalewicz, *J. Phys. Chem. A* **108**, 3211 (2004).
- <sup>141</sup>K. Patkowski, W. Cencek, M. Jeziorska, B. Jeziorski, and K. Szalewicz, *J. Phys. Chem. A* **111**, 7611 (2007).
- <sup>142</sup>M. Jeziorska, W. Cencek, K. Patkowski, B. Jeziorski, and K. Szalewicz, *J. Chem. Phys.* **127**, 124303 (2007).
- <sup>143</sup>W. Cencek and K. Szalewicz, *Int. J. Quantum Chem.* **108**, 2191 (2008).
- <sup>144</sup>M. Przybytek, W. Cencek, J. Komasa, G. Łach, B. Jeziorski, and K. Szalewicz, *Phys. Rev. Lett.* **104**, 183003 (2010).
- <sup>145</sup>W. Cencek, M. Przybytek, J. Komasa, J. B. Mehl, B. Jeziorski, and K. Szalewicz, *J. Chem. Phys.* **136**, 224303 (2012).
- <sup>146</sup>B. W. Bakr, D. G. A. Smith, and K. Patkowski, *J. Chem. Phys.* **139**, 144305 (2013).
- <sup>147</sup>K. Patkowski, W. Cencek, P. Jankowski, K. Szalewicz, J. B. Mehl, G. Garberoglio, and A. H. Harvey, *J. Chem. Phys.* **129**, 094304 (2008).
- <sup>148</sup>G. Garberoglio, K. Patkowski, and A. H. Harvey, *Int. J. Thermophys.* **35**, 1435 (2014).
- <sup>149</sup>G. Garberoglio, P. Jankowski, K. Szalewicz, and A. H. Harvey, *J. Chem. Phys.* **141**, 044119 (2014).
- <sup>150</sup>Y. Wan, B. H. Yang, P. C. Stancil, N. Balakrishnan, N. J. Parekh, and R. C. Forrey, *Astrophys. J.* **862**, 132 (2018).
- <sup>151</sup>F. Thibault, K. Patkowski, P. S. Żuchowski, H. Jóźwiak, R. Ciuryło, and P. Wcisło, *J. Quant. Spectrosc. Radiat. Transfer* **202**, 308 (2017).
- <sup>152</sup>R. Z. Martínez, D. Bermejo, F. Thibault, and P. Wcisło, *J. Raman Spectrosc.* **49**, 1339 (2018).
- <sup>153</sup>E. Lavert-Ofir, Y. Shagam, A. B. Henson, S. Gersten, J. Klos, P. S. Żuchowski, J. Narevicius, and E. Narevicius, *Nat. Chem.* **6**, 332 (2014).
- <sup>154</sup>A. Klein, Y. Shagam, W. Skomorowski, P. S. Żuchowski, M. Pawlak, L. M. C. Janssen, N. Moiseyev, S. Y. T. van de Meerakker, A. van der Avoird, C. P. Koch *et al.*, *Nat. Phys.* **13**, 35 (2017).
- <sup>155</sup>A. R. W. McKellar, *J. Chem. Phys.* **108**, 1811 (1998).
- <sup>156</sup>P. Jankowski and K. Szalewicz, *J. Chem. Phys.* **123**, 104301 (2005).
- <sup>157</sup>J. Noga, M. Kállay, and P. Valiron, *Mol. Phys.* **104**, 2337 (2006).
- <sup>158</sup>P. Jankowski, L. A. Surin, A. Potapov, S. Schlemmer, A. R. W. McKellar, and K. Szalewicz, *J. Chem. Phys.* **138**, 084307 (2013).
- <sup>159</sup>S. Chefdeville, T. Stoecklin, C. Naulin, P. Jankowski, K. Szalewicz, A. Faure, M. Costes, and A. Bergeat, *Astrophys. J. Lett.* **799**, L9 (2015).
- <sup>160</sup>G. Garberoglio, P. Jankowski, K. Szalewicz, and A. H. Harvey, *J. Chem. Phys.* **146**, 054304 (2017).
- <sup>161</sup>D. Hou, X.-L. Zhang, Y. Zhai, and H. Li, *Chin. J. Chem. Phys.* **30**, 776 (2017).
- <sup>162</sup>K. Harada, K. Tanaka, T. Tanaka, S. Nanbu, and M. Aoyagi, *J. Chem. Phys.* **117**, 7041 (2002).
- <sup>163</sup>S. N. Vogels, T. Karman, J. Klos, M. Besemer, J. Onvlee, A. van der Avoird, G. C. Groenenboom, and S. Y. T. van de Meerakker, *Nat. Chem.* **10**, 435 (2018).
- <sup>164</sup>T. de Jongh, T. Karman, S. N. Vogels, M. Besemer, J. Onvlee, A. G. Suits, J. O. F. Thompson, G. C. Groenenboom, A. van der Avoird, and S. Y. T. van de Meerakker, *J. Chem. Phys.* **147**, 013918 (2017).
- <sup>165</sup>J. Klos, Q. Ma, M. H. Alexander, and P. J. Dagdigian, *J. Chem. Phys.* **146**, 114301 (2017).
- <sup>166</sup>A. D. Boese, *J. Chem. Theory Comput.* **9**, 4403 (2013).
- <sup>167</sup>E. V. Dornshuld and G. S. Tschumper, *J. Chem. Theory Comput.* **12**, 1534 (2016).
- <sup>168</sup>R. Hellmann, *Mol. Phys.* **111**, 387 (2013).
- <sup>169</sup>J.-M. Liu, Y. Zhai, X.-L. Zhang, and H. Li, *Phys. Chem. Chem. Phys.* **20**, 2036 (2018).
- <sup>170</sup>L. A. Surin, I. V. Tarabukin, S. Schlemmer, Y. N. Kalugina, and A. van der Avoird, *J. Chem. Phys.* **148**, 044313 (2018).

- <sup>171</sup>H. Cybulski, C. Henriksen, R. Dawes, X.-G. Wang, N. Bora, G. Avila, T. Carrington, Jr., and B. Fernández, *Phys. Chem. Chem. Phys.* **20**, 12624 (2018).
- <sup>172</sup>M. Rode, J. Sadlej, R. Moszyński, P. E. S. Wormer, and A. van der Avoird, *Chem. Phys. Lett.* **314**, 326 (1999).
- <sup>173</sup>R. Dawes, X.-G. Wang, and T. Carrington, Jr., *J. Phys. Chem. A* **117**, 7612 (2013).
- <sup>174</sup>S. A. Ndengué, R. Dawes, and F. Gatti, *J. Phys. Chem. A* **119**, 7712 (2015).
- <sup>175</sup>J. G. Hill, S. Mazumder, and K. A. Peterson, *J. Chem. Phys.* **132**, 054108 (2010).
- <sup>176</sup>J. G. Hill, K. A. Peterson, G. Knizia, and H.-J. Werner, *J. Chem. Phys.* **131**, 194105 (2009).
- <sup>177</sup>A. Hesselmann, *J. Chem. Phys.* **128**, 144112 (2008).
- <sup>178</sup>J. Řezáč, K. E. Riley, and P. Hobza, *J. Chem. Theory Comput.* **8**, 4285 (2012).
- <sup>179</sup>M. Melicherčík, M. Pitoňák, V. Kellö, P. Hobza, and P. Neogrady, *J. Chem. Theory Comput.* **9**, 5296 (2013).
- <sup>180</sup>M. Melicherčík, D. Suchá, P. Neogrady, and M. Pitoňák, *Int. J. Quantum Chem.* **118**, e25580 (2018).
- <sup>181</sup>F.-M. Tao and Y.-K. Pan, *J. Phys. Chem.* **95**, 3582 (1991).
- <sup>182</sup>F.-M. Tao, *Int. Rev. Phys. Chem.* **20**, 617 (2001).
- <sup>183</sup>R. Podeszwa, R. Bukowski, and K. Szalewicz, *J. Phys. Chem. A* **110**, 10345 (2006).
- <sup>184</sup>M. Jeziorska, W. Cencek, K. Patkowski, B. Jeziorski, and K. Szalewicz, *Int. J. Quantum Chem.* **108**, 2053 (2008).
- <sup>185</sup>S. Li, D. G. A. Smith, and K. Patkowski, *Phys. Chem. Chem. Phys.* **17**, 16560 (2015).
- <sup>186</sup>R. A. Shaw and J. G. Hill, *Mol. Phys.* **116**, 1460 (2018).
- <sup>187</sup>S. N. Steinmann and C. Corminboeuf, *J. Chem. Theory Comput.* **8**, 4305 (2012).
- <sup>188</sup>P. R. Tentscher and J. S. Arey, *J. Chem. Theory Comput.* **9**, 1568 (2013).
- <sup>189</sup>B. Alday, R. Johnson, J. Li, and H. Guo, *Theor. Chem. Acc.* **133**, 1540 (2014).
- <sup>190</sup>D. Hait and M. Head-Gordon, *J. Chem. Theory Comput.* **14**, 1969 (2018).
- <sup>191</sup>J. C. Howard and G. S. Tschumper, *J. Chem. Theory Comput.* **11**, 2126 (2015).
- <sup>192</sup>J. G. McDaniel and J. R. Schmidt, *J. Phys. Chem. A* **117**, 2053 (2013).
- <sup>193</sup>S. Vandenbrande, M. Waroquier, V. Van Speybroeck, and T. Verstraelen, *J. Chem. Theory Comput.* **13**, 161 (2017).
- <sup>194</sup>T. Bereau, R. A. DiStasio, A. Tkatchenko, and O. A. von Lilienfeld, *J. Chem. Phys.* **148**, 241706 (2018).
- <sup>195</sup>T. M. Parker, L. A. Burns, R. M. Parrish, A. G. Ryno, and C. D. Sherrill, *J. Chem. Phys.* **140**, 094106 (2014).
- <sup>196</sup>T. Korona, *Mol. Phys.* **111**, 3705 (2013).
- <sup>197</sup>Y. S. Al-Hamdani and A. Tkatchenko, *J. Chem. Phys.* **150**, 010901 (2019).
- <sup>198</sup>R. Sedlak, T. Janowski, M. Pitoňák, J. Řezáč, P. Pulay, and P. Hobza, *J. Chem. Theory Comput.* **9**, 3364 (2013).
- <sup>199</sup>S. Grimme, *Chem. Eur. J.* **18**, 9955 (2012).
- <sup>200</sup>R. Sure and S. Grimme, *J. Chem. Theory Comput.* **11**, 3785 (2015).
- <sup>201</sup>J. Calbo, E. Ortí, J. C. Sancho-García, and J. Aragó, *J. Chem. Theory Comput.* **11**, 932 (2015).
- <sup>202</sup>A. Ambrosetti, D. Alfè, R. A. DiStasio, Jr., and A. Tkatchenko, *J. Phys. Chem. Lett.* **5**, 849 (2014).
- <sup>203</sup>C. Riplinger and F. Neese, *J. Chem. Phys.* **138**, 034106 (2013).
- <sup>204</sup>M. Dubecký, L. Mitas, and P. Jurečka, *Chem. Rev.* **116**, 5188 (2016).

## **Appendix C**

### **Explicitly correlated dispersion and exchange dispersion energies in symmetry-adapted perturbation theory**

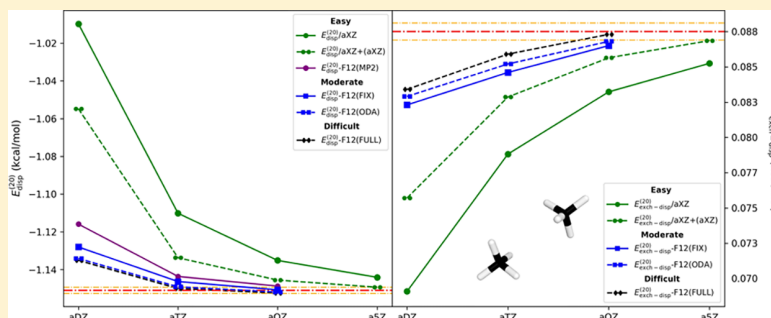
# Explicitly Correlated Dispersion and Exchange Dispersion Energies in Symmetry-Adapted Perturbation Theory

Monika Kodrycka,<sup>†</sup> Christof Holzer,<sup>‡</sup> Wim Klopper,<sup>‡</sup> and Konrad Patkowski<sup>\*,†</sup>

<sup>†</sup>Department of Chemistry and Biochemistry, Auburn University, Auburn, Alabama 36849, United States

<sup>‡</sup>Theoretical Chemistry Group, Institute of Physical Chemistry, Karlsruhe Institute of Technology (KIT), KIT Campus South, P.O. Box 6980, D-76049 Karlsruhe, Germany

## Supporting Information



**ABSTRACT:** The individual interaction energy terms in symmetry-adapted perturbation theory (SAPT) not only have different physical interpretations but also converge to their complete basis set (CBS) limit values at quite different rates. Dispersion energy is notoriously the slowest converging interaction energy contribution, and exchange dispersion energy, while smaller in absolute value, converges just as poorly in relative terms. To speed up the basis set convergence of the lowest-order SAPT dispersion and exchange dispersion energies, we borrow the techniques from explicitly correlated (F12) electronic structure theory and develop practical expressions for the closed-shell  $E_{\text{disp}}^{(20)}$ -F12 and  $E_{\text{exch-disp}}^{(20)}$ -F12 contributions. While the latter term has been derived and implemented for the first time, the former correction was recently proposed by Przybytek [*J. Chem. Theory Comput.* **2018**, *14*, 5105–5117] using an Ansatz with a full optimization of the explicitly correlated amplitudes. In addition to reimplementing the fully optimized variant of  $E_{\text{disp}}^{(20)}$ -F12, we propose three approximate Ansätze that substantially improve the scaling of the method and at the same time avoid the numerical instabilities of the unrestricted optimization. The performance of all four resulting flavors of  $E_{\text{disp}}^{(20)}$ -F12 and  $E_{\text{exch-disp}}^{(20)}$ -F12 is first tested on helium, neon, argon, water, and methane dimers, with orbital and auxiliary basis sets up to aug-cc-pV5Z and aug-cc-pV5Z-RL, respectively. The double- and triple- $\zeta$  basis set calculations are then extended to the entire A24 database of noncovalent interaction energies and compared with CBS estimates for  $E_{\text{disp}}^{(20)}$  and  $E_{\text{exch-disp}}^{(20)}$  computed using conventional SAPT with basis sets up to aug-cc-pV6Z with midbond functions. It is shown that the F12 treatment is highly successful in improving the basis set convergence of the SAPT terms, with the F12 calculations in an  $X$ -tuple  $\zeta$  basis about as accurate as conventional calculations in bases with cardinal numbers  $(X + 2)$  for  $E_{\text{disp}}^{(20)}$  and either  $(X + 1)$  or  $(X + 2)$  for  $E_{\text{exch-disp}}^{(20)}$ . While the full amplitude optimization affords the highest accuracy for both corrections, the much simpler and numerically stable optimized diagonal Ansatz is a very close second. We have also tested the performance of the simple F12 correction based on the second-order Møller–Plesset perturbation theory, SAPT-F12(MP2) [Frey, J. A.; et al. *Chem. Rev.* **2016**, *116*, 5614–5641] and observed that it is also quite successful in speeding up the basis set convergence of conventional  $E_{\text{disp}}^{(20)} + E_{\text{exch-disp}}^{(20)}$ , albeit with some outliers.

## 1. INTRODUCTION

Noncovalent intermolecular interactions are quite a demanding case for electronic structure theory. The electron correlation is essential to obtain even qualitatively correct interaction energies: an uncorrelated, Hartree–Fock (HF) description completely misses the dispersion forces. On the other hand, correlated wave function methods such as the Møller–Plesset perturbation theory (MP $n$ ) or the coupled-cluster approaches with singles and doubles (CCSD) or singles, doubles, and perturbative triples (CCSD(T)) exhibit slow convergence with

respect to the one-electron basis set. The reason for this slow convergence has been tracked down to the inability of products of one-electron functions to describe the interelectronic cusp, that is, to provide the proper form of the wave function at the  $r_{ij} \rightarrow 0$  limit when two electrons approach each other.<sup>1,2</sup> A successful remedy to the cusp problem involves going beyond the one-electron picture, that is, enriching the wave function

Received: June 4, 2019

Published: September 10, 2019

Ansatz with terms that explicitly depend on the interelectronic separations  $r_{ij}$ .<sup>3,4</sup> While a full variational optimization of such an Ansatz is only possible for few-electron systems,<sup>5</sup> a single frozen  $r_{12}$ -dependent function (correlation factor) is all it takes to substantially improve the basis set convergence of the correlation energy. After an initial exploration phase of different correlation factors, the exponential  $e^{-\gamma r_{12}}$ <sup>6</sup> emerged as the best performer.<sup>7–9</sup> For practical calculations of the required two-electron integrals, the exponential (or other correlation factors) is fitted to a linear combination of Gaussian  $e^{-\alpha r_{12}^2}$  terms.<sup>7</sup> While such Gaussian functions obviously have no cusp at  $r_{12} \rightarrow 0$ , the additional basis space flexibility in the small- $r_{12}$  region is sufficient to provide nearly converged molecular correlation energies using double- or triple- $\zeta$  orbital basis sets. An extension of a parent correlated approach with nonlinear  $r_{12}$ -dependent terms is referred to as the F12 method, with the MP2-F12 approach<sup>10,11</sup> and different CCSD(T)-F12 variants<sup>12–17</sup> being particularly popular.

As many studies have shown,<sup>8,18–22</sup> the improved basis set convergence of MP2-F12 and/or CCSD(T)-F12 molecular correlation energies does translate to an improved convergence of supermolecular interaction energies at the same levels of theory. At the level of double- and triple- $\zeta$  basis sets, the improvement in interaction energies is comparable to the improvement in molecular energies, with approximate CCSD(T)-F12 results in the augmented correlation consistent  $X$ -tuple  $\zeta$  basis sets aug-cc-pVXZ  $\equiv$  aXZ reaching similar level of complete basis set (CBS) convergence as conventional CCSD(T) in a much larger  $a(X+2)Z$  (or even  $a(X+3)Z$ ) basis.<sup>23</sup> The CBS interaction energy estimates can also be improved in an alternative manner, by augmenting the atom-centered basis functions with a set of functions centered on the intermolecular bond.<sup>24</sup> Moreover, the benefits of the F12 Ansatz and of the bond functions can be combined: this combination often leads to both the most accurate CCSD(T)/CBS estimates available<sup>22</sup> and the best-performing CBS estimate possible with only a double- $\zeta$  CCSD(T)-level calculation.<sup>25</sup>

Symmetry-adapted perturbation theory (SAPT)<sup>26–28</sup> provides a decomposition of the interaction energy into its physically meaningful electrostatic, induction, dispersion, and exchange contributions. Such a decomposition has many benefits, from explaining interaction energy and property trends in a group of similar complexes<sup>29,30</sup> to providing reference data for a term-by-term construction of physically sound, ab initio-based force fields.<sup>31</sup> An additional, often overlooked benefit of SAPT is that the CBS convergence of individual energy contributions can be studied separately, which might lead to a recommendation of using different basis sets for different SAPT corrections. It has been observed that while some SAPT corrections, especially those not involving electron correlation, converge quickly with the basis set, other corrections converge just as poorly as MP2 and CCSD(T) correlation energies. A particularly important example is the dispersion energy, which, when calculated in a small basis set, typically dominates the error with respect to the SAPT/CBS result. Dispersion energy is also the singular SAPT component that is significantly improved by the addition of bond functions.<sup>32</sup> Clearly, dispersion energy is sensitive to the representation of the dispersion wave function (see below for a precise definition) in the space between the interacting molecules. This region is not the direct target of the F12 Ansatz, and the mechanism of CBS convergence improvement of supermolecular MP2-F12 or CCSD(T)-F12 interaction

energies is not entirely clear (although the improvement itself is undisputable). It should be noted that another component of SAPT, the second-order exchange dispersion energy, converges with the basis set just as poorly in relative terms: however, this is less of a practical issue as this correction is typically an order of magnitude smaller than the dispersion energy.

The logical next step for the assessment of CBS convergence of different SAPT corrections is finding out whether individual SAPT terms can be improved by an explicitly correlated approach, and the logical first choice for an F12 treatment is the dispersion energy, followed by the exchange dispersion term. It should be kept in mind that different levels of SAPT involve different approximations to the dispersion energy: the intermolecular interaction is always included within the second order of perturbation theory but the intramolecular electron correlation can be treated in many different ways, from a complete neglect (within the SAPT0 approach) to a truncated second perturbation expansion in powers of the Møller–Plesset fluctuation potential<sup>33</sup> (in the SAPT2, SAPT2+, SAPT2+3, ... variants<sup>34</sup>) to a generalized Casimir–Polder integral involving linear response functions of the electron density,<sup>35</sup> computed at the time-dependent HF, density functional theory [DFT, leading to the SAPT(DFT) approach<sup>36,37</sup>], or higher levels of theory.<sup>38</sup> The SAPT0 approximation to dispersion energy is not always accurate: the famous binding energy overestimation by MP2 in  $\pi$ -stacked complexes<sup>39</sup> is a direct consequence of the dispersion energy overestimation by its SAPT0 approximation (the dispersion energy contained in supermolecular MP2 is roughly equivalent to SAPT0). As a result, it is often suggested<sup>34</sup> to compute SAPT0 interaction energies in a small basis set (such as the “calendar” set jun-cc-pVDZ<sup>40</sup>) instead of trying to converge them to CBS, in order to facilitate an (empirical but surprisingly consistent) error cancellation between the overestimation of dispersion energy by SAPT0 and the underestimation of dispersion energy by an incomplete basis set. Nevertheless, the SAPT0 level provides the bulk of dispersion energy and should be the first target for improvement associated with an F12 Ansatz.

In this work, we develop rigorous F12 expressions for the SAPT0-level dispersion and exchange dispersion energies, expecting to overcome the slow CBS convergence for the leading-order dispersion effects. This level of approximation is also the easiest to transform into an F12 approach for three reasons. First, the SAPT0 dispersion energy is a variational quantity that can be accessed by minimizing a suitably defined Hylleraas functional<sup>41</sup> (in direct analogy to the MP2-F12 development via the Hylleraas functional of MP2<sup>11</sup>). Second, the resulting F12-enabled dispersion pair functions can be directly inserted into the standard expression for exchange dispersion energy in place of conventional dispersion pair functions [very much like converged CCSD-F12 amplitudes are typically inserted<sup>15,42</sup> into the conventional expression for the perturbative (T) correction]. Third, if intramolecular correlation effects on dispersion and exchange dispersion are desired, a double F12 Ansatz is likely required: one for the intermolecular (dispersion) pair functions and another for the intramolecular pair functions (note that such a double explicitly correlated Ansatz has been proposed for the lowest-level intramolecular correlation correction to dispersion in the specific case of the helium dimer<sup>43</sup>). Therefore, while an F12 extension of higher-level treatments of dispersion is certainly worthwhile (and such an extension is the subject of an ongoing research in our groups), in this work, we restrict ourselves to the simplest, SAPT0-level



dispersion (also referred to as uncoupled Hartree–Fock dispersion) and exchange dispersion corrections.

The problem of calculating explicitly correlated dispersion energies has been addressed by several earlier studies. For the helium dimer system, as already mentioned, the SAPT0 dispersion and exchange dispersion terms, as well as the leading intramolecular correlation correction to SAPT0 dispersion within the double perturbation formalism, have been derived and computed using a Gaussian-type geminal (GTG) basis.<sup>43–45</sup> An approximate F12 correction to the SAPT0 dispersion and exchange dispersion by selecting the intermolecular pair functions out of a local MP2-F12 computation for the complex has recently been proposed and tested by some of us.<sup>46</sup> Here, this approach will be tested alongside the newly developed SAPT-F12 corrections and referred to as SAPT-F12(MP2). Very recently, when this work was well advanced, Przybytek presented<sup>47</sup> an independent derivation and pilot implementation of an F12 correction to the SAPT0 dispersion energy (but not exchange dispersion energy). Przybytek's recommended approach is equivalent to the optimized-amplitude variant of our F12 dispersion correction (presented below) up to technical details of little practical significance. In addition, Przybytek examined the performance of two additional variants of the F12 Ansatz and two additional correlation factors (which will not be discussed in this work) and performed a detailed study of the significance of the length-scale parameter  $\gamma$  in the correlation factor for several complexes.

The structure of the rest of this paper is as follows. In Section II, we derive the expression for an F12 correction to the second-order dispersion energy, and in Section III, we develop the corresponding correction to the second-order exchange dispersion energy. The pertinent details of the computer implementation of our algorithms are presented in Section IV. The numerical results for a number of test complexes are presented and analyzed in Section V. Finally, Section VI contains conclusions.

## II. F12 DISPERSION ENERGY

Throughout this work, we will use the notation similar to ref 11 with one important extension: the indices  $(i,k,m),a,r,x,\alpha$  (with primes if necessary) always relate to monomer A, and the indices  $(j,l,n),b,s,y,\beta$  relate to monomer B. As far as the range of each orbital index is concerned, indices  $ij,kl,m,n$  label occupied orbitals  $a,b$ , virtual orbitals [those that are unoccupied in the monomer Hartree–Fock references but are within the space spanned by the atomic-orbital (AO) basis functions];  $r,s$ , all molecular orbitals (MOs), both occupied and virtual;  $x,y$ , the complementary auxiliary (CA) functions approximately spanning the orthogonal complement of the MO space; and  $\alpha,\beta$ , the formally complete orthonormal set that is the union of the MO and CA subspaces. We will assume the dimer-centered basis set (DCBS) approach<sup>32</sup> so that the MOs of both monomers (that is,  $r$  and  $s$ ) are built from the same set of AO basis functions, centered on the atoms of both monomers (and possibly in between the monomers), and thus span the same space. Similarly, the CA orbitals for both monomers (that is,  $x$  and  $y$ ) span the same space so that also the monomer-A and monomer-B approximations to the complete orbital space (that is,  $\alpha$  and  $\beta$ ) are identical.

The zeroth-order wave function in SAPT is the product of monomer ground-state Hartree–Fock determinants  $|\phi_{\text{HF}}^{\text{A}}\phi_{\text{HF}}^{\text{B}}\rangle$ , and the zeroth-order Hamiltonian is the sum of the monomer Fock operators,  $F^{\text{A}} + F^{\text{B}}$

$$F^{\text{A}}\phi_{\text{HF}}^{\text{A}} = E_{\text{A}}^0\phi_{\text{HF}}^{\text{A}} = \left(2 \sum_i \epsilon_i^{\text{A}}\right)\phi_{\text{HF}}^{\text{A}} \quad (1)$$

and similarly for  $F^{\text{B}}$ . In eq 1,  $\epsilon_i^{\text{A}}$  denotes the HF orbital energy for monomer A. Now, the complete second-order correction in the Rayleigh–Schrödinger perturbation theory, utilizing  $F^{\text{A}} + F^{\text{B}}$  as the zeroth-order perturbation and the intermolecular interaction operator  $V$  as the perturbation (neglecting intramonomer correlation completely), can be written as

$$E^{(20)} = \sum_{m \neq 0} \frac{|\langle \phi_{\text{HF}}^{\text{A}}\phi_{\text{HF}}^{\text{B}} | V | \phi_m^{\text{A}}\phi_{\text{HF}}^{\text{B}} \rangle|^2}{E_{\text{A}}^0 - E_m^{\text{A}}} + \sum_{n \neq 0} \frac{|\langle \phi_{\text{HF}}^{\text{A}}\phi_{\text{HF}}^{\text{B}} | V | \phi_{\text{HF}}^{\text{A}}\phi_n^{\text{B}} \rangle|^2}{E_{\text{B}}^0 - E_n^{\text{B}}} + \sum_{m \neq 0} \sum_{n \neq 0} \frac{|\langle \phi_{\text{HF}}^{\text{A}}\phi_{\text{HF}}^{\text{B}} | V | \phi_m^{\text{A}}\phi_n^{\text{B}} \rangle|^2}{E_{\text{A}}^0 + E_{\text{B}}^0 - E_m^{\text{A}} - E_n^{\text{B}}} \quad (2)$$

where the three consecutive sums represent  $E_{\text{ind,B} \rightarrow \text{A}}^{(20)}$ ,  $E_{\text{ind,A} \rightarrow \text{B}}^{(20)}$ , and  $E_{\text{disp}}^{(20)}$ , respectively, and  $\phi_m^{\text{A}}$  and  $\phi_n^{\text{B}}$  are excited eigenfunctions of  $F^{\text{A}}$  and  $F^{\text{B}}$ , respectively. The related formula for the first-order wave function  $\Psi^{(1)} = \Psi_{\text{ind,B} \rightarrow \text{A}}^{(1)} + \Psi_{\text{ind,A} \rightarrow \text{B}}^{(1)} + \Psi_{\text{disp}}^{(1)}$  is

$$\Psi^{(1)} = \sum_{m \neq 0} \frac{\langle \phi_m^{\text{A}}\phi_{\text{HF}}^{\text{B}} | V | \phi_{\text{HF}}^{\text{A}}\phi_{\text{HF}}^{\text{B}} \rangle}{E_{\text{A}}^0 - E_m^{\text{A}}} |\phi_m^{\text{A}}\phi_{\text{HF}}^{\text{B}}\rangle + \sum_{n \neq 0} \frac{\langle \phi_{\text{HF}}^{\text{A}}\phi_n^{\text{B}} | V | \phi_{\text{HF}}^{\text{A}}\phi_{\text{HF}}^{\text{B}} \rangle}{E_{\text{B}}^0 - E_n^{\text{B}}} |\phi_{\text{HF}}^{\text{A}}\phi_n^{\text{B}}\rangle + \sum_{m \neq 0} \sum_{n \neq 0} \frac{\langle \phi_m^{\text{A}}\phi_n^{\text{B}} | V | \phi_{\text{HF}}^{\text{A}}\phi_{\text{HF}}^{\text{B}} \rangle}{E_{\text{A}}^0 + E_{\text{B}}^0 - E_m^{\text{A}} - E_n^{\text{B}}} |\phi_m^{\text{A}}\phi_n^{\text{B}}\rangle \quad (3)$$

Let  $|\phi^{\text{A}}\rangle$  depend on the coordinates of electrons 1, 2, ...,  $N_{\text{A}}$ , and  $|\phi^{\text{B}}\rangle$ —on the coordinates of electrons  $N_{\text{A}} + 1, N_{\text{A}} + 2, \dots, N_{\text{A}} + N_{\text{B}}$ . For the purpose of separating out the induction and dispersion effects, we will define the operators projecting out the ground state for a given monomer

$$Q_{\text{A}} = 1 - |\phi_{\text{HF}}^{\text{A}}\rangle\langle\phi_{\text{HF}}^{\text{A}}|; \quad Q_{\text{B}} = 1 - |\phi_{\text{HF}}^{\text{B}}\rangle\langle\phi_{\text{HF}}^{\text{B}}| \quad (4)$$

and consider the operator which will be written simply as  $Q_{\text{A}}Q_{\text{B}}$ , but it is implied that  $Q_{\text{A}}$  acts on electrons 1, 2, ...,  $N_{\text{A}}$  and  $Q_{\text{B}}$  acts on electrons  $N_{\text{A}} + 1, N_{\text{A}} + 2, \dots, N_{\text{A}} + N_{\text{B}}$  (obviously,  $Q_{\text{A}}$  and  $Q_{\text{B}}$  commute with each other and each of them is idempotent, e.g.,  $Q_{\text{A}}^2 = Q_{\text{A}}$ ). It is easy to see that the Hermitian operator  $Q_{\text{A}}Q_{\text{B}}$  annihilates the induction parts of the first-order wave function

$$Q_{\text{A}}Q_{\text{B}}\Psi^{(1)} = \Psi_{\text{disp}}^{(1)} \quad (5)$$

We can now define a “dispersion-only” Hylleraas functional that is a straightforward generalization of the functional used in earlier studies of interactions between two-electron systems<sup>43–45</sup>

$$J_{\text{disp}}[\chi] = \langle \chi | Q_{\text{A}}Q_{\text{B}}(F^{\text{A}} + F^{\text{B}} - E_{\text{A}}^0 - E_{\text{B}}^0)Q_{\text{A}}Q_{\text{B}} | \chi \rangle + \langle \chi | Q_{\text{A}}Q_{\text{B}}(V - \langle V \rangle) | \phi_{\text{HF}}^{\text{A}}\phi_{\text{HF}}^{\text{B}} \rangle + \langle \phi_{\text{HF}}^{\text{A}}\phi_{\text{HF}}^{\text{B}} | (V - \langle V \rangle) Q_{\text{A}}Q_{\text{B}} | \chi \rangle \quad (6)$$

where  $\langle V \rangle \equiv \langle \phi_{\text{HF}}^{\text{A}}\phi_{\text{HF}}^{\text{B}} | V | \phi_{\text{HF}}^{\text{A}}\phi_{\text{HF}}^{\text{B}} \rangle$  is the first-order electrostatic correction  $E_{\text{elst}}^{(1)}$ . It can be shown that the dispersion wave

function  $Q_A Q_B \Psi^{(1)}$  minimizes  $J_{\text{disp}}$  and that the minimum value  $J_{\text{disp}}[Q_A Q_B \Psi^{(1)}]$  equals the second-order dispersion energy  $E_{\text{disp}}^{(2)}$  as expressed by eq 2.

We will now minimize  $J_{\text{disp}}$  using a trial function fully analogous to, e.g., the MP2-F12 theory<sup>11</sup>

$$\chi = T_{ab}^{ij} |\Phi_{ij}^{ab}\rangle + T_{kl}^{ij} \mathcal{F}_{\alpha\beta}^{kl} |\Phi_{ij}^{\alpha\beta}\rangle \quad (7)$$

where  $|\Phi_{ij}^{\alpha\beta}\rangle = \hat{E}_{\alpha i} \hat{E}_{\beta j} |\phi_{\text{HF}}^A \phi_{\text{HF}}^B\rangle$  is a doubly excited (once on A, once on B) determinant. The Einstein summation convention will be employed from now on for every repeated upper and lower indices. Each unitary group generator  $\hat{E}_{\alpha i}$  produces a singlet excitation combining two spin cases,  $i\uparrow \rightarrow \alpha\uparrow$  and  $i\downarrow \rightarrow \alpha\downarrow$ . Thus,  $\hat{E}_{\alpha i} \hat{E}_{\beta j}$  generates a sum of four spin cases where each pair of orbital indices  $(i, \alpha)$  and  $(j, \beta)$  occurs with both spin up and spin down in  $|\Phi_{ij}^{\alpha\beta}\rangle$ . Consequently, in the closed-shell case

$$\langle \Phi_{\alpha\beta}^{ij} | \Phi_{i'j'}^{\alpha'\beta'} \rangle = 4 \delta_{\alpha\alpha'} \delta_{\beta\beta'} \delta_{ii'} \delta_{jj'} \quad (8)$$

which results in a factor of 4 in the dispersion energy expression due to spin adaptation (a spin-up or spin-down excitation on A interacts in the same way with a spin-up or spin-down excitation on B). As usual in the F12 approaches, the excitations to a formally complete space are included via a compact set of amplitudes  $T_{kl}^{ij}$  and a suitable internal contraction

$$\mathcal{F}_{\alpha\beta}^{kl} = \langle kl | \hat{E}_{12} \hat{Q}_{12} | \alpha\beta \rangle \quad (9)$$

where  $\hat{E}_{12} \equiv F(r_{12})$  is the correlation factor [we use the standard exponential  $\exp(-\gamma r_{12})$  factor in this work], and  $\hat{Q}_{12}$  is the projection operator ensuring strong orthogonality. We will use what is known as Ansatz 3 (cf. eq 9 of ref 11) for  $\hat{Q}_{12}$

$$\hat{Q}_{12} = \left( 1_1 - \sum_i |i\rangle \langle i| \right) \left( 1_2 - \sum_j |j\rangle \langle j| \right) \left( 1_{12} - \sum_{ab} |ab\rangle \langle ab| \right) \quad (10)$$

with the subscripts specifying which electron coordinates are affected by a given part of the projector. Note that, unlike in the case of an F12 correction to the correlation energy of a single molecule, different spaces (belonging to monomers A and B) are projected out for electron 1 and electron 2, and there is no left-right index symmetry in the  $|\Phi_{ij}^{ab}\rangle$  and  $|\Phi_{ij}^{\alpha\beta}\rangle$  functions in eq 7.

We will now evaluate  $J_{\text{disp}}[\chi]$ , eq 6, for  $\chi$  given by eq 7 in terms of two-electron integrals involving molecular and/or complementary auxiliary orbitals. In the process of doing this, we will use the fact that for Ansatz 3  $\mathcal{F}_{ab}^{kl} = 0$  and employ a simplified form of the Fock operator. Specifically, we will assume that the occupied and virtual orbitals for a given monomer are canonical solutions of the Hartree–Fock equations for this monomer in the MO basis and that the occupied orbitals cannot be improved by the complementary auxiliary basis set (CABS). The latter condition is referred to in ref 11 as the generalized Brillouin condition (GBC). Thus, we will assume GBC but not necessarily the extended Brillouin condition (EBC) (stating that the virtual orbitals are not improved by the complementary auxiliary basis functions), which would be a more drastic approximation. As a result

$$\begin{aligned} \hat{f}^A |i\rangle &= \epsilon_i^A |i\rangle & \hat{f}^A |a\rangle &= \epsilon_a^A |a\rangle + (f^A)_a^x |x\rangle \\ \hat{f}^A |x\rangle &= (f^A)_x^a |a\rangle + (f^A)_x^a |a\rangle \end{aligned} \quad (11)$$

and similarly for  $\hat{f}^B$ . Obviously, the one-electron Fock operator  $\hat{f}^A$  is related to the complete operator  $F^A$  of eq 1 as  $F^A = \sum_{i=1}^{N_A} \hat{f}_i^A$ .

Let us substitute eq 7 into eq 6

$$\begin{aligned} J_{\text{disp}}[\chi] &= T_{ij}^{ab} T_{a'b'}^{i'j'} \langle \Phi_{ab}^{ij} | Q_A Q_B (F^A + F^B - E_A^0 - E_B^0) Q_A Q_B | \Phi_{i'j'}^{a'b'} \rangle \\ &+ T_{ij}^{ab} T_{kl}^{i'j'} \mathcal{F}_{\alpha\beta}^{kl} \langle \Phi_{ab}^{ij} | Q_A Q_B (F^A + F^B - E_A^0 - E_B^0) Q_A Q_B | \Phi_{i'j'}^{\alpha\beta} \rangle \\ &+ T_{ij}^{kl} \mathcal{F}_{\alpha\beta}^{i'j'} \langle \Phi_{\alpha\beta}^{ij} | Q_A Q_B (F^A + F^B - E_A^0 - E_B^0) Q_A Q_B | \Phi_{i'j'}^{\alpha\beta} \rangle \\ &+ T_{ij}^{kl} \mathcal{F}_{\alpha\beta}^{i'j'} \mathcal{F}_{\alpha'\beta'}^{k'l'} \langle \Phi_{\alpha\beta}^{ij} | Q_A Q_B (F^A + F^B - E_A^0 - E_B^0) Q_A Q_B | \Phi_{i'j'}^{\alpha'\beta'} \rangle \\ &+ T_{ij}^{ab} \langle \Phi_{ab}^{ij} | Q_A Q_B (V - E^{(10)}) \phi_{\text{HF}}^A \phi_{\text{HF}}^B \rangle \\ &+ T_{ij}^{kl} \mathcal{F}_{\alpha\beta}^{i'j'} \langle \Phi_{\alpha\beta}^{ij} | Q_A Q_B (V - E^{(10)}) \phi_{\text{HF}}^A \phi_{\text{HF}}^B \rangle \\ &+ T_{ab}^{ij} \langle \phi_{\text{HF}}^A \phi_{\text{HF}}^B | (V - E^{(10)}) Q_A Q_B | \Phi_{ij}^{ab} \rangle \\ &+ T_{kl}^{ij} \mathcal{F}_{\alpha\beta}^{kl} \langle \phi_{\text{HF}}^A \phi_{\text{HF}}^B | (V - E^{(10)}) Q_A Q_B | \Phi_{ij}^{\alpha\beta} \rangle \end{aligned} \quad (12)$$

To start simplifying eq 12, we first note that the contributions to the last four terms that involve  $E^{(10)}$  vanish because  $Q_A Q_B | \phi_{\text{HF}}^A \phi_{\text{HF}}^B \rangle = 0$ . Second,  $Q_A Q_B | \Phi_{ij}^{ab} \rangle = | \Phi_{ij}^{ab} \rangle$ ,  $Q_A Q_B | \Phi_{ij}^{\alpha\beta} \rangle = | \Phi_{ij}^{\alpha\beta} \rangle$ , and  $Q_A Q_B | \Phi_{ij}^{\alpha'\beta'} \rangle = | \Phi_{ij}^{\alpha'\beta'} \rangle$  as all of these functions involve excitations on both monomers and thus belong to the space of dispersion excitations. Third

$$\begin{aligned} (F^A + F^B - E_A^0 - E_B^0) | \Phi_{ij}^{ab} \rangle &= (\epsilon_a^A + \epsilon_b^B - \epsilon_i^A - \epsilon_j^B) | \Phi_{ij}^{ab} \rangle + (f^A)_x^a | \Phi_{ij}^{xb} \rangle \\ &+ (f^B)_y^b | \Phi_{ij}^{ay} \rangle \end{aligned} \quad (13)$$

In view of these three identities, eq 12 becomes

$$\begin{aligned} J_{\text{disp}}[\chi] &= 4 T_{ij}^{ab} T_{ab}^{i'j'} (\epsilon_a^A + \epsilon_b^B - \epsilon_i^A - \epsilon_j^B) \\ &+ T_{ij}^{ab} T_{kl}^{i'j'} \mathcal{F}_{\alpha\beta}^{kl} (\epsilon_a^A + \epsilon_b^B - \epsilon_i^A - \epsilon_j^B) \langle \Phi_{ab}^{ij} | \Phi_{i'j'}^{\alpha\beta} \rangle \\ &+ T_{ij}^{ab} T_{kl}^{i'j'} \mathcal{F}_{\alpha\beta}^{kl} (f^A)_x^a \langle \Phi_{ab}^{ij} | \Phi_{i'j'}^{\alpha\beta} \rangle \\ &+ T_{ij}^{ab} T_{kl}^{i'j'} \mathcal{F}_{\alpha\beta}^{kl} (f^B)_y^b \langle \Phi_{ab}^{ij} | \Phi_{i'j'}^{\alpha\beta} \rangle \\ &+ T_{ij}^{kl} \mathcal{F}_{\alpha\beta}^{i'j'} \langle \epsilon_a^A + \epsilon_b^B - \epsilon_i^A - \epsilon_j^B \rangle \langle \Phi_{\alpha\beta}^{ij} | \Phi_{i'j'}^{\alpha\beta} \rangle \\ &+ T_{ij}^{kl} \mathcal{F}_{\alpha\beta}^{i'j'} (f^A)_x^a \langle \Phi_{\alpha\beta}^{ij} | \Phi_{i'j'}^{\alpha\beta} \rangle \\ &+ T_{ij}^{kl} \mathcal{F}_{\alpha\beta}^{i'j'} (f^B)_y^b \langle \Phi_{\alpha\beta}^{ij} | \Phi_{i'j'}^{\alpha\beta} \rangle \\ &+ T_{ij}^{kl} \mathcal{F}_{\alpha\beta}^{i'j'} \mathcal{F}_{\alpha'\beta'}^{k'l'} \langle \Phi_{\alpha\beta}^{ij} | Q_A Q_B (F^A + F^B - E_A^0 - E_B^0) Q_A Q_B | \Phi_{i'j'}^{\alpha'\beta'} \rangle \\ &+ T_{ij}^{ab} \langle \Phi_{ab}^{ij} | V | \phi_{\text{HF}}^A \phi_{\text{HF}}^B \rangle \\ &+ T_{ij}^{kl} \mathcal{F}_{\alpha\beta}^{i'j'} \langle \Phi_{\alpha\beta}^{ij} | Q_A Q_B V | \phi_{\text{HF}}^A \phi_{\text{HF}}^B \rangle \\ &+ T_{ab}^{ij} \langle \phi_{\text{HF}}^A \phi_{\text{HF}}^B | V | \Phi_{ij}^{ab} \rangle \\ &+ T_{kl}^{ij} \mathcal{F}_{\alpha\beta}^{kl} \langle \phi_{\text{HF}}^A \phi_{\text{HF}}^B | V Q_A Q_B | \Phi_{ij}^{\alpha\beta} \rangle \end{aligned} \quad (14)$$

Now, terms 2 and 5 of eq 14 vanish because  $\langle \Phi_{ab}^{ij} | \Phi_{i'j'}^{\alpha\beta} \rangle = 4 \delta_{ii'} \delta_{jj'} \delta_{\alpha\alpha'} \delta_{\beta\beta'}$  and the resulting matrix element  $\mathcal{F}_{ab}^{kl} = 0$  is zero in the employed Ansatz. The terms 9 and 11 are equal to each other and add up to  $8 T_{ab}^{ij} K_{ij}^{ab}$ , with the standard two-electron integrals

$$K_{ij}^{ab} = \langle ij | r_{12}^{-1} | ab \rangle \quad (15)$$

To simplify the remaining terms in eq 14, we need to understand how the projector  $Q_A Q_B$  acts on  $|\Phi_{ij}^{\alpha\beta}\rangle$ . Splitting the complete indices  $\alpha, \beta$  into their occupied, virtual, and CA ranges and projecting out nondispersion parts, we obtain

$$\sum_{ij\alpha\beta} Q_A Q_B |\Phi_{ij}^{\alpha\beta}\rangle = \sum_{ijab} |\Phi_{ij}^{ab}\rangle + \sum_{ijxb} |\Phi_{ij}^{xb}\rangle + \sum_{ijay} |\Phi_{ij}^{ay}\rangle + \sum_{ijxy} |\Phi_{ij}^{xy}\rangle \quad (16)$$

Using the decomposition of eq 16, we find that the terms 10 and 12 in eq 14 are equal to each other and add up to

$$8T_{ij}^{kl} \mathcal{F}_{kl}^{ab} K_{ab}^{ij} + 8T_{ij}^{kl} \mathcal{F}_{kl}^{xb} K_{xb}^{ij} + 8T_{ij}^{kl} \mathcal{F}_{kl}^{ay} K_{ay}^{ij} + 8T_{ij}^{kl} \mathcal{F}_{kl}^{xy} K_{xy}^{ij} \quad (17)$$

where, in addition, the first term vanishes because of the presence of  $\mathcal{F}_{kl}^{ab}$ .

The terms 3, 4, 6, and 7 in eq 14 couple the ordinary and explicitly correlated dispersion amplitudes and would vanish if the EBC approximation was employed. Using eq 8, we find that the pairs of terms (3, 6) and (4, 7) are identical to each other, and these four terms add up to

$$8T_{ij}^{ab} T_{kl}^{ij} \mathcal{F}_{kl}^{ab} (f^A)_a^x + 8T_{ij}^{ab} T_{kl}^{ij} \mathcal{F}_{kl}^{ab} (f^B)_b^y \quad (18)$$

The last part remaining to be cast into two-electron integrals and similar quantities is the term 8 in eq 14. To process this term, we employ eq 16 and invoke the structure of the Fock matrix in canonical molecular orbitals within the GBC approximation (eq 11), specifically, the result of the action of a Fock operator on a singly excited monomer state. If the excitation is to the virtual space, we get

$$F^A |\Phi_{ij}^{ab}\rangle = (E_A^0 + \epsilon_a^A - \epsilon_i^A) |\Phi_{ij}^{ab}\rangle + (f^A)_x^a |\Phi_{ij}^{xb}\rangle \quad (19)$$

and for an occupied  $\rightarrow$  CA excitation, the result is

$$F^A |\Phi_{ij}^{xb}\rangle = (E_A^0 - \epsilon_i^A) |\Phi_{ij}^{xb}\rangle + (f^A)_x^a |\Phi_{ij}^{xb}\rangle + (f^A)_a^x |\Phi_{ij}^{ab}\rangle \quad (20)$$

Thus

$$\begin{aligned} \sum_{ij\alpha\beta} (F^A + F^B - E_A^0 - E_B^0) Q_A Q_B |\Phi_{ij}^{\alpha\beta}\rangle = & \sum_{ijab} (\epsilon_a^A + \epsilon_b^B - \epsilon_i^A - \epsilon_j^B) |\Phi_{ij}^{ab}\rangle + \sum_{ijab} (f^A)_x^a |\Phi_{ij}^{xb}\rangle + \\ & \sum_{ijab} (f^B)_y^b |\Phi_{ij}^{ay}\rangle + \sum_{ijxb} (\epsilon_b^B - \epsilon_i^A - \epsilon_j^B) |\Phi_{ij}^{xb}\rangle + \\ & \sum_{ijxb} (f^A)_x^a |\Phi_{ij}^{xb}\rangle + \sum_{ijxb} (f^A)_a^x |\Phi_{ij}^{ab}\rangle + \sum_{ijxb} (f^B)_y^b |\Phi_{ij}^{xy}\rangle + \\ & \sum_{ijay} (\epsilon_a^A - \epsilon_i^A - \epsilon_j^B) |\Phi_{ij}^{ay}\rangle + \sum_{ijay} (f^A)_x^a |\Phi_{ij}^{xy}\rangle + \\ & \sum_{ijay} (f^B)_y^b |\Phi_{ij}^{ay}\rangle + \sum_{ijay} (f^B)_b^y |\Phi_{ij}^{ab}\rangle + \\ & \sum_{ijxy} (-\epsilon_i^A - \epsilon_j^B) |\Phi_{ij}^{xy}\rangle + \sum_{ijxy} (f^A)_x^a |\Phi_{ij}^{xy}\rangle + \\ & \sum_{ijxy} (f^A)_a^x |\Phi_{ij}^{ay}\rangle + \sum_{ijxy} (f^B)_y^b |\Phi_{ij}^{xy}\rangle + \sum_{ijxy} (f^B)_b^y |\Phi_{ij}^{xb}\rangle \end{aligned} \quad (21)$$

Note that all doubly excited functions in eq 21 belong to the dispersion space and are unchanged by the projector  $Q_A Q_B$ . Therefore, we can use eq 8 to evaluate all dot products, and the term 8 in eq 14 becomes

$$\begin{aligned} T_{ij}^{kl} \mathcal{F}_{kl}^{\alpha\beta} T_{k'l'}^{ij} \mathcal{F}_{a'\beta'}^{k'l'} \langle \Phi_{ij}^{\alpha\beta} | Q_A Q_B (F^A + F^B - E_A^0 - E_B^0) Q_A \\ Q_B | \Phi_{i'j'}^{\alpha'\beta'} \rangle = 4T_{ij}^{kl} \mathcal{F}_{kl}^{xb} T_{k'l'}^{ij} \mathcal{F}_{xb}^{k'l'} (\epsilon_b^B - \epsilon_i^A - \epsilon_j^B) \\ + 4T_{ij}^{kl} \mathcal{F}_{kl}^{x'b} T_{k'l'}^{ij} \mathcal{F}_{xb}^{k'l'} (f^A)_{x'}^x + 4T_{ij}^{kl} \mathcal{F}_{kl}^{xy} T_{k'l'}^{ij} \mathcal{F}_{xb}^{k'l'} (f^B)_y^b \\ + 4T_{ij}^{kl} \mathcal{F}_{kl}^{ay} T_{k'l'}^{ij} \mathcal{F}_{ay}^{k'l'} (\epsilon_a^A - \epsilon_i^A - \epsilon_j^B) \\ + 4T_{ij}^{kl} \mathcal{F}_{kl}^{xy} T_{k'l'}^{ij} \mathcal{F}_{ay}^{k'l'} (f^A)_x^a \\ + 4T_{ij}^{kl} \mathcal{F}_{kl}^{ay'} T_{k'l'}^{ij} \mathcal{F}_{ay}^{k'l'} (f^B)_y^y \\ + 4T_{ij}^{kl} \mathcal{F}_{kl}^{xy} T_{k'l'}^{ij} \mathcal{F}_{xy}^{k'l'} (-\epsilon_i^A - \epsilon_j^B) \\ + 4T_{ij}^{kl} \mathcal{F}_{kl}^{x'y} T_{k'l'}^{ij} \mathcal{F}_{xy}^{k'l'} (f^A)_{x'}^x + 4T_{ij}^{kl} \mathcal{F}_{kl}^{ay} T_{k'l'}^{ij} \mathcal{F}_{xy}^{k'l'} (f^A)_x^a \\ + 4T_{ij}^{kl} \mathcal{F}_{kl}^{xy'} T_{k'l'}^{ij} \mathcal{F}_{xy}^{k'l'} (f^B)_y^y + 4T_{ij}^{kl} \mathcal{F}_{kl}^{xb} T_{k'l'}^{ij} \mathcal{F}_{xy}^{k'l'} (f^B)_y^b \end{aligned} \quad (22)$$

where we used  $\mathcal{F}_{ab}^{kl} = 0$  to eliminate the  $|\Phi_{i'j'}^{ab}\rangle$  terms.

Combining all terms, the complete expression for  $J_{\text{disp}}[\chi]$  becomes

$$\begin{aligned} J_{\text{disp}}[\chi] = 4T_{ij}^{ab} T_{ab}^{ij} (\epsilon_a^A + \epsilon_b^B - \epsilon_i^A - \epsilon_j^B) + 8T_{ij}^{ab} T_{kl}^{ij} \mathcal{F}_{kl}^{ab} (f^A)_a^x \\ + 8T_{ij}^{ab} T_{kl}^{ij} \mathcal{F}_{kl}^{ab} (f^B)_b^y + 4T_{ij}^{kl} \mathcal{F}_{kl}^{xb} T_{k'l'}^{ij} \mathcal{F}_{xb}^{k'l'} (\epsilon_b^B - \epsilon_i^A - \epsilon_j^B) \\ + 4T_{ij}^{kl} \mathcal{F}_{kl}^{x'b} T_{k'l'}^{ij} \mathcal{F}_{xb}^{k'l'} (f^A)_{x'}^x + 4T_{ij}^{kl} \mathcal{F}_{kl}^{xy} T_{k'l'}^{ij} \mathcal{F}_{xb}^{k'l'} (f^B)_y^b \\ + 4T_{ij}^{kl} \mathcal{F}_{kl}^{ay} T_{k'l'}^{ij} \mathcal{F}_{ay}^{k'l'} (\epsilon_a^A - \epsilon_i^A - \epsilon_j^B) + 4T_{ij}^{kl} \mathcal{F}_{kl}^{xy} T_{k'l'}^{ij} \mathcal{F}_{ay}^{k'l'} (f^A)_x^a \\ + 4T_{ij}^{kl} \mathcal{F}_{kl}^{ay'} T_{k'l'}^{ij} \mathcal{F}_{ay}^{k'l'} (f^B)_y^y + 4T_{ij}^{kl} \mathcal{F}_{kl}^{xy} T_{k'l'}^{ij} \mathcal{F}_{xy}^{k'l'} (-\epsilon_i^A - \epsilon_j^B) \\ + 4T_{ij}^{kl} \mathcal{F}_{kl}^{x'y} T_{k'l'}^{ij} \mathcal{F}_{xy}^{k'l'} (f^A)_{x'}^x + 4T_{ij}^{kl} \mathcal{F}_{kl}^{ay} T_{k'l'}^{ij} \mathcal{F}_{xy}^{k'l'} (f^A)_x^a \\ + 4T_{ij}^{kl} \mathcal{F}_{kl}^{xy'} T_{k'l'}^{ij} \mathcal{F}_{xy}^{k'l'} (f^B)_y^y + 4T_{ij}^{kl} \mathcal{F}_{kl}^{xb} T_{k'l'}^{ij} \mathcal{F}_{xy}^{k'l'} (f^B)_y^b \\ + 8T_{ij}^{ab} K_{ij}^{ab} + 8T_{ij}^{kl} \mathcal{F}_{kl}^{xb} K_{xb}^{ij} + 8T_{ij}^{kl} \mathcal{F}_{kl}^{ay} K_{ay}^{ij} \\ + 8T_{ij}^{kl} \mathcal{F}_{kl}^{xy} K_{xy}^{ij} \end{aligned} \quad (23)$$

While eq 23 is a complete expression for  $J_{\text{disp}}[\chi]$  in terms of one- and two-electron quantities, it is not well suited for practical applications due to the presence of several CA indices at the same time that necessitate slowly convergent double resolutions of identity. Instead, we will rewrite eq 23 to identify several intermediates found in the standard MP2-F12 theory, whose efficient evaluation avoiding a double resolution of identity (RI) whenever possible<sup>11</sup> can be reused for the computation of  $E_{\text{disp}}^{(20)}$ -F12. To this end, we first expand the  $(\hat{f}_1^A + \hat{f}_2^B)$  operator via a double resolution of identity and eliminate the occupied and double-virtual terms by the strong orthogonality projector

$$\begin{aligned} \hat{Q}_{12} (\hat{f}_1^A + \hat{f}_2^B) \hat{Q}_{12} = |ay\rangle \epsilon_a^A \langle ay| \\ + |ay\rangle (f^A)_a^x \langle xyl + lxy\rangle (f^A)_x^a \langle ay| \\ + |xb\rangle (f^A)_{x'}^x \langle x'bl + lxy\rangle (f^A)_{x'}^x \langle x'y| \\ + |xb\rangle \epsilon_b^B \langle xbl + lxb\rangle (f^B)_b^y \langle xyl \\ + |xy\rangle (f^B)_y^b \langle xbl + lxy\rangle (f^B)_y^y \langle ay'| \\ + |xy\rangle (f^B)_y^y \langle xy'l \end{aligned} \quad (24)$$

Consequently

$$\begin{aligned}
\langle kll\hat{F}_{12}\hat{Q}_{12}(\hat{f}_1^A + \hat{f}_2^B)\hat{Q}_{12}\hat{F}_{12}|k'l'\rangle &= \mathcal{F}_{kl}^{ay}\epsilon_a^A\mathcal{F}_{ay}^{k'l'} \\
&+ \mathcal{F}_{kl}^{ay}(f^A)_a^x\mathcal{F}_{xy}^{k'l'} + \mathcal{F}_{kl}^{xy}(f^A)_x^a\mathcal{F}_{ay}^{k'l'} \\
&+ \mathcal{F}_{kl}^{xb}(f^A)_x^a\mathcal{F}_{x'b}^{k'l'} + \mathcal{F}_{kl}^{xy}(f^A)_x^a\mathcal{F}_{x'y}^{k'l'} \\
&+ \mathcal{F}_{kl}^{xb}\epsilon_b^B\mathcal{F}_{xb}^{k'l'} + \mathcal{F}_{kl}^{xy}(f^B)_b^y\mathcal{F}_{xy}^{k'l'} \\
&+ \mathcal{F}_{kl}^{xy}(f^B)_y^b\mathcal{F}_{xb}^{k'l'} + \mathcal{F}_{kl}^{ay}(f^B)_y^b\mathcal{F}_{ay}^{k'l'} \\
&+ \mathcal{F}_{kl}^{xy}(f^B)_y^b\mathcal{F}_{xy}^{k'l'} \quad (25)
\end{aligned}$$

All 10 resulting terms are found in eq 23 multiplied by the same factor  $4T_{ij}^{kl}T_{k'l'}^{ij}$ . Moreover, the matrix element of eq 25 is the same as the standard  $B_{kl,k'l'}$  intermediate of the MP2-F12 theory (see, e.g., eq 27 of ref 11) except for the fact that the Fock operators  $\hat{f}_1^A$  and  $\hat{f}_2^B$  now refer to two different molecules.

Three other contributions in eq 23 can be added together as follows

$$\begin{aligned}
4(-\epsilon_i^A - \epsilon_j^B)T_{ij}^{kl}T_{k'l'}^{ij}(\mathcal{F}_{kl}^{xb}\mathcal{F}_{x'b}^{k'l'} + \mathcal{F}_{kl}^{ay}\mathcal{F}_{ay}^{k'l'} + \mathcal{F}_{kl}^{xy}\mathcal{F}_{xy}^{k'l'}) \\
= 4(-\epsilon_i^A - \epsilon_j^B)T_{ij}^{kl}T_{k'l'}^{ij}\langle kll\hat{F}_{12}\hat{Q}_{12}\hat{F}_{12}|k'l'\rangle \quad (26)
\end{aligned}$$

which involves another common MP2-F12 intermediate  $X_{kl,k'l'}$ , cf. eq 28 of ref 11. The last three terms in eq 23 can be written as

$$8T_{ij}^{kl}(\mathcal{F}_{kl}^{xb}K_{xb}^{ij} + \mathcal{F}_{kl}^{ay}K_{ay}^{ij} + \mathcal{F}_{kl}^{xy}K_{xy}^{ij}) = 8T_{ij}^{kl}\langle kll\hat{F}_{12}\hat{Q}_{12}r_{12}^{-1}|ij\rangle \quad (27)$$

with the intermediate  $V_{kb}^{ij}$ , eq 26 of ref 11, present this time. Finally, the second and third terms in eq 23 can be expressed as

$$\begin{aligned}
8T_{ij}^{ab}T_{kl}^{ij}\mathcal{F}_{xb}^{kl}(f^A)_a^x + 8T_{ij}^{ab}T_{kl}^{ij}\mathcal{F}_{ay}^{kl}(f^B)_b^y \\
= 8T_{ij}^{ab}T_{kl}^{ij}\langle kll\hat{F}_{12}\hat{Q}_{12}\hat{f}_1^A|lab\rangle + 8T_{ij}^{ab}T_{kl}^{ij}\langle kll\hat{F}_{12}\hat{Q}_{12}\hat{f}_2^B|lab\rangle \quad (28)
\end{aligned}$$

The resulting matrix elements add up to the  $C_{ab}^{kl}$  MP2-F12 intermediate, defined, e.g., in eq 29 of ref 11, except that the Fock operators  $f_1$  and  $f_2$  pertain to different molecules. Thus, the final formula for  $J_{\text{disp}}[\chi]$ , utilizing intermediates similar to the MP2-F12 theory, reads

$$\begin{aligned}
J_{\text{disp}}[\chi] &= 4T_{ij}^{ab}T_{ab}^{ij}(\epsilon_a^A + \epsilon_b^B - \epsilon_i^A - \epsilon_j^B) + 8T_{ab}^{ij}K_{ij}^{ab} \\
&+ 4T_{ij}^{kl}T_{k'l'}^{ij}B_{kl,k'l'} - 4(\epsilon_i^A + \epsilon_j^B)T_{ij}^{kl}T_{k'l'}^{ij}X_{kl,k'l'} \\
&+ 8T_{ij}^{kl}V_{kl}^{ij} + 8T_{ij}^{ab}T_{kl}^{ij}C_{ab}^{kl} \quad (29)
\end{aligned}$$

It may be verified that all of the resolution of identity and commutator transformations used to evaluate the  $V$ ,  $X$ ,  $B$ , and  $C$  matrices in the MP2-F12(3C) context<sup>11</sup> remain valid in the case of explicitly correlated dispersion energy as long as one is careful to employ the Fock operator for the correct monomer.

We now need to find the amplitudes  $T_{ij}^{ab}$  and  $T_{ij}^{kl}$  that minimize eq 29. The partial derivatives of the Hylleraas functional with respect to the amplitudes are (writing the summations explicitly this time)

$$\frac{\partial J_{\text{disp}}}{\partial T_{ij}^{ab}} = 8T_{ij}^{ab}(\epsilon_a^A + \epsilon_b^B - \epsilon_i^A - \epsilon_j^B) + 8K_{ij}^{ab} + 8 \sum_{kl} T_{kl}^{ij}C_{ab}^{kl} \quad (30)$$

$$\begin{aligned}
\frac{\partial J_{\text{disp}}}{\partial T_{ij}^{kl}} &= 8 \sum_{k'l'} T_{ij}^{k'l'}B_{kl,k'l'} - 8(\epsilon_i^A + \epsilon_j^B) \sum_{k'l'} T_{ij}^{k'l'}X_{kl,k'l'} \\
&+ 8V_{kl}^{ij} + 8 \sum_{ab} T_{ij}^{ab}C_{ab}^{kl} \quad (31)
\end{aligned}$$

As expected, the equations for the standard dispersion amplitudes  $T_{ij}^{ab}$  and explicitly correlated amplitudes  $T_{ij}^{kl}$  are coupled since we have not assumed the extended Brillouin condition. Setting both gradients to zero gives a separate system of linear equations for each pair  $(ij)$ . Inserting the solutions of these linear equations into eq 29, we get a simplified formula for  $E_{\text{disp}}^{(20)}$ -F12 valid for optimized amplitudes only

$$E_{\text{disp}}^{(20)}\text{-F12} = 4T_{ab}^{ij}K_{ij}^{ab} + 4T_{ij}^{kl}V_{kl}^{ij} \quad (32)$$

The full optimization of amplitudes  $T_{ij}^{ab}$  and  $T_{ij}^{kl}$  proceeds by solving eq 30 for  $T_{ij}^{ab}$  and substituting the result into eq 31

$$\begin{aligned}
T_{ij}^{ab} &= \frac{K_{ij}^{ab} + \sum_{kl} T_{kl}^{ij}C_{ab}^{kl}}{\epsilon_i^A + \epsilon_j^B - \epsilon_a^A - \epsilon_b^B} \quad (33) \\
\sum_{k'l'} T_{ij}^{k'l'} &\left[ B_{kl,k'l'} - (\epsilon_i^A + \epsilon_j^B)X_{kl,k'l'} \right. \\
&+ \left. \sum_{ab} \frac{C_{ab}^{k'l'}C_{ab}^{kl}}{\epsilon_i^A + \epsilon_j^B - \epsilon_a^A - \epsilon_b^B} \right] \\
&= -V_{kl}^{ij} - \sum_{ab} \frac{K_{ij}^{ab}C_{ab}^{kl}}{\epsilon_i^A + \epsilon_j^B - \epsilon_a^A - \epsilon_b^B} \quad (34)
\end{aligned}$$

Let us denote by  $o_A$ ,  $v_A$  ( $o_B$ ,  $v_B$ ) the numbers of occupied and virtual orbitals for monomer A (B), respectively. For a given pair  $(ij)$ , eq 34 is a system of  $o_A o_B$  linear equations for the explicitly correlated amplitudes  $T_{ij}^{kl}$ . Unfortunately, the formation of the matrix for this linear system scales like  $o_A^2 v_A o_B^2 v_B$  and has to be repeated for each of the  $o_A o_B$  pairs, bringing the overall scaling of the full amplitude optimization to a highly unfavorable  $o_A^3 v_A o_B^3 v_B$ , that is,  $N^8$ . This nonapproximate but expensive variant of  $E_{\text{disp}}^{(20)}$ -F12 was very recently proposed and investigated by Przybytek.<sup>47</sup> In this work, in addition to the full amplitude optimization, we propose and test three simplified Ansätze that exhibit reduced computational scaling.

- **EBC Ansatz:** Assuming the extended Brillouin condition simplifies eq 11 by zeroing out the  $(f^A)_x^a$  and  $(f^B)_a^x$  coupling matrices, which results in  $C_{ab}^{kl} = 0$  so that eqs 30 and 31 are decoupled (in addition, the  $B_{kl,k'l'}$  intermediate is somewhat simplified, see eq 25). Most importantly, eq 34 simplifies to

$$\sum_{k'l'} (T^{\text{EBC}})_{ij}^{k'l'} [B_{kl,k'l'} - (\epsilon_i^A + \epsilon_j^B)X_{kl,k'l'}] = -V_{kl}^{ij} \quad (35)$$

In such a case, the matrix for the system of equations can trivially be formed from the same  $B_{kl,k'l'}$  and  $X_{kl,k'l'}$  intermediates (which require on the order of  $N^5$  operations to evaluate), and the limiting factor becomes the solution of eq 35 for every pair  $(ij)$ . This brings the overall scaling of the approach to  $o_A^4 o_B^4$  if a complete noniterative solution of each linear system is performed, which is more favorable than for the non-EBC variant but still  $N^8$ . However, an iterative (e.g., conjugate gradient)

solution of the systems of equations can deliver better scaling as a single iteration (matrix–vector multiplication) for all pairs scales like  $\sigma_A^3 \sigma_B^3$  or  $N^6$ .

- **Optimized Diagonal Ansatz (ODA):** In this approximation, we assume that the amplitudes  $T_{ij}^{kl}$  are diagonal, that is

$$T_{ij}^{kl} = T_{ij}^{ij} \delta_{ik} \delta_{jl} \quad (36)$$

With this simplification (and without assuming EBC), eqs 33 and 34 become

$$T_{ij}^{ab} = \frac{K_{ij}^{ab} + T_{ij}^{ij} C_{ab}^{ij}}{\epsilon_i^A + \epsilon_j^B - \epsilon_a^A - \epsilon_b^B} \quad (37)$$

$$T_{ij}^{ij} \left[ B_{ij,ij} - (\epsilon_i^A + \epsilon_j^B) X_{ij,ij} + \sum_{ab} \frac{C_{ab}^{ij} C_{ab}^{ij}}{\epsilon_i^A + \epsilon_j^B - \epsilon_a^A - \epsilon_b^B} \right] = -V_{ij}^{ij} - \sum_{ab} \frac{K_{ij}^{ab} C_{ab}^{ij}}{\epsilon_i^A + \epsilon_j^B - \epsilon_a^A - \epsilon_b^B} \quad (38)$$

Thus, no systems of equations need to be solved, and all amplitudes can be recovered in  $\sigma_A \nu_A \sigma_B \nu_B$  ( $N^4$ ) operations once all of the intermediates  $V, X, C, B$  are ready.

- **Fixed-Amplitude Ansatz:** In this simplest approximation, we assume that  $T_{ij}^{kl}$  is not only diagonal (eq 36) but all diagonal  $T_{ij}^{ij} = \lambda$  for some common value of the single parameter  $\lambda$ . In this case, the Hylleraas functional  $J_{\text{disp}}[\chi]$ , eq 29, is quadratic in  $\lambda$  and it is trivial to find the value of  $\lambda$  that minimizes it. One should note that the  $T_{ij}^{ab}$  amplitudes in this approximation are still calculated from eq 37; thus, they do contain a nonzero contribution from the conventional-F12 amplitude coupling. We have observed that the optimal  $\lambda$  values for various systems are typically in a fairly narrow, 0.3–0.6 range. It should be noted that the molecular MP2-F12 and CCSD(T)-F12 calculations commonly employ a similar fixed-amplitude Ansatz where the values for the singlet and triplet pair functions are fixed by the cusp conditions.<sup>6</sup> As the SAPT dispersion wave function does not allow for electron exchanges between monomers (exchange corrections are added in SAPT at a later stage, using symmetrized energy expressions with unsymmetrized wave function corrections<sup>26</sup>), the exact singlet and triplet coalescence conditions cannot be enforced and we chose to treat  $\lambda$  as an adjustable parameter instead. It should be noted, however, that the fixed-amplitude Ansatz leads to negligible computational savings over the optimized diagonal one as the limiting factor is still the computation of intermediates, in particular  $B$ .

### III. F12 EXCHANGE DISPERSION ENERGY

In conventional SAPT, the second-order exchange dispersion energy is usually computed in the single exchange approximation, also called the  $S^2$  approximation as it neglects terms of order higher than 2 in the intermolecular overlap integrals.<sup>26</sup> The value of the  $E_{\text{exch-disp}}^{(20)}$  ( $S^2$ ) correction (the qualifier ( $S^2$ ) will be dropped from now on) is obtained from dispersion amplitudes  $T_{ab}^{ij}$ , taken straight from the dispersion energy

calculation, and a host of various one- and two-electron integrals. As we have assumed the DCBS case, that is, both the molecular-orbital and CA bases span the same spaces for monomers A and B, the  $E_{\text{exch-disp}}^{(20)}$  correction can be computed from two equivalent expressions: the conventional one derived using density matrices<sup>48</sup> and the less popular, DCBS-only one employing the second-quantized form of the single exchange operator.<sup>49</sup> The latter formalism will be employed here as it contains far fewer different integral types. The standard  $E_{\text{exch-disp}}^{(20)}$  correction within the second-quantized formalism is given, e.g., by eq 12 of ref 50, which, transcribed to our notation, reads

$$E_{\text{exch-disp}}^{(20)} = 2T_{ij}^{ij} [-K_{ij}^{a'b'} S_a^a S_{b'}^{b'} + K_{i'i'}^{ab'} S_i^a S_{b'}^{b'} - 2K_{ij}^{ab'} S_i^a S_{b'}^{b'} + K_{ij}^{a'b} S_j^a S_{b'}^{b'} - 2K_{ij}^{a'b} S_j^a S_{b'}^{b'} - K_{i'i'}^{ab} S_i^a S_{j'}^{b'} + 2K_{ij}^{ab} S_i^a S_{j'}^{b'} + 2K_{i'i'}^{ab} S_i^a S_{j'}^{b'} - 2(\omega_B)_i^a S_i^a S_{j'}^{b'} + (\omega_B)_i^a S_i^a S_{j'}^{b'} - (\omega_B)_i^a S_i^a S_{j'}^{b'} - 2(\omega_A)_j^b S_j^b S_{i'}^{a'} + (\omega_A)_j^b S_j^b S_{i'}^{a'} - (\omega_A)_j^b S_j^b S_{i'}^{a'}] \quad (39)$$

where  $S_j^i = \langle ij | j \rangle$  is the overlap integral and  $(\omega_B)_i^a$  is the matrix element of the electrostatic potential of monomer B, that is

$$(\omega_B)_i^a = \langle a | V_B | i \rangle + 2K_{ij}^{aj} \quad (40)$$

and  $V_B$  is the nuclear potential of molecule B. A similar definition holds for the  $(\omega_A)_j^b$  matrix elements. Let us now imagine that we are running the same SAPT calculation in a complete one-electron basis  $|\alpha\rangle$  for A and  $|\beta\rangle$  for B. Then, eq 39 holds, with the occupied orbitals  $ij$  the same as for the standard SAPT calculation (according to GBC, the addition of CA functions does not improve  $ij$ ) but the virtual orbitals  $a, b$  replaced by larger sets  $\gamma, \delta$ , which will denote unoccupied orbitals on A and B, respectively (that is, the index  $\gamma$  runs over both  $a$  and  $x$ , and the index  $\delta$  runs over both  $b$  and  $y \equiv x$ ). The calculation with such large virtual spaces is, in general, unfeasible, but the F12 Ansatz provides a compact internally contracted representation of these spaces

$$T_{\gamma\delta}^{ij} |\Phi_{ij}^{\gamma\delta}\rangle \rightarrow T_{ab}^{ij} |\Phi_{ij}^{ab}\rangle + T_{kl}^{ij} \mathcal{F}_{\alpha\beta}^{kl} |\Phi_{ij}^{\alpha\beta}\rangle \quad (41)$$

where both  $T_{ab}^{ij}$  and  $T_{kl}^{ij}$  have been determined in the preceding  $E_{\text{disp}}^{(20)}$ -F12 calculation. One should note that the presence of the projector  $\hat{Q}_{12}$ , eq 10, in the  $\mathcal{F}_{\alpha\beta}^{kl}$  matrix element means that (1) neither  $\alpha$  nor  $\beta$  can be an occupied index so there are no contributions outside of the  $|\Phi_{ij}^{\gamma\delta}\rangle$  space, and (2)  $\alpha$  and  $\beta$  cannot both be virtual so there is no double counting between the  $|\Phi_{ij}^{ab}\rangle$  and  $|\Phi_{ij}^{\alpha\beta}\rangle$  terms. In other words, out of different doubly excited configurations  $|\Phi_{ij}^{\gamma\delta}\rangle$ , the first term in eq 41 accounts for  $|\Phi_{ij}^{ab}\rangle$  and the second term for  $|\Phi_{ij}^{\alpha\gamma}\rangle$ ,  $|\Phi_{ij}^{\alpha\delta}\rangle$ , and  $|\Phi_{ij}^{\beta\gamma}\rangle$ . If we now substitute the Ansatz of eq 41 into eq 39, the  $T_{ab}^{ij} |\Phi_{ij}^{ab}\rangle$  term will give the standard exchange dispersion energy and the second term will provide the F12 correction  $\delta E_{\text{exch-disp}}^{(20)}$ -F12. Accordingly, the latter correction takes the following form (note the ranges of different indices)

$$\delta E_{\text{exch-disp}}^{(20)}\text{-F12} = 2T_{kl}^{ij} \mathcal{F}_{\alpha\beta}^{kl} [-K_{ij}^{\gamma\delta} S_\gamma^\beta S_\delta^\alpha + K_{i'i'}^{\alpha\delta} S_i^\alpha S_{j'}^\beta S_\delta^\alpha - 2K_{ij}^{\alpha\delta} S_i^\alpha S_{j'}^\beta S_\delta^\alpha + K_{ij}^{\gamma\beta} S_j^\alpha S_\gamma^\beta - 2K_{ij}^{\gamma\beta} S_j^\alpha S_\gamma^\beta - K_{i'i'}^{\alpha\beta} S_i^\alpha S_{j'}^\beta S_\delta^\alpha + 2K_{ij}^{\alpha\beta} S_i^\alpha S_{j'}^\beta S_\delta^\alpha + 2K_{i'i'}^{\alpha\beta} S_i^\alpha S_{j'}^\beta S_\delta^\alpha - 2(\omega_B)_i^\alpha S_i^\alpha S_{j'}^\beta S_\delta^\alpha + (\omega_B)_i^\alpha S_i^\alpha S_{j'}^\beta S_\delta^\alpha - (\omega_B)_i^\alpha S_i^\alpha S_{j'}^\beta S_\delta^\alpha - 2(\omega_A)_j^\beta S_j^\beta S_{i'}^\alpha S_\delta^\alpha + (\omega_A)_j^\beta S_j^\beta S_{i'}^\alpha S_\delta^\alpha - (\omega_A)_j^\beta S_j^\beta S_{i'}^\alpha S_\delta^\alpha] \quad (42)$$

The first step to transform eq 42 to a practical equation is to eliminate the projectors  $\hat{Q}_{12}$  from the  $\mathcal{F}_{\alpha\beta}^{kl}$  matrix elements. We have two forms of this projector that are equivalent in the limit of complete RI basis, but the first form converges faster with the RI basis as the second form involves an undesirable, slowly converging double CABS expansion<sup>11</sup>

$$\begin{aligned}\hat{Q}_{12} &= 1 - |xn\rangle\langle xnl - lmy\rangle\langle myl - lrs\rangle\langle rsl \\ &= |ay\rangle\langle ayl + |xb\rangle\langle xbl + |xy\rangle\langle xyl\end{aligned}\quad (43)$$

For the reasons that will become clear below, we will use the first form of eq 43 for the underlined terms in eq 42 and the second form for the terms that are not underlined. In short, we will show that the latter terms do not lead to a double RI expansion (over  $x,y$ ) in the end, while the underlined terms would lead to such an expansion unless explicitly prevented. On the other hand, if we tried treating the nonunderlined terms with the first form of eq 43, three-electron integrals would appear.

Let us start with the nonunderlined terms in eq 42

$$\begin{aligned}\delta E_{\text{exch-disp}}^{(20)}\text{-F12}(1) &= 2T_{kl}^{ij}\langle kll\hat{F}_{12}(lay)\langle ayl + |xb\rangle\langle xbl \\ &+ |xy\rangle\langle xyl|\alpha\beta\rangle[K_{i'j'}^{\alpha\delta}S_i^{\beta}S_j^{\alpha} - 2K_{ij}^{\alpha\delta}S_i^{\beta}S_j^{\alpha} + K_{ij'}^{\gamma\beta}S_i^{\alpha}S_j^{\gamma} \\ &- 2K_{ij}^{\gamma\beta}S_j^{\alpha}S_i^{\gamma} - 2(\omega_B)_i^{\alpha}S_i^{\beta}S_j^{\alpha} + (\omega_B)_i^{\alpha}S_i^{\beta}S_j^{\alpha} \\ &- (\omega_B)_i^{\gamma}S_i^{\beta}S_j^{\alpha} - 2(\omega_A)_j^{\beta}S_j^{\alpha}S_i^{\gamma} + (\omega_A)_j^{\beta}S_j^{\alpha}S_i^{\gamma} - (\omega_A)_j^{\delta}S_j^{\beta}S_i^{\alpha}]\end{aligned}\quad (44)$$

Each term in eq 44 contains an overlap integral of the type  $S_j^{\alpha}$  or  $S_i^{\beta}$ . Such an integral is zero if the orbital  $\alpha(\beta)$  belongs to the CA space as all complementary functions are orthogonal to the molecular orbitals of both monomers, e.g.,  $S_j^{\alpha} = 0$ . Therefore, for each of the terms in eq 44, only one of the three contributions,  $|ay\rangle\langle ayl$  or  $|xb\rangle\langle xbl$ , survives (the term  $|xy\rangle\langle xyl$  always vanishes so that the danger of a double RI expansion has been averted). The surviving terms are

$$\begin{aligned}\delta E_{\text{exch-disp}}^{(20)}\text{-F12}(1) &= 2T_{kl}^{ij}[F_{xb}^{kl}K_{i'j'}^{\alpha\delta}S_i^{\beta}S_j^{\alpha} \\ &- 2F_{xb}^{kl}K_{ij}^{\alpha\delta}S_i^{\beta}S_j^{\alpha} + F_{ay}^{kl}K_{ij'}^{\gamma\beta}S_j^{\alpha}S_i^{\gamma} \\ &- 2F_{ay}^{kl}K_{ij}^{\gamma\beta}S_j^{\alpha}S_i^{\gamma} - 2F_{xb}^{kl}(\omega_B)_i^{\alpha}S_i^{\beta}S_j^{\alpha} \\ &+ F_{xb}^{kl}(\omega_B)_i^{\alpha}S_i^{\beta}S_j^{\alpha} - F_{ay}^{kl}(\omega_B)_i^{\gamma}S_j^{\alpha}S_i^{\gamma} \\ &- 2F_{ay}^{kl}(\omega_A)_j^{\beta}S_j^{\alpha}S_i^{\gamma} + F_{ay}^{kl}(\omega_A)_j^{\beta}S_j^{\alpha}S_i^{\gamma} \\ &- F_{xb}^{kl}(\omega_A)_j^{\delta}S_j^{\beta}S_i^{\alpha}]\end{aligned}\quad (45)$$

To finalize the derivation of this part of the F12 correction to the exchange dispersion energy, we need to split the unoccupied indices  $\gamma,\delta$  into their virtual and CA ranges and identify surviving terms. Taking into account the orthogonality of the complementary auxiliary space to the orbital space and the mutual orthogonality of the complementary functions ( $S_j^{\alpha} = \delta_{xy}$ ), we obtain the final expression for this part

$$\begin{aligned}\delta E_{\text{exch-disp}}^{(20)}\text{-F12}(1) &= 2T_{kl}^{ij}[F_{xb}^{kl}K_{i'j'}^{\alpha\delta}S_i^{\beta}S_j^{\alpha} \\ &- 2F_{xb}^{kl}K_{ij}^{\alpha\delta}S_i^{\beta}S_j^{\alpha} + F_{ay}^{kl}K_{ij'}^{\gamma\beta}S_j^{\alpha}S_i^{\gamma} \\ &- 2F_{ay}^{kl}K_{ij}^{\gamma\beta}S_j^{\alpha}S_i^{\gamma} - 2F_{xb}^{kl}(\omega_B)_i^{\alpha}S_i^{\beta}S_j^{\alpha} \\ &+ F_{xb}^{kl}(\omega_B)_i^{\alpha}S_i^{\beta}S_j^{\alpha} - F_{ay}^{kl}(\omega_B)_i^{\gamma}S_j^{\alpha}S_i^{\gamma} \\ &- 2F_{ay}^{kl}(\omega_A)_j^{\beta}S_j^{\alpha}S_i^{\gamma} + F_{ay}^{kl}(\omega_A)_j^{\beta}S_j^{\alpha}S_i^{\gamma} \\ &- F_{xb}^{kl}(\omega_A)_j^{\delta}S_j^{\beta}S_i^{\alpha}]\end{aligned}\quad (46)$$

We can now move on to the underlined terms in eq 42, substituting the first form of the projector from eq 43

$$\begin{aligned}\delta E_{\text{exch-disp}}^{(20)}\text{-F12}(2) &= 2T_{kl}^{ij}\langle kll\hat{F}_{12}(1 - |xn\rangle\langle xnl - lmy)\langle myl \\ &- |rs\rangle\langle rsl|\alpha\beta\rangle \times [-K_{ij}^{\gamma\delta}S_j^{\alpha}S_i^{\beta} - K_{i'j'}^{\alpha\beta}S_i^{\gamma}S_j^{\delta} \\ &+ 2K_{ij}^{\alpha\beta}S_i^{\gamma}S_j^{\delta} + 2K_{i'j'}^{\alpha\beta}S_i^{\gamma}S_j^{\delta}] \\ &= 2T_{kl}^{ij}[-F_{\alpha\beta}^{kl}K_{ij}^{\gamma\delta}S_j^{\alpha}S_i^{\beta} + F_{\alpha\beta}^{kl}K_{i'j'}^{\gamma\delta}S_i^{\alpha}S_j^{\beta} + F_{\alpha\beta}^{kl}K_{ij}^{\gamma\delta}S_j^{\alpha}S_i^{\beta} \\ &+ F_{rs}^{kl}K_{ij}^{\gamma\delta}S_j^{\alpha}S_i^{\beta} - F_{\alpha\beta}^{kl}K_{i'j'}^{\alpha\beta}S_i^{\gamma}S_j^{\delta} + F_{\alpha\beta}^{kl}K_{i'j'}^{\alpha\beta}S_i^{\gamma}S_j^{\delta} \\ &+ F_{\alpha\beta}^{kl}K_{i'j'}^{\alpha\beta}S_i^{\gamma}S_j^{\delta} + F_{rs}^{kl}K_{ij}^{\gamma\delta}S_j^{\alpha}S_i^{\beta} + 2F_{\alpha\beta}^{kl}K_{ij}^{\alpha\beta}S_i^{\gamma}S_j^{\delta} \\ &- 2F_{\alpha\beta}^{kl}K_{ij}^{\alpha\beta}S_i^{\gamma}S_j^{\delta} - 2F_{\alpha\beta}^{kl}K_{i'j'}^{\alpha\beta}S_i^{\gamma}S_j^{\delta} - 2F_{rs}^{kl}K_{ij}^{\gamma\delta}S_j^{\alpha}S_i^{\beta} \\ &+ 2F_{\alpha\beta}^{kl}K_{i'j'}^{\alpha\beta}S_i^{\gamma}S_j^{\delta} - 2F_{\alpha\beta}^{kl}K_{i'j'}^{\alpha\beta}S_i^{\gamma}S_j^{\delta} - 2F_{\alpha\beta}^{kl}K_{i'j'}^{\alpha\beta}S_i^{\gamma}S_j^{\delta} \\ &- 2F_{rs}^{kl}K_{ij}^{\gamma\delta}S_j^{\alpha}S_i^{\beta}]\end{aligned}\quad (47)$$

Let us now first examine the terms in eq 47 that result from the unit operator in the expansion of  $\hat{Q}_{12}$ . In three of these terms, it is easy to identify and eliminate the identity operator  $1 = |\alpha\beta\rangle\langle\alpha\beta|$

$$\begin{aligned}2T_{kl}^{ij}[-F_{\alpha\beta}^{kl}K_{i'j'}^{\alpha\beta}S_i^{\gamma}S_j^{\delta} + 2F_{\alpha\beta}^{kl}K_{ij}^{\alpha\beta}S_i^{\gamma}S_j^{\delta} + 2F_{\alpha\beta}^{kl}K_{i'j'}^{\alpha\beta}S_i^{\gamma}S_j^{\delta}] \\ = 2T_{kl}^{ij}[-\langle kll\hat{F}_{12}r_{12}^{-1}|i'j'\rangle S_i^{\gamma}S_j^{\delta} + 2\langle kll\hat{F}_{12}r_{12}^{-1}|ij'\rangle S_i^{\gamma}S_j^{\delta} \\ + 2\langle kll\hat{F}_{12}r_{12}^{-1}|i'j'\rangle S_i^{\gamma}S_j^{\delta}]\end{aligned}\quad (48)$$

leading to the integrals identical to eq 55 of ref 11, which were already present in the formula for the F12 dispersion energy. The first term in eq 47 also involves the resolutions of identity  $|\alpha\rangle\langle\alpha|$  and  $|\beta\rangle\langle\beta|$ , and it can be proven that

$$F_{\alpha\beta}^{kl}S_i^{\alpha}S_j^{\beta} = F_{\delta\beta}^{kl}S_i^{\alpha}S_j^{\beta} = F_{\delta\gamma}^{kl} = F_{\gamma\delta}^{kl}\quad (49)$$

The resulting operator  $|\gamma\delta\rangle\langle\gamma\delta|$  is not a complete resolution of identity because the terms involving occupied orbitals on either monomer are missing

$$\begin{aligned}|\gamma\delta\rangle\langle\gamma\delta| &= 1 - |ij\rangle\langle ij| - |aj\rangle\langle aj| - |ib\rangle\langle ib| - |xj\rangle\langle xj| \\ &- |iy\rangle\langle iy|\end{aligned}\quad (50)$$

The substitution of eq 50 into the first term of eq 47 gives

$$\begin{aligned}-2T_{kl}^{ij}F_{\gamma\delta}^{kl}K_{ij}^{\alpha\beta} &= -2T_{kl}^{ij}\langle kll\hat{F}_{12}(1 - |i'j'\rangle\langle i'j'| - |aj'\rangle\langle aj'| \\ &- |i'b\rangle\langle i'b| - |xj'\rangle\langle xj'| - |i'y\rangle\langle i'y|)r_{12}^{-1}|ij\rangle \\ &- 2T_{kl}^{ij}\langle kll\hat{F}_{12}r_{12}^{-1}|ij\rangle + 2T_{kl}^{ij}F_{ij'}^{kl}K_{ij}^{\alpha\beta} \\ &+ 2T_{kl}^{ij}F_{aj'}^{kl}K_{ij}^{\alpha\beta} + 2T_{kl}^{ij}F_{ib}^{kl}K_{ij}^{\alpha\beta} + 2T_{kl}^{ij}F_{xj'}^{kl}K_{ij}^{\alpha\beta} \\ &+ 2T_{kl}^{ij}F_{i'y}^{kl}K_{ij}^{\alpha\beta}\end{aligned}\quad (51)$$

All resulting integral types have been already encountered in the calculation of intermediates for  $E_{\text{disp}}^{(20)}$ -F12: the only difference is that the integrals involving  $\hat{F}_{12}$  and  $\hat{F}_{12}r_{12}^{-1}$  are of the exchange type:  $F_{\text{AB}}^{\text{BA}}$ . This requires the same atomic-orbital integrals but a slightly modified integral transformation employing the SCF vectors of the appropriate monomer.

All that remains to be evaluated are the 12 terms from eq 47 except for the ones resulting from the identity operator in eq 43. These terms are straightforward: we just need to determine the proper range for the unoccupied indices  $\gamma, \delta$

$$\begin{aligned}
 & 2T_{kl}^{ij}[F_{\text{xt}}^{kl}K_{ij}^{\gamma\delta}S_{\gamma}^nS_{\delta}^x + F_{\text{my}}^{kl}K_{ij}^{\gamma\delta}S_{\gamma}^yS_{\delta}^m + F_{\text{rs}}^{kl}K_{ij}^{\gamma\delta}S_{\gamma}^rS_{\delta}^s \\
 & + F_{\text{xt}}^{kl}K_{ij}^{\text{xn}}S_i^jS_j^{i'} + F_{\text{my}}^{kl}K_{ij}^{\text{my}}S_i^jS_j^{i'} + F_{\text{rs}}^{kl}K_{ij}^{\text{rs}}S_i^jS_j^{i'} \\
 & - 2F_{\text{xt}}^{kl}K_{ij}^{\text{xn}}S_i^jS_j^{i'} - 2F_{\text{my}}^{kl}K_{ij}^{\text{my}}S_i^jS_j^{i'} - 2F_{\text{rs}}^{kl}K_{ij}^{\text{rs}}S_i^jS_j^{i'} \\
 & - 2F_{\text{xt}}^{kl}K_{ij}^{\text{xn}}S_i^jS_j^{i'} - 2F_{\text{my}}^{kl}K_{ij}^{\text{my}}S_i^jS_j^{i'} - 2F_{\text{rs}}^{kl}K_{ij}^{\text{rs}}S_i^jS_j^{i'}] \\
 & = 2T_{kl}^{ij}[F_{\text{xt}}^{kl}K_{ij}^{\text{ax}}S_a^n + F_{\text{my}}^{kl}K_{ij}^{\text{yb}}S_b^m + F_{\text{rs}}^{kl}K_{ij}^{\text{cs}}S_c^r \\
 & + F_{\text{xt}}^{kl}K_{ij}^{\text{xn}}S_i^jS_j^{i'} + F_{\text{my}}^{kl}K_{ij}^{\text{my}}S_i^jS_j^{i'} + F_{\text{rs}}^{kl}K_{ij}^{\text{rs}}S_i^jS_j^{i'} \\
 & - 2F_{\text{xt}}^{kl}K_{ij}^{\text{xn}}S_i^jS_j^{i'} - 2F_{\text{my}}^{kl}K_{ij}^{\text{my}}S_i^jS_j^{i'} - 2F_{\text{rs}}^{kl}K_{ij}^{\text{rs}}S_i^jS_j^{i'} \\
 & - 2F_{\text{xt}}^{kl}K_{ij}^{\text{xn}}S_i^jS_j^{i'} - 2F_{\text{my}}^{kl}K_{ij}^{\text{my}}S_i^jS_j^{i'} - 2F_{\text{rs}}^{kl}K_{ij}^{\text{rs}}S_i^jS_j^{i'}]
 \end{aligned} \quad (52)$$

We have now derived all parts of the F12 correction to  $E_{\text{exch-disp}}^{(20)}$ . Collecting them together, we obtain

$$\begin{aligned}
 \delta E_{\text{exch-disp}}^{(20)}\text{-F12} &= 2T_{kl}^{ij}[F_{\text{xt}}^{kl}K_{ij}^{\text{xb}}S_i^aS_j^{b'} - 2F_{\text{xt}}^{kl}K_{ij}^{\text{xb}}S_i^aS_j^{b'} \\
 & + F_{\text{ay}}^{kl}K_{ij}^{\text{ay}}S_j^aS_i^{a'} - 2F_{\text{ay}}^{kl}K_{ij}^{\text{ay}}S_j^aS_i^{a'} - 2F_{\text{ab}}^{kl}(\omega_{\text{B}})_i^a S_j^b S_i^{b'} \\
 & + F_{\text{ab}}^{kl}(\omega_{\text{B}})_i^a S_j^b S_i^{b'} - F_{\text{ay}}^{kl}(\omega_{\text{B}})_i^a S_j^a S_i^{a'} - 2F_{\text{ay}}^{kl}(\omega_{\text{A}})_i^a S_j^a S_i^{a'} \\
 & + F_{\text{ay}}^{kl}(\omega_{\text{A}})_i^a S_j^a S_i^{a'} - F_{\text{ab}}^{kl}(\omega_{\text{A}})_i^a S_j^b S_i^{b'} - \langle kl|\hat{F}_{12}r_{12}^{-1}i'j\rangle S_i^j S_j^{i'} \\
 & + 2\langle kl|\hat{F}_{12}r_{12}^{-1}ij\rangle S_i^j S_j^{i'} + 2\langle kl|\hat{F}_{12}r_{12}^{-1}i'j\rangle S_i^j S_j^{i'} - \langle kl|\hat{F}_{12}r_{12}^{-1}ij\rangle \\
 & + F_{ij}^{lk}K_{ij}^{i'j'} + F_{aj}^{lk}K_{ij}^{aj'} + F_{ib}^{lk}K_{ij}^{ib'} + F_{sj}^{lk}K_{ij}^{sj'} \\
 & + F_{ij}^{lk}K_{ij}^{i'y} + F_{\text{xt}}^{kl}K_{ij}^{\text{ax}}S_a^n + F_{\text{my}}^{kl}K_{ij}^{\text{yb}}S_b^m + F_{\text{rs}}^{kl}K_{ij}^{\text{cs}}S_c^r \\
 & + F_{\text{xt}}^{kl}K_{ij}^{\text{xn}}S_i^jS_j^{i'} + F_{\text{my}}^{kl}K_{ij}^{\text{my}}S_i^jS_j^{i'} + F_{\text{rs}}^{kl}K_{ij}^{\text{rs}}S_i^jS_j^{i'} \\
 & - 2F_{\text{xt}}^{kl}K_{ij}^{\text{xn}}S_i^jS_j^{i'} - 2F_{\text{my}}^{kl}K_{ij}^{\text{my}}S_i^jS_j^{i'} - 2F_{\text{rs}}^{kl}K_{ij}^{\text{rs}}S_i^jS_j^{i'} \\
 & - 2F_{\text{xt}}^{kl}K_{ij}^{\text{xn}}S_i^jS_j^{i'} - 2F_{\text{my}}^{kl}K_{ij}^{\text{my}}S_i^jS_j^{i'} - 2F_{\text{rs}}^{kl}K_{ij}^{\text{rs}}S_i^jS_j^{i'}]
 \end{aligned} \quad (53)$$

Thus, the F12-improved second-order exchange dispersion energy in a DCBS treatment is equal to the conventional  $E_{\text{exch-disp}}^{(20)}$  eq 39, plus the F12 correction given by eq 53.

#### IV. COMPUTATIONAL DETAILS

The new expressions for  $E_{\text{disp}}^{(20)}$ -F12 and  $E_{\text{exch-disp}}^{(20)}$ -F12 developed in the preceding sections were implemented within the Psi4NUMPY framework,<sup>51</sup> utilizing the integrals and monomer Hartree-Fock vectors computed by the Psi4 code<sup>52</sup> and the NUMPY library to manipulate the resulting tensors Python-side. The calculations require the same four types of F12 integrals (over some combinations of AO and RI basis indices) as a conventional MP2-F12 calculation, namely,  $F_{vw}^{\text{tu}} \equiv \langle \text{tu}|\hat{F}_{12}|vw\rangle$ ,  $\langle \text{tu}|\hat{F}_{12}r_{12}^{-1}|vw\rangle$ ,  $\langle \text{tu}|\hat{F}_{12}r_{12}^{-1}|vw\rangle$ , and the double commutator integrals  $\langle \text{tu}|\hat{F}_{12}[\hat{t}_{12}, \hat{F}_{12}]]|vw\rangle$ , with  $\hat{t}_{12} = \hat{t}_1 + \hat{t}_2$  being the kinetic energy

operator. These integrals were computed using the LIBINT library<sup>53</sup> performing the Obara-Saika angular momentum recursion<sup>54</sup> on top of auxiliary s-type integrals already implemented in Psi4 following the formulas given in ref 55. The intermediates involving the Fock operators,  $B_{kl,k'l'}$  and  $C_{ab}^{kl}$ , were computed in exactly the same fashion as within the 3C approximation to conventional MP2-F12,<sup>11</sup> taking care to pick the Fock operator of the appropriate monomer (cf. eqs 25 and 28) for the respective orbital transformations. Compared to the simplest and most transparent implementation utilized, e.g., in the SAPT0 code included in the official Psi4NUMPY release,<sup>51</sup> two modifications were made to reduce the memory and CPU time requirements, which are both dominated by the integral evaluation and transformation. First, the integrals of each type were not computed all at once, but in  $N^3$  chunks where one shell index was frozen and the other three indices ran over all shells in the (orbital or auxiliary) basis set. This required a minor modification of the Psi4 code so that the required subset of integrals could be exported to the Python layer. Second, the partially transformed integrals were reused whenever possible so that the number of the (most expensive) transformations of the first index was minimized. These enhancements to the Psi4NUMPY implementation were sufficient to compute all quantities obtained in the present work, including all  $E_{\text{disp}}^{(20)}$ -F12 and  $E_{\text{exch-disp}}^{(20)}$ -F12 values in an augmented triple- $\zeta$  basis for all complexes in the A24 benchmark database.<sup>56</sup> However, a further improvement to the computational efficiency of the new algorithms requires a robust density fitting of all four index quantities present.<sup>57,58</sup> While density fitting was not pursued in the present benchmark study to avoid an additional source of residual error in the calculations, the work on production-level density-fitted  $E_{\text{disp}}^{(20)}$ -F12 and  $E_{\text{exch-disp}}^{(20)}$ -F12 implementations is in progress in the Auburn research group.

The SAPT-F12(MP2) corrections to the second-order dispersion and exchange dispersion energies proposed in ref 46 were computed using a development version of the TURBOMOLE program. To compute the -F12(MP2) correction for each dimer, the Hartree-Fock vectors of the corresponding monomers are combined to the dimer orbitals, sorted by energy. No density fitting was used in this step. The resulting dimer Hartree-Fock vectors are orthogonalized, and an MP2-F12 calculation is carried out. The final -F12(MP2) correction is obtained by summing the MP2-F12 pair energies of occupied-occupied pairs where each occupied index is located on a different monomer fragment, while the pairs with two occupied indices on the same monomer fragment are discarded. Although, in principle, all approximations used for MP2-F12<sup>11</sup> can also be applied to the  $E_{\text{disp}}^{(20)}$ -F12(MP2) scheme, the 2<sup>\*A</sup> approximation was used in conjunction with the T+V commutator approximation<sup>59</sup> to evaluate the  $E_{\text{disp}}^{(20)}$ -F12(MP2) correction.

The orbital basis sets employed in the present work were the augmented correlation consistent aug-cc-pVXZ  $\equiv$  aXZ sets of Dunning and co-workers,<sup>60,61</sup> with X ranging from D to 6. We have chosen not to use the cc-pVXZ-F12 basis sets optimized specifically for the F12 calculations<sup>62</sup> as these sets were proven to be inferior to the standard aXZ ones in intermolecular interaction energy calculations at the supermolecular counterpoise-corrected CCSD(T)-F12 level,<sup>23</sup> a conclusion that is unchanged<sup>25</sup> by the recently proposed aug-cc-pVXZ-F12 extension.<sup>63</sup> The resolution-of-identity (CABS) bases used to expand the CA functions were the aXZ-RI sets, also termed aXZ/MP2FIT,<sup>64,65</sup> with the cardinal number X equal or larger to the corresponding X for the orbital set. Note that the use of

**Table 1.**  $E_{\text{disp}}^{(20)}$ -F12 Values (in kcal/mol) for the Helium Dimer for Different Combinations of the Orbital Basis aXZ and CABS Basis aXZ-RI<sup>a</sup>

basis	$E_{\text{disp}}^{(20)}$	aDZ-RI	aTZ-RI	aQZ-RI	aSZ-RI	a6Z-RI
Fixed-Amplitude/Optimized Diagonal/Fully Optimized Ansatz						
aDZ	-0.0243	-0.0597	-0.0455	-0.0422	-0.0403	-0.0360
aTZ	-0.0297		-0.0363	-0.0357	-0.0352	-0.0345
aQZ	-0.0314			-0.0341	-0.0341	-0.0349
aSZ	-0.0325				-0.0340	-0.0339
a6Z	-0.0332					-0.0340
EBC Ansatz						
aDZ	-0.0243	-0.0598	-0.0456	-0.0423	-0.0404	-0.0360
aTZ	-0.0297		-0.0360	-0.0354	-0.0348	-0.0342
aQZ	-0.0314			-0.0338	-0.0338	-0.0346
aSZ	-0.0325				-0.0337	-0.0336
a6Z	-0.0332					-0.0339
F12(MP2) Ansatz						
aDZ	-0.0243	-0.0380	-0.0345	-0.0329	-0.0316	-0.0303
aTZ	-0.0297		-0.0331	-0.0327	-0.0325	-0.0322
aQZ	-0.0314			-0.0326	-0.0325	-0.0325
aSZ	-0.0325				-0.0334	-0.0334
a6Z	-0.0332					-0.0337
GTG	$-0.0341 \pm 1.6 \times 10^{-7}$					

<sup>a</sup>The fully optimized, optimized diagonal, and fixed-amplitude Ansätze are equivalent for this specific system. EBC stands for the extended Brillouin condition Ansatz, eq 35, and F12(MP2) denotes the approach of ref 46. The benchmark  $E_{\text{disp}}^{(20)}$ /CBS value given at the bottom of the table was computed in ref 45 using Gaussian-type geminals (GTGs). Note that the variational character of the  $E_{\text{disp}}^{(20)}$ -F12 expression, eq 29, holds only in the limit of the complete RI basis and breaks down for finite auxiliary bases employed in this table.

extended auxiliary basis sets, with  $X$  larger than for the orbital basis, has been extensively tested before in the explicitly correlated MP2<sup>66</sup> context, and it has also been recommended<sup>67</sup> for density-fitted SAPT(DFT) calculations. The exponential correlation factor  $\exp(-\gamma r_{12})$  was used throughout the present work, with the length-scale parameter  $\gamma$  equal to  $1.0a_0^{-1}$ . For the purpose of integral calculation, this correlation factor was fitted to a sum of six Gaussian terms.<sup>7</sup> All  $E_{\text{disp}}^{(20)}$ -F12(MP2) results were calculated using the resolution-of-identity approximation for Coulomb and exchange integrals, which were fitted using the same aXZ/MP2FIT basis as the one chosen as the CABS. The SAPT-F12 corrections were computed with all electrons correlated. For technical reasons, the SAPT-F12(MP2) results were obtained by adding a frozen-core F12 correction on top of an all-electron conventional SAPT result and with the length-scale parameter  $\gamma$  equal to  $1.4a_0^{-1}$ . Both values should converge to the all-electron CBS limit, and the partial freezing of the core in SAPT-F12(MP2) is of little practical consequence (note that for the systems considered in this work, unlike, e.g., alkali or alkaline earth metal dimers, the contribution of core correlation to the interaction energy is very minor).

Extensive tests of the convergence of different  $E_{\text{disp}}^{(20)}$ -F12 and  $E_{\text{exch-disp}}^{(20)}$ -F12 variants with the orbital and auxiliary bases were initially performed on five small complexes: the homodimers of helium, neon, argon, water, and methane. The atom-atom distances in He-He, Ne-Ne, and Ar-Ar were fixed at their near-equilibrium values of 5.6 bohr, 3.1 Å, and 3.75 Å, respectively, and the geometries for the water and methane dimers were taken from the A24 benchmark database.<sup>56</sup> Subsequently, the entire A24 set was employed to investigate the performance of  $E_{\text{disp}}^{(20)}$ -F12 and  $E_{\text{exch-disp}}^{(20)}$ -F12 corrections in the aDZ and aTZ orbital bases. The F12 data were compared with conventional CBS limit estimates of  $E_{\text{disp}}^{(20)}$  and  $E_{\text{exch-disp}}^{(20)}$  computed using the a6Z+(a6Z) basis set, where the aXZ+(aXZ)

notation signifies that the aXZ atom-centered orbital basis has been augmented by the set of midbond functions from the same aXZ basis, with the exponents and contraction coefficients appropriate for hydrogen. It should be stressed that the midbond basis functions and the RI basis functions are used in fundamentally different contexts. The midbond set is added to the atom-centered part of the orbital basis. In the limit of a complete midbond set,  $E_{\text{disp}}^{(20)}$  (or any other electronic structure theory) reaches its CBS limit: a complete set of functions centered on any one point in space is a formally sufficient, although woefully inefficient, way to saturate the one-electron basis set. For a specific complex, the  $E_{\text{disp}}^{(20)}$  calculation (without density fitting) scales like  $N^4$  with the number of midbond functions. In contrast, the RI basis is needed to approximate the many-electron integrals of the F12 theory. In the limit of a complete RI set,  $E_{\text{disp}}^{(20)}$ -F12 attains its value characteristic to the orbital basis set employed, with all many-electron integrals computed exactly. For a specific complex, the  $E_{\text{disp}}^{(20)}$ -F12 calculation scales quadratically with the number of RI basis functions.

The conventional SAPT0 calculations utilized the PSl4 code<sup>52,68</sup> and employed density fitting with the a6Z-RI auxiliary basis used for both HF and SAPT0 parts of the calculation. A different benchmark was adopted for the helium dimer, for which very accurate estimates of the  $E_{\text{disp}}^{(20)}$  and  $E_{\text{exch-disp}}^{(20)}$  CBS limits are available from Gaussian-type geminal (GTG) calculations with nonlinearly optimized amplitudes.<sup>45</sup> The (tiny) estimated uncertainty of these CBS limits was also taken from ref 45: as only the uncertainty of the complete  $E_{\text{disp}}^{(20)}$  +  $E_{\text{disp}}^{(21)}$  +  $E_{\text{exch-disp}}^{(20)}$  term was given in this reference, that value was used for both corrections investigated here. For other systems, the uncertainty of the a6Z+(a6Z) CBS values was conservatively estimated as the absolute value of the difference between the results computed in the a6Z+(a6Z) and aSZ+(aSZ) basis sets.



**Table 2.**  $E_{\text{disp}}^{(20)}$ -F12 Values (in kcal/mol) for the Neon Dimer for Different Combinations of the Orbital Basis aXZ and CABS Basis aXZ-RI<sup>a</sup>

basis	$E_{\text{disp}}^{(20)}$	aDZ-RI	aTZ-RI	aQZ-RI	aSZ-RI
Fixed-Amplitude Ansatz					
aDZ	-0.0816	-0.1883	-0.1496	-0.1385	-0.1223
aTZ	-0.1087		-0.1536	-0.1434	-0.1338
aQZ	-0.1203			-0.1405	-0.1364
aSZ	-0.1270				-0.1341
Optimized Diagonal Ansatz					
aDZ	-0.0816	-0.1948	-0.1549	-0.1438	-0.1267
aTZ	-0.1087		-0.1577	-0.1471	-0.1366
aQZ	-0.1203			-0.1424	-0.1380
aSZ	-0.1270				-0.1350
EBC Ansatz					
aDZ	-0.0816	-0.1910	-0.1514	-0.1370	-0.1221
aTZ	-0.1087		-0.1551	-0.1447	-0.1333
aQZ	-0.1203			-0.1413	-0.1364
aSZ	-0.1270				-0.1343
Fully Optimized Amplitudes					
aDZ	-0.0816	-0.1964	-0.1556	-0.1440	-0.1269
aTZ	-0.1087		-0.1584	-0.1477	-0.1367
aQZ	-0.1203			-0.1430	-0.1384
aSZ	-0.1270				-0.1365
F12(MP2) Ansatz					
aDZ	-0.0816	-0.1293	-0.1196	-0.1145	-0.1120
aTZ	-0.1087		-0.1403	-0.1348	-0.1325
aQZ	-0.1203			-0.1469	-0.1441
aSZ	-0.1270				
a6Z+(a6Z)	-0.1344 ± 0.0002				

<sup>a</sup>EBC stands for the extended Brillouin condition Ansatz, eq 35, and F12(MP2) denotes the approach of ref 46. The benchmark  $E_{\text{disp}}^{(20)}$ /CBS value given at the bottom of the table was computed using the a6Z atom-centered basis augmented by the hydrogenic a6Z midbond set.

## V. RESULTS AND DISCUSSION

A detailed analysis of the  $E_{\text{disp}}^{(20)}$ -F12 and  $E_{\text{exch-disp}}^{(20)}$ -F12 corrections was performed on a set of five weakly interacting dimers: He-He, Ne-Ne, Ar-Ar, H<sub>2</sub>O-H<sub>2</sub>O, and CH<sub>4</sub>-CH<sub>4</sub> at their van der Waals minimum geometries. Explicitly correlated calculations employed basis sets up to a5Z along with auxiliary sets up to a5Z-RI. The exceptions are the helium dimer, for which the use of a6Z and a6Z-RI was possible, and the methane dimer for which calculations were limited to aQZ. We studied the performance of the F12 approach with fully optimized amplitudes (FULL), as well as three approximate Ansätze: optimized diagonal (ODA), EBC, and fixed amplitude (FIX). These four variants will be collectively referred to as SAPT-F12, as opposed to the SAPT-F12(MP2) approach of ref 46 whose performance was also investigated. The results were compared with benchmark CBS values determined as detailed in Section IV.

Tables 1–10 present the  $E_{\text{disp}}^{(20)}$ -F12 and  $E_{\text{exch-disp}}^{(20)}$ -F12 values for the abovementioned complexes with different ways of calculating the explicitly correlated amplitudes. Tables SI–SV in the Supporting Information display the corresponding  $E_{\text{disp}}^{(20)}$ -F12 +  $E_{\text{exch-disp}}^{(20)}$ -F12 sums. As the helium dimer has only one occupied orbital on each monomer and thus only one  $T_{ki}^j$  amplitude, the FULL, ODA, and FIX Ansätze are identical for this system; only the EBC one is slightly different as it neglects the coupling between the conventional and F12 amplitudes. Interestingly,  $E_{\text{disp}}^{(20)}$ -F12 energies obtained for all rare gas dimers break the variational principle in the aXZ/aXZ-RI basis set combinations, converging to the benchmark result from below.

Further investigation shows that this is caused by a very slow convergence of the energy with the CABS. Although  $E_{\text{exch-disp}}^{(20)}$ -F12 is not a variational quantity, so an improvement of results is not guaranteed when enlarging the basis set, the same slow convergence pattern is noticeable. Tables 1–3 indicate that the aDZ orbital result is not converged with respect to the RI basis even at the largest available a5Z-RI level (a6Z-RI for He-He), with all  $E_{\text{disp}}^{(20)}$ -F12(FULL)/aDZ values still below the variational limit for the helium dimer. Therefore, we tested an even larger CABS, a (17s15p13d11f9g7h5i) set obtained from the a6Z-RI one by inserting one additional exponent (a geometric mean) between each pair of successive exponents and then adding one exponent larger than the largest one and one exponent smaller than the smallest one so that the three largest and three smallest exponents form two geometric sequences. Using this RI basis, the helium dimer  $E_{\text{disp}}^{(20)}$ -F12(FULL)/aDZ energy amounted to -0.0332 kcal/mol, finally above the variational limit but quite close to it. The origin of slow convergence of noble gas dimer interaction energies can possibly be traced down to the auxiliary basis sets being insufficiently optimized for the purposes of dispersion energy calculation. In contrast, the dispersion and exchange dispersion energies for the water and methane dimers converge rapidly with the RI basis. Moreover, we observed occasional convergence issues in the full optimization of dispersion amplitudes since the systems of equations that need to be solved<sup>47</sup> are quite ill-conditioned. This motivated us to replace  $E_{\text{disp}}^{(20)}$ -F12(FULL) by  $E_{\text{disp}}^{(20)}$ -F12(ODA) for each pair of orbitals ( $i, j$ ) whenever the fully optimized approach encountered numerical issues as evidenced by the resulting pair

**Table 3.**  $E_{\text{disp}}^{(20)}$ -F12 Values (in kcal/mol) for the Argon Dimer for Different Combinations of the Orbital Basis aXZ and CABS Basis aXZ-RI<sup>a</sup>

basis	$E_{\text{disp}}^{(20)}$	aDZ-RI	aTZ-RI	aQZ-RI	aSZ-RI
Fixed-Amplitude Ansatz					
aDZ	-0.4613	-0.7317	-0.6383	-0.6167	-0.6013
aTZ	-0.5758		-0.6615	-0.6523	-0.6440
aQZ	-0.6243			-0.6573	-0.6571
aSZ	-0.6505				-0.6695
Optimized Diagonal Ansatz					
aDZ	-0.4613	-0.7634	-0.6675	-0.6456	-0.6295
aTZ	-0.5758		-0.6789	-0.6695	-0.6609
aQZ	-0.6243			-0.6681	-0.6676
aSZ	-0.6505				-0.6737
EBC Ansatz					
aDZ	-0.4613	-0.7371	-0.6668	-0.6404	-0.6224
aTZ	-0.5758		-0.6755	-0.6607	-0.6432
aQZ	-0.6243			-0.6596	-0.6632
aSZ	-0.6505				-0.6722
Fully Optimized Amplitudes					
aDZ	-0.4613	-0.7738	-0.6830	-0.6555	-0.6374
aTZ	-0.5758		-0.8042	-0.6777	-0.6644
aQZ	-0.6243			-0.6723	-0.6711
aSZ	-0.6505				-0.6748
F12(MP2) Ansatz					
aDZ	-0.4613	-0.6017	-0.6125	-0.5937	-0.6242
aTZ	-0.5758		-0.6483	-0.6459	-0.6506
aQZ	-0.6243			-0.6603	-0.6590
aSZ	-0.6505				-0.6772
a6Z+(a6Z)	-0.6762 ± 0.0020				

<sup>a</sup>EBC stands for the extended Brillouin condition Ansatz, eq 35, and F12(MP2) denotes the approach of ref 46. The benchmark  $E_{\text{disp}}^{(20)}$ /CBS value given at the bottom of the table was computed using the a6Z atom-centered basis augmented by the hydrogenic a6Z midbond set.

correlation energy above the ODA value (which is against the variational principle). While all results in the FULL Ansatz presented in this work include this simple correction, there is no equally simple way to detect convergence issues that result in the  $E_{\text{disp}}^{(20)}$ -F12(FULL) pair correlation energy being too low instead of too high. Thus, a small subset of the FULL results presented here (and possibly also some EBC ones where no sanity check is performed) likely contain artifacts related to the ill-conditioned systems of equations, which on very rare occasions is evident in the final results. The most drastic example of these convergence issues is the  $E_{\text{disp}}^{(20)}$ -F12(FULL)/aTZ/aTZ-RI result for the argon dimer in Table 3. The ODA and FIX Ansätze do not require solving systems of equations and are completely free of this instability problem.

The results in Tables 1–10 clearly show the enhanced convergence of the new SAPT-F12 methods over conventional  $E_{\text{disp}}^{(20)}$  and  $E_{\text{exch-disp}}^{(20)}$ . The  $E_{\text{disp}}^{(20)}$ -F12 energies computed in the aDZ orbital basis along with the largest auxiliary basis set for He–He, Ne–Ne, and Ar–Ar, as well as in aDZ/aTZ-RI for H<sub>2</sub>O–H<sub>2</sub>O and CH<sub>4</sub>–CH<sub>4</sub>, are almost as good or superior to conventional  $E_{\text{disp}}^{(20)}$  computed in the aQZ basis set for all investigated SAPT-F12 flavors. The same effect is observed for  $E_{\text{exch-disp}}^{(20)}$ -F12; however, the improvement of the F12 approach is somewhat diminished. Thus, the new F12 methods are equivalent, accuracy-wise, to adding two (for  $E_{\text{disp}}^{(20)}$ -F12) or more than one (for  $E_{\text{exch-disp}}^{(20)}$ -F12) additional shell of basis functions to conventional SAPT calculations. It is worth mentioning that for all rare gas dimers, the explicitly correlated dispersion energies calculated in the aDZ/aDZ-RI basis set combination

overestimate the CBS results due to an incomplete error cancellation of the effects of orbital and auxiliary basis set truncations. This effect explains the occasional superb performance of  $E_{\text{exch-disp}}^{(20)}$ -F12 in these small basis sets; however, this combination of orbital and auxiliary bases is not reliable, providing the right answer for the wrong reason.

Increasing the basis set size up to aTZ for  $E_{\text{disp}}^{(20)}$ -F12 and up to aQZ for  $E_{\text{exch-disp}}^{(20)}$ -F12, we obtain impressive results very close to the benchmark, or possibly even better depending on the SAPT-F12 variant. Therefore, the investigation of the F12 dispersion energy with different explicitly correlated amplitudes leads to the deduction of the most accurate and the most computationally efficient approach. As expected, the  $E_{\text{disp}}^{(20)}$ -F12 energies with the full optimization of amplitudes exhibit the best performance with the relative errors for the aDZ basis in the range of -5.7 to 5.6% for the five systems. The combination of this F12 variant with the aTZ orbital basis set (still in the largest RI set available) leads to a further substantial improvement, with the largest errors of 1.7 and -1.7% attained for the neon and argon dimers, respectively. The exchange dispersion effects for the helium and neon dimers are so tiny that relative errors would be misleading, but the convergence is still smooth: e.g., the absolute  $E_{\text{exch-disp}}^{(20)}$ -F12(FULL) errors for the neon dimer amount to 0.0022, 0.0003, and 0.0005 kcal/mol in the aDZ, aTZ, and aQZ orbital bases, respectively, with the largest auxiliary basis used each time. Thus, the results are essentially converged (up to the RI basis incompleteness effects) at the aTZ level, where the conventional  $E_{\text{exch-disp}}^{(20)}$  value is still in error by 0.0020 kcal/mol.

**Table 4.**  $E_{\text{disp}}^{(20)}$ -F12 Values (in kcal/mol) for the Water Dimer for Different Combinations of the Orbital Basis aXZ and CABS Basis aXZ-RI<sup>a</sup>

basis	$E_{\text{disp}}^{(20)}$	aDZ-RI	aTZ-RI	aQZ-RI	aSZ-RI
Fixed-Amplitude Ansatz					
aDZ	-2.1519	-2.5120	-2.5026	-2.5017	-2.5022
aTZ	-2.4625		-2.5671	-2.5665	-2.5666
aQZ	-2.5514			-2.5956	-2.5956
aSZ	-2.5806				-2.6042
Optimized Diagonal Ansatz					
aDZ	-2.1519	-2.5684	-2.5584	-2.5572	-2.5579
aTZ	-2.4625		-2.5953	-2.5947	-2.5949
aQZ	-2.5514			-2.6084	-2.6084
aSZ	-2.5806				-2.6117
EBC Ansatz					
aDZ	-2.1519	-2.5576	-2.5461	-2.5447	-2.5457
aTZ	-2.4625		-2.5939	-2.5931	-2.5934
aQZ	-2.5514			-2.6082	-2.6082
aSZ	-2.5806				-2.6119
Fully Optimized Amplitudes					
aDZ	-2.1519	-2.5829	-2.5716	-2.5703	-2.5713
aTZ	-2.4625		-2.6020	-2.6014	-2.6016
aQZ	-2.5514			-2.6110	-2.6110
aSZ	-2.5806				-2.6130
F12(MP2) Ansatz					
aDZ	-2.1519	-2.6070	-2.5989	-2.5977	-2.5979
aTZ	-2.4625		-2.6087	-2.6078	-2.6079
aQZ	-2.5514			-2.6101	-2.6100
aSZ	-2.5806				-2.6097
a6Z+(a6Z)	-2.6047 ± 0.0070				

<sup>a</sup>EBC stands for the extended Brillouin condition Ansatz, eq 35, and F12(MP2) denotes the approach of ref 46. The benchmark  $E_{\text{disp}}^{(20)}$ /CBS value given at the bottom of the table was computed using the a6Z atom-centered basis augmented by the hydrogenic a6Z midbond set.

**Table 5.**  $E_{\text{disp}}^{(20)}$ -F12 Values (in kcal/mol) for the Methane Dimer for Different Combinations of the Orbital Basis aXZ and CABS Basis aXZ-RI<sup>a</sup>

basis	$E_{\text{disp}}^{(20)}$	aDZ-RI	aTZ-RI	aQZ-RI	aSZ-RI
Fixed-Amplitude Ansatz					
aDZ	-1.0096	-1.1336	-1.1280	-1.1270	-1.1269
aTZ	-1.1101		-1.1463	-1.1461	-1.1461
aQZ	-1.1351			-1.1507	
Optimized Diagonal Ansatz					
aDZ	-1.0096	-1.1398	-1.1341	-1.1331	-1.1330
aTZ	-1.1101		-1.1491	-1.1489	-1.1489
aQZ	-1.1351			-1.1519	
EBC Ansatz					
aDZ	-1.0096	-1.1367	-1.1313	-1.1302	-1.1302
aTZ	-1.1101		-1.1470	-1.1468	-1.1468
aQZ	-1.1351			-1.1509	
Fully Optimized Amplitudes					
aDZ	-1.0096	-1.1409	-1.1351	-1.1340	-1.1340
aTZ	-1.1101		-1.1500	-1.1499	-1.1499
aQZ	-1.1351			-1.1524	
F12(MP2) Ansatz					
aDZ	-1.0096	-1.1180	-1.1159	-1.1152	-1.1152
aTZ	-1.1101		-1.1436	-1.1435	-1.1435
aQZ	-1.1351			-1.1487	-1.1486
a6Z+(a6Z)	-1.1510 ± 0.0017				

<sup>a</sup>EBC stands for the extended Brillouin condition Ansatz, eq 35, and F12(MP2) denotes the approach of ref 46. The benchmark  $E_{\text{disp}}^{(20)}$ /CBS value given at the bottom of the table was computed using the a6Z atom-centered basis augmented by the hydrogenic a6Z midbond set.

**Table 6.**  $E_{\text{exch-disp}}^{(20)}$ -F12 Values (in kcal/mol) for the Helium Dimer for Different Combinations of the Orbital Basis aXZ and CABS Basis aXZ-RI<sup>a</sup>

basis	$E_{\text{exch-disp}}^{(20)}$	aDZ-RI	aTZ-RI	aQZ-RI	aSZ-RI	a6Z-RI
Fixed-Amplitude/Optimized Diagonal/Fully Optimized Ansatz						
aDZ	0.0004	0.0011	0.0010	0.0009	0.0009	0.0008
aTZ	0.0007		0.0009	0.0009	0.0009	0.0009
aQZ	0.0008			0.0009	0.0009	0.0010
aSZ	0.0009				0.0010	0.0010
a6Z	0.0009					0.0010
EBC Ansatz						
aDZ	0.0004	0.0011	0.0010	0.0009	0.0009	0.0008
aTZ	0.0007		0.0009	0.0009	0.0009	0.0009
aQZ	0.0008			0.0009	0.0009	0.0010
aSZ	0.0009				0.0010	0.0010
a6Z	0.0009					0.0010
GTG	$0.0011 \pm 1.6 \times 10^{-7}$					

<sup>a</sup>The fully optimized, optimized diagonal, and fixed-amplitude Ansätze are equivalent for this specific system. EBC stands for the extended Brillouin condition Ansatz, eq 35. The benchmark  $E_{\text{exch-disp}}^{(20)}$ /CBS value given at the bottom of the table was computed in ref 45 using Gaussian-type geminals (GTGs).

**Table 7.**  $E_{\text{exch-disp}}^{(20)}$ -F12 Values (in kcal/mol) for the Neon Dimer for Different Combinations of the Orbital Basis aXZ and CABS Basis aXZ-RI<sup>a</sup>

basis	$E_{\text{exch-disp}}^{(20)}$	aDZ-RI	aTZ-RI	aQZ-RI	aSZ-RI
Fixed-Amplitude Ansatz					
aDZ	0.0024	0.0039	0.0038	0.0038	0.0035
aTZ	0.0037		0.0048	0.0048	0.0046
aQZ	0.0044			0.0052	0.0051
aSZ	0.0048				0.0052
Optimized Diagonal Ansatz					
aDZ	0.0024	0.0040	0.0039	0.0041	0.0037
aTZ	0.0037		0.0050	0.0050	0.0047
aQZ	0.0044			0.0053	0.0052
aSZ	0.0048				0.0053
EBC Ansatz					
aDZ	0.0024	0.0038	0.0039	0.0040	0.0037
aTZ	0.0037		0.0049	0.0050	0.0047
aQZ	0.0044			0.0053	0.0052
aSZ	0.0048				0.0053
Fully Optimized Amplitudes					
aDZ	0.0024	0.0037	0.0039	0.0036	0.0035
aTZ	0.0037		0.0055	0.0051	0.0054
aQZ	0.0044			0.0053	0.0052
aSZ	0.0048				0.0052
a6Z+(a6Z)	$0.0057 \pm 0.0001$				

<sup>a</sup>EBC stands for the extended Brillouin condition Ansatz, eq 35. The benchmark  $E_{\text{exch-disp}}^{(20)}$ /CBS value given at the bottom of the table was computed using the a6Z atom-centered basis augmented by the hydrogenic a6Z midbond set.

The  $E_{\text{disp}}^{(20)}$ -F12 and  $E_{\text{exch-disp}}^{(20)}$ -F12 corrections calculated with the optimized diagonal Ansatz perform nearly as phenomenally as the variant with fully optimized amplitudes while being much cheaper computationally. When the best converged auxiliary basis sets are used, the largest difference between the two levels of F12 treatment amounts to 1.2% (aSZ/aSZ-RI) and -12.2% (aTZ/aSZ-RI) for  $E_{\text{disp}}^{(20)}$ -F12 and  $E_{\text{exch-disp}}^{(20)}$ -F12, respectively, both for the neon dimer (note that the  $E_{\text{exch-disp}}^{(20)}$  value is tiny for this system so that even the -12.2% error is not an issue).

Considering  $E_{\text{disp}}^{(20)}$ -F12 with the EBC Ansatz, it produces slightly worse results than the optimized diagonal Ansatz. However, this trend is flipped for  $E_{\text{exch-disp}}^{(20)}$ -F12. The sum  $E_{\text{disp}}^{(20)}$ -

F12 +  $E_{\text{exch-disp}}^{(20)}$ -F12 with the EBC Ansatz is not as accurate as its cheaper optimized diagonal Ansatz counterpart. Therefore, the EBC variant was excluded from further tests because of its cost and lower accuracy. While applying the least expensive SAPT-F12 approximation, the fixed-amplitude Ansatz, we observe it to be the worst performer: as long as a sufficiently converged RI basis is used, the highest relative  $E_{\text{disp}}^{(20)}$ -F12 error amounts to -11.1% for the argon dimer in aDZ. The  $E_{\text{disp}}^{(20)}$ -F12 +  $E_{\text{exch-disp}}^{(20)}$ -F12 sum results in the largest error of -10.8% for the argon dimer in aDZ. Nevertheless, even the simplest fixed-amplitude treatment considerably improves upon conventional  $E_{\text{disp}}^{(20)}$  and  $E_{\text{exch-disp}}^{(20)}$ .

**Table 8.**  $E_{\text{exch-disp}}^{(20)}$ -F12 Values (in kcal/mol) for the Argon Dimer for Different Combinations of the Orbital Basis aXZ and CABS Basis aXZ-RI<sup>a</sup>

basis	$E_{\text{exch-disp}}^{(20)}$	aDZ-RI	aTZ-RI	aQZ-RI	aSZ-RI
Fixed-Amplitude Ansatz					
aDZ	0.0279	0.0441	0.0413	0.0406	0.0400
aTZ	0.0345		0.0423	0.0422	0.0419
aQZ	0.0392			0.0431	0.0433
aSZ	0.0421				0.0448
Optimized Diagonal Ansatz					
aDZ	0.0279	0.0459	0.0431	0.0425	0.0418
aTZ	0.0345		0.0439	0.0438	0.0436
aQZ	0.0392			0.0445	0.0446
aSZ	0.0421				0.0455
EBC Ansatz					
aDZ	0.0279	0.0466	0.0449	0.0418	0.0424
aTZ	0.0345		0.0433	0.0466	0.0469
aQZ	0.0392			0.0447	0.0449
aSZ	0.0421				0.0460
Fully Optimized Amplitudes					
aDZ	0.0279	0.0463	0.0443	0.0431	0.0452
aTZ	0.0345		0.0271	0.0443	0.0443
aQZ	0.0392			0.0446	0.0433
aSZ	0.0421				0.0452
a6Z+(a6Z)	0.0470 ± 0.0005				

<sup>a</sup>EBC stands for the extended Brillouin condition Ansatz, eq 35. The benchmark  $E_{\text{exch-disp}}^{(20)}$ /CBS value given at the bottom of the table was computed using the a6Z atom-centered basis augmented by the hydrogenic a6Z midbond set.

**Table 9.**  $E_{\text{exch-disp}}^{(20)}$ -F12 Values (in kcal/mol) for the Water Dimer for Different Combinations of the Orbital Basis aXZ and CABS Basis aXZ-RI<sup>a</sup>

basis	$E_{\text{exch-disp}}^{(20)}$	aDZ-RI	aTZ-RI	aQZ-RI	aSZ-RI
Fixed-Amplitude Ansatz					
aDZ	0.3852	0.4430	0.4421	0.4420	0.4421
aTZ	0.4420		0.4668	0.4668	0.4668
aQZ	0.4665			0.4798	0.4798
aSZ	0.4763				0.4846
Optimized Diagonal Ansatz					
aDZ	0.3852	0.4519	0.4507	0.4506	0.4507
aTZ	0.4420		0.4735	0.4734	0.4735
aQZ	0.4665			0.4835	0.4835
aSZ	0.4763				0.4871
EBC Ansatz					
aDZ	0.3852	0.4569	0.4551	0.4549	0.4552
aTZ	0.4420		0.4768	0.4767	0.4767
aQZ	0.4665			0.4856	0.4856
aSZ	0.4763				0.4883
Fully Optimized Amplitudes					
aDZ	0.3852	0.4577	0.4560	0.4558	0.4560
aTZ	0.4420		0.4772	0.4772	0.4772
aQZ	0.4665			0.4854	0.4854
aSZ	0.4763				0.4881
a6Z+(a6Z)	0.4857 ± 0.0029				

<sup>a</sup>EBC stands for the extended Brillouin condition Ansatz, eq 35. The benchmark  $E_{\text{exch-disp}}^{(20)}$ /CBS value given at the bottom of the table was computed using the a6Z atom-centered basis augmented by the hydrogenic a6Z midbond set.

The  $E_{\text{disp}}^{(20)}$ -F12(MP2) results, obtained from a purely perturbative correction, perform worst when the -F12 correction is large. Especially for the neon dimer, the corrections needed to achieve a converged result are too large to be recovered by the -F12(MP2) Ansatz. The -F12(MP2) approach even fails to

obtain a physically meaningful correction for the largest aSZ/aSZ-RI orbital and auxiliary basis set combination. Overall,  $E_{\text{disp}}^{(20)}$ -F12(MP2) still improves upon the conventional result for the neon dimer, but to a lesser extent than the other Ansätze, especially for larger basis sets. For the other four dimers

**Table 10.**  $E_{\text{exch-disp}}^{(20)}$ -F12 Values (in kcal/mol) for the Methane Dimer for Different Combinations of the Orbital Basis aXZ and CABS Basis aXZ-RI<sup>a</sup>

basis	$E_{\text{exch-disp}}^{(20)}$	aDZ-RI	aTZ-RI	aQZ-RI	aSZ-RI
Fixed-Amplitude Ansatz					
aDZ	0.0695	0.0826	0.0823	0.0822	0.0822
aTZ	0.0790		0.0846	0.0846	0.0846
aQZ	0.0833			0.0865	
Optimized Diagonal Ansatz					
aDZ	0.0695	0.0832	0.0829	0.0829	0.0829
aTZ	0.0790		0.0852	0.0852	0.0852
aQZ	0.0833			0.0868	
EBC Ansatz					
aDZ	0.0695	0.0835	0.0835	0.0835	0.0835
aTZ	0.0790		0.0858	0.0858	0.0859
aQZ	0.0833			0.0873	
Fully Optimized Amplitudes					
aDZ	0.0695	0.0834	0.0834	0.0834	0.0835
aTZ	0.0790		0.0859	0.0859	0.0860
aQZ	0.0833			0.0873	
a6Z+(a6Z)	0.0875 ± 0.0006				

<sup>a</sup>EBC stands for the extended Brillouin condition Ansatz, eq 35. The benchmark  $E_{\text{exch-disp}}^{(20)}/\text{CBS}$  value given at the bottom of the table was computed using the a6Z atom-centered basis augmented by the hydrogenic a6Z midbond set.

presented in Tables 1–5,  $E_{\text{disp}}^{(20)}$ -F12(MP2) performs well and considerably improves the dispersion energy, with sufficient convergence often being reached already with the aTZ basis set. The results obtained by the simplistic -F12(MP2) Ansatz are in these cases comparable to those from the more sophisticated Ansätze discussed above, justifying its usage for systems too large to be currently treated by the newly developed methods.

To investigate the performance of our methods on a larger set of complexes, we carried out further computations on all systems from the A24 database,<sup>56</sup> using up to aTZ/aTZ-RI basis sets. The convergence of  $E_{\text{disp}}^{(20)}$ -F12 for individual systems is illustrated in Figures 1, 2, S1, and S2 (Supporting Information) in comparison to conventional  $E_{\text{disp}}^{(20)}$  results computed with and without a hydrogenic set of midbond functions. It should be noted that the +(aXZ) set of midbond functions is used in this work to provide an example of the convergence benefits achievable by this approach and, at the largest basis set level, to serve as a benchmark against which small basis results are evaluated. The results with bond functions could be made more (less) accurate by adding a larger (smaller) set of midbond functions, and the most popular choice in SAPT calculations, the addition of a constant midbond set such as (3s3p2d2f), would likely result in more accurate aDZ and aTZ values [because the (3s3p2d2f) set is larger than the hydrogenic aXZ set] but less accurate aSZ and a6Z ones [because the (3s3p2d2f) set is smaller than the hydrogenic aXZ set]. For the latter reason, we selected the +(aXZ) midbond set as the most appropriate one for generating benchmark data, but results for small orbital bases could be obviously improved by adding a larger set of bond functions. Overall, the bond function and F12 approaches are complementary rather than competitive, and it is likely that the combination of both methods, which will be investigated in a subsequent publication, outperforms either one of them taken separately.

Overall, we observe a very fast convergence of  $E_{\text{disp}}^{(20)}$ -F12 with fully optimized amplitudes and optimized diagonal Ansatz going from aDZ/aTZ-RI to aTZ/aTZ-RI. Employing these F12 variants, energies are converged to the benchmark level in

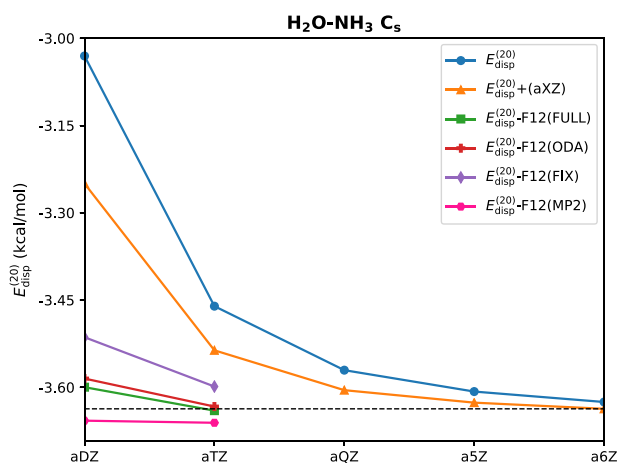


**Figure 1.** Convergence of  $E_{\text{disp}}^{(20)}$  and  $E_{\text{disp}}^{(20)}$ -F12 as a function of basis set for the  $\text{H}_2\text{O}-\text{NH}_3$  system from the A24 database. The fully optimized, optimized diagonal, and fixed-amplitude Ansätze for the explicitly correlated amplitudes are denoted by (FULL), (ODA), and (FIX), respectively, and (MP2) stands for the F12(MP2) approach of ref 46. The aTZ-RI basis was used as CABS in all F12 calculations. The notation +(aXZ) signifies that the hydrogenic aXZ set of midbond functions has been added to the aXZ atom-centered basis, and the conventional a6Z+(a6Z) value has been used as a reference.

aTZ/aTZ-RI or even earlier (e.g., the  $\text{NH}_3-\text{H}_2\text{O}$  complex, Figure 1). However, this trend is challenged by complexes containing a noble gas atom. For  $\text{Ar}-\text{CH}_4$  (Figure 2) and  $\text{Ar}-\text{C}_2\text{H}_4$  (Figure S2),  $E_{\text{disp}}^{(20)}$ -F12/aTZ with ODA is slightly inferior to conventional  $E_{\text{disp}}^{(20)}/\text{aQZ}+(\text{aQZ})$  level, while the FULL aTZ result is nearly identical ( $\text{Ar}-\text{CH}_4$ ) or somewhat more converged ( $\text{Ar}-\text{C}_2\text{H}_4$ ) than the conventional aQZ+(aQZ) one. The FULL Ansatz provides a minuscule but consistent improvement over ODA, although in rare cases (such as the  $\text{NH}_3-\text{CH}_4$  results, Figure S1), the numerical instabilities of the FULL method appear to affect the results slightly. The performance of  $E_{\text{disp}}^{(20)}$ -F12 combined with the fixed-amplitude

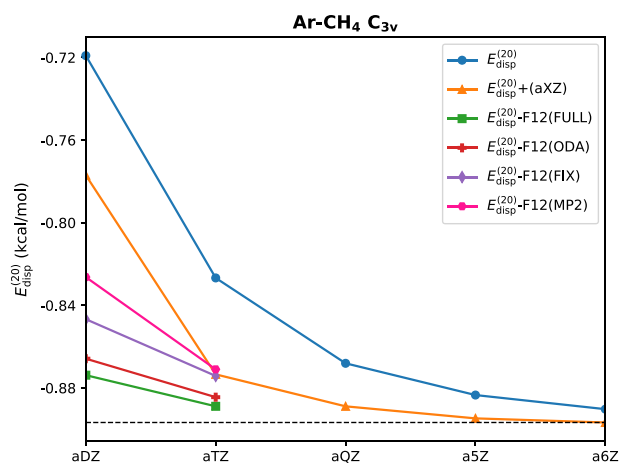


**Figure 2.** Convergence of  $E_{\text{disp}}^{(20)}$  and  $E_{\text{disp}}^{(20)}$ -F12 as a function of basis set for the Ar-CH<sub>4</sub> system from the A24 database. The fully optimized, optimized diagonal, and fixed-amplitude Ansätze for the explicitly correlated amplitudes are denoted by (FULL), (ODA), and (FIX), respectively, and (MP2) stands for the F12(MP2) approach of ref 46. The aTZ-RI basis was used as CABS in all F12 calculations. The notation +(aXZ) signifies that the hydrogenic aXZ set of midbond functions has been added to the aXZ atom-centered basis, and the conventional a6Z+(a6Z) value has been used as a reference.

Ansatz is less impressive, with the aTZ results converging to the point of  $E_{\text{disp}}^{(20)}$  computed in aQZ+(aQZ) for most systems and in aTZ+(aTZ) for the Ar-CH<sub>4</sub> and Ar-C<sub>2</sub>H<sub>4</sub> complexes. The  $E_{\text{disp}}^{(20)}$ -F12(MP2) Ansatz exhibits two convergence patterns. For complexes containing at least one polar monomer (H<sub>2</sub>O, NH<sub>3</sub>, HF),  $E_{\text{disp}}^{(20)}$ -F12(MP2) in the aDZ and aTZ bases is usually the best-performing variant, producing energies close to the CBS limit (even though overshooting slightly in some cases). However, for nonpolar complexes,  $E_{\text{disp}}^{(20)}$ -F12(MP2) tends to be the least accurate of the explicitly correlated Ansätze presented in Figures S1 and S2.

As demonstrated in Figures 3 and 4, as well as Figures S3 and S4 in the Supporting Information, the  $E_{\text{exch-disp}}^{(20)}$ -F12 energies also show a fast convergence with increasing X, converging from below to a reference value. Not surprisingly, the fixed-amplitude Ansatz is the least effective compared to the remaining SAPT0 F12 variants. For this Ansatz,  $E_{\text{exch-disp}}^{(20)}$ -F12/aTZ is of better quality than conventional  $E_{\text{exch-disp}}^{(20)}$ /aQZ but worse than  $E_{\text{exch-disp}}^{(20)}$ /aQZ+(aQZ), thus providing a little over one cardinal number of improvement. Moving on to  $E_{\text{exch-disp}}^{(20)}$ -F12 with fully optimized amplitudes and the optimized diagonal Ansatz, we see that both methods in the aDZ basis are converged close to the level corresponding to conventional  $E_{\text{exch-disp}}^{(20)}$  with the aTZ+(aTZ) basis set. In the aTZ basis, the FULL variant provides consistent improvement even upon  $E_{\text{exch-disp}}^{(20)}$ /a5Z. Even though ODA is less accurate, in most cases,  $E_{\text{exch-disp}}^{(20)}$ -F12/aTZ still works as well or even better than  $E_{\text{exch-disp}}^{(20)}$ /a5Z.

Having these observations in mind, it is very interesting to examine the convergence behavior for the sum of  $E_{\text{disp}}^{(20)}$ -F12 and  $E_{\text{exch-disp}}^{(20)}$ -F12. Figures S5 and S6 in the Supporting Information clearly show the rapid convergence of this sum computed with fully optimized amplitudes and the optimized diagonal Ansatz, converging at aTZ to the reference value or even lower. Again, the two systems containing a noble gas atom, Ar-CH<sub>4</sub> and Ar-C<sub>2</sub>H<sub>4</sub>, follow a slightly different pattern with a somewhat larger improvement of FULL over ODA. Outside of these two complexes, the cheapest SAPT-F12 variant, the fixed-amplitude

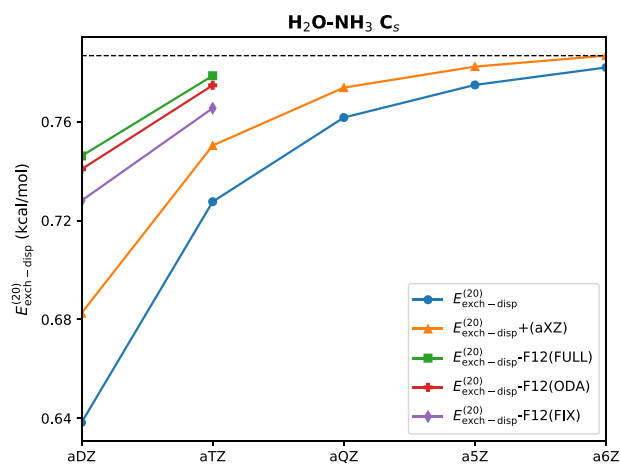


**Figure 3.** Convergence of  $E_{\text{exch-disp}}^{(20)}$  and  $E_{\text{exch-disp}}^{(20)}$ -F12 as a function of basis set for the H<sub>2</sub>O-NH<sub>3</sub> system from the A24 database. The fully optimized, optimized diagonal, and fixed-amplitude Ansätze for the explicitly correlated amplitudes are denoted by (FULL), (ODA), and (FIX), respectively. The aTZ-RI basis was used as CABS in all F12 calculations. The notation +(aXZ) signifies that the hydrogenic aXZ set of midbond functions has been added to the aXZ atom-centered basis, and the conventional a6Z+(a6Z) value has been used as a reference.

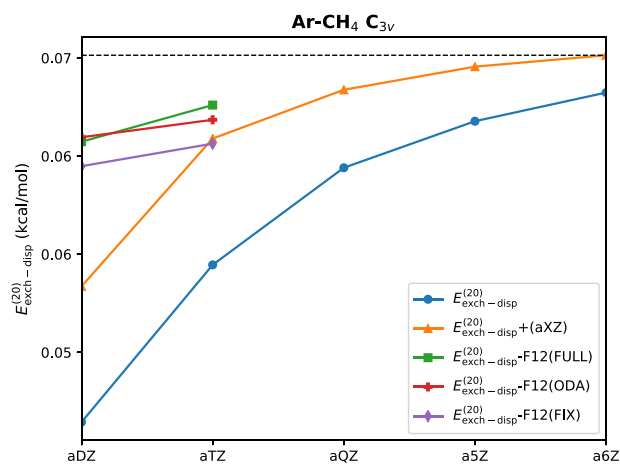


**Figure 4.** Convergence of  $E_{\text{exch-disp}}^{(20)}$  and  $E_{\text{exch-disp}}^{(20)}$ -F12 as a function of basis set for the Ar-CH<sub>4</sub> system from the A24 database. The fully optimized, optimized diagonal, and fixed-amplitude Ansätze for the explicitly correlated amplitudes are denoted by (FULL), (ODA), and (FIX), respectively. The aTZ-RI basis was used as CABS in all F12 calculations. The notation +(aXZ) signifies that the hydrogenic aXZ set of midbond functions has been added to the aXZ atom-centered basis, and the conventional a6Z+(a6Z) value has been used as a reference.

Ansatz, in the aTZ basis provides modest but consistent improvement over conventional  $E_{\text{disp}}^{(20)} + E_{\text{exch-disp}}^{(20)}$  in the aTZ+(aTZ) basis. When the -F12(MP2) correction is added, the  $E_{\text{disp}}^{(20)} + E_{\text{exch-disp}}^{(20)}$  energies in the aDZ and aTZ basis sets are generally overestimated.

The relative errors with respect to the benchmark for  $E_{\text{disp}}^{(20)}$ -F12,  $E_{\text{exch-disp}}^{(20)}$ -F12, and their sum using various options of calculating amplitudes are plotted in Figures 5–8, S7, and S8. The performance of explicitly correlated methods even in the aDZ basis set is definitely encouraging, significantly reducing the error with respect to conventional results with and without midbond functions. In fact,  $E_{\text{disp}}^{(20)}$ -F12 with fully optimized amplitudes (Figure 5) is consistently the top performer,

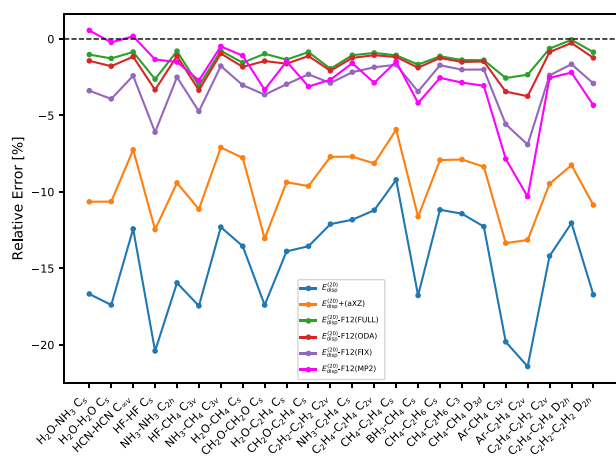


**Figure 5.** Relative errors on the A24 database<sup>56</sup> for the  $E_{\text{disp}}^{(20)}$  and  $E_{\text{disp}}^{(20)}$ -F12 corrections computed with the aDZ orbital basis set and the aTZ-RI auxiliary basis set. The fully optimized, optimized diagonal, and fixed-amplitude Ansätze for the explicitly correlated amplitudes are denoted by (FULL), (ODA), and (FIX), respectively, and (MP2) stands for the F12(MP2) approach of ref 46. The notation +(aXZ) signifies that the hydrogenic aXZ set of midbond functions has been added to the aXZ atom-centered basis, and the conventional a6Z +(a6Z) values have been used as a reference.

producing the largest error of  $-3.1\%$  for HF-CH<sub>4</sub>/aDZ. Nevertheless, the variant with optimized diagonal amplitudes leads to results of similar accuracy with the maximum error of  $-3.7\%$  for Ar-C<sub>2</sub>H<sub>4</sub>/aDZ. Not surprisingly, the fixed-amplitude Ansatz constitutes the least accurate variant (among the SAPT-F12 Ansätze) at the  $E_{\text{disp}}^{(20)}$ -F12/aDZ level, with the largest error of  $-6.9\%$  for Ar-C<sub>2</sub>H<sub>4</sub>. As already mentioned, the SAPT-F12(MP2) approach works well for polar complexes but is somewhat inferior to the other F12 flavors for nonpolar ones.

Analyzing the aTZ/aTZ-RI level of basis set (Figure 6),  $E_{\text{disp}}^{(20)}$ -F12 with fully optimized amplitudes and the optimized diagonal

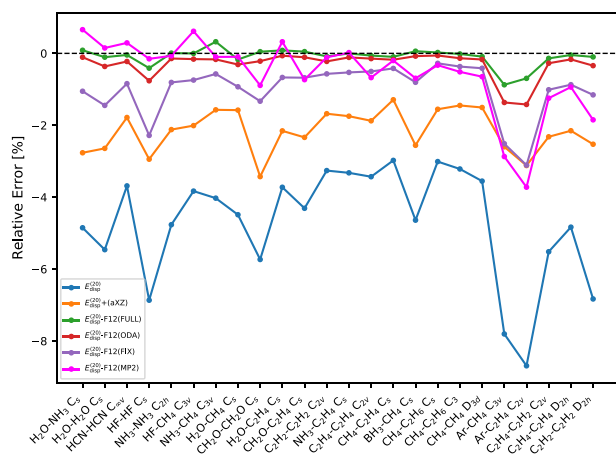


**Figure 6.** Relative errors on the A24 database<sup>56</sup> for the  $E_{\text{disp}}^{(20)}$  and  $E_{\text{disp}}^{(20)}$ -F12 corrections computed with the aTZ orbital basis set and the aTZ-RI auxiliary basis set. The fully optimized, optimized diagonal, and fixed-amplitude Ansätze for the explicitly correlated amplitudes are denoted by (FULL), (ODA), and (FIX), respectively, and (MP2) stands for the F12(MP2) approach of ref 46. The notation +(aXZ) signifies that the hydrogenic aXZ set of midbond functions has been added to the aXZ atom-centered basis, and the conventional a6Z +(a6Z) values have been used as a reference.

Ansatz work impressively, leading to mean unsigned relative errors (MUREs) of 0.2 and 0.3%, respectively. The fixed-amplitude and -F12(MP2) variants exhibit a somewhat worse performance (although still much better than conventional  $E_{\text{disp}}^{(20)}$ ), with the respective MURE values of 1.0 and 0.7%. It is worth emphasizing that the largest errors turn out to come from complexes containing the argon atom. This result is in line with our preliminary study on noble gas dimers, which showed a very slow convergence of F12 dispersion energies with respect to the auxiliary basis set size.

The relative errors of  $E_{\text{exch-disp}}^{(20)}$ -F12 in the aDZ/aTZ-RI basis set are presented in Figure 7. All F12 variants are superior to

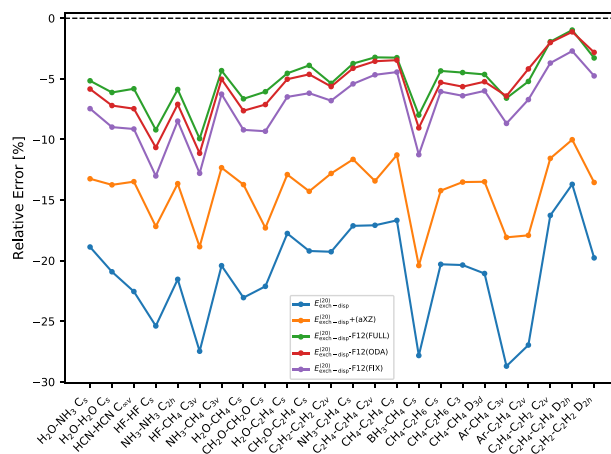


**Figure 7.** Relative errors on the A24 database<sup>56</sup> for the  $E_{\text{exch-disp}}^{(20)}$  and  $E_{\text{exch-disp}}^{(20)}$ -F12 corrections computed with the aDZ orbital basis set and the aTZ-RI auxiliary basis set. The fully optimized, optimized diagonal, and fixed-amplitude Ansätze for the explicitly correlated amplitudes are denoted by (FULL), (ODA), and (FIX), respectively. The notation +(aXZ) signifies that the hydrogenic aXZ set of midbond functions has been added to the aXZ atom-centered basis, and the conventional a6Z +(a6Z) values have been used as a reference.

conventional  $E_{\text{exch-disp}}^{(20)}$  and show comparable performance with the largest error of  $-13.0\%$  for the HF-HF dimer computed with the fixed-amplitude Ansatz.  $E_{\text{exch-disp}}^{(20)}$ -F12 evaluated in the aTZ/aTZ-RI basis set (Figure 8) brings an additional enhancement for all F12 treatments with the overall performance being the worst for the FIX Ansatz (maximum error  $-6.9\%$ ). It is noticeable that  $E_{\text{exch-disp}}^{(20)}$ -F12 provides larger relative errors than  $E_{\text{disp}}^{(20)}$ -F12; nevertheless, the second-order exchange dispersion energy is a small effect that brings about a minor absolute error.

Figures S7 and S8 show the quality of results for the total  $E_{\text{disp}}^{(20)}$ -F12 +  $E_{\text{exch-disp}}^{(20)}$ -F12 values in the aDZ/aTZ-RI and aTZ/aTZ-RI basis sets, respectively. Overall, the  $E_{\text{disp}}^{(20)}$ -F12 +  $E_{\text{exch-disp}}^{(20)}$ -F12 CBS values are recovered amazingly well, and while the simplest SAPT-F12 approximation with a fixed-amplitude Ansatz is somewhat less accurate, the optimized diagonal Ansatz is practically as good as the full optimization leading to important computational savings. The -F12(MP2) variant is the least effective F12 correction among all examined ones, most of the time overestimating the energies. However, it still brings improvement over the conventional  $E_{\text{disp}}^{(20)}$  +  $E_{\text{exch-disp}}^{(20)}$  treatment with and without midbond functions, especially for the aDZ basis set.

Figures 9 and 10 display the relative errors for the F12 dispersion and exchange dispersion energies calculated with the optimized diagonal Ansatz with various CABS bases. Acciden-



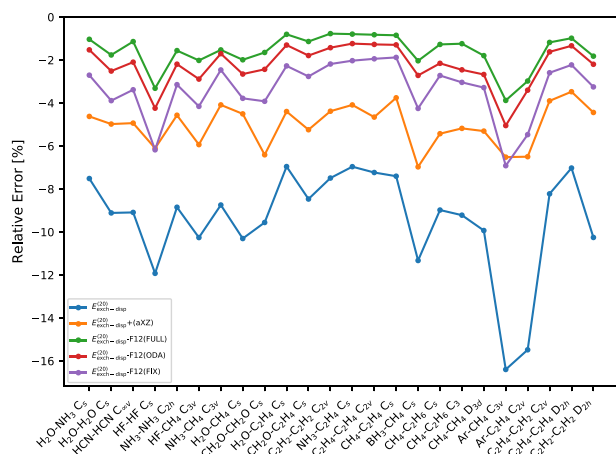


**Figure 8.** Relative errors on the A24 database<sup>56</sup> for the  $E_{\text{exch-disp}}^{(20)}$  and  $E_{\text{disp}}^{(20)}$ -F12 corrections computed with the aTZ orbital basis set and the aTZ-RI auxiliary basis set. The fully optimized, optimized diagonal, and fixed-amplitude Ansätze for the explicitly correlated amplitudes are denoted by (FULL), (ODA), and (FIX), respectively. The notation +(aXZ) signifies that the hydrogenic aXZ set of midbond functions has been added to the aXZ atom-centered basis, and the conventional a6Z +(a6Z) values have been used as a reference.

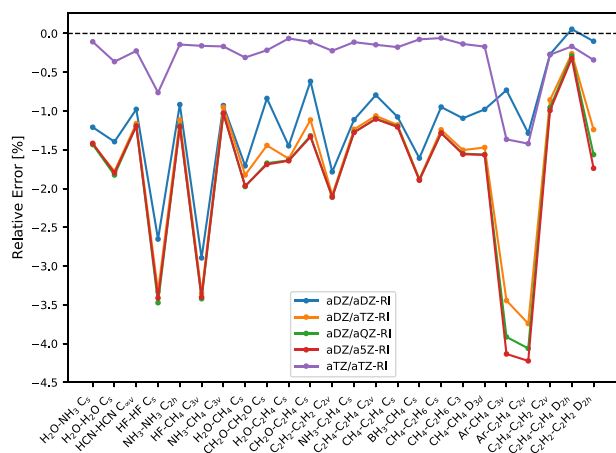


**Figure 9.** Dependence of the  $E_{\text{disp}}^{(20)}$ -F12 relative errors for the A24 database,<sup>56</sup> computed with the optimized diagonal Ansatz, on the orbital basis set aXZ and the CABS set aXZ-RI. The conventional a6Z +(a6Z) values have been used as a reference.

tally, the aDZ/aDZ-RI variant shows the best aDZ-level performance that confirms previous observations about the error cancellations. To avoid relying on error cancellations, we recommend using the aDZ/aTZ-RI level of theory for near-benchmark accuracy. The differences between the aDZ/aTZ-RI, aDZ/aQZ-RI, and aDZ/a5Z-RI results are very small, confirming that the aTZ-RI auxiliary set is sufficiently converged in this case.

## VI. SUMMARY

We have derived and implemented compact expressions for the explicitly correlated SAPT0-level dispersion and exchange dispersion energies. The resulting expressions involve the same types of F12 integrals (over orbital and auxiliary basis functions) as the popular MP2-F12 approach,<sup>11</sup> the integrals just have to be transformed to the molecular-orbital and complementary auxiliary bases using the orbitals and Fock

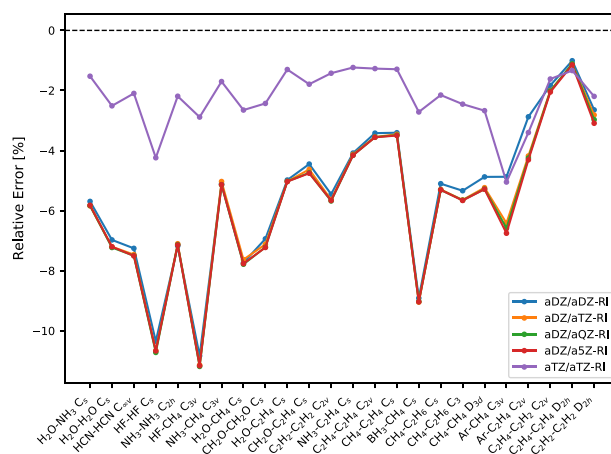


**Figure 10.** Dependence of the  $E_{\text{exch-disp}}^{(20)}$ -F12 relative errors for the A24 database,<sup>56</sup> computed with the optimized diagonal Ansatz, on the orbital basis set aXZ and the CABS set aXZ-RI. The conventional a6Z +(a6Z) values have been used as a reference.

operators of the appropriate monomer. Our pilot implementation makes use of the Psi4NUMPY framework<sup>51</sup> interfaced to the LIBINT integral library<sup>53</sup> via the Python and C++ layers of the Psi4 code.<sup>52</sup> At this stage, the evaluation of three- and four-electron integrals is completely avoided by the resolutions of identity, but the two-electron quantities are evaluated conventionally, without density fitting. Thus, our pilot code is not nearly as efficient as a production-level, density-fitted MP2-F12 implementation, but it is more than sufficient to complete all calculations presented here, including the aTZ-level computations for all systems in the A24 database.

In this work, the  $E_{\text{exch-disp}}^{(20)}$ -F12 correction is derived and implemented for the first time, following a generalization of the second-quantized SAPT exchange formalism.<sup>49</sup> The  $E_{\text{disp}}^{(20)}$ -F12 correction with fully optimized amplitudes (FULL) was recently proposed by Przybytek;<sup>47</sup> here, we reimplement Przybytek's fully optimized Ansatz and propose three new approximate Ansätze: optimized diagonal (ODA), EBC, and fixed amplitude (FIX). An exhaustive investigation of the two corrections is presented on five weakly interacting dimers: He–He, Ne–Ne, Ar–Ar, H<sub>2</sub>O–H<sub>2</sub>O, and CH<sub>4</sub>–CH<sub>4</sub> at their van der Waals minimum geometries. Subsequently, the performance of  $E_{\text{disp}}^{(20)}$ -F12,  $E_{\text{exch-disp}}^{(20)}$ -F12, and  $E_{\text{disp}}^{(20)}$ -F12 +  $E_{\text{exch-disp}}^{(20)}$ -F12 with basis sets up to aTZ/aTZ-RI was studied on the A24 database<sup>56</sup> and compared with SAPT-F12(MP2).<sup>46</sup> The most accurate and most computationally efficient Ansätze have been established, and the convergence with respect to the RI basis was assessed, as well.

Our calculations show that the explicitly correlated F12 methods significantly speed up the basis set convergence compared to the conventional second-order dispersion and exchange dispersion approaches.  $E_{\text{disp}}^{(20)}$ -F12 with fully optimized amplitudes and optimized diagonal Ansatz leads to results being converged to the CBS limit already at the aTZ/aTZ-RI level, while  $E_{\text{exch-disp}}^{(20)}$ -F12 provides energies close to the level of  $E_{\text{exch-disp}}^{(20)}/\text{aQZ}+(\text{aQZ})$  using the same basis sets. As far as the sum  $E_{\text{disp}}^{(20)}$ -F12 +  $E_{\text{exch-disp}}^{(20)}$ -F12 is concerned, its values computed with the FULL and ODA variants are nearly converged to the CBS limit. The  $E_{\text{disp}}^{(20)}$ -F12 Ansatz employing the extended Brillouin condition is overall less accurate and more expensive than the ODA approximation and cannot be recommended for practical calculations. The FIX and -F12(MP2) flavors are the

least accurate, but even they provide a substantial improvement over standard  $E_{\text{disp}}^{(20)}$  and  $E_{\text{exch-disp}}^{(20)}$ . It should be stressed that the simplest, local-MP2-F12-based  $E_{\text{disp}}^{(20)}$ -F12(MP2) correction does not strictly represent dispersion energy but likely contains an exchange dispersion contribution as well. The -F12(MP2) corrected sum  $E_{\text{disp}}^{(20)} + E_{\text{exch-disp}}^{(20)}$  is markedly more accurate than its conventional counterpart, but the precise accuracy of the -F12(MP2) treatment varies, with a few outliers present in the A24 set. For all variants, the A24 systems containing the argon atom show somewhat slower convergence. We expect that the inclusion of midbond functions in the F12 approach, quite beneficial in supermolecular CCSD(T)-F12 interaction energy calculations,<sup>25</sup> can bring about further enhancement of results.

The relative errors with respect to the benchmarks for  $E_{\text{disp}}^{(20)}$ -F12,  $E_{\text{exch-disp}}^{(20)}$ -F12, and  $E_{\text{disp}}^{(20)}$ -F12 +  $E_{\text{exch-disp}}^{(20)}$ -F12 averaged over the A24 database revealed the most efficient approaches in terms of accuracy and computational time. The fully optimized-amplitude flavor is the most accurate out of all SAPT0 dispersion corrections, leading to remarkably small MURE of 0.2, 1.6, and 0.2% for  $E_{\text{disp}}^{(20)}$ -F12/aTZ,  $E_{\text{exch-disp}}^{(20)}$ -F12/aTZ, and  $E_{\text{disp}}^{(20)}$ -F12/aTZ +  $E_{\text{exch-disp}}^{(20)}$ -F12/aTZ, respectively. However, this variant suffers from serious drawbacks: it is very expensive (scales like  $N^8$ ) and shows numerical instabilities due to the need to solve potentially ill-conditioned systems of linear equations. While the FIX and -F12(MP2) Ansätze provide somewhat less accurate energies, the ODA variant is in a very good agreement with the FULL Ansatz. Therefore, we propose to replace the more expensive FULL treatment of  $E_{\text{disp}}^{(20)}$ -F12<sup>47</sup> with the cheaper ODA one which scales like  $N^5$  without losing much accuracy. In this way, we not only significantly reduce the computational effort but also remove numerical issues.

For the investigated rare gas dimers, we observed an extremely slow auxiliary basis set convergence of  $E_{\text{disp}}^{(20)}$ -F12. This issue was attributed to the auxiliary basis sets probably being inadequately optimized for the purposes of noncovalent interaction energy calculations. Therefore, noble gas dimers have to be calculated close to the complete RI basis set limit, employing the largest CABS possible. The rare gas dimer dispersion energies calculated with the aDZ/aDZ-RI basis sets overestimate the CBS values, which is caused by an incomplete error cancellation of the effects of orbital and CABS set truncations. Thus, we recommend the aTZ-RI auxiliary basis set in calculations with the aDZ orbital basis.

Building on our successful application of explicitly correlated methods to SAPT0, it will be beneficial to extend the F12 treatment to higher-order corrections, e.g., to the effects of intramolecular electron correlation on the second-order dispersion energy. Until this is accomplished, computing  $E_{\text{disp}}^{(20)}$ -F12 and adding intramolecular correlation corrections computed without F12 is a valid approach—no double counting occurs. While an investigation of the performance of such a dispersion treatment is outside of the scope of this paper, we do expect a significant improvement of the CBS convergence compared to, say, that of standard SAPT2+3, in the same way as the composite “MP2/CBS plus CCSD(T) correction” interaction energies converge much faster with the basis set than stand-alone CCSD(T).<sup>69</sup> On a different note, the introduction of density-fitting techniques is necessary to extend the SAPT-F12 calculations to medium and large systems and to make them competitive with conventional (density-fitted) large-basis SAPT. All of these enhancements are subjects of ongoing research in our groups.

## ■ ASSOCIATED CONTENT

### 📄 Supporting Information

The Supporting Information is available free of charge on the ACS Publications website at DOI: 10.1021/acs.jctc.9b00547.

Tables and figures illustrating the convergence of the sum  $E_{\text{disp}}^{(20)}$ -F12 +  $E_{\text{exch-disp}}^{(20)}$ -F12 for all systems studied in this work; counterparts of Figures 1–4 for all complexes in the A24 database (PDF)

## ■ AUTHOR INFORMATION

### Corresponding Author

\*E-mail: patkowski@auburn.edu (K.P.).

### ORCID

Wim Klopper: 0000-0002-5219-9328

Konrad Patkowski: 0000-0002-4468-207X

### Notes

The authors declare no competing financial interest.

## ■ ACKNOWLEDGMENTS

This work was supported by the U.S. National Science Foundation (NSF) CAREER award CHE-1351978. The authors furthermore gratefully acknowledge support by the Deutsche Forschungsgemeinschaft (DFG) through the Priority Programme SPP 1807 “Control of London Dispersion Interactions in Molecular Chemistry” (Project No. KL 721/5-2). M.K. was supported by a fellowship from the Molecular Sciences Software Institute (MolSSI) under NSF Grant No. ACI-1547580.

## ■ REFERENCES

- (1) Kato, T. On the eigenfunctions of many-particle systems in quantum mechanics. *Commun. Pure Appl. Math.* **1957**, *10*, 151–177.
- (2) Pack, R. T.; Brown, W. B. Cusp Conditions for Molecular Wavefunctions. *J. Chem. Phys.* **1966**, *45*, 556–559.
- (3) Kutzelnigg, W.  $r_{12}$ -Dependent terms in the wave function as closed sums of partial wave amplitudes for large  $l$ . *Theor. Chim. Acta* **1985**, *68*, 445–469.
- (4) Klopper, W.; Kutzelnigg, W. Møller-Plesset calculations taking care of the correlation cusp. *Chem. Phys. Lett.* **1987**, *134*, 17–22.
- (5) Mitroy, J.; Bubin, S.; Horiuchi, W.; Suzuki, Y.; Adamowicz, L.; Cencek, W.; Szalewicz, K.; Komasa, J.; Blume, D.; Varga, K. Theory and application of explicitly correlated Gaussians. *Rev. Mod. Phys.* **2013**, *85*, 693–749.
- (6) Ten-no, S. Initiation of explicitly correlated Slater-type geminal theory. *Chem. Phys. Lett.* **2004**, *398*, 56–61.
- (7) Tew, D. P.; Klopper, W. New correlation factors for explicitly correlated electronic wave functions. *J. Chem. Phys.* **2005**, *123*, No. 074101.
- (8) Tew, D. P.; Klopper, W. A comparison of linear and nonlinear correlation factors for basis set limit Møller-Plesset second order binding energies and structures of He<sub>2</sub>, Be<sub>2</sub>, and Ne<sub>2</sub>. *J. Chem. Phys.* **2006**, *125*, No. 094302.
- (9) Valeev, E. F. Combining explicitly correlated R12 and Gaussian geminal electronic structure theories. *J. Chem. Phys.* **2006**, *125*, No. 244106.
- (10) Klopper, W.; Samson, C. C. M. Explicitly correlated second-order Møller-Plesset methods with auxiliary basis sets. *J. Chem. Phys.* **2002**, *116*, 6397–6410.
- (11) Werner, H.-J.; Adler, T. B.; Manby, F. R. General orbital invariant MP2-F12 theory. *J. Chem. Phys.* **2007**, *126*, No. 164102.
- (12) Fliegl, H.; Klopper, W.; Hättig, C. Coupled-cluster theory with simplified linear- $r_{12}$  corrections: The CCSD(R12) model. *J. Chem. Phys.* **2005**, *122*, No. 084107.

- (13) Adler, T. B.; Knizia, G.; Werner, H.-J. A Simple and Efficient CCSD(T)-F12 Approximation. *J. Chem. Phys.* **2007**, *127*, No. 221106.
- (14) Torheyden, M.; Valeev, E. F. Variational formulation of perturbative explicitly-correlated coupled-cluster methods. *Phys. Chem. Chem. Phys.* **2008**, *10*, 3410–3420.
- (15) Knizia, G.; Adler, T. B.; Werner, H.-J. Simplified CCSD(T)-F12 Methods: Theory and Benchmarks. *J. Chem. Phys.* **2009**, *130*, No. 054104.
- (16) Shiozaki, T.; Valeev, E. F.; Hirata, S. Explicitly correlated combined coupled-cluster and perturbation methods. *J. Chem. Phys.* **2009**, *131*, No. 044118.
- (17) Hättig, C.; Tew, D. P.; Köhn, A. Accurate and efficient approximations to explicitly correlated coupled-cluster singles and doubles, CCSD-F12. *J. Chem. Phys.* **2010**, *132*, No. 231102.
- (18) Marchetti, O.; Werner, H.-J. Accurate calculations of intermolecular interaction energies using explicitly correlated wave functions. *Phys. Chem. Chem. Phys.* **2008**, *10*, 3400–3409.
- (19) Marchetti, O.; Werner, H.-J. Accurate Calculations of Intermolecular Interaction Energies Using Explicitly Correlated Coupled Cluster Wave Functions and a Dispersion-Weighted MP2 Method. *J. Phys. Chem. A* **2009**, *113*, 11580–11585.
- (20) McMahan, J. D.; Lane, J. R. Explicit correlation and basis set superposition error: The structure and energy of carbon dioxide dimer. *J. Chem. Phys.* **2011**, *135*, No. 154309.
- (21) Patkowski, K. On the accuracy of explicitly correlated coupled-cluster interaction energies - have orbital results been beaten yet? *J. Chem. Phys.* **2012**, *137*, No. 034103.
- (22) Patkowski, K. Basis Set Converged Weak Interaction Energies from Conventional and Explicitly Correlated Coupled-Cluster Approach. *J. Chem. Phys.* **2013**, *138*, No. 154101.
- (23) Sirianni, D. A.; Burns, L. A.; Sherrill, C. D. Comparison of Explicitly Correlated Methods for Computing High-Accuracy Benchmark Energies for Noncovalent Interactions. *J. Chem. Theory Comput.* **2017**, *13*, 86–99.
- (24) Tao, F.-M.; Pan, Y.-K. Validity of the function counterpoise method and ab initio calculations of van der Waals interaction energy. *J. Phys. Chem. A* **1991**, *95*, 3582–3588.
- (25) Dutta, N. N.; Patkowski, K. Improving ‘Silver-Standard’ Benchmark Interaction Energies with Bond Functions. *J. Chem. Theory Comput.* **2018**, *14*, 3053–3070.
- (26) Jeziorski, B.; Moszyński, R.; Szalewicz, K. Perturbation Theory Approach to Intermolecular Potential Energy Surfaces of van der Waals Complexes. *Chem. Rev.* **1994**, *94*, 1887–1930.
- (27) Szalewicz, K.; Patkowski, K.; Jeziorski, B. Intermolecular Interactions via Perturbation Theory: from Diatoms to Biomolecules. *Struct. Bonding* **2005**, *116*, 43–117.
- (28) Hohenstein, E. G.; Sherrill, C. D. Wavefunction Methods for Noncovalent Interactions. *Wiley Interdiscip. Rev.: Comput. Mol. Sci.* **2012**, *2*, 304–326.
- (29) Parrish, R. M.; Sherrill, C. D. Quantum-Mechanical Evaluation of  $\pi$ - $\pi$  versus Substituent- $\pi$  Interactions in  $\pi$  Stacking: Direct Evidence for the Wheeler-Houk Picture. *J. Am. Chem. Soc.* **2014**, *136*, 17386–17389.
- (30) Gryn'ova, G.; Corminboeuf, C. Implications of Charge Penetration for Heteroatom-Containing Organic Semiconductors. *J. Phys. Chem. Lett.* **2016**, *7*, 5198–5204.
- (31) McDaniel, J. G.; Yu, K.; Schmidt, J. R. Ab Initio, Physically Motivated Force Fields for CO<sub>2</sub> Adsorption in Zeolitic Imidazolate Frameworks. *J. Phys. Chem. C* **2012**, *116*, 1892–1903.
- (32) Williams, H. L.; Mas, E. M.; Szalewicz, K.; Jeziorski, B. On the effectiveness of monomer-, dimer-, and bond-centered basis functions in calculations of intermolecular interaction energies. *J. Chem. Phys.* **1995**, *103*, 7374–7391.
- (33) Rybak, S.; Jeziorski, B.; Szalewicz, K. Many-body symmetry-adapted perturbation theory of intermolecular interactions - H<sub>2</sub>O and HF dimers. *J. Chem. Phys.* **1991**, *95*, 6579–6601.
- (34) Parker, T. M.; Burns, L. A.; Parrish, R. M.; Ryno, A. G.; Sherrill, C. D. Levels of Symmetry Adapted Perturbation Theory (SAPT). I. Efficiency and Performance for Interaction Energies. *J. Chem. Phys.* **2014**, *140*, No. 094106.
- (35) Jaszunski, M.; McWeeny, R. Time-dependent Hartree-Fock calculations of dispersion energy. *Mol. Phys.* **1985**, *55*, 1275–1286.
- (36) Misquitta, A. J.; Jeziorski, B.; Szalewicz, K. Dispersion energy from density-functional theory description of monomers. *Phys. Rev. Lett.* **2003**, *91*, No. 033201.
- (37) Heßelmann, A.; Jansen, G. Intermolecular dispersion energies from time-dependent density functional theory. *Chem. Phys. Lett.* **2003**, *367*, 778–784.
- (38) Holzer, C.; Klopper, W. Communication: Symmetry-adapted perturbation theory with intermolecular induction and dispersion energies from the Bethe-Salpeter equation. *J. Chem. Phys.* **2017**, *147*, No. 181101.
- (39) Hobza, P.; Selzle, H. L.; Schlag, E. W. Potential Energy Surface for the Benzene Dimer. Results of ab Initio CCSD(T) Calculations Show Two Nearly Isoenergetic Structures: T-Shaped and Parallel-Displaced. *J. Phys. Chem.* **1996**, *100*, 18790–18794.
- (40) Papajak, E.; Zheng, J.; Xu, X.; Leverentz, H. R.; Truhlar, D. G. Perspectives on Basis Sets Beautiful: Seasonal Plantings of Diffuse Basis Functions. *J. Chem. Theory Comput.* **2011**, *7*, 3027–3034.
- (41) Jeziorski, B.; van Hemert, M. C. Variation-perturbation treatment of the hydrogen bond between water molecules. *Mol. Phys.* **1976**, *31*, 713–729.
- (42) Tew, D. P.; Klopper, W.; Neiss, C.; Hättig, C. Quintuple-zeta quality coupled-cluster correlation energies with triple-zeta basis sets. *Phys. Chem. Chem. Phys.* **2007**, *9*, 1921–1930.
- (43) Szalewicz, K.; Jeziorski, B. Symmetry-adapted double-perturbation analysis of intramolecular correlation effects in weak intermolecular interactions: the He-He interaction. *Mol. Phys.* **1979**, *38*, 191–208.
- (44) Korona, T.; Williams, H. L.; Bukowski, R.; Jeziorski, B.; Szalewicz, K. Symmetry-Adapted Perturbation Theory Calculation of He-He Interaction Energy. *J. Chem. Phys.* **1997**, *106*, 5109–5122.
- (45) Jeziorski, M.; Cencek, W.; Patkowski, K.; Jeziorski, B.; Szalewicz, K. Pair potential for helium from symmetry-adapted perturbation theory calculations and from supermolecular data. *J. Chem. Phys.* **2007**, *127*, No. 124303.
- (46) Frey, J. A.; Holzer, C.; Klopper, W.; Leutwyler, S. Experimental and Theoretical Determination of Dissociation Energies of Dispersion-Dominated Aromatic Molecular Complexes. *Chem. Rev.* **2016**, *116*, 5614–5641.
- (47) Przybytek, M. Dispersion Energy of Symmetry-Adapted Perturbation Theory from the Explicitly Correlated F12 Approach. *J. Chem. Theory Comput.* **2018**, *14*, 5105–5117.
- (48) Moszyński, R.; Jeziorski, B.; Rybak, S.; Szalewicz, K.; Williams, H. L. Many-body theory of exchange effects in intermolecular interactions. Density matrix approach and applications to He-F<sup>-</sup>, He-HF, H<sub>2</sub>-HF, and Ar-H<sub>2</sub> dimers. *J. Chem. Phys.* **1994**, *100*, 5080–5093.
- (49) Moszyński, R.; Jeziorski, B.; Szalewicz, K. Many-body theory of exchange effects in intermolecular interactions. Second-quantization approach and comparison with full configuration interaction results. *J. Chem. Phys.* **1994**, *100*, 1312–1325.
- (50) Patkowski, K.; Szalewicz, K. Frozen core and effective core potentials in symmetry-adapted perturbation theory. *J. Chem. Phys.* **2007**, *127*, No. 164103.
- (51) Smith, D. G. A.; et al. Psi4NumPy: An Interactive Quantum Chemistry Programming Environment for Reference Implementations and Rapid Development. *J. Chem. Theory Comput.* **2018**, *14*, 3504–3511.
- (52) Parrish, R. M.; et al. Psi4 1.1: An Open-Source Electronic Structure Program Emphasizing Automation, Advanced Libraries, and Interoperability. *J. Chem. Theory Comput.* **2017**, *13*, 3185–3197.
- (53) Valeev, E. F. *Libint: A Library for the Evaluation of Molecular Integrals of Many-Body Operators over Gaussian Functions*, version 2.5.0-beta.1, 2018. <http://libint.valeev.net/>.
- (54) Obara, S.; Saika, A. Efficient recursive computation of molecular integrals over Cartesian Gaussian functions. *J. Chem. Phys.* **1986**, *84*, 3963–3974.
- (55) Höfener, S.; Bischoff, F. A.; Glöß, A.; Klopper, W. Slater-type geminals in explicitly-correlated perturbation theory: application to n-

alkanols and analysis of errors and basis-set requirements. *Phys. Chem. Chem. Phys.* **2008**, *10*, 3390–3399.

(56) Rezáč, J.; Hobza, P. Describing Noncovalent Interactions beyond the Common Approximations: How Accurate Is the 'Gold Standard,' CCSD(T) at the Complete Basis Set Limit? *J. Chem. Theory Comput.* **2013**, *9*, 2151–2155.

(57) Manby, F. R. Density fitting in second-order linear-R12 Møller-Plesset perturbation theory. *J. Chem. Phys.* **2003**, *119*, 4607–4613.

(58) May, A. J.; Manby, F. R. An explicitly correlated second order Møller-Plesset theory using a frozen Gaussian geminal. *J. Chem. Phys.* **2004**, *121*, 4479–4485.

(59) Bachorz, R. A.; Bischoff, F. A.; Glöß, A.; Hättig, C.; Höfener, S.; Klopper, W.; Tew, D. P. The MP2-F12 method in the TURBOMOLE program package. *J. Comput. Chem.* **2011**, *32*, 2492–2513.

(60) Dunning, T. H., Jr. Gaussian-Basis Sets for Use in Correlated Molecular Calculations. 1. The Atoms Boron through Neon and Hydrogen. *J. Chem. Phys.* **1989**, *90*, 1007–1023.

(61) Kendall, R. A.; Dunning, T. H., Jr.; Harrison, R. J. Electron Affinities of the 1st-Row Atoms Revisited - Systematic Basis Sets and Wave Functions. *J. Chem. Phys.* **1992**, *96*, 6796–6806.

(62) Peterson, K. A.; Adler, T. B.; Werner, H.-J. Systematically convergent basis sets for explicitly correlated wavefunctions: The atoms H, He, B-Ne, and Al-Ar. *J. Chem. Phys.* **2008**, *128*, No. 084102.

(63) Sylvetsky, N.; Kesharwani, M. K.; Martin, J. M. L. The aug-cc-pVnZ-F12 basis set family: Correlation consistent basis sets for explicitly correlated benchmark calculations on anions and noncovalent complexes. *J. Chem. Phys.* **2017**, *147*, No. 134106.

(64) Weigend, F.; Köhn, A.; Hättig, C. Efficient use of the correlation consistent basis sets in resolution of the identity MP2 calculations. *J. Chem. Phys.* **2002**, *116*, 3175–3183.

(65) Hättig, C. Optimization of auxiliary basis sets for RI-MP2 and RI-CC2 calculations: Core-valence and quintuple-zeta basis sets for H to Ar and QZVPP basis sets for Li to Kr. *Phys. Chem. Chem. Phys.* **2005**, *7*, 59–66.

(66) May, A. J.; Valeev, E.; Polly, R.; Manby, F. R. Analysis of the errors in explicitly correlated electronic structure theory. *Phys. Chem. Chem. Phys.* **2005**, *7*, 2710–2713.

(67) Misquitta, A. J. Intermolecular Interactions. In *Handbook of Computational Chemistry*; Leszczynski, J., Ed.; Springer International Publishing: Switzerland, 2017; pp 295–335.

(68) Hohenstein, E. G.; Sherrill, C. D. Density fitting and Cholesky decomposition approximations in symmetry-adapted perturbation theory: Implementation and application to probe the nature of pi-pi interactions in linear acenes. *J. Chem. Phys.* **2010**, *132*, No. 184111.

(69) Burns, L. A.; Marshall, M. S.; Sherrill, C. D. Appointing silver and bronze standards for noncovalent interactions: A comparison of spin-component-scaled (SCS), explicitly correlated (F12), and specialized wavefunction approaches. *J. Chem. Phys.* **2014**, *141*, No. 234111.

**Supporting Information for**  
**Explicitly correlated dispersion and exchange dispersion energies**  
**in symmetry-adapted perturbation theory**

Monika Kodrycka

*Department of Chemistry and Biochemistry,  
Auburn University, Auburn, AL 36849, United States*

Christof Holzer and Wim Klopper

*Theoretical Chemistry Group, Institute of Physical Chemistry,  
Karlsruhe Institute of Technology (KIT), KIT Campus South,  
P.O. Box 6980, D-76049 Karlsruhe, Germany*

Konrad Patkowski

*Department of Chemistry and Biochemistry,  
Auburn University, Auburn, AL 36849, United States*

(Dated: August 9, 2019)

TABLE SI: The  $E_{\text{disp}}^{(20)}$ -F12+ $E_{\text{exch-disp}}^{(20)}$ -F12 sum (in kcal/mol) for the helium dimer for different combinations of the orbital basis aXZ and CABS basis aXZ-RI. The fully optimized, optimized diagonal, and fixed-amplitude Ansätze are equivalent for this specific system. EBC stands for the extended Brillouin condition Ansatz, and F12(MP2) denotes the approach of Ref. 1. The benchmark  $E_{\text{disp}}^{(20)} + E_{\text{exch-disp}}^{(20)}$ /CBS value given at the bottom of the table was computed in Ref. 2 using Gaussian-type geminals (GTGs).

Fixed-amplitude/Optimized diagonal/Fully optimized Ansatz						
Basis	$E_{\text{disp}}^{(20)} + E_{\text{exch-disp}}^{(20)}$	aDZ-RI	aTZ-RI	aQZ-RI	a5Z-RI	a6Z-RI
aDZ	-0.0239	-0.0586	-0.0445	-0.0413	-0.0394	-0.0352
aTZ	-0.0290		-0.0354	-0.0348	-0.0343	-0.0336
aQZ	-0.0306			-0.0332	-0.0332	-0.0339
a5Z	-0.0316				-0.0330	-0.0329
a6Z	-0.0323					-0.0330
EBC Ansatz						
Basis	$E_{\text{disp}}^{(20)} + E_{\text{exch-disp}}^{(20)}$	aDZ-RI	aTZ-RI	aQZ-RI	a5Z-RI	a6Z-RI
aDZ	-0.0239	-0.0587	-0.0447	-0.0414	-0.0394	-0.0352
aTZ	-0.0291		-0.0351	-0.0344	-0.0339	-0.0333
aQZ	-0.0307			-0.0328	-0.0329	-0.0336
a5Z	-0.0316				-0.0327	-0.0327
a6Z	-0.0323					-0.0329
F12(MP2) Ansatz						
Basis	$E_{\text{disp}}^{(20)} + E_{\text{exch-disp}}^{(20)}$	aDZ-RI	aTZ-RI	aQZ-RI	a5Z-RI	a6Z-RI
aDZ	-0.0239	-0.0376	-0.0341	-0.0325	-0.0312	-0.0299
aTZ	-0.0290		-0.0324	-0.0320	-0.0318	-0.0315
aQZ	-0.0306			-0.0318	-0.0317	-0.0317
a5Z	-0.0316				-0.0325	-0.0325
a6Z	-0.0323					-0.0328
<b>GTG</b>	<b>-0.0330</b>	$\pm 1.6 \cdot 10^{-7}$				

TABLE SII: The  $E_{\text{disp}}^{(20)}$ -F12+ $E_{\text{exch-disp}}^{(20)}$ -F12 sum (in kcal/mol) for the neon dimer for different combinations of the orbital basis aXZ and CABS basis aXZ-RI. EBC stands for the extended Brillouin condition Ansatz, and F12(MP2) denotes the approach of Ref. 1.

The benchmark  $E_{\text{disp}}^{(20)} + E_{\text{exch-disp}}^{(20)}$ /CBS value given at the bottom of the table was computed using the a6Z atom-centered basis augmented by the hydrogenic a6Z midbond set.

Fixed-amplitude Ansatz					
Basis	$E_{\text{disp}}^{(20)} + E_{\text{exch-disp}}^{(20)}$	aDZ-RI	aTZ-RI	aQZ-RI	a5Z-RI
aDZ	-0.0792	-0.1844	-0.1458	-0.1347	-0.1188
aTZ	-0.1050		-0.1488	-0.1386	-0.1292
aQZ	-0.1159			-0.1353	-0.1313
a5Z	-0.1222				-0.1289
Optimized diagonal Ansatz					
Basis	$E_{\text{disp}}^{(20)} + E_{\text{exch-disp}}^{(20)}$	aDZ-RI	aTZ-RI	aQZ-RI	a5Z-RI
aDZ	-0.0792	-0.1908	-0.1510	-0.1397	-0.1230
aTZ	-0.1050		-0.1527	-0.1421	-0.1319
aQZ	-0.1159			-0.1371	-0.1328
a5Z	-0.1222				-0.1297
EBC Ansatz					
Basis	$E_{\text{disp}}^{(20)} + E_{\text{exch-disp}}^{(20)}$	aDZ-RI	aTZ-RI	aQZ-RI	a5Z-RI
aDZ	-0.0792	-0.1872	-0.1475	-0.1330	-0.1184
aTZ	-0.1050		-0.1502	-0.1397	-0.1286
aQZ	-0.1159			-0.1360	-0.1312
a5Z	-0.1222				-0.1290
Fully optimized amplitudes					
Basis	$E_{\text{disp}}^{(20)} + E_{\text{exch-disp}}^{(20)}$	aDZ-RI	aTZ-RI	aQZ-RI	a5Z-RI
aDZ	-0.0792	-0.1927	-0.1517	-0.1404	-0.1234
aTZ	-0.1050		-0.1529	-0.1426	-0.1313
aQZ	-0.1159			-0.1377	-0.1332
a5Z	-0.1222				-0.1313
F12(MP2) Ansatz					
Basis	$E_{\text{disp}}^{(20)} + E_{\text{exch-disp}}^{(20)}$	aDZ-RI	aTZ-RI	aQZ-RI	a5Z-RI
aDZ	-0.0792	-0.1269	-0.1172	-0.1121	-0.1096
aTZ	-0.1050		-0.1366	-0.1311	-0.1288
aQZ	-0.1159			-0.1425	-0.1397
a5Z	-0.1222				
<b>a6Z+(a6Z)</b>	<b>-0.1287</b>	$\pm 0.0001$			

TABLE SIII: The  $E_{\text{disp}}^{(20)}$ -F12+ $E_{\text{exch-disp}}^{(20)}$ -F12 sum (in kcal/mol) for the argon dimer for different combinations of the orbital basis aXZ and CABS basis aXZ-RI. EBC stands for the extended Brillouin condition Ansatz, and F12(MP2) denotes the approach of Ref. 1.

The benchmark  $E_{\text{disp}}^{(20)} + E_{\text{exch-disp}}^{(20)}$ /CBS value given at the bottom of the table was computed using the a6Z atom-centered basis augmented by the hydrogenic a6Z midbond set.

Fixed-amplitude Ansatz					
Basis	$E_{\text{disp}}^{(20)} + E_{\text{exch-disp}}^{(20)}$	aDZ-RI	aTZ-RI	aQZ-RI	a5Z-RI
aDZ	-0.4334	-0.6876	-0.5970	-0.5761	-0.5613
aTZ	-0.5413		-0.6192	-0.6101	-0.6021
aQZ	-0.5851			-0.6142	-0.6138
a5Z	-0.6084				-0.6247
Optimized diagonal Ansatz					
Basis	$E_{\text{disp}}^{(20)} + E_{\text{exch-disp}}^{(20)}$	aDZ-RI	aTZ-RI	aQZ-RI	a5Z-RI
aDZ	-0.4334	-0.7175	-0.6244	-0.6031	-0.5877
aTZ	-0.5413		-0.6350	-0.6257	-0.6173
aQZ	-0.5851			-0.6236	-0.6230
a5Z	-0.6084				-0.6282
EBC Ansatz					
Basis	$E_{\text{disp}}^{(20)} + E_{\text{exch-disp}}^{(20)}$	aDZ-RI	aTZ-RI	aQZ-RI	a5Z-RI
aDZ	-0.4334	-0.6905	-0.6219	-0.5986	-0.5800
aTZ	-0.5413		-0.6322	-0.6141	-0.5963
aQZ	-0.5851			-0.6149	-0.6183
a5Z	-0.6084				-0.6262
Fully optimized amplitudes					
Basis	$E_{\text{disp}}^{(20)} + E_{\text{exch-disp}}^{(20)}$	aDZ-RI	aTZ-RI	aQZ-RI	a5Z-RI
aDZ	-0.4334	-0.7275	-0.6387	-0.6124	-0.5922
aTZ	-0.5413		-0.7771	-0.6334	-0.6201
aQZ	-0.5851			-0.6277	-0.6278
a5Z	-0.6084				-0.6296
F12(MP2) Ansatz					
Basis	$E_{\text{disp}}^{(20)} + E_{\text{exch-disp}}^{(20)}$	aDZ-RI	aTZ-RI	aQZ-RI	a5Z-RI
aDZ	-0.4334	-0.5738	-0.5846	-0.5658	-0.5963
aTZ	-0.5413		-0.6138	-0.6114	-0.6161
aQZ	-0.5851			-0.6211	-0.6198
a5Z	-0.6084				-0.6351
<b>a6Z+(a6Z)</b>	<b>-0.6292</b>	$\pm$ 0.0015			



TABLE SIV: The  $E_{\text{disp}}^{(20)}$ -F12+ $E_{\text{exch-disp}}^{(20)}$ -F12 sum (in kcal/mol) for the water dimer for different combinations of the orbital basis aXZ and CABS basis aXZ-RI. EBC stands for the extended Brillouin condition Ansatz, and F12(MP2) denotes the approach of Ref. 1.

The benchmark  $E_{\text{disp}}^{(20)} + E_{\text{exch-disp}}^{(20)}$ /CBS value given at the bottom of the table was computed using the a6Z atom-centered basis augmented by the hydrogenic a6Z midbond set.

Fixed-amplitude Ansatz					
Basis	$E_{\text{disp}}^{(20)} + E_{\text{exch-disp}}^{(20)}$	aDZ-RI	aTZ-RI	aQZ-RI	a5Z-RI
aDZ	-1.7667	-2.069	-2.0605	-2.0597	-2.0601
aTZ	-2.0205	0.000	-2.1003	-2.0997	-2.0998
aQZ	-2.0849	0.000	0.0000	-2.1158	-2.1158
a5Z	-2.1043	0.000	0.0000	0.0000	-2.1196
Optimized diagonal Ansatz					
Basis	$E_{\text{disp}}^{(20)} + E_{\text{exch-disp}}^{(20)}$	aDZ-RI	aTZ-RI	aQZ-RI	a5Z-RI
aDZ	-1.7667	-2.1165	-2.1077	-2.1066	-2.1072
aTZ	-2.0205		-2.1218	-2.1213	-2.1214
aQZ	-2.0849			-2.1249	-2.1249
a5Z	-2.1043				-2.1246
EBC Ansatz					
Basis	$E_{\text{disp}}^{(20)} + E_{\text{exch-disp}}^{(20)}$	aDZ-RI	aTZ-RI	aQZ-RI	a5Z-RI
aDZ	-1.7667	-2.1007	-2.0910	-2.0898	-2.0905
aTZ	-2.0205		-2.1171	-2.1164	-2.1167
aQZ	-2.0849			-2.1226	-2.1226
a5Z	-2.1043				-2.1236
Fully optimized amplitudes					
Basis	$E_{\text{disp}}^{(20)} + E_{\text{exch-disp}}^{(20)}$	aDZ-RI	aTZ-RI	aQZ-RI	a5Z-RI
aDZ	-1.7667	-2.1252	-2.1156	-2.1145	-2.1153
aTZ	-2.0205		-2.1248	-2.1242	-2.1244
aQZ	-2.0849			-2.1256	-2.1256
a5Z	-2.1043				-2.1249
F12(MP2) Ansatz					
Basis	$E_{\text{disp}}^{(20)} + E_{\text{exch-disp}}^{(20)}$	aDZ-RI	aTZ-RI	aQZ-RI	a5Z-RI
aDZ	-1.7667	-2.2218	-2.2137	-2.2125	-2.2127
aTZ	-2.0205		-2.1667	-2.1658	-2.1659
aQZ	-2.0849			-2.1436	-2.1435
a5Z	-2.1043				-2.1334
<b>a6Z+(a6Z)</b>	<b>-2.1190</b>	$\pm$ 0.0041			

TABLE SV: The  $E_{\text{disp}}^{(20)}$ -F12+ $E_{\text{exch-disp}}^{(20)}$ -F12 sum (in kcal/mol) for the methane dimer for different combinations of the orbital basis aXZ and CABS basis aXZ-RI. EBC stands for the extended Brillouin condition Ansatz, and F12(MP2) denotes the approach of Ref. 1.

The benchmark  $E_{\text{disp}}^{(20)} + E_{\text{exch-disp}}^{(20)}$ /CBS value given at the bottom of the table was computed using the a6Z atom-centered basis augmented by the hydrogenic a6Z midbond set.

Fixed-amplitude Ansatz					
Basis	$E_{\text{disp}}^{(20)} + E_{\text{exch-disp}}^{(20)}$	aDZ-RI	aTZ-RI	aQZ-RI	a5Z-RI
aDZ	-0.9401	-1.0511	-1.0457	-1.0448	-1.0447
aTZ	-1.0311	0.0000	-1.0617	-1.0615	-1.0615
aQZ	-1.0518	0.0000	0.0000	-1.0642	
Optimized diagonal Ansatz					
Basis	$E_{\text{disp}}^{(20)} + E_{\text{exch-disp}}^{(20)}$	aDZ-RI	aTZ-RI	aQZ-RI	a5Z-RI
aDZ	-0.9401	-1.0566	-1.0512	-1.0502	-1.0501
aTZ	-1.0311		-1.0639	-1.0637	-1.0637
aQZ	-1.0518			-1.0651	
EBC Ansatz					
Basis	$E_{\text{disp}}^{(20)} + E_{\text{exch-disp}}^{(20)}$	aDZ-RI	aTZ-RI	aQZ-RI	a5Z-RI
aDZ	-0.9401	-1.0532	-1.0478	-1.0467	-1.0467
aTZ	-1.0311		-1.0612	-1.0610	-1.0609
aQZ	-1.0518			-1.0636	
Fully optimized amplitudes					
Basis	$E_{\text{disp}}^{(20)} + E_{\text{exch-disp}}^{(20)}$	aDZ-RI	aTZ-RI	aQZ-RI	a5Z-RI
aDZ	-0.9401	-1.0575	-1.0517	-1.0506	-1.0505
aTZ	-1.0311		-1.0641	-1.0640	-1.0639
aQZ	-1.0518			-1.0651	
F12(MP2) Ansatz					
Basis	$E_{\text{disp}}^{(20)} + E_{\text{exch-disp}}^{(20)}$	aDZ-RI	aTZ-RI	aQZ-RI	a5Z-RI
aDZ	-0.9401	-1.0485	-1.0464	-1.0457	-1.0457
aTZ	-1.0311		-1.0646	-1.0645	-1.0645
aQZ	-1.0518			-1.0654	-1.0653
<b>a6Z+(a6Z)</b>	<b>-1.0635</b>	$\pm$ 0.0011			

FIG. S1: Convergence of  $E_{\text{disp}}^{(20)}$  and  $E_{\text{disp}}^{(20)}$ -F12 as a function of basis set for the A24 database. The fully optimized, optimized diagonal, and fixed-amplitude Ansätze for the explicitly correlated amplitudes are denoted by (FULL), (ODA), and (FIX), respectively, and (MP2) stands for the F12(MP2) approach of Ref. 1. The aTZ-RI basis was used as CABS in all F12 calculations. The notation +(aXZ) signifies that the hydrogenic aXZ set of midbond functions has been added to the aXZ atom-centered basis, and the conventional a6Z+(a6Z) value has been used as a reference.

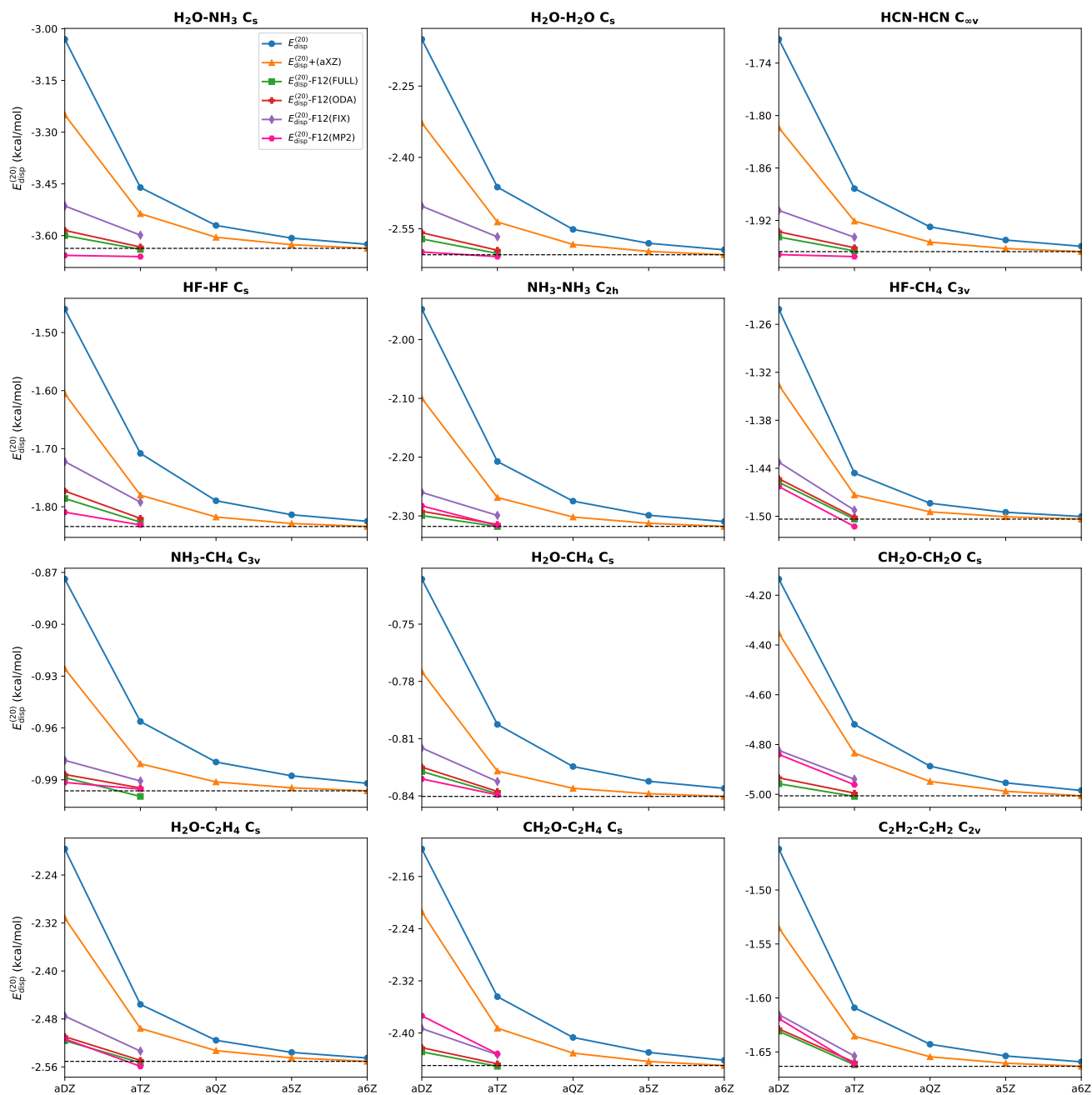


FIG. S2: Convergence of  $E_{\text{disp}}^{(20)}$  and  $E_{\text{disp}}^{(20)}$ -F12 as a function of basis set for the A24 database. The fully optimized, optimized diagonal, and fixed-amplitude Ansätze for the explicitly correlated amplitudes are denoted by (FULL), (ODA), and (FIX), respectively, and (MP2) stands for the F12(MP2) approach of Ref. 1. The aTZ-RI basis was used as CABS in all F12 calculations. The notation +(aXZ) signifies that the hydrogenic aXZ set of midbond functions has been added to the aXZ atom-centered basis, and the conventional a6Z+(a6Z) value has been used as a reference.

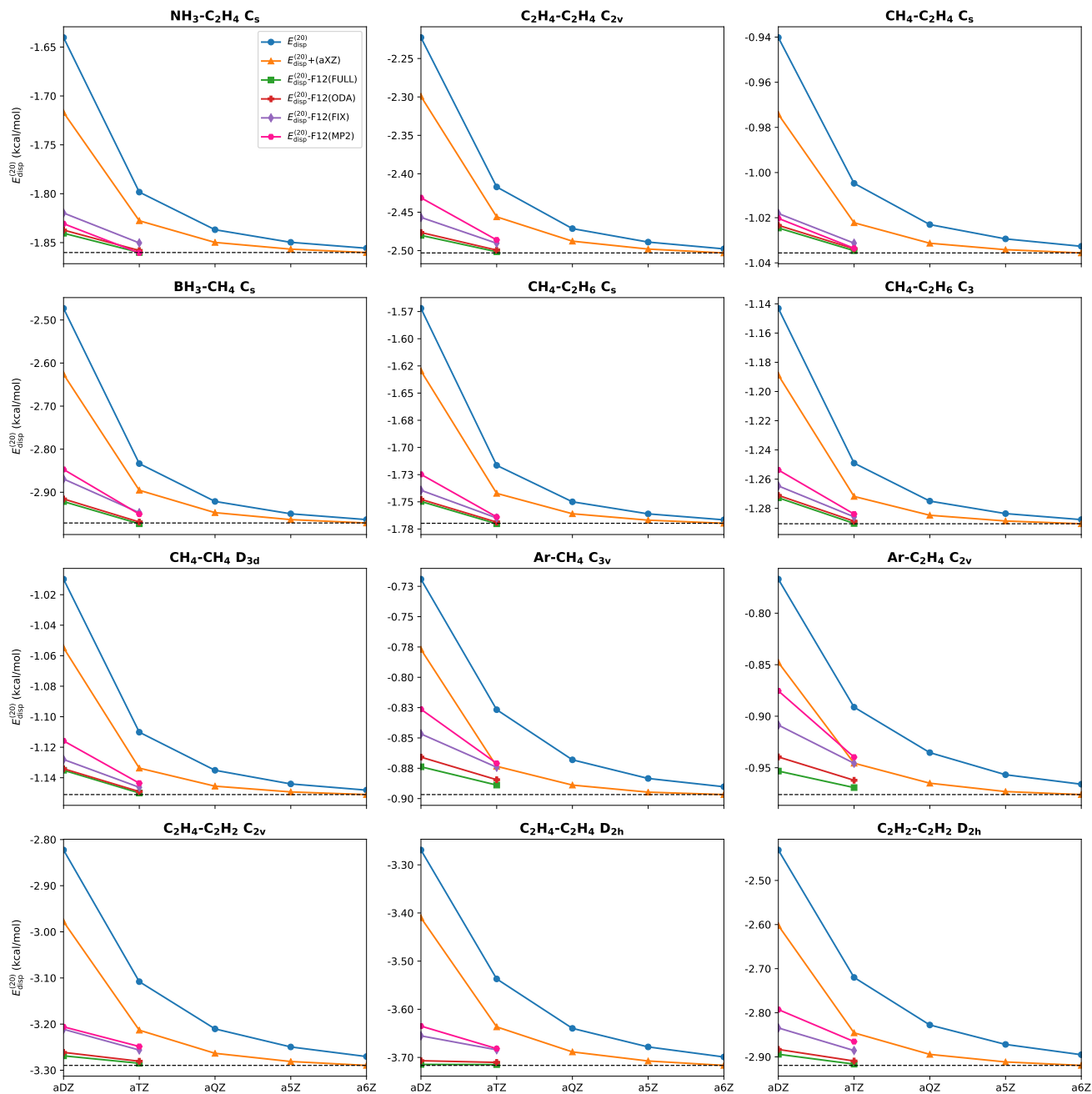


FIG. S3: Convergence of  $E_{\text{exch-disp}}^{(20)}$  and  $E_{\text{exch-disp}}^{(20)}$ -F12 as a function of basis set for the A24 database. The fully optimized, optimized diagonal, and fixed-amplitude Ansätze for the explicitly correlated amplitudes are denoted by (FULL), (ODA), and (FIX), respectively.

The aTZ-RI basis was used as CABS in all F12 calculations. The notation +(aXZ) signifies that the hydrogenic aXZ set of midbond functions has been added to the aXZ atom-centered basis, and the conventional a6Z+(a6Z) value has been used as a reference.

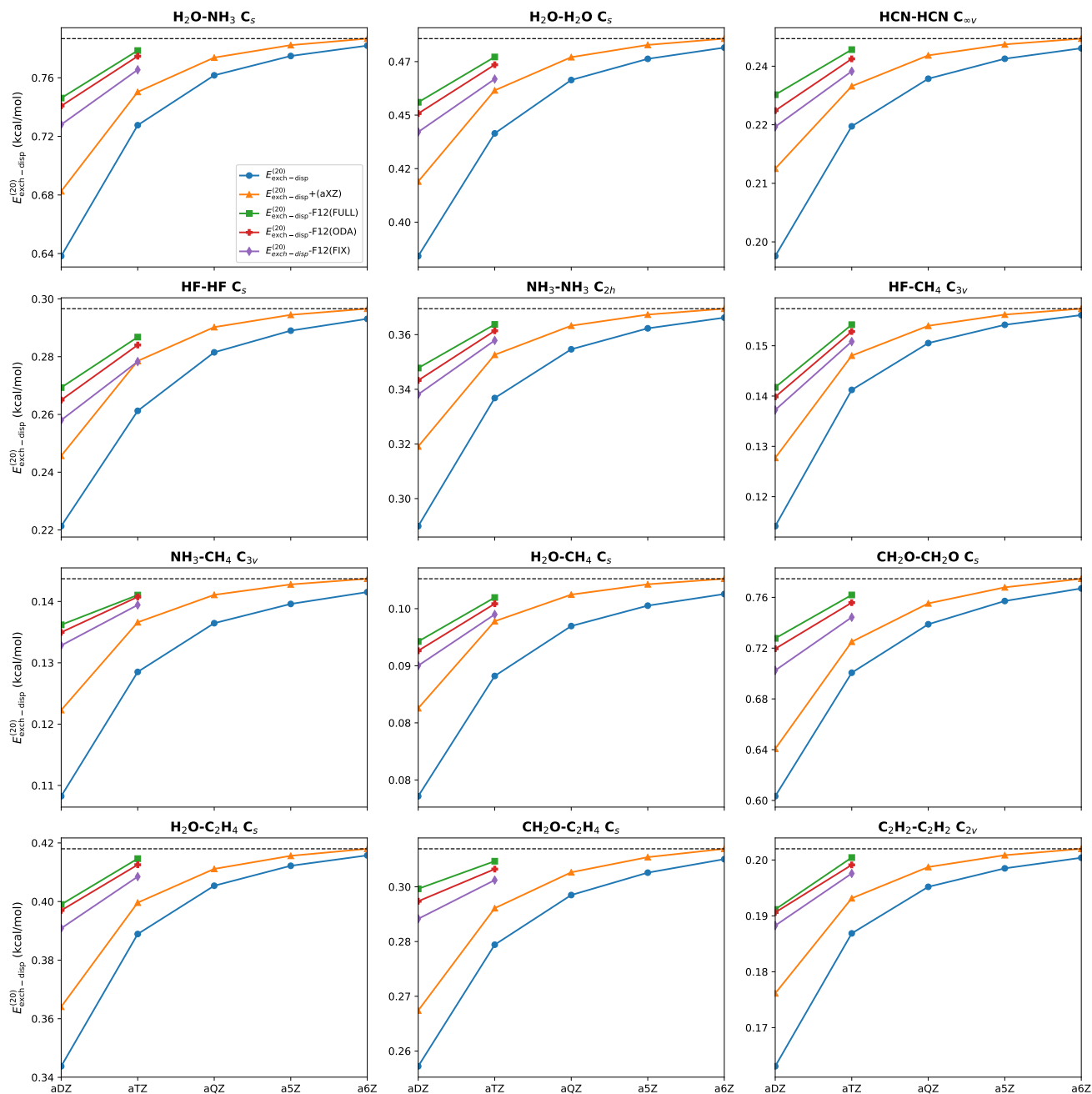


FIG. S4: Convergence of  $E_{\text{exch-disp}}^{(20)}$  and  $E_{\text{exch-disp}}^{(20)}$ -F12 as a function of basis set for the A24 database. The fully optimized, optimized diagonal, and fixed-amplitude Ansätze for the explicitly correlated amplitudes are denoted by (FULL), (ODA), and (FIX), respectively.

The aTZ-RI basis was used as CABS in all F12 calculations. The notation +(aXZ) signifies that the hydrogenic aXZ set of midbond functions has been added to the aXZ atom-centered basis, and the conventional a6Z+(a6Z) value has been used as a reference.

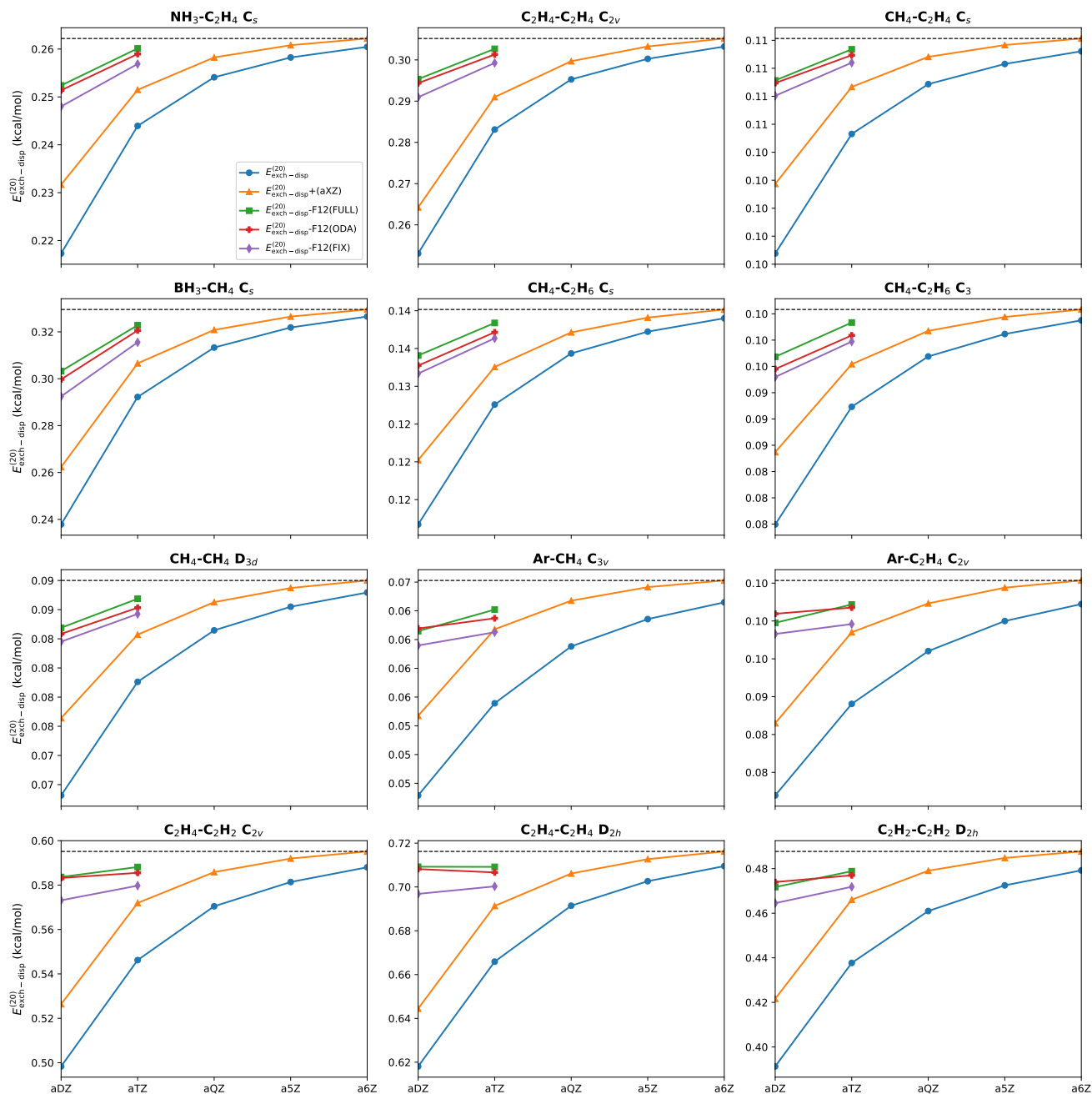


FIG. S5: Convergence of the sums  $E_{\text{disp}}^{(20)} + E_{\text{exch-disp}}^{(20)}$  and  $E_{\text{disp}}^{(20)}\text{-F12} + E_{\text{exch-disp}}^{(20)}\text{-F12}$  as a function of basis set for the A24 database. The fully optimized, optimized diagonal, and fixed-amplitude Ansätze for the explicitly correlated amplitudes are denoted by (FULL), (ODA), and (FIX), respectively, and (MP2) stands for the F12(MP2) approach of Ref. 1.

The aTZ-RI basis was used as CABS in all F12 calculations. The notation +(aXZ) signifies that the hydrogenic aXZ set of midbond functions has been added to the aXZ atom-centered basis, and the conventional a6Z+(a6Z) value has been used as a reference.

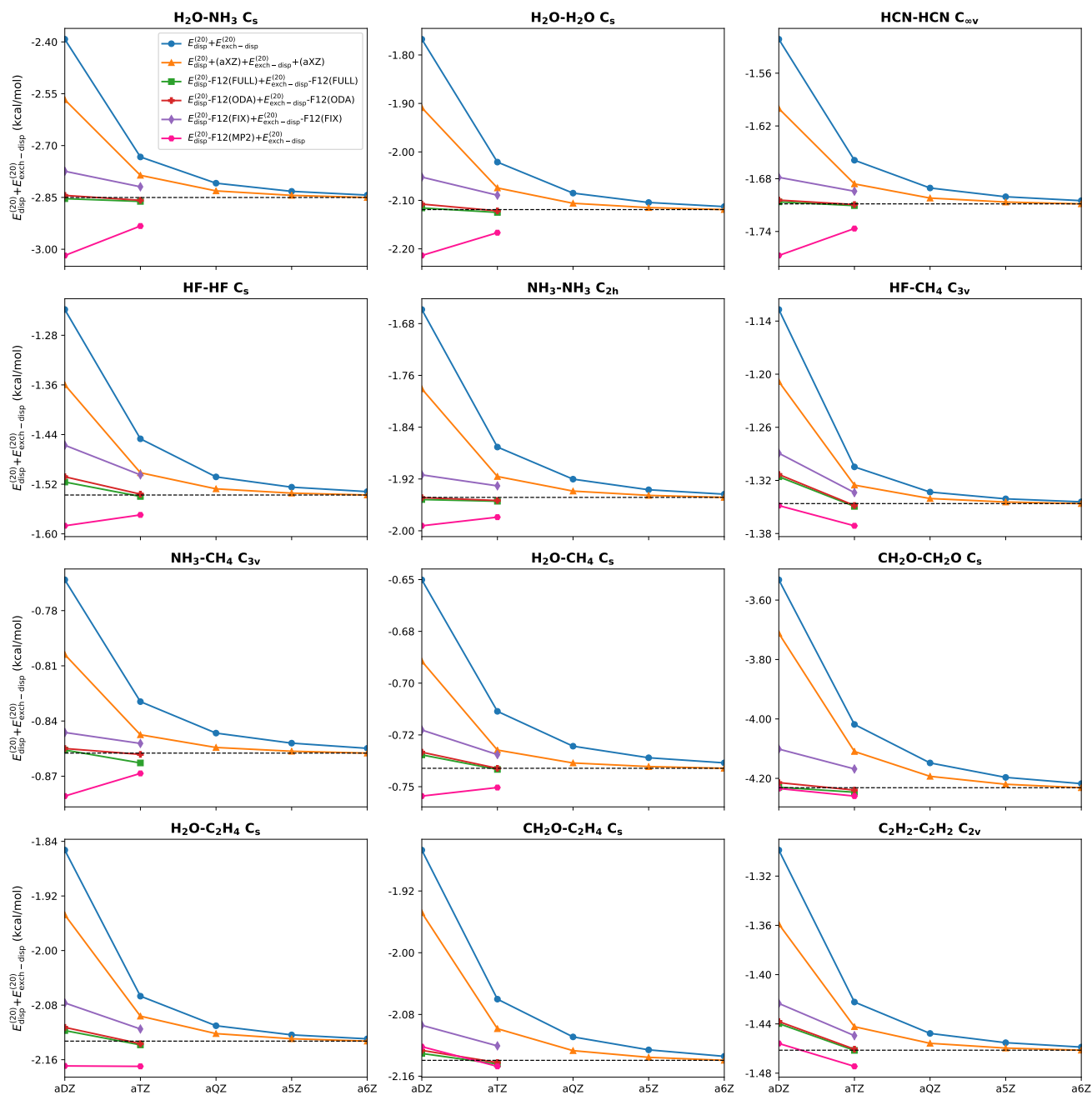


FIG. S6: Convergence of the sums  $E_{\text{disp}}^{(20)} + E_{\text{exch-disp}}^{(20)}$  and  $E_{\text{disp}}^{(20)}\text{-F12} + E_{\text{exch-disp}}^{(20)}\text{-F12}$  as a function of basis set for the A24 database. The fully optimized, optimized diagonal, and fixed-amplitude Ansätze for the explicitly correlated amplitudes are denoted by (FULL), (ODA), and (FIX), respectively, and (MP2) stands for the F12(MP2) approach of Ref. 1.

The aTZ-RI basis was used as CABS in all F12 calculations. The notation +(aXZ) signifies that the hydrogenic aXZ set of midbond functions has been added to the aXZ atom-centered basis, and the conventional a6Z+(a6Z) value has been used as a reference.

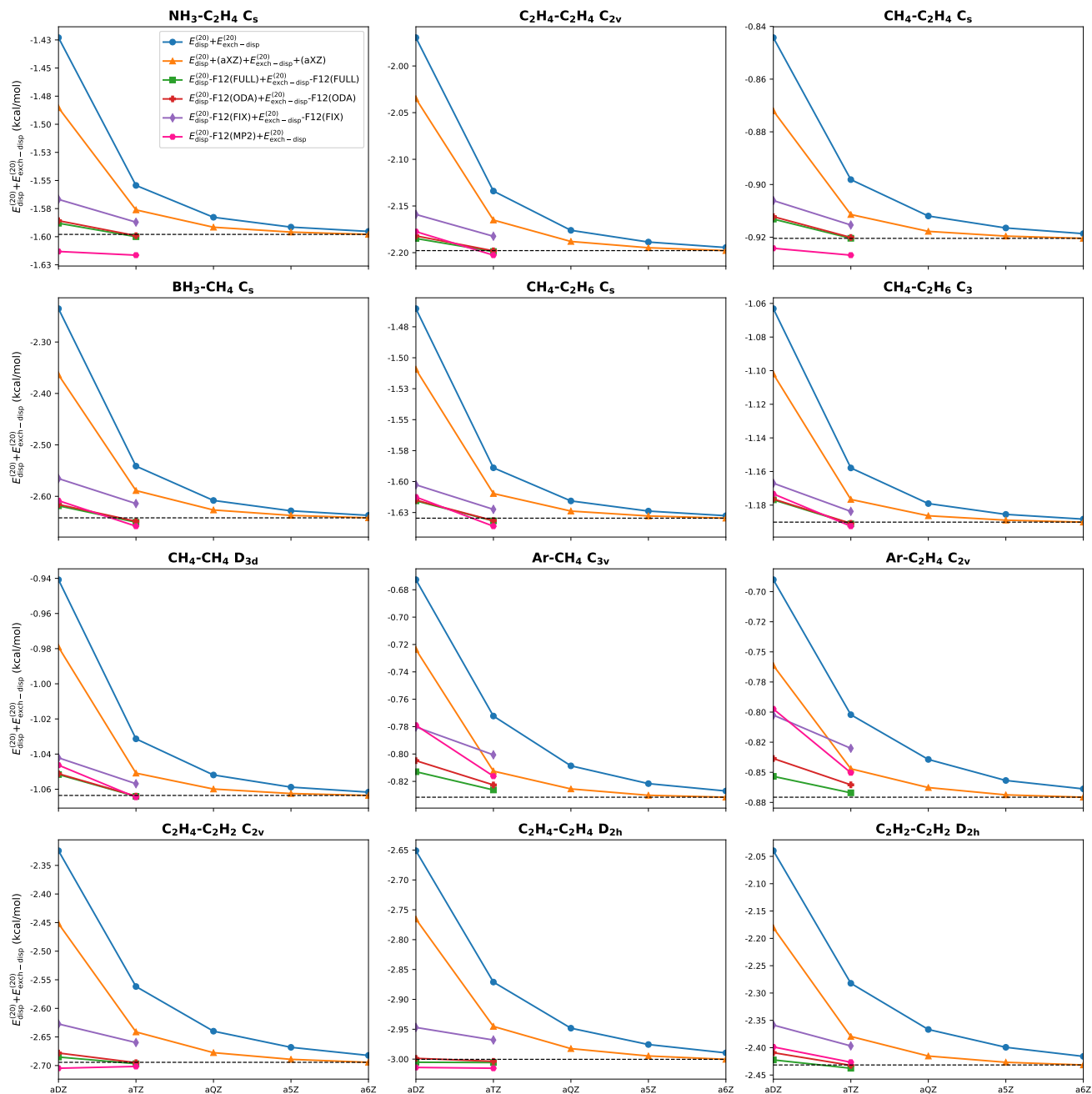




FIG. S7: Relative errors on the A24 database<sup>3</sup> for the sums  $E_{\text{disp}}^{(20)} + E_{\text{exch-disp}}^{(20)}$  and  $E_{\text{disp}}^{(20)} - \text{F12} + E_{\text{exch-disp}}^{(20)} - \text{F12}$  computed with the aDZ orbital basis set and the aTZ-RI auxiliary basis set. The fully optimized, optimized diagonal, and fixed-amplitude Ansätze for the explicitly correlated amplitudes are denoted by (FULL), (ODA), and (FIX), respectively, and (MP2) stands for the F12(MP2) approach of Ref. 1. The notation +(aXZ) signifies that the hydrogenic aXZ set of midbond functions has been added to the aXZ atom-centered basis, and the conventional a6Z+(a6Z) value has been used as a reference.

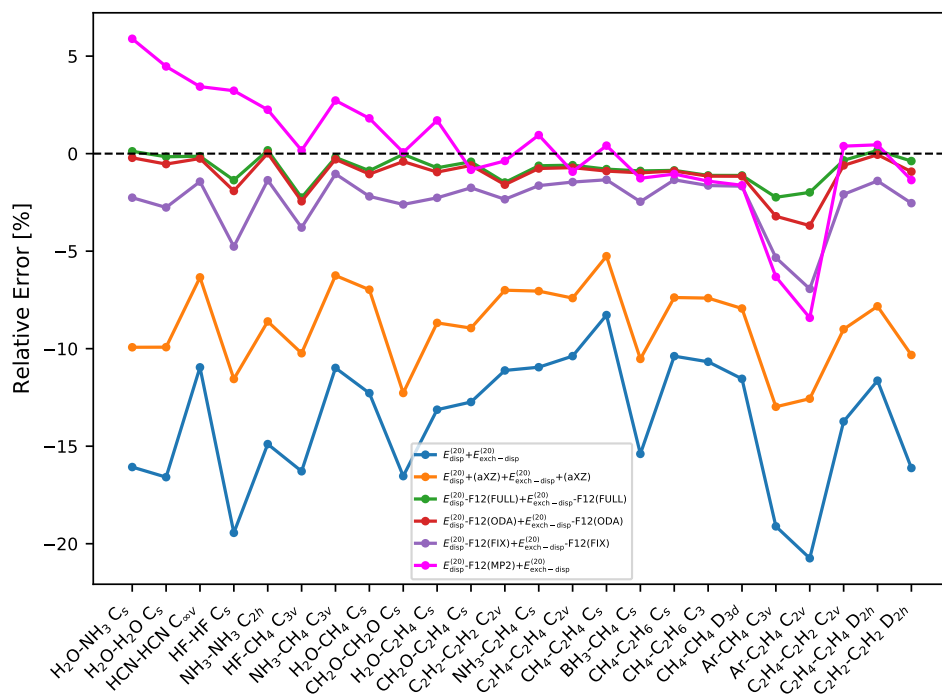


FIG. S8: Relative errors on the A24 database<sup>3</sup> for the sums  $E_{\text{disp}}^{(20)} + E_{\text{exch-disp}}^{(20)}$  and  $E_{\text{disp}}^{(20)}\text{-F12} + E_{\text{exch-disp}}^{(20)}\text{-F12}$  computed with the aTZ orbital basis set and the aTZ-RI auxiliary basis set. The fully optimized, optimized diagonal, and fixed-amplitude Ansätze for the explicitly correlated amplitudes are denoted by (FULL), (ODA), and (FIX), respectively, and (MP2) stands for the F12(MP2) approach of Ref. 1. The notation +(aXZ) signifies that the hydrogenic aXZ set of midbond functions has been added to the aXZ atom-centered basis, and the conventional a6Z+(a6Z) value has been used as a reference.

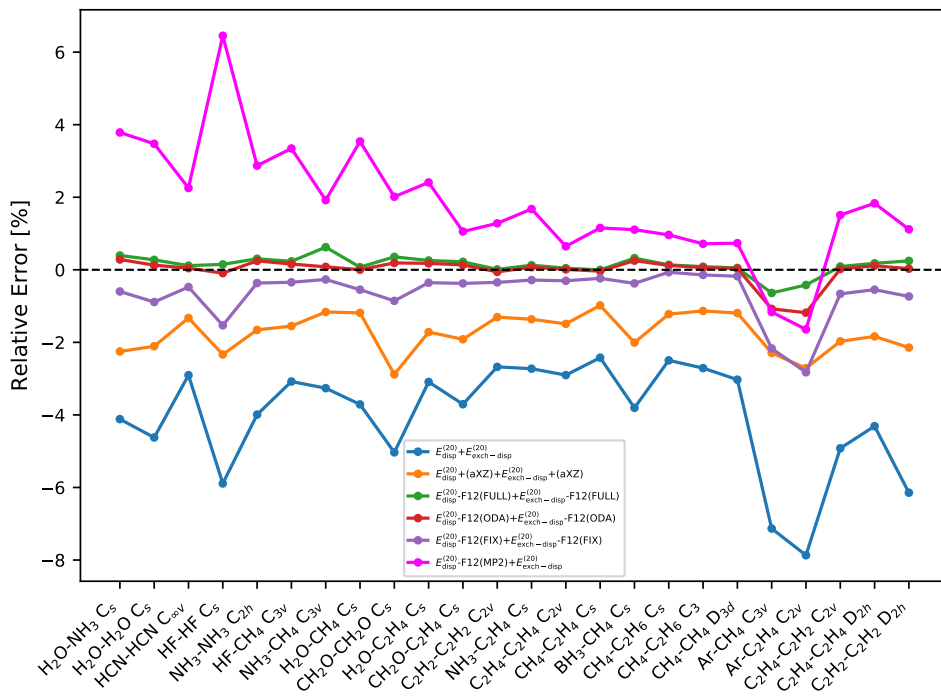
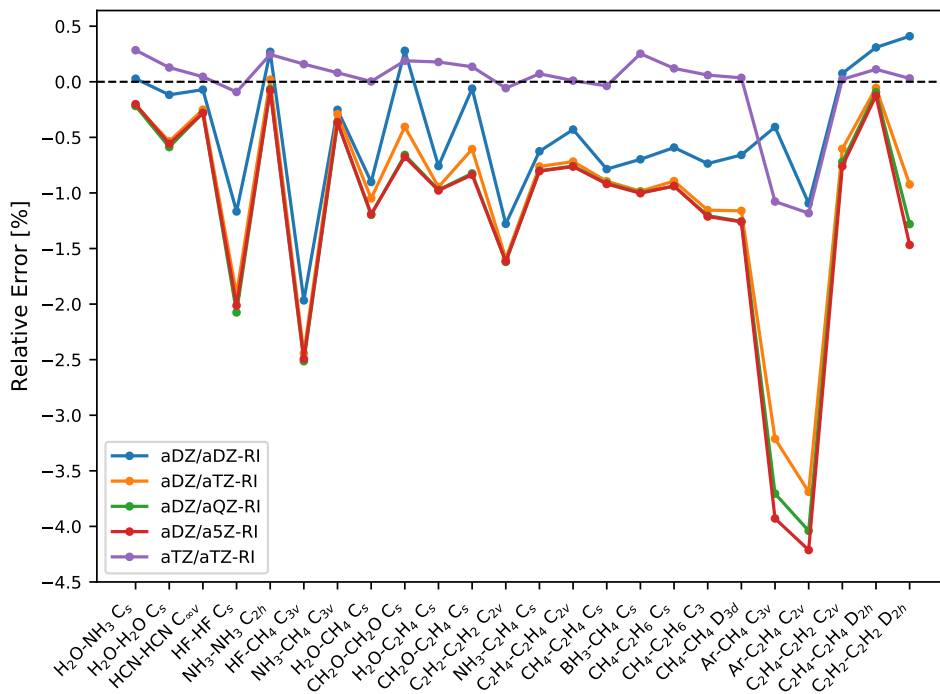


FIG. S9: Dependence of the  $E_{\text{disp}}^{(20)}\text{-F12} + E_{\text{exch-disp}}^{(20)}\text{-F12}$  relative errors for the A24 database<sup>3</sup>, computed with the optimized diagonal Ansatz, on the orbital basis set aXZ and the CABS set aXZ-RI. The conventional a6Z+(a6Z) value has been used as a reference



- 
- <sup>1</sup> Frey, J. A.; Holzer, C.; Klopper, W.; Leutwyler, S. Experimental and Theoretical Determination of Dissociation Energies of Dispersion-Dominated Aromatic Molecular Complexes. *Chem. Rev.* **2016**, *116*, 5614–5641.
- <sup>2</sup> Jeziorska, M.; Cencek, W.; Patkowski, K.; Jeziorski, B.; Szalewicz, K. Pair potential for helium from symmetry-adapted perturbation theory calculations and from supermolecular data. *J. Chem. Phys.* **2007**, *127*, 124303.
- <sup>3</sup> Řezáč, J.; Hobza, P. Describing Noncovalent Interactions beyond the Common Approximations: How Accurate Is the 'Gold Standard,' CCSD(T) at the Complete Basis Set Limit? *J. Chem. Theory Comput.* **2013**, *9*, 2151–2155.